Calhoun: The NPS Institutional Archive

DSpace Repository

Theses and Dissertations | 1. Thesis and Dissertation Collection, all items

2017-09

Synthetic modifications in the frequency domain for finite element model update and damage detection

Konze, Ryun J.C.

Monterey, California: Naval Postgraduate School

https://hdl.handle.net/10945/56148

This publication is a work of the U.S. Government as defined in Title 17, United States Code, Section 101. Copyright protection is not available for this work in the United States.

Downloaded from NPS Archive: Calhoun

http://www.nps.edu/library

Calhoun is the Naval Postgraduate School's public access digital repository for research materials and institutional publications created by the NPS community. Calhoun is named for Professor of Mathematics Guy K. Calhoun, NPS's first appointed -- and published -- scholarly author.

Dudley Knox Library / Naval Postgraduate School
411 Dyer Road / 1 University Circle
Monterey, California USA 93943

NAVAL POSTGRADUATE SCHOOL

MONTEREY, CALIFORNIA

THESIS

SYNTHETIC MODIFICATIONS IN THE FREQUENCY DOMAIN FOR FINITE ELEMENT MODEL UPDATE AND DAMAGE DETECTION

by

Ryun J. C. Konze

September 2017

Thesis Advisor:	Joshua H. Gordis
Second Reader:	Young W. Kwon

Approved for public release. Distribution is unlimited.

THIS PAGE INTENTIONALLY LEFT BLANK

REPORT DOCUMENTATION PAGE			Form Approved OMB No. 0704–0188
Public reporting burden for this collection of information is estimated to average 1 hour per response, including the time for reviewing instruction, searching existing data sources, gathering and maintaining the data needed, and completing and reviewing the collection of information. Send comments regarding this burden estimate or any other aspect of this collection of information, including suggestions for reducing this burden, to Washington headquarters Services, Directorate for Information Operations and Reports, 1215 Jefferson Davis Highway, Suite 1204, Arlington, VA 22202-4302, and to the Office of Management and Budget, Paperwork Reduction Project (0704-0188) Washington, DC 20503.			
1. AGENCY USE ONLY ***(Leave blank)***	**2. REPORT DATE** September 2017	**3. REPORT TYPE AND DATES COVERED** Master's thesis	
4. TITLE AND SUBTITLE SYNTHETIC MODIFICATIONS IN THE FREQUENCY DOMAIN FOR FINITE ELEMENT MODEL UPDATE AND DAMAGE DETECTION			**5. FUNDING NUMBERS**
6. AUTHOR(S) Ryun J. C. Konze			
7. PERFORMING ORGANIZATION NAME(S) AND ADDRESS(ES) Naval Postgraduate School Monterey, CA 93943-5000			**8. PERFORMING ORGANIZATION REPORT NUMBER**
9. SPONSORING /MONITORING AGENCY NAME(S) AND ADDRESS(ES) N/A			**10. SPONSORING / MONITORING AGENCY REPORT NUMBER**
11. SUPPLEMENTARY NOTES The views expressed in this thesis are those of the author and do not reflect the official policy or position of the Department of Defense or the U.S. Government. IRB number N/A.			
12a. DISTRIBUTION / AVAILABILITY STATEMENT Approved for public release. Distribution is unlimited.			**12b. DISTRIBUTION CODE**

13. ABSTRACT (maximum 200 words)

Sensitivity-based finite element model updating and structural damage detection has been limited by the number of modes available in a vibration test and also by the corresponding amount of natural frequency sensitivity data. The method of Artificial Boundary Conditions (ABC) has been shown to greatly increase the number of modes and corresponding sensitivity data by artificially constraining the structure under test, producing a large number of alternative test configurations and associated sensitivity data. This thesis explores an extension of this concept by the application of synthetic structural modifications to the measured data, including both springs-to-ground and mass modifications. This is accomplished with frequency domain structural synthesis. The ability of this technique to generate additional sensitivity data for use in model update and damage detection is explored and compared with the use of Artificial Boundary Conditions. Frequency response functions from a simulated damaged structure are used as well as measured frequency response functions from a lab-scale damaged structure.

14. SUBJECT TERMS artificial boundary conditions, artificial beam modification, finite element model, model update, damage identification, natural frequencies, sensitivity matrix			**15. NUMBER OF PAGES** 227
			16. PRICE CODE
17. SECURITY CLASSIFICATION OF REPORT Unclassified	**18. SECURITY CLASSIFICATION OF THIS PAGE** Unclassified	**19. SECURITY CLASSIFICATION OF ABSTRACT** Unclassified	**20. LIMITATION OF ABSTRACT** UU

NSN 7540–01-280-5500 Standard Form 298 (Rev. 2–89)
Prescribed by ANSI Std. 239–18

THIS PAGE INTENTIONALLY LEFT BLANK

Approved for public release. Distribution is unlimited.

SYNTHETIC MODIFICATIONS IN THE FREQUENCY DOMAIN FOR FINITE ELEMENT MODEL UPDATE AND DAMAGE DETECTION

Ryun J. C. Konze
Lieutenant, United States Coast Guard
B.S., California Maritime Academy, 2010

Submitted in partial fulfillment of the
requirements for the degree of

MASTER OF SCIENCE IN MECHANICAL ENGINEERING

from the

NAVAL POSTGRADUATE SCHOOL
September 2017

Approved by: Joshua H. Gordis
Thesis Advisor

Young W. Kwon
Second Reader

Garth V. Hobson
Chair, Department of Mechanical and Aerospace Engineering

THIS PAGE INTENTIONALLY LEFT BLANK

ABSTRACT

Sensitivity-based finite element model updating and structural damage detection has been limited by the number of modes available in a vibration test and also by the corresponding amount of natural frequency sensitivity data. The method of Artificial Boundary Conditions (ABC) has been shown to greatly increase the number of modes and corresponding sensitivity data by artificially constraining the structure under test, producing a large number of alternative test configurations and associated sensitivity data. This thesis explores an extension of this concept by the application of synthetic structural modifications to the measured data, including both springs-to-ground and mass modifications. This is accomplished with frequency domain structural synthesis. The ability of this technique to generate additional sensitivity data for use in model update and damage detection is explored and compared with the use of Artificial Boundary Conditions. Frequency response functions from a simulated damaged structure are used as well as measured frequency response functions from a lab-scale damaged structure.

THIS PAGE INTENTIONALLY LEFT BLANK

TABLE OF CONTENTS

I. INTRODUCTION 1
A. BACKGROUND 1
B. LITERATURE REVIEW 5
C. SCOPE OF THESIS 8
D. NOTES ON THESIS 8

II. THEORY 9
A. STRUCTURAL DYNAMICS 9
1. Shape Functions 10
2. Finite Element Model 13
B. NATURAL FREQUENCY SENSITIVITY 14
1. Modal Frequencies 15
2. Analytical and Omitted Coordinates 16
3. Building the Modal Sensitivity Matrix 18
4. Determining the Modal Sensitivity Matrix Using Eigenvectors and Eigen Values 20
C. FREQUENCY RESPONSE FUNCTION 21
D. DAMAGE DETECTION AND MODEL UPDATING 23
E. STRUCTURAL SYNTHESIS 24
1. Artificial Boundary Condition Synthesis 27
2. Artificial Spring or Mass Synthesis 28
F. COMPOSITE SENSITIVITY MATRIX 30
G. CONCLUDING REMARKS 32

III. EXPERIMENTAL SETUP AND TESTING 33
A. EXPERIMENTAL SETUP 33
B. EXPERIMENTAL TESTING 35
C. CONCLUDING REMARKS 38

IV. FINITE ELEMENT MODELING AND SIMULATION 39
A. FINITE ELEMENT MODELING 39
B. FINITE ELEMENT MODEL TESTING 40
C. FEM INITIAL SENSITIVITY MATRIX AND FRF 43
1. Initial Sensitivity Matrix 43
2. Initial Calculated FRF 44
D. SINGLE SPRING DYNAMIC RESPONSE 46
1. FRF Synthesis 46
2. Single Spring FRF Synthesis 47

3. Single Spring Sensitivity Analysis 56
E. SINGLE MASS SYSTEM DYNAMIC RESPONSE 83
1. Single Mass FRF Synthesis 83
2. Single Mass Sensitivity Analysis 86
F. TWO SPRING SYSTEM 106
1. Two Spring FRF Analysis 106
2. Two Spring Sensitivity Analysis 110
G. CONCLUDING REMARKS 129

V. MODEL UPDATING AND DAMAGE DETECTION 131
A. INTRODUCTION 131
B. VERIFICATION OF DATA IMPORT 131
C. MODEL UPDATING USING SINGLE SPRING 132
D. MODEL UPDATING USING SINGLE MASS 141
E. MODEL UPDATING USING TWO SPRINGS 148
F. MODEL UPDATING USING LOWER MODES 155
G. CONCLUDING REMARKS 161

VI. CONCLUSIONS AND RECOMMENDATIONS 163
A. CONCLUSIONS 163
B. RECOMMENDATIONS 166

APPENDIX A. BEAM MODIFICATION BASE CODE 169

APPENDIX B. STIFFNESS AND MASS MATRIX BUILDING FUNCTION 175

APPENDIX C. EIGENVALUE FUNCTION 179

APPENDIX D. SYSTEM FREQUENCY LIMITING FUNCTION 181

APPENDIX E. SENSITIVITY MATRIX BUILDING FUNCTION 183

APPENDIX F. SENSITIVITY MATRIX CHECK FUNCTION 185

APPENDIX G. FRF SYNTHESIS FUNCTION 187

APPENDIX H. SENSITIVITY CALCULATION FOR SYNTHESIZED BEAM 193

LIST OF REFERENCES 197

INITIAL DISTRIBUTION LIST 201

LIST OF FIGURES

Figure 1. Euler-Bernoulli Beam Assumption Characteristics. Source: [3]. 2

Figure 2. Frequency Response Function 3

Figure 3. 2-D Euler-Bernoulli Beam 10

Figure 4. Cubic Hermite Shape Functions. Source: [18]. 11

Figure 5. 16-Element Structure with Beam Modification. 25

Figure 6. 16-Element Structure with Artificial Boundary Condition. 27

Figure 7. 16-Element Structure with Artificial Spring. 29

Figure 8. Experimental Beam Node Numbering 33

Figure 9. Testing Signal Comparison 37

Figure 10. Single Impact Hammer Testing Mode Selection 38

Figure 11. FEM Node Numbering 39

Figure 12. 2-D Euler-Bernoulli Element DOF Setup. Adapted from [25]. 40

Figure 13. FEM Initial FRF Response, $H_{1,1}$ 44

Figure 14. Initial FEM vs Measured FEM Response, $H_{1,1}$ 45

Figure 15. Initial FRF Response vs Synthesized Pin Located at Node 13, $H_{33,33}$ 46

Figure 16. Pin FRF Response Check, Pin Located at Node 13, $H_{33,33}$ 47

Figure 17. 178.579 kg/mm (10,000lb/in)Spring Synthesis at Node 2 Check, $H_{3,3}$ 48

Figure 18. FRF Progression for Spring Synthesis at Node 13, $H_{25,25}$ 48

Figure 19. Magnification of FRF Progression for Spring Synthesis at Node 13, $H_{25,25}$ 49

Figure 20. Modal Resonance Frequency Progression for Spring Strength 0–8.928 kg/mm (0–500lb/in) Located at Node 13 50

Figure 21. Modal Resonance Frequency Progression for Spring Strength 0–178.579 kg/mm (0–10,000lb/in) Located at Node 13 50

Figure 22. Mode Shapes with 0 kg/mm(0 lb/in) Spring Located at Node 13 (Resonance Frequency in Parentheses) 51

Figure 23. Mode Shapes with 0.017 kg/mm (1 lb/in) Spring Located at Node 13 (Resonance Frequency in Parentheses) 51

Figure 24. Mode Shapes with 0.357 kg/mm(20 lb/in) Spring Located at Node 13 (Resonance Frequency in Parentheses) 52

Figure 25. Mode Shapes with 0.892 kg/mm(50 lbf/in)Spring Located at Node 13 (Resonance Frequency in Parentheses) 52

Figure 26. Mode Shapes with 0.982 kg/mm(55 lb/in) Spring Located at Node 13 (Resonance Frequency in Parentheses) 53

Figure 27. Mode Shapes with 1.00 kg/mm (56 lb/in) Spring Located at Node 13 (Resonance Frequency in Parentheses) 53

Figure 28. Mode Shapes with 1.79 kg/mm (100 lb/in) Spring Located at Node 13 (Resonance Frequency in Parentheses) 54

Figure 29. Mode Shapes with 8.93 kg/mm(500 lbf/in)Spring Located at Node 13 (Resonance Frequency in Parentheses) 54

Figure 30. Mode Shapes with 178.579 kg/mm (10,000 lb/in) Spring Located at Node 13 (Resonance Frequency in Parentheses) 55

Figure 31. Mode Shapes with a Pin Connection Located at Node 13 (Resonance Frequency in Parentheses) 55

Figure 32. Effects of Spring Strength Variance on Sensitivity Value for Node 2 57

Figure 33. Effects of Spring Strength Variance on Sensitivity Value for Node 3 57

Figure 34. Effects of Spring Strength Variance on Sensitivity Value for Node 4 58

Figure 35. Effects of Spring Strength Variance on Sensitivity Value for Node 5 58

Figure 36. Effects of Spring Strength Variance on Sensitivity Value for Node 6 59

Figure 37. Effects of Spring Strength Variance on Sensitivity Value for Node 7 59

Figure 38. Effects of Spring Strength Variance on Sensitivity Value for Node 8 60

Figure 39. Effects of Spring Strength Variance on Sensitivity Value for Node 9 60

Figure 40. Effects of Spring Strength Variance on Sensitivity Value for Node 10 61

Figure 41. Effects of Spring Strength Variance on Sensitivity Value for Node 11 61

Figure 42. Effects of Spring Strength Variance on Sensitivity Value for Node 12 62

Figure 43. Effects of Spring Strength Variance on Sensitivity Value for Node 13 62

Figure 44. Effects of Spring Strength Variance on Sensitivity Value for Node 14 63

Figure 45. Effects of Spring Strength Variance on Sensitivity Value for Node 15 63

Figure 46. Effects of Spring Strength Variance on Sensitivity Value for Node 16 64

Figure 47. Model Error vs True Error Using Poorly Conditioned Sensitivity Matrix 65

Figure 48. Model Error vs True Error Using a Well Conditioned Sensitivity Matrix 66

Figure 49. Effect of Number of Baseline Modes Used in Sensitivity Matrix on Condition Number, Single Node, 178.579 kg/mm (10,000 lb/in) Artificial Spring 69

Figure 50. Effect of Number of Baseline Modes Used in Sensitivity Matrix on Condition Number, 71.431kg/mm (4000lb/in) (Node 13) 116.076 kg/mm (6500lb/in) (Node 7) 69

Figure 51. Effect of Number of Baseline Modes Used in Sensitivity Matrix on Condition Number, 71.431 & 178.579kg/mm (4,000&10,000lb/in) on Node 13, 116.076 & 178.579kg/mm (6,500&10,000lb/in) on Node 7 70

Figure 52. Sensitivity Matrix Condition Number Index Example 73

Figure 53. Sensitivity Matrix Combination Condition Number Indicator, Single Spring 74

Figure 54. Single Spring Error Identification with Damage at Element 1 76

Figure 55. Single Spring Error Identification with Damage at Element 2 77

Figure 56. Single Spring Error Identification with Damage at Element 3 77

Figure 57. Single Spring Error Identification with Damage at Element 4 78

Figure 58. Single Spring Error Identification with Damage at Element 5 78

Figure 59. Single Spring Error Identification with Damage at Element 6 79

Figure 60. Single Spring Error Identification with Damage at Element 7 79

Figure 61. Single Spring Error Identification with Damage at Element 8 80

Figure 62. Single Spring Error Identification with Damage at Element 9 80

Figure 63. Single Spring Error Identification with Damage at Element 10 81

Figure 64. Single Spring Error Identification with Damage at Element 11 81

Figure 65. Single Spring Error Identification with Damage at Element 12 82

Figure 66. Single Spring Error Identification with Damage at Element 13 82

Figure 67. Single Spring Error Identification with Damage at Element 14 83

Figure 68. 0.227 kg (0.5 lb) Lumped Mass on Node 13 FRF Synthesis Check, $H_{25,25}$ 84

Figure 69. Lumped Mass on Node 13 FRF Synthesis Progression, $H_{25,25}$ 85

Figure 70. Modal Frequency Variance Due to Mass Addition at Node 13 86

Figure 71. Effects on Sensitivity Value for Mass Addition Variance on Node 2 87

Figure 72. Effects on Sensitivity Value for Mass Addition Variance on Node 3 88

Figure 73. Effects on Sensitivity Value for Mass Addition Variance on Node 4 88

Figure 74. Effects on Sensitivity Value for Mass Addition Variance on Node 5 89

Figure 75. Effects on Sensitivity Value for Mass Addition Variance on Node 6 89

Figure 76. Effects on Sensitivity Value for Mass Addition Variance on Node 7 90

Figure 77. Effects on Sensitivity Value for Mass Addition Variance on Node 8 90

Figure 78. Effects on Sensitivity Value for Mass Addition Variance on Node 9 91

Figure 79. Effects on Sensitivity Value for Mass Addition Variance on Node 10 91

Figure 80. Effects on Sensitivity Value for Mass Addition Variance on Node 11 92

Figure 81. Effects on Sensitivity Value for Mass Addition Variance on Node 12 92

Figure 82. Effects on Sensitivity Value for Mass Addition Variance on Node 13 93

Figure 83. Effects on Sensitivity Value for Mass Addition Variance on Node 14 93

Figure 84. Effects on Sensitivity Value for Mass Addition Variance on Node 15 94

Figure 85. Effects on Sensitivity Value for Mass Addition Variance on Node 16 94

Figure 86. Sensitivity Matrix Combination Condition Number Indicator, Single Mass 97

Figure 87. Single Mass Error Identification with Damage at Element 1 99

Figure 88. Single Mass Error Identification with Damage at Element 2 99

Figure 89. Single Mass Error Identification with Damage at Element 3 100

Figure 90. Single Mass Error Identification with Damage at Element 4 100

Figure 91. Single Mass Error Identification with Damage at Element 5 101

Figure 92. Single Mass Error Identification with Damage at Element 6 101

Figure 93. Single Mass Error Identification with Damage at Element 7 102

Figure 94. Single Mass Error Identification with Damage at Element 8 102

Figure 95. Single Mass Error Identification with Damage at Element 9 103

Figure 96. Single Mass Error Identification with Damage at Element 10 103

Figure 97. Single Mass Error Identification with Damage at Element 11 104

Figure 98. Single Mass Error Identification with Damage at Element 12 104

Figure 99. Single Mass Error Identification with Damage at Element 13 105

Figure 100. Single Mass Error Identification with Damage at Element 14 105

Figure 101. Two Springs at Nodes 5 and 12 FRF Synthesis Check, $H_{33,33}$, 178.579 kg/mm (10,000 lb/in) Springs 107

Figure 102. Frequency Progression with Springs Installed at Nodes 5 and 12, Varying strength from 0–178.579 kg/mm (0-10,000 lb/in) Equally 108

Figure 103. FRF Progression with Springs Installed at Nodes 5 and 12, Varying strength from 0–178.579 kg/mm (0-10,000 lb/in) Equally, $H_{9,9}$ 109

Figure 104. Magnified FRF Variance with Springs Installed at Nodes 5 and 12, Varying strength from 0–178.579 kg/mm (0-10,000 lb/in) Equally,$H_{9,9}$ 109

Figure 105. Effects on Sensitivity Value with Increasing Spring Strength for Springs Located on Nodes 2 and 6 from 0–178.579 kg/mm (0-10,000 lb/in) Equally 110

Figure 106. Effects on Sensitivity Value with Increasing Spring Strength for Springs Located on Nodes 2 and 16 from 0–178.579 kg/mm (0-10,000 lb/in) Equally 111

Figure 107. Effects on Sensitivity Value with Increasing Spring Strength for Springs Located on Nodes 3 and 15 from 0–178.579 kg/mm (0-10,000 lb/in) Equally 111

Figure 108. Effects on Sensitivity Value with Increasing Spring Strength for Springs Located on Nodes 4 and 8 from 0–178.579 kg/mm (0-10,000 lb/in) Equally 112

Figure 109. Effects on Sensitivity Value with Increasing Spring Strength for Springs Located on Nodes 4 and 15 from 0–178.579 kg/mm (0-10,000 lb/in) Equally 112

Figure 110. Effects on Sensitivity Value with Increasing Spring Strength for Springs Located on Nodes 5 and 8 from 0–178.579 kg/mm (0-10,000 lb/in) Equally 113

Figure 111. Effects on Sensitivity Value with Increasing Spring Strength for Springs Located on Nodes 5 and 12 from 0–178.579 kg/mm (0-10,000 lb/in) Equally 113

Figure 112. Effects on Sensitivity Value with Increasing Spring Strength for Springs Located on Nodes 5 and 16 from 0–178.579 kg/mm (0-10,000 lb/in) Equally 114

Figure 113. Effects on Sensitivity Value with Increasing Spring Strength for Springs Located on Nodes 7 and 11 from 0–178.579 kg/mm (0-10,000 lb/in) Equally 114

Figure 114. Effects on Sensitivity Value with Increasing Spring Strength for Springs Located on Nodes 7 and 15 from 0–178.579 kg/mm (0-10,000 lb/in) Equally 115

Figure 115. Effects on Sensitivity Value with Increasing Spring Strength for Springs Located on Nodes 9 and 13 from 0–178.579 kg/mm (0-10,000 lb/in) Equally 115

Figure 116. Effects on Sensitivity Value with Increasing Spring Strength for Springs Located on Nodes 9 and 16 from 0–178.579 kg/mm (0-10,000 lb/in) Equally 116

Figure 117. Effects on Sensitivity Value with Increasing Spring Strength for Springs Located on Nodes 12 and 15 from 0–178.579 kg/mm (0-10,000 lb/in) Equally 116

Figure 118. Effects on Sensitivity Value with Increasing Spring Strength for Springs Located on Nodes 15 and 16 from 0–178.579 kg/mm (0-10,000 lb/in) Equally 117

Figure 119. Sensitivity Matrix Condition Number Evaluation, Two Springs 120
Figure 120. Two Spring Error Identification at Element 1 122
Figure 121. Two Spring Error Identification at Element 2 122
Figure 122. Two Spring Error Identification at Element 3 123
Figure 123. Two Spring Error Identification at Element 4 123
Figure 124. Two Spring Error Identification at Element 5 124
Figure 125. Two Spring Error Identification at Element 6 124
Figure 126. Two Spring Error Identification at Element 7 125
Figure 127. Two Spring Error Identification at Element 8 125
Figure 128. Two Spring Error Identification at Element 9 126
Figure 129. Two Spring Error Identification at Element 10 126
Figure 130. Two Spring Error Identification at Element 11 127
Figure 131. Two Spring Error Identification at Element 12 127
Figure 132. Two Spring Error Identification at Element 13 128
Figure 133. Two Spring Error Identification at Element 14 128
Figure 134. Experimental Beam Response Driving Point Data Verification.... 132
Figure 135. Synthesized Measured Data, 178.579 kg/mm (10,000 lb/in) Spring Synthesized on Node 1 133
Figure 136. Synthesized Measured Data, 178.579 kg/mm (10,000 lb/in) on Node 1, Averaged Driving Points compared against FEM.... 134
Figure 137. Synthesized Measured Data, 178.579 kg/mm (10,000 lb/in) Spring Synthesized on Node 7 135
Figure 138. Synthesized Measured Data, 178.579 kg/mm (10,000 lb/in) on Node 7, Averaged Driving Points compared against FEM.... 136
Figure 139. Identified Error in FEM Flexural Rigidity Using Single Spring Synthesis 137

Figure 140. Updated FEM FRF compared to Prototype FRF Using Element Specific Correction, $H_{1,1}$ 139

Figure 141. Updated FEM FRF Compared to Prototype FRF Using Average Element Correction 140

Figure 142. Synthesized Measured Data, 0.1588 kg (0.35 lb) on Node 5 141

Figure 143. Synthesized Measured Data, Averaged Driving Points 0.1588 kg (0.35 lb) on Node 5 142

Figure 144. Synthesized Measured Data, 1.81437kg (4lb) on Node 13 143

Figure 145. Synthesized Measured Data, Average Driving Points, 1.81437kg (4lb) on Node 13 143

Figure 146. Identified Error in FEM Flexural Rigidity using Single Mass Synthesis 144

Figure 147. Updated FEM FRF compared to Prototype FRF Using Mass Synthesis Element Specific Correction, $H_{1,1}$ 146

Figure 148. Updated FEM FRF compared to Prototype FRF Using Mass Synthesis Average Element Correction, $H_{1,1}$ 147

Figure 149. Synthesized Measured Data, 178.579 kg/mm (10,000 lb/in) on Nodes 4 and 11 148

Figure 150. Synthesized Measured Data, Averaged Driving Points 178.579 kg/mm (10,000 lb/in) on Nodes 4 and 11 149

Figure 151. Synthesized Measured Data, 178.579 kg/mm (10,000 lb/in) on Nodes 4 and 15 150

Figure 152. Synthesized Measured Data, Average Driving Points, 1178.579 kg/mm (10,000 lb/in) on Nodes 4 and 15 150

Figure 153. Identified Error in FEM Flexural Rigidity Using Two Spring Synthesis 151

Figure 154. Updated FEM FRF compared to Prototype FRF Using Two Spring Synthesis Element Specific Correction, $H_{1,1}$ 153

Figure 155. Updated FEM FRF compared to Prototype FRF Using Two Spring Synthesis Average Element Correction, $H_{1,1}$ 154

Figure 156. Synthesized Measured Data, 178.579 kg/mm (10,000 lb/in) on Nodes 4 and 11 156

Figure 157. Synthesized Measured Data, Driving Point Average, 178.579 kg/mm (10,000 lb/in) on Nodes 4 and 11 156

Figure 158. Synthesized Measured Data, 178.579 kg/mm (10,000 lb/in) on Nodes 8 and 15 157

Figure 159. Synthesized Measured Data, Driving Point Average, 178.579 kg/mm (10,000 lb/in) on Nodes 8 and 15 157

Figure 160. Identified Error in FEM Flexural Rigidity Using Two Spring Synthesis, Low Modes 158

Figure 161. Updated FEM FRF compared to Prototype FRF Using Two Spring Synthesis Element Specific Correction, Low Modes, $H_{1,1}$ 160

Figure 162. Effect on Sensitivity Value as Single Spring Strength Increases from 0–8928.984 kg/mm (500,000 lb/in) on Node 13 .. 166

Figure 163. Effect on Sensitivity Value as Two Spring Strength increases from 0–8928.984 kg/mm (500,000 lb/in) on Nodes 5 and 12 equally 167

LIST OF TABLES

Table 1. Properties of 6061 Aluminum Beam 33

Table 2. Accelerometer Properties 34

Table 3. Accelerometer Locations 34

Table 4. Load Cell Specifications 35

Table 5. Properties of Beam FEM 39

Table 6. Analytical and FEM Frequency Comparison 41

Table 7. FEM Resonance Frequencies 42

Table 8. FEM Resonance Frequencies with Correction Factor 42

Table 9. Useable Single Spring Strengths 67

Table 10. Single Spring Index for Evaluating Condition Number 71

Table 11. Useable Single Mass Additions 95

Table 12. Single Mass Addition Index for Evaluating Condition Number 96

Table 13. Useable Two Spring Sensitivity Matrices 118

Table 14. Index of Two Spring Sensitivity Matrices for Evaluating Condition Number 119

Table 15. Updated FEM Resonance Frequencies Using Single Spring Synthesis Element Specific Correction 139

Table 16. Updated FEM Resonance Frequencies Using Single Spring Synthesis Average Element Correction 140

Table 17. Updated FEM Resonance Frequencies Using Mass Synthesis Element Specific Correction 146

Table 18. Updated FEM Resonance Frequencies Using Mass Synthesis Average Element Correction 147

Table 19. Updated FEM Resonance Frequencies Using Two Spring Synthesis Element Specific Correction 153

Table 20. Updated FEM Resonance Frequencies Using Two Spring Synthesis Average Element Correction 154

Table 21. Updated FEM Resonance Frequencies Using Low Modes Synthesis Element Specific Correction 160

Table 22. Single Mass Solution Comparison to Previous Work 164

Table 23. Single Mass Solution Comparison to Previous Work 164

Table 24. Two Spring Solution Comparison to Previous Work 165

Table 25. Two Spring, Low Modes Comparison to Previous Work 165

LIST OF ACRONYMS AND ABBREVIATIONS

Abbreviations

ABC	Artificial Boundary Conditions
ABM	Artificial Beam Modifications
ASET	Analytic Set
CSET	Connected Set
ISET	Internal Set
DOF	Degree of Freedom
FE	Finite Element
FEA	Finite Element Analysis
FEM	Finite Element Model
FRF	Frequency Response Function
OSET	Omitted Set
PBC	Perturbed Boundary Condition
QR	Orthogonal-Triangular Matrix Decomposition

Symbols

$[\ ]$	Matrix
$\{\ \}$	Vector
$\{\ \}_{\exp}$	Experimental Vector
$\{\ \}_{FE}$	Finite Element Vector

THIS PAGE INTENTIONALLY LEFT BLANK

ACKNOWLEDGMENTS

I would like to express my utmost gratitude to Dr. Joshua Gordis. This thesis would not have been possible without his guidance and patience in helping me to understand the many concepts interweaving toward one solid goal.

I would like to thank my wife for her patience and support in the many long nights spent developing this work and making sure I was still eating and breathing every once in a while.

THIS PAGE INTENTIONALLY LEFT BLANK

I. INTRODUCTION

A. BACKGROUND

The finite element (FEM) method is the representation of structures by a discretized set of elements and nodes for the purpose of engineering calculations. This method has permeated almost every form of engineering due to its adaptability and capability to handle everything from heat transfer to structural dynamics. The FEM utilizes shape functions and boundary conditions formulated from the prediction of how an element reacts to the stimuli provided and interpolated throughout each element. As this thesis focuses on the field of structural dynamics, the finite element method is typically paired with the theory of elasticity in order to formulate the shape functions required for calculation.

The theory of elasticity is a mathematical interpretation of the deformation of structures and objects [1]. For the purposes of structural dynamics and its applicability to this thesis, we will use the linear formulation, which assumes the following: The structure experiences small deformations (infinitesimal strain), the material has a linear stress/strain relationship, and the material does not experience yielding (as yielding is a non-linear process). The theory of elasticity can be applied using any coordinate system or in the direct tensor form. The theory of elasticity is the basis of many common engineering equations such as Hooke's law and the bi-harmonic wave equation; however, we will focus on a simplified version of the theory called the Euler-Bernoulli beam theory.

The Euler-Bernoulli beam theory, as will be re-iterated in Chapter II, was derived from the theory of elasticity based on the load carrying and deflection characteristics of beams [1, 2]. To simplify the calculation of stress and deflection of a beam, the Euler-Bernoulli beam theory assumes the neutral axis does not change length, all cross sections remain plane to the neutral axis, and the material is homogeneous between ends as demonstrated in Figure 1.

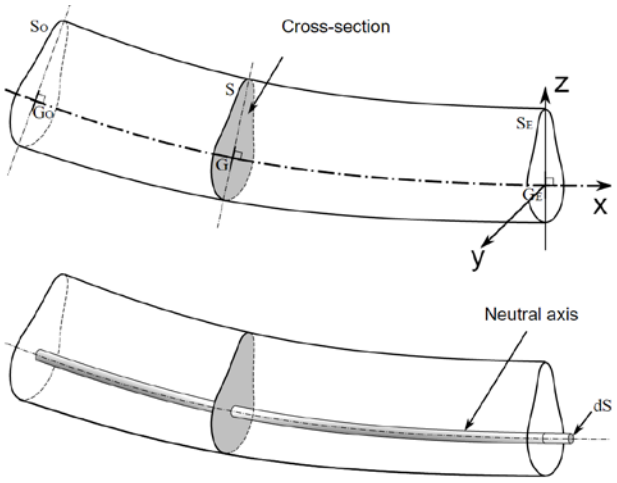

Figure 1. Euler-Bernoulli Beam Assumption Characteristics. Source: [3].

As described earlier, the finite element method and Euler-Bernoulli beam theory are combined in structural dynamics to predict the response of a beam under static and dynamic forces [4]. The Euler-Bernoulli beam theory and finite element method are applicable to a three-dimensional structure; however, we will simplify their application to two dimensions for this thesis based on the assumption that movement will be planar. The simulated model of the beam comprises several discrete beam elements assembled computationally in accordance with the finite element method, whereas each element of the beam reflects and responds as dictated by the Euler-Bernoulli beam theory. While there is no guidance as to how many elements need to exist, the larger number of elements that comprise the model will develop a better prediction for the response of a prototype beam. However, as the number of elements increase, so does the amount of calculations. Other considerations into how many elements should comprise the simulation may be influenced by testing equipment and measurement capabilities. As such, the resolution of the elements is just one possible cause of which the simulated model may be required to be updated to better reflect a prototype beam.

Of the many issues that exist between simulation and prototype, one of the most common is an inaccurate beam dynamic response prediction as shown

in [2, 5]. There are many potential causes for the error, including material property inaccuracies, manufacturing discrepancies, measurement errors, improper assumptions, etc. Conversely, some of these errors may also indicate locations of potential damage in the prototype, if the simulated model proved to be an accurate representation upon initial build. One of the indicators of a discrepancy between simulation and prototype is the beam harmonic response in response to a force input, also known as the frequency response. The frequency response function (FRF) is a measure of the magnitude and phase of beam displacement per unit force as described in [6]. An example of this can be found in Figure 2.

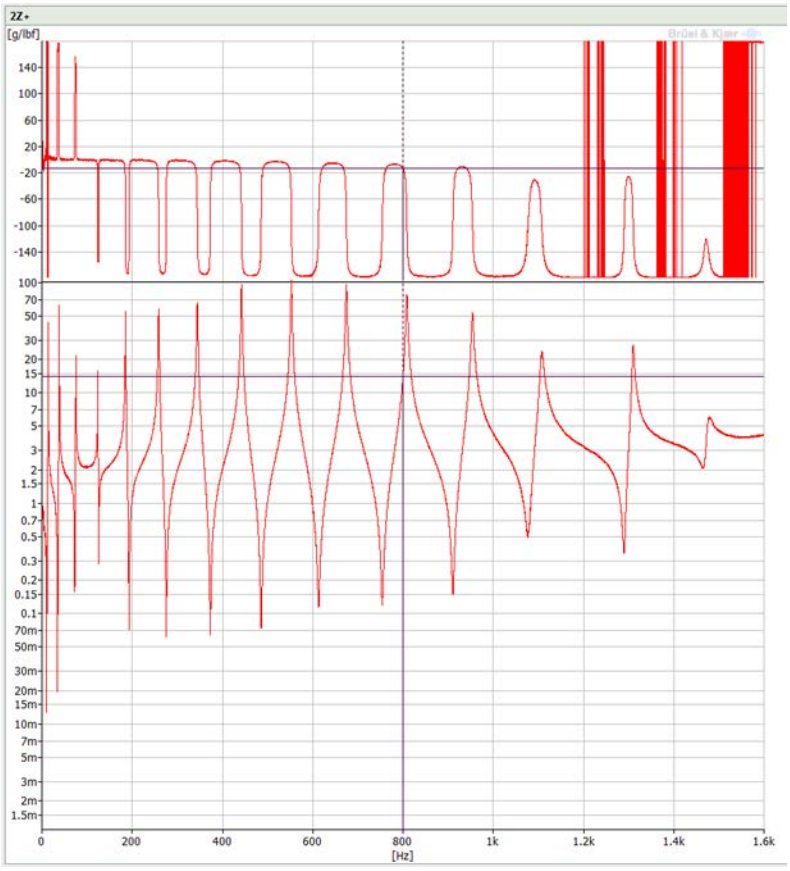

Image created using [7].

Figure 2. Frequency Response Function

The FRF provides details as to resonance frequencies for the structure, which correlate to the modes of bending and correlate to the associated resonance frequencies calculated from the finite element model (FEM). The FRF can be computationally derived or physically measured. The computation is described more thoroughly in Chapter II, but consists of determining the beam response at a specific node and specific degree of freedom given a harmonic forcing function applied at another degree of freedom in the beam. This computation can also be found in [4]. Similarly, the measured FRF is the ratio of the harmonic excitation force provided by an impact hammer or shaker, to the response force measured by an accelerometer, as demonstrated by [7]. Many types of programs exist that can gather and calculate FRF data from such an experiment, but typically are limited by equipment costs and in frequency bandwidth. By comparing the FRF from the computation to the measured FRF, we are able to determine if there are discrepancies between the two. If there are, we can use a method known as “Sensitivity-Based Finite Element Model Updating and Structural Damage Detection” [5, 8] to determine where the discrepancies for the FRF’s originate

The sensitivity matrix used for updating the model is calculated from the FEM eigenvectors and the FEM reaction to a perturbation at one element [5]. The process of this is discussed further in Chapter II, but the resulting matrix relates the change in resonance frequencies given a change in a physical parameter of an element. However, this method is restricted to the amount of modes/resonance frequencies that are shown in both measured and calculated FRF plots, and thus the bandwidth of the experimental equipment. Typically, equipment falls far short of capturing all modes of vibration [5, 9], which can lead to mode truncation errors when comparing the FRFs and give incomplete or incorrect indications of errors. It is from this issue that this thesis will focus and develop a new method for model updating and damage detection.

The method that this thesis explores involves the installation of either a massless spring or a lumped mass into the structure in an attempt to provide new

and unique data for damage detection or model updating. Frequency domain structural synthesis as shown in [5, 10] is an exact method to calculate changes to the FRF of a structure after structural modification or substructure coupling. The synthesis technique is useful because of its capability to handle large model reductions, frequency dependencies, and provide an exact solution based on the baseline response of the structure and the impedance descriptions of the structural modifications. Previous explorations in this field, such as [11], utilized the artificial synthesis of pin connections to provide unique data and proved successful.

B. LITERATURE REVIEW

"Classic beam theory," as derived from the theory of elasticity, was developed by Jacob Bernoulli and applied by Daniel Bernoulli and Leonhard Euler to describe static and dynamic beam elements in response from stimuli. This is more thoroughly described in [12]. The dynamic response produces a FRF from which the resonance frequencies can be determined and later used for damage detection or model updating. As discussed earlier, the dynamic response can be determined two ways, though measurements or though calculation. The measurement process consists of placing one or more accelerometers along the prototype beam and exciting the structure with either a special hammer, or attaching an electrodynamic shaker. Software is used provide a suitable excitation signal for an electrodynamic shaker and to measure the dynamic response of the structure to produce a highly detailed FRF, as demonstrated in [7]. However, the measureable bandwidth captures far fewer modes than the full dynamic response of the beam, estimated on the order of 10^1–10^2 times less, as described in [5]. The calculated dynamic response is determined by calculating the eigenvectors and eigenvalues of the global mass and stiffness matrices developed from the FEM [5]. The eigenvalues directly correlate to the resonance frequencies in the structure, and the eigenvalues are the mass-normalized positions of the nodes of the FEM for each resonance

frequency, otherwise known as a mode. Further explanation can be found in [13, 4]. This method can determine as many frequencies and modes as there are degrees of freedom (DOF) in the model, but higher frequencies will have increasingly larger error from the actual frequencies unless node count increases to infinite, which is obviously not possible. As such, one possible measure for determining a minimum amount of nodes is the convergence of the resonance frequencies within the measurable bandwidth.

Another beam theory exists known as the Timoshenko theory and is explored in [1, 12]. As Timoshenko and Han explain, instead of assuming that cross-sections remain perpendicular to the neutral axis, the Timoshenko theory assumes there is angular deformation, but the neutral axis remains the same length. This method has proven to be more accurate in the representation of the bending of structures where the cross-section does not remain perpendicular to the neutral axis, however has minor gains in accuracy for a rigid, smaller structure [12]. As such, this thesis will continue to use the Euler-Bernoulli beam theory.

As discussed earlier, the current effort is to utilize both the measured FRF and the calculated FRF to determine the possible location of either damage or necessity for model updating, which are described in [5, 14]. When calculating the sensitivity matrix, the number of modes that are within the measureable bandwidth typically are fewer than the number of modes available to the whole FEM. This creates a rectangular matrix that is typically not full rank, and thus computationally cannot be reliably solved for damage detection or for model updating. In an effort to correct this, several methods have been attempted.

One method to provide new information into the measured FRF is to modify the physical structure with known boundary conditions, as demonstrated by [15]. This method would physically place a pin condition or add a mass at a node of the prototype beam to impart a “perturbed boundary condition” (PBC). Each modification would alter the FRF and provide more, relevant data to the calculations. However, the implementation of the method has in increasing risk of

introducing inaccuracies in the characterization of boundary conditions. Additionally, this method requires increasing amounts of testing and a laboratory work, becoming increasingly expensive.

Another proposed method for model updating uses the anti-resonance frequencies of the FRF as opposed to the resonance frequencies, as explored in [16]. Where resonance in an FRF is a peak value where a node has the most displacement at a specific mode, anti-resonance is where there is minimal to no movement at a specific node given a certain frequency on the FRF. Typical accelerometers send a milli-voltage back to the measuring equipment based on the rate of movement they experience, demonstrated by [7]. Because the anti-resonance point is determined to have no movement, the signal the accelerometers provide would be subject to noise, making the anti-resonance point difficult to measure accurately.

Finally, this thesis focuses on modifying a method that introduces “artificial boundary conditions” to provide new and relevant information to the sensitivity matrix as originally explored by [5]. The method computationally modifies test data through a process called synthesis to apply a boundary condition, thus no-longer requiring the expensive and time consuming physical alterations. Boundary conditions can be systematically applied to any FEM and quickly: calculate the eigenvectors and eigenvalues, calculate a new FRF, create a new sensitivity matrix based on the new conditions, and provide relevant and new information for model updating and damage detection. The synthesized test data compared to the modified FEM will provide new information to the modal sensitivity matrix of which, with the previous calculations appended to the new information, provides a much more reasonable and reliable method for model updating and damage detection.

Based on the ABC method developed in [5, 11], an updated procedure was developed to identify parameter-specific optimal artificial boundary conditions [8]. When calculating the differences in frequencies of a damaged or undamaged beam, the likelihood to correctly find discrepancies between the

model and the prototype per each FEM element is predominantly determined by the decomposition of the sensitivity matrix. In this method, artificial boundary conditions are chosen based on the QR method for matrix decomposition. The matrix decomposition is accomplished by using MATLAB proprietary coding to provide a stable decomposition, explored in [8, 17]. The method then analyzes the sequence of pivots of the decomposition and utilizes the rows most likely to find damage within each element. The method eventually creates a composite square, full rank sensitivity matrix that is far more effective and accurate in determining damage or updating the model.

C. SCOPE OF THESIS

This thesis will explore the use of an artificial spring or dimensionless mass added to the beam and connected to ground in-lieu of a pin connection. By varying the spring stiffness at a single node, we determine if new and relevant frequency data and subsequent sensitivity matrices can be used in damage detection/model updating. Additionally, the beam should react the same as a pin connection when using a spring of near-infinite stiffness.

For the purpose of the exploration of this new method, finite element model will be limited to a two dimensional Euler-Bernoulli beam structure and discretized using the finite element method. This model reflects a prototype structure for practical comparison. If there is new and relevant information, this new method explores the accuracy of its application.

D. NOTES ON THESIS

As mentioned earlier, the FEM reflects a prototype beam. Beam measurements are conducted using Pulse Reflex software [7] and calculations are conducted in MATLAB software [17].

II. THEORY

A. STRUCTURAL DYNAMICS

It is theorized a structure can experience a near infinite number of resonance frequencies as a continuous beam has an infinite number of degrees of freedom(DOF). However, while we can use a significant number of elements, the finite element process discretizes the beam and number of degrees of freedom to form a finite element model based on the Euler-Bernoulli beam theory.

The Euler-Bernoulli Beam describes the relationship of a beam in reaction to static and dynamic forces derived through Newton's second law and Rayleigh energy equations as found in [4]. As described before, this beam theory operates on the following assumptions:

1. The cross-section plane of the beam remains plane during deformation.
2. The beam has a neutral axis that does not experience expansion or contraction.
3. Cross sections that are perpendicular to the neutral axis remain perpendicular through deformation.
4. The beam is homogenous and has a linear modulus of elasticity E(x).
5. Primary stresses perpendicular to the neutral axis are negligible when compared to primary stresses parallel with the neutral axis.
6. The rotary inertia of the beam is neglected in the moment equation.
7. Displacements are relatively small.

Figure 3 displays the coordinate system of a typical 2-D Euler-Bernoulli Beam.

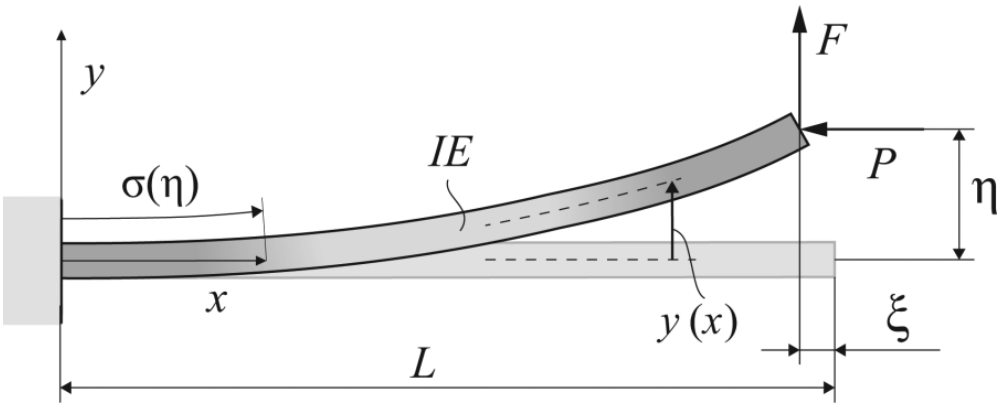

Figure 3. 2-D Euler-Bernoulli Beam

With these assumptions, the differential equation of motion for a transverse vibration of a beam is [4]:

$$\frac{\partial^2}{\partial x^2}\left(EI\frac{\partial^2 y}{\partial x^2}\right)+\rho A\frac{\partial^2 y}{\partial t^2}=f(x,t)\rightarrow 0<x<L \ , \tag{2.1}$$

where EI is the flexural rigidity consisting of the modulus of elasticity (E) and the moment of inertia(I) for the cross sectional area, ρ is the mass density, A is the cross sectional area, f is the force experiences by the beam. However, when the beam is experiencing transverse loads only, and no forcing function, the equilibrium equation, as explained by [4], reduces to:

$$\frac{\partial^2}{\partial x^2}\left(EI\frac{\partial^2 y}{\partial x^2}\right)=f(x,\mathrm{t}) \tag{2.2}$$

1. Shape Functions

We approximate the dynamic transverse displacement of the beam over the length of the beam using the following equation, as explained by [4],:

$$y(x,t)=\sum_{i=1}^{4}\psi_i(x)\,\mathrm{y_i(t)} \tag{2.3}$$

Where ψ represents the shape functions (assumed modes) of the beam. Because the general solution to equation 2.2 is:

$$y(x) = c_1 + c_2\left(\frac{x}{L}\right) + c_3\left(\frac{x}{L}\right)^2 + c_4\left(\frac{x}{L}\right)^3, \tag{2.4}$$

as explained by [4],we can assume that the shape functions take the form of a cubic. However, those shape functions must fulfill the boundary conditions found in equation (2.5) and displayed in Figure 4 [4]:

$$\begin{aligned}
&1.\ \psi(0) = 1 \quad \psi'(0) = \psi(L) = \psi'(L) = 0 \\
&2.\ \psi'(0) = 1 \quad \psi(0) = \psi(L) = \psi'(L) = 0 \\
&3.\ \psi(L) = 1 \quad \psi(0) = \psi'(0) = \psi'(L) = 0 \\
&4.\ \psi'(L) = 1 \quad \psi(0) = \psi'(0) = \psi(L) = 0
\end{aligned} \tag{2.5}$$

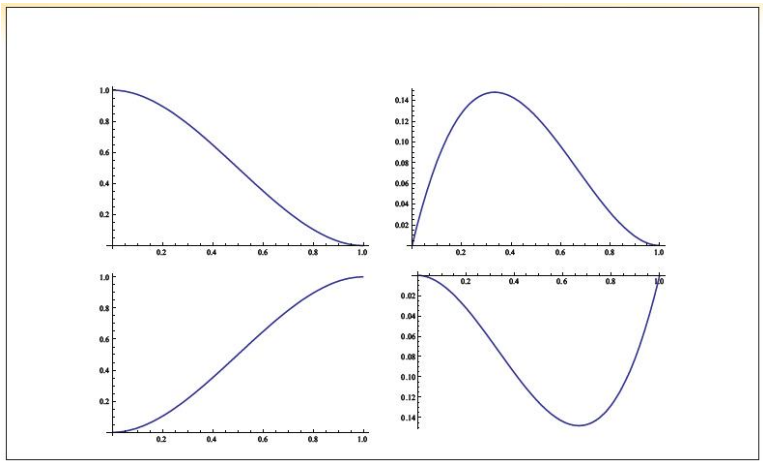

Figure 4. Cubic Hermite Shape Functions. Source: [18].

By entering the boundary conditions from equation (2.5) into (2.4), we get the following shape function for the beam as developed by [4]:

$$\psi_1(x) = 1 - 3\left(\frac{x}{L}\right)^2 + 2\left(\frac{x}{L}\right)^3$$
$$\psi_2(x) = x - 2L\left(\frac{x}{L}\right)^2 + L\left(\frac{x}{L}\right)^3$$
$$\psi_3(x) = 3\left(\frac{x}{L}\right)^2 - 2\left(\frac{x}{L}\right)^3 \qquad (2.6)$$
$$\psi_4(x) = -L\left(\frac{x}{L}\right)^2 + L\left(\frac{x}{L}\right)^3$$

By using the equations for strain and kinetic energy in a beam, we are able to determine the coefficients for the stiffness or mass matrices using the following equations as identified in [4]:

$$k_{ij} = \int_0^L EI\psi_i'' \psi_j'' \, \mathrm{dx} \qquad \text{i,j=1,2,3,4} \qquad (2.7)$$

$$m_{ij} = \int_0^L \rho A \psi_i \, \psi_j \, \mathrm{dx} \qquad \text{i,j=1,2,3,4} \qquad (2.8)$$

By plugging in the shape functions (2.6) into the coefficient equations (2.7,2.8), we are able to determine the stiffness and mass matrices of a uniform beam element that is loaded only by end shears and moments. The result is the following, as calculated in [4]:

$$[K]_e = \frac{EI}{L^3}\begin{bmatrix} 12 & 6L & -12 & 6L \\ 6L & 4L^2 & -6L & 2L^2 \\ -12 & -6L & 12 & -6L \\ 6L & 2L^2 & -6L & 4L^2 \end{bmatrix} \qquad (2.9)$$

$$[M]_e = \frac{\rho AL}{420}\begin{bmatrix} 156 & 22L & 54 & -13L \\ 22L & 4L^2 & 13L & -3L^2 \\ 54 & 13L & 156 & -22L \\ -13L & -3L^2 & -22L & 4L^2 \end{bmatrix} \qquad (2.10)$$

Equations 2.9 and 2.10 are used in the construction of the finite element model.

2. Finite Element Model

The FEM is a structure that is comprised of multiple Euler-Bernoulli beam elements connected in an effort to predict overall dynamic response. As such, the governing equation for a dynamic system is the following, as derived by [4]:

$$[M]\{\ddot{x}\}+[C]\{\dot{x}\}+[K]\{x\}=\{f(\mathrm{t})\} \tag{2.11}$$

In this instance, $[M]$ and $[K]$ are the mass and stiffness matrices for the whole system, otherwise known as global matrices. $[C]$ is the global damping coefficient matrix. $[M]$, $[K]$, and $[C]$ each is an nxn matrix where n is the number of degrees of freedom in the structure. $\{f(\mathrm{t})\}$ is an nx1 array comprising of the external forces on the structure at all degrees of freedom. $\{x\}$ is the displacement and rotation position of the beam, $\{\dot{x}\}$ is the transverse and rotational velocity, and $\{\ddot{x}\}$ is the transverse and rotational acceleration of the beam.

For the purposes of this thesis, we will assume that our beam experiences undamped, free vibrations. The reason we assume the structure is undamped is because damping cannot be predicted, and has little influence on the frequency of resonance peaks. Typically, modal damping is measured in a vibration test; however, without a test, damping is assumed at 2% (ξ=0.02) and proportional to the stiffness and mass matrices. The influence of damping is determined from the typical conversion from an undamped resonance frequency to a damped resonance frequency, found in [4]:

$$\omega_d=\omega_n\sqrt{1-\zeta^2} \tag{2.12}$$

Based on equation (2.12), the typical assumed damping would change the resonance frequency by 0.04%, which is a small enough change to safely neglect.

By neglecting damping in the system, the governing equation for a dynamic system changes to the following, as derived by [4]:

$$[M]\{\ddot{x}\}+[K]\{x\}=0 \tag{2.13}$$

The assembly of global $[M]$ and $[K]$ is determined by the degrees of freedom and node connections. Because we are using a four DOF beam element, the assembly of these matrices follows this pattern:

$$[M]=\begin{bmatrix} M_{e1,11} & M_{e1,12} & M_{e1,13} & M_{e1,14} & & & & \\ M_{e1,21} & M_{e1,22} & M_{e1,23} & M_{e1,24} & & & & \\ M_{e1,31} & M_{e1,32} & M_{e1,33}+M_{e2,11} & M_{e1,34}+M_{e2,12} & M_{e2,13} & M_{e2,14} & & \\ M_{e1,41} & M_{e1,42} & M_{e1,43}+M_{e2,21} & M_{e1,44}+M_{e2,22} & M_{e2,23} & M_{e2,24} & & \\ & & M_{e2,31} & M_{e2,32} & M_{e2,33}+M_{e3,11} & M_{e2,34}+M_{e3,12} & & \\ & & M_{e2,41} & M_{e2,42} & M_{e2,43}+M_{e3,21} & M_{e2,44}+M_{e3,22} & & \\ & & & & & & \ddots & M_{e\,\mathrm{m},34} \\ & & & & & & M_{e\,\mathrm{m},43} & M_{e\,\mathrm{m},44} \end{bmatrix} \tag{2.14}$$

$$[K]=\begin{bmatrix} K_{e1,11} & K_{e1,12} & K_{e1,13} & K_{e1,14} & & & & \\ K_{e1,21} & K_{e1,22} & K_{e1,23} & K_{e1,24} & & & & \\ K_{e1,31} & K_{e1,32} & K_{e1,33}+K_{e2,11} & K_{e1,34}+K_{e2,12} & K_{e2,13} & K_{e2,14} & & \\ K_{e1,41} & K_{e1,42} & K_{e1,43}+K_{e2,21} & K_{e1,44}+K_{e2,22} & K_{e2,23} & K_{e2,24} & & \\ & & K_{e2,31} & K_{e2,32} & K_{e2,33}+K_{e3,11} & K_{e2,34}+K_{e3,12} & & \\ & & K_{e2,41} & K_{e2,42} & K_{e2,43}+K_{e3,21} & K_{e2,44}+K_{e3,22} & & \\ & & & & & & \ddots & K_{e\,\mathrm{m},34} \\ & & & & & & K_{e\,\mathrm{m},43} & K_{e\,\mathrm{m},44} \end{bmatrix} \tag{2.15}$$

The final product produces a set of global matrices that are nxn where n=number of DOFs=(DOF/node)*m elements.

B. NATURAL FREQUENCY SENSITIVITY

One of the benefits of the FEM is the capability to determine the modal frequencies and mode shapes inherent to the structure without the necessity of performing a test. However, after building and testing a prototype, we want to be able to use the differences between the FEM and the prototype modal frequencies to find errors in the FEM. Some possibilities of errors could be

incorrect assumptions in the model or unmodeled joint mechanics in a prototype. A method of determining these errors is the use of the Sensitivity matrix

1. Modal Frequencies

Continuing with the assumption of an undamped bar experiencing free vibrations, we can assume a harmonic solution for equation (2.13) is the following, as determined by [4, 9]:

$$\{x\} = \{\phi\} C e^{j\omega t}, \tag{2.16}$$

where ϕ is the eigenvector for the mode of vibration. The eigenvector is a product of the eigenvalue problem that details the position of each degree of freedom in the structure for the corresponding eigenvalue. The resulting algebraic eigenvalue problem as described in [4], [14], and [19] is:

$$\left[[K] - \lambda_i [M]\right]\{\phi_i\} = 0 \tag{2.17}$$

We are looking for more than a trivial solution of $\{\phi\} \neq 0$ and therefore the eigenvalue, λ_i, must take on a value to render the matrix non-invertable and thus yielding non trivial solutions for $\{\phi\}$. As such, the values of λ_i are found by setting the determinant of the difference to zero, as determined by [4, 9]:

$$Det\left[[K] - \lambda_i [M]\right] = 0 \tag{2.18}$$

There are as may roots to this equation as there are DOF in the structure. As $\lambda_i = \omega_i^2$, the eigenvalue can quickly be converted to the resonance frequencies of the structure. This method is validated by the use of a secondary dynamic system defined though analytical and omitted coordinates.

2. Analytical and Omitted Coordinates

As alluded in Chapter I, it is theorized that any given structure may have resonance frequencies on the order of 10^2–10^3 , which is further discussed in [5]. However, a vibration test may only measure modal parameters on the order of 10^1. In order to validate the applicability of the FEM and the vibration test, we take a look at the analytical and omitted coordinates of the beam. The analytical coordinates (ASET) are the measured coordinates where instrumentation is applied to the structure and is annotated in equations using “a.” The omitted coordinates (OSET) are the coordinates that are not directly measured and are annotated in equations using “o.” For the purposes of the FEM, the OSET is of finite dimension; however, the OSET is of infinite dimension in a vibration test.

The OSET is also referred as a secondary dynamic system and is defined by the process of representing a large order dynamic system with a smaller order dynamic system [14]. The secondary dynamic system is obtained by fully constraining a coordinate from the ASET. This effectively removes a row and column from the stiffness and mass matrices in the FEM. This introduces singularities into the undamped system which translate to modal frequencies.

Re-evaluating equation (2.17) for a forced system of analytical and omitted coordinates, as described in [14, 20]:

$$\left[\begin{pmatrix} K_{\alpha\alpha} & K_{\alpha o} \\ K_{o\alpha} & K_{oo} \end{pmatrix} - \omega^2 \begin{pmatrix} M_{aa} & M_{\alpha o} \\ M_{oa} & M_{oo} \end{pmatrix}\right] \begin{Bmatrix} x_\alpha \\ x_o \end{Bmatrix} = \begin{Bmatrix} f_a \\ f_o \end{Bmatrix} \tag{2.19}$$

However, we assume there is no excitation acting on the omitted coordinates. As such, equation (2.19) becomes, [14, 20]:

$$\left[\begin{pmatrix} K_{\alpha\alpha} & K_{\alpha o} \\ K_{o\alpha} & K_{oo} \end{pmatrix} - \omega^2 \begin{pmatrix} M_{aa} & M_{\alpha o} \\ M_{oa} & M_{oo} \end{pmatrix}\right] \begin{Bmatrix} x_\alpha \\ x_o \end{Bmatrix} = \begin{Bmatrix} f_a \\ 0 \end{Bmatrix} \tag{2.20}$$

If we examine the two row partitions of equation 2.20, we get the following, [14, 20]:

$$\left[K_{aa}\right]\left\{x_a\right\}+\left[K_{ao}\right]\left\{x_o\right\}-\omega^2\left[\left[M_{aa}\right]\left\{x_a\right\}+\left[M_{ao}\right]\left\{x_o\right\}\right]=f_a \tag{2.21}$$

$$\left[K_{o\alpha}\right]\left\{x_a\right\}+\left[K_{oo}\right]\left\{x_o\right\}-\omega^2\left[\left[M_{o\alpha}\right]\left\{x_a\right\}+\left[M_{oo}\right]\left\{x_o\right\}\right]=0 \tag{2.22}$$

Using equation (2.22), we can find the exact dynamic relationship between the omitted and analytic coordinates as calculated in [14]:

$$\left\{x_0\right\}=\left[\mathrm{I}-\omega^2 K_{00}^{-1}\mathrm{M}_{00}\right]^{-1}\left[-\mathrm{K}_{00}^{-1}\mathrm{K}_{oa}+\omega^2 K_{00}^{-1}M_{oa}\right]\left\{x_a\right\} \tag{2.23}$$

While equation (2.23) is an exact reduction of the model, it provides some issues with regards to the conditioning of the matrix. As such, we use the Improved Reduction System (IRS) developed and tested in [8, 14, 20]. Using the static Test Analysis Model (TAM) reduction:

$$\left\{\ddot{x}_a\right\}=\omega^2\left\{\ddot{x}_a\right\}=\left[M_{stat}\right]^{-1}\left[M_{stat}\right]\left\{x_a\right\} \tag{2.24}$$

The new exact model reduction is frequency independent [8, 14, 20]:

$$\left\{x_0\right\}=\left[-\mathrm{K}_{00}^{-1}\mathrm{K}_{oa}+\left(-K_{oo}^{-1}M_{oa}-K_{oo}^{-1}M_{oo}K_{oo}^{-1}K_{oa}\right)M_{stat}^{-1}K_{stat}\right]\left\{x_a\right\} \tag{2.25}$$

However, in order for equation (2.23) to work, $\left[\mathrm{I}-\omega^2 K_{00}^{-1}\mathrm{M}_{00}\right]^{-1}$ needs to be invertible. A matrix can be inverted by dividing the adjoint (Adj) by the determinant (Det). In equation form, the formula for an inversion is [8, 14, 20].:

$$\left[A\right]^{-1}=\frac{1}{Det\left[A\right]}Adj\left[A\right] \tag{2.26}$$

So, using equation (2.23), the following needs to be satisfied [8, 14, 20].

$$\left[\mathrm{I}-\omega^2 K_{00}^{-1}\mathrm{M}_{00}\right]^{-1}=\frac{1}{Det\left[\mathrm{I}-\omega^2 K_{00}^{-1}\mathrm{M}_{00}\right]}Adj\left[\mathrm{I}-\omega^2 K_{00}^{-1}\mathrm{M}_{00}\right] \tag{2.27}$$

Similarly to what was identified in equation (2.18), the roots of the following characteristic equation [8, 14, 20].:

$$\mathrm{Det}\left[\mathrm{I}-\omega^2 K_{00}^{-1}\mathrm{M}_{00}\right]^{-1}=0 \tag{2.28}$$

are the resonance frequencies for the OSET system, made up of $[K_{oo}]$ and $[M_{oo}]$, when the ASET frequencies are constrained to ground.

3. Building the Modal Sensitivity Matrix

The purpose of the modal sensitivity matrix is to assist in predicting the change in dynamic response of a structure based on the change of a given parameter. As such, it is developed by perturbing, or increasing, a parameter a minor amount, such as 1 percent, on a single element of the structure and determining change in the resonance frequency for that mode. To put it mathematically, as found in [14, 21]:

$$S_{ij} = \frac{\partial \lambda_i}{\partial p_j} \tag{2.29}$$

Where λ_i is the eigenvalue for mode *i,* p_j is the perturbed parameter at element *j*, and S_{ij} is the sensitivity value for mode *i* and with a modification in element *j*.

The sensitivity matrix is calculated by perturbing an element in the structure and calculating the modal response. More specifically, we calculate the change in the resonance frequencies by using the eigenvector for that mode, as demonstrated in [4, 21].

$$S_{ij} = \{\phi_i\}^T \left[\frac{\partial K}{\partial p_j} - \lambda_i \frac{\partial M}{\partial p_j} \right] \{\phi_i\}, \tag{2.30}$$

where $\{\phi_i\}$ is the eigenvector for mode *i*, $\{\phi_i\}^T$ is the transpose of the eigenvector, and $\left[\frac{\partial K}{\partial p_j} - \lambda_i \frac{\partial M}{\partial p_j} \right]$ is the change in the stiffness and mass matrices with respect to the change in a parameter at element j. $\{\phi_i\}$ is of size nx1 where n is the number

of modes/DOFs in the FEM, and $\left[\frac{\partial K}{\partial p_j} - \lambda_i \frac{\partial M}{\partial p_j}\right]$ is sized n x n. Equation 2.30 yields a singular entry of the sensitivity matrix

The sensitivity matrix should be sized n x m, where m is the number of elements in the structure, and n is the number of modes. For example:

$$[S] = \begin{bmatrix} S_{1,1} & S_{1,2} & \cdots & S_{1,\mathrm{m}-1} & S_{1,\mathrm{m}} \\ S_{2,1} & S_{2,2} & \cdots & S_{2,\mathrm{m}-1} & S_{2,\mathrm{m}} \\ \vdots & \vdots & \vdots & \vdots & \vdots \\ S_{n-1,1} & S_{n-1,2} & \cdots & S_{n-1,\mathrm{m}-1} & S_{n-1,\mathrm{m}} \\ S_{\mathrm{n},1} & S_{\mathrm{n},2} & \cdots & S_{\mathrm{n},\mathrm{m}-1} & S_{\mathrm{n},\mathrm{m}} \end{bmatrix} \tag{2.31}$$

The importance of the size of the sensitivity matrix will be discussed later in this chapter. Several different types of parameters can vary in the structure. Some examples of these are the flexural rigidity (E*I), width, or depth of the beam. Once the sensitivity value has been calculated, it can be used to predict future eigenvalues/resonance frequencies given an arbitrary change in that parameter. As found in [14, 21]:

$$\lambda_i^* = \lambda_i + S_{ij} \cdot (p_j^* - p_j), \tag{2.32}$$

where λ_i^* is the new eigenvalue/resonance frequency given the updated parameter p_j^* at element *j*. Alternatively, we can reduce Equation 2.19 to simply needing to know the change in a resonance frequency based on the change of a parameter at a given element. [21]

$$\Delta\omega_i^2 = \Delta\lambda_i = S_{ij} \cdot (\Delta p_j) \tag{2.33}$$

For example, assuming we need to know what the change is to the 4th mode of vibration due to a change in the EI value of element 2, the calculation would look something like this:

$$\Delta\omega_4^2 = \Delta\lambda_4 = S_{4,2} \cdot (\Delta EI) \tag{2.34}$$

4. Determining the Modal Sensitivity Matrix Using Eigenvectors and Eigen Values

The development of equation (2.29) as developed by [14] and [22] starts with equation (2.17) where $[M]$ and $[K]$ are the mass and stiffness matrices as developed by the FEM. As identified in equation (2.30) the parameter that is being modified may be a part of either or both matrices. For example, if modal parameter p_j is the density of the jth element, only the mass will be effected. However, if p_j is the thickness of the jth element, p_j is then a function of the stiffness and mass matrices. As such, the derivative for both matrices must be calculated, as developed by [9, 13, 21, 23]:

$$\left[\frac{\partial K}{\partial p_j}\right] \tag{2.34}$$

$$\left[\frac{\partial M}{\partial p_j}\right] \tag{2.35}$$

As such, if we take the derivative of equation (2.17) with respect to p_j, we get the following equation [9, 13, 21, 23]:

$$\left[\frac{\partial K}{\partial p_j} - \lambda_i \frac{\partial M}{\partial p_j} - \frac{\partial \lambda_i}{\partial p_j} M\right]\{\phi_i\} + \left[[K] - \lambda_i [M]\right]\left\{\frac{\partial \phi_i}{\partial p_j}\right\} = 0 \tag{2.36}$$

By pre-multiplying equation (2.36) by $\{\phi_i\}^T$, we get the following as demonstrated by [14] and [22]:

$$\{\phi_i\}^T\left[\frac{\partial K}{\partial p_j} - \lambda_i \frac{\partial M}{\partial p_j} - \frac{\partial \lambda_i}{\partial p_j} M\right]\{\phi_i\} + \{\phi_i\}^T\left[[K] - \lambda_i [M]\right]\left\{\frac{\partial \phi_i}{\partial p_j}\right\} = 0 \tag{2.37}$$

By recognizing $[M] = [M]^T$ and $[K] = [K]^T$ and invoking equation (2.17) gives the following:

$$\{\phi_i\}^T \left[\frac{\partial K}{\partial p_j} - \lambda_i \frac{\partial M}{\partial p_j} - \frac{\partial \lambda_i}{\partial p_j} M \right] \{\phi_i\} = 0 \tag{2.38}$$

If we assume a mass normalized mode shape $\{\phi_i\}^T [M] \{\phi_i\} = 1$, we get the following:

$$S_{ij} = \frac{\partial \lambda_i}{\partial p_j} = \{\phi_i\}^T \left[\frac{\partial K}{\partial p_j} - \lambda_i \frac{\partial M}{\partial p_j} \right] \{\phi_i\} \tag{2.39}$$

Which is equation (2.29). However, if we are conducting a test on a prototype, we most likely will not know the changed parameter, or on which element has been altered. As such, we can conduct a vibration test of the structure and determine the resonance frequencies from the frequency response functions.

C. FREQUENCY RESPONSE FUNCTION

The frequency response function (FRF) is a measure of the dynamic response of the structure and can be both calculated and measured. The FRF is a transfer function from the input (force) to the output (acceleration). The derivation of the calculation can be found in [4].

The quantity $\left[[K] - \Omega [M] \right]$ as discussed when determining the modal frequencies is known as the impedance, $[Z]$. The impedance of a structure is a calculation of the structure's resistance to dynamic movement when subjected to harmonic motion. The inverse of the impedance is the FRF, $[H]$. With regard to the viewpoint of a transfer function, the input is a harmonic signal, at some frequency Ω, and the output is the beam response [21]:

$$\left[[K] - \Omega [M] \right]^{-1} = [Z]^{-1} = [H] \tag{2.40}$$

The calculated FRF, $[H]$, records the beam response of every DOF as each node is separately excited, for a specific excitation frequency. As such, if the beam response was needed from 1 hertz to 1000 hertz with a 0.1 hertz step, the FRF calculation, equation (2.40), would need to be performed for each step of the range.

Once the FRF matrix has been calculated, we can extract the displacement of the DOF by multiplying the FRF by the force at that frequency, as explained in [21]:

$$\{X(\Omega)\} = [H]\{F(\Omega)\} \tag{2.41}$$

By expanding this to an n DOF system, the system of equations would look something like this:

$$\begin{Bmatrix} X_1 \\ X_2 \\ \vdots \\ X_{n-1} \\ X_n \end{Bmatrix} = \begin{bmatrix} H_{11} & H_{12} & \cdots & H_{1,n-1} & H_{1,n} \\ H_{21} & H_{22} & \cdots & H_{2,n-1} & H_{2,n} \\ \vdots & \vdots & \ddots & \vdots & \vdots \\ H_{n-1,1} & H_{n-1,2} & \cdots & H_{n-1,n-1} & H_{n-1,n} \\ H_{n,1} & H_{n,2} & \cdots & H_{n,n-1} & H_{n,n} \end{bmatrix} \begin{Bmatrix} F_1 \\ F_2 \\ \vdots \\ F_{n-1} \\ F_n \end{Bmatrix} \tag{2.42}$$

Where X_n is the complex amplitude response of the n-th DOF, H_{jk} is the j-th DOF response due to harmonic excitation at the k-th DOF, and F_n if the harmonic force at the n-th DOF. All of these terms are frequency dependent.

When measuring the beam response for the FRF, high fidelity measurement devices are required to determine the structure's dynamic response to excitation. As will be discussed in Chapter III, each node needs to be excited separately while measuring the response of the beam with measurement software for processing to develop a full FRF matrix. Ultimately, a measured FRF will produce a set of resonance frequencies, ω, that can be converted into eigenvalues. This allows for the most complete comparison when performing damage detection/model updating calculations.

D. DAMAGE DETECTION AND MODEL UPDATING

When we are looking at the differences between a FEM and a structure using the FRF comparison method, we are typically looking for “hidden” damage, or something that would produce relatively minor differences in resonance frequencies between the model and the structure. Model updating is the process of updating the FEM based on the dynamic response of a recently built prototype. Damage detection is the process of identifying problematic elements based on the differences between dynamic response of the updated FEM and the response of the same structure that has many hours of use. In both cases, the goal of using this method is to identify where the FEM does not correlate to the reaction of the prototype.

Ultimately, we want to use the resonance frequency data for damage detection and/or model updating. For the purposes of this thesis, we will assume the parameter in question is the flexural rigidity (E*I), and the sensitivity matrix has been calculated to reflect as such. To accomplish damage detection or model updating, we change the perspective of how we view equation (2.33) to the following equations, as detailed in [14]:

$$\Delta\lambda_i = S_{ij}\Delta EI_j \tag{2.43}$$

$$\left(\lambda_{i,FEM} - \lambda_{i,Measured}\right) = S_{ij}\Delta EI_j \tag{2.44}$$

$$\{\Delta\lambda\} = [S]\{\Delta EI\} \tag{2.45}$$

$$[S]^{-1}\{\Delta\lambda\} = \{\Delta EI\} \tag{2.46}$$

Where $[S]$ is the full sensitivity matrix, $\{\Delta\lambda\}$ is a vector consisting of the difference in eigenvalues for each mode, and $\{\Delta EI\}$ is a vector identifying which element the suspected parameter differs. However, in order for this process to work, the sensitivity matrix must be invertible and full rank. This means that the measuring software will need to capture as many modes in the structure as there

are elements, at a minimum. Unfortunately, the bandwidth of most measuring equipment is not capable of measuring higher order frequencies [5] and thus cannot include modes above some practical bandwidth in the calculations. This limitation leads to a non-square sensitivity matrix, also known as modal truncation. The other limitation of the sensitivity matrix being full rank becomes an issue when you have a symmetrical structure. The rank refers to the number of linearly independent rows and columns in a matrix. If the structure is symmetrical, the columns of the sensitivity matrix may be close enough in value to be considered linearly dependent. In an effort to correct these issues, we implement a derivative of the Artificial Boundary Condition (ABC) method detailed in [5].

E. STRUCTURAL SYNTHESIS

A typical structural dynamic design cycle will involve repeated creation of finite element models due to unacceptable errors or results from the previous iteration [21]. For large FEMs, this can be very computationally demanding and expensive in manpower and time. The synthesis method eliminates the necessity to re-create and re-solve an entire FEM after the baseline evaluation. The method is able to accomplish this by applying models of structural changes to the baseline dynamic response and effectively transform the baseline response into the modified response. The speed of the computation comes into effect by only including the FRF for the DOF involved in the synthesis and additional DOF in which we have interest.

DOFs involved in synthesis typically fall under two conditions: The connection set (CSET), or the internal set (ISET). The CSET describes the DOFs of connection of a modification to the original structure. In this instance, the CSET will be limited to a single DOF for a boundary condition or a spring/mass addition. DOFs that might not be involved in the connection, but need to be recorded, are known as the internal set (ISET). Together, these points are known as the analytical set (ASET). For example, if we have a beam modification that

will be connected to nodes 6 and 10, and we want to record the translational response at node 15 and 16, we identify DOF 11,12,19 and 20 as the CSET DOF and DOF 29 and 31 as the ISET DOF. This example is displayed in Figure 5 and equation (2.47)

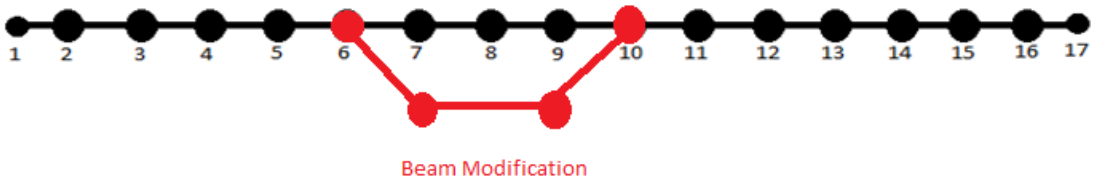

Figure 5. 16-Element Structure with Beam Modification.

$$\begin{aligned} CSET &= [11,12,19,20] \\ ISET &= [29,31] \\ ASET &= [CSET, \text{ISET}] = [11,12,19,20,29,31] \end{aligned} \tag{2.47}$$

Once these sets have been identified, we can pull them out of the primary FRF matrix:

$$\begin{Bmatrix} X_{11} \\ X_{12} \\ X_{19} \\ X_{20} \\ X_{29} \\ X_{31} \end{Bmatrix} = \begin{bmatrix} H_{11,11} & H_{11,12} & H_{11,19} & H_{11,20} & H_{11,29} & H_{11,31} \\ H_{12,11} & H_{12,12} & H_{12,19} & H_{12,20} & H_{12,29} & H_{12,31} \\ H_{19,11} & H_{19,12} & H_{19,19} & H_{19,20} & H_{19,29} & H_{19,31} \\ H_{20,11} & H_{20,12} & H_{20,19} & H_{20,20} & H_{20,29} & H_{20,31} \\ H_{29,11} & H_{29,12} & H_{29,19} & H_{29,20} & H_{29,29} & H_{29,31} \\ H_{31,11} & H_{31,12} & H_{31,19} & H_{31,20} & H_{31,29} & H_{31,31} \end{bmatrix} \begin{Bmatrix} F_{11} \\ F_{12} \\ F_{19} \\ F_{20} \\ F_{29} \\ F_{31} \end{Bmatrix} \tag{2.48}$$

Or, with the analytical set definitions, we can re-write equation (2.47) to something like this, as demonstrated in [21]:

$$\begin{Bmatrix} X_c \\ X_i \end{Bmatrix} = \begin{bmatrix} H_{cc} & H_{ci} \\ H_{ic} & H_{ii} \end{bmatrix} \begin{Bmatrix} F_c \\ F_i \end{Bmatrix} \tag{2.49}$$

In the process of determining the effects of the modification, we need to determine the force exerted by the modification on the structure. As such, we modify equation (2.41) to solve for force as opposed to displacement:

$$\left\{F_c^*\right\} = -\left[\Delta K + \omega^2 \Delta M\right]\left\{X_c^*\right\} = -\left[\Delta Z\right]\left\{X_c^*\right\} \tag{2.50}$$

Where $\left\{F_c^*\right\}$ is the force of the modification at the CSET DOF, $\left\{X_c^*\right\}$ is the response the modification "sees," and $\left[\Delta K + \omega^2 \Delta M\right]$ or $\left[\Delta Z\right]$ is the added modification. Additionally, if there is any external force on the modification or structure, it can be annotated with $\left\{F_c^{(e)}\right\}$. Therefore, as described in [5], the overall force applied to the CSET is:

$$\left\{F_c\right\} = \left\{F_c^{(e)}\right\} + \left\{F_c^*\right\} = \left\{F_c^{(e)}\right\} - \left[\Delta Z\right]\left\{X_c^*\right\} \tag{2.51}$$

As such, we can expand equation (2.49) to the following:

$$\begin{Bmatrix} X_c^* \\ X_c^* \\ X_i^* \end{Bmatrix} = \begin{bmatrix} H_{cc} & H_{cc} & H_{ci} \\ H_{cc} & H_{cc} & H_{ci} \\ H_{ic} & H_{ii} & H_{ii} \end{bmatrix} \begin{Bmatrix} F_c^* \\ F_c^{(e)} \\ F_i^{(e)} \end{Bmatrix} \tag{2.52}$$

Based on our definition of ASET, we can re-write equation (2.52) to the following:

$$\begin{Bmatrix} X_c^* \\ X_a^* \end{Bmatrix} = \begin{bmatrix} H_{cc} & H_{ca} \\ H_{ac} & H_{aa} \end{bmatrix} \begin{Bmatrix} F_c^* \\ F_a^{(e)} \end{Bmatrix} \tag{2.53}$$

We can break equation (2.53) into its system of equations like so:

$$\left\{X_c^*\right\} = \left[H_{cc}\right]\left\{F_c^*\right\} + \left[H_{ca}\right]\left\{F_a^{(e)}\right\} \tag{2.54}$$

$$\left\{X_a^*\right\} = \left[H_{ac}\right]\left\{F_c^*\right\} + \left[H_{aa}\right]\left\{F_a^{(e)}\right\} \tag{2.55}$$

By using equation (2.45) and solving for $\left\{X_c^*\right\}$ in equation (2.49), we get the following:

$$\left\{X_c^*\right\} = \left[I + \left[H_{cc}\right]\left[\Delta Z(\omega)\right]\right]^{-1}\left[H_{ca}\right]\left\{F_a^{(e)}\right\} \tag{2.56}$$

Now, by using equation (2.50) and equation (2.56) in equation (2.55), we get the following:

$$\left\{X_a^*\right\} = \left[\left[H_{aa}\right] - \left[H_{ac}\right]\left[\Delta Z(\omega)\right]\left[I + \left[H_{cc}\right]\left[\Delta Z(\omega)\right]\right]^{-1}\left[H_{ca}\right]\right]\left\{F_a^{(e)}\right\} \tag{2.57}$$

The final form of the synthesized matrix is:

$$\left\{X_a^*\right\} = \left[H_{aa}^*\right]\left\{F_a\right\} \tag{2.58}$$

As such, the synthesized FRF matrix is:

$$\left[H_{aa}^*\right] = \left[\left[H_{aa}\right] - \left[H_{ac}\right]\left[\Delta Z(\omega)\right]\left[I + \left[H_{cc}\right]\left[\Delta Z(\omega)\right]\right]^{-1}\left[H_{ca}\right]\right] \tag{2.59}$$

1. Artificial Boundary Condition Synthesis

The Artificial Boundary Condition (ABC) method computationally applies restrictions to the test data to simulate a pin connected to ground [5]. Finding these resonance frequencies for known changes helps to provide new information to the sensitivity matrix and provide reliability in damage detection. For the purpose of this thesis, we will be identifying a connection point to apply our conditions, and we will be interested in the response of the remaining DOFs of the structure. As such, [CSET]=restricted DOF and [ISET]=remaining DOF. An example of an artificial pin constraint is displayed in Figure 6.

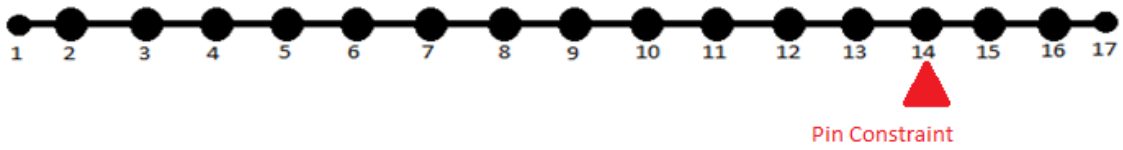

Figure 6. 16-Element Structure with Artificial Boundary Condition.

Because the CSET will have no movement, $\left\{X_c\right\} = \left\{0\right\}$. As such, equation (2.48) changes to the following:

$$\begin{Bmatrix} 0 \\ X_i \end{Bmatrix} = \begin{bmatrix} H_{cc} & H_{ci} \\ H_{ic} & H_{ii} \end{bmatrix} \begin{Bmatrix} F_c \\ F_i \end{Bmatrix} \tag{2.60}$$

By using the top row of equation (2.60), we can solve for the forces from synthesis (the asterisk indicating the effects of the modification):

$$\{F_c^*\} = -[H_{cc}]^{-1}[H_{ci}]\{F_i\} \tag{2.61}$$

By plugging equation (2.61) into the bottom row of equation (2.60) and re-arranging terms, we get the following:

$$\{X_i^*\} = \left[[H_{ii}] - [H_{ic}][H_{cc}]^{-1}[H_{ci}]\right]\{F_i\} \tag{2.62}$$

Similarly to equation (2.58), $\{X_i^*\}$ represents the beam response as a result of the ABC synthesis. Therefore, the modified FRF response is:

$$[H_{ii}^*] = \left[[H_{ii}] - [H_{ic}][H_{cc}]^{-1}[H_{ci}]\right] \tag{2.63}$$

Similarly to when we analyzed the analytical and omitted coordinates, the act of putting a pin connection into a FEM structure removes the column and row associated with the DOF in the stiffness and mass matrices. This an easy method to check the synthesis calculations. By recalculating the baseline FRF matrix with the associated modifications, we can overlay the graph onto the synthesized version. If done correctly, the check and the synthesized FRF should be exact.

2. Artificial Spring or Mass Synthesis

The focus of this thesis is the introduction of an artificial, massless spring or lumped mass into the FEM and determining the response. An example of using synthesizing an artificial spring is in Figure 7.

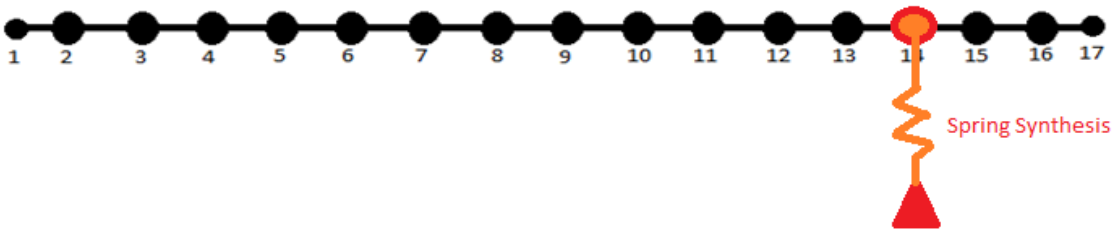

Figure 7. 16-Element Structure with Artificial Spring.

The two DOF massless spring is connected from the node to ground. Similar to the ABC, the DOF that would have been introduced from the end connected to ground is no longer considered. The spring value is synthesized into the structure FRF without adding DOF to the system.

For the instance of a lumped mass, we are attaching the mass directly to the node. Because it is an idealized condition known as “lumped,” there are no rotational inertial components to account for and so the added artificial mass will only effect the translational DOF.

For both instances, the CSET is the DOF that we are synthesizing the spring or mass onto, and the ISET are the remaining DOFs of the structure.

Because we are using only a single value to synthesize, equation (2.58) becomes:

$$\left[H_{aa}^{*}\right]=\left[\left[H_{aa}\right]-\left[H_{ac}\right]\left[\left[H_{cc}\right]+\left[\Delta Z(\omega)\right]\right]^{-1}\left[H_{ca}\right]\right] \tag{2.64}$$

As demonstrated in [21]. In this instance:

$$\begin{aligned}&\left[\Delta Z(\omega)\right]=\Delta k_{spring}\\ &or\\ &\left[\Delta Z(\omega)\right]=-\omega^{2}\Delta m_{mass}\end{aligned} \tag{2.65}$$

The benefit of this method is the wide range of variability for either value. By using a mass, we should see the FRF resonance peaks shift down in the measurable bandwidth. By using a spring, we should see the FRF resonance

values shift upward in the measureable bandwidth. Ultimately, a spring of infinite stiffness will act as a pin connection.

F. COMPOSITE SENSITIVITY MATRIX

As discussed earlier, one of the primary issues in damage detection and model updating is modal truncation. Modal truncation occurs due to a difference in the number of modes that can be identified in a vibration test as opposed to those that can be calculated from a FEM. For instance, a 2-dimensional beam with 20 elements will produce 40 modes; however, testing equipment may be limited to measuring up to 1000 Hz, and thus can only capture 14 modes. As such, we calculate the sensitivity matrix with the 14 modes and get a sensitivity matrix that is 14 modes x 20 elements. In this configuration, the sensitivity matrix is underdetermined and rank deficient. As such, it cannot reliably be used in damage detection or model updating as its use in equation (2.46) will produce false indications of damage in an attempt to solve the equation.

Another issue presents itself when you are given a symmetric structure such as a free-free beam. If 20 modes where available for our 20 element beam, we have a fully developed sensitivity matrix, but we may still have an issue as the structure is symmetrical. Symmetry in a structure will produce a symmetric sensitivity matrix, thus making it rank deficient since it will not have enough unique values to solve the system of equations.

Because of modal truncation and/or rank deficiency in the sensitivity matrix, we use the Artificial Boundary Condition method to calculate a new sensitivity matrix and new frequencies. The process of which requires the FEM to be re-calculated for each condition presented.

Additionally, as this is for the initial development of the sensitivity matrix, we create a second FEM of the structure identical except for a known amount of damage. This allows us to develop a $\{\Delta\lambda\}$ and $\{\Delta EI\}$ matrix based on the conditions provided.

For the development of the composite sensitivity matrix, we will modify equation (2.40) to the following:

$$\left\{\Delta\lambda^{(0)}\right\} = \left[S^{(0)}\right]\left\{\Delta EI_n\right\} \tag{2.66}$$

Where the superscript 0 indicates the baseline configuration. Using the process described for ABC FRF development, we recalculate the baseline damaged and baseline undamaged structure to include an ABC:

$$\left\{\Delta\lambda^{(1)}\right\} = \left[S^{(1)}\right]\left\{\Delta EI_n\right\} \tag{2.67}$$

Where the superscript (1) indicates a specific ABC condition like a pin connection on the first node. This equation is then appended onto the bottom of equation (2.66)

$$\begin{Bmatrix}\left\{\Delta\lambda^{(0)}\right\}\\ \left\{\Delta\lambda^{(1)}\right\}\end{Bmatrix} = \begin{bmatrix}\left[S^{(0)}\right]\\ \left[S^{(1)}\right]\end{bmatrix}\left\{\Delta EI\right\} \tag{2.68}$$

This process is then repeated to the damaged and undamaged beams as many times as necessary to develop a full rank, square matrix.

$$\begin{Bmatrix}\left\{\Delta\lambda^{(0)}\right\}\\ \left\{\Delta\lambda^{(1)}\right\}\\ \vdots\\ \left\{\Delta\lambda^{(n)}\right\}\end{Bmatrix} = \begin{bmatrix}\left[S^{(0)}\right]\\ \left[S^{(1)}\right]\\ \vdots\\ \left[S^{(n)}\right]\end{bmatrix}\left\{\Delta EI\right\} \tag{2.68}$$

Ultimately, because the damage and change in frequencies are known, we can input the new resonance frequencies and sensitivity matrices, as determined in equation (2.68), into equation (2.46) to prove that the new sensitivity values can find damage in all elements.

The thesis presented by Damanakis [11, 24] took this a step further. For a specific beam, he was able to utilize the QR decomposition of each sensitivity

matrix and extract specific rows from a large variety of ABC conditions that provided a good correlation for damage detection for a specific element. This method also develops a full rank, square matrix and has proven reliable in damage detection.

For this thesis, we are exploring the placement of a massless spring of variable stiffness or a lumped mass of variable value on a single node of the damaged and undamaged beam. Then, using the process described in this chapter, develop a new composite sensitivity matrix for damage detection and model updating.

By placing a spring or mass on the node as opposed to a pin connection, we can provide a near infinite amount of new sensitivity matrices. However, this new method needs to be verified that the change in resonance frequencies is sufficient enough to provide a well conditioned sensitivity matrix that will detect damage accurately.

G. CONCLUDING REMARKS

As has been detailed in this chapter, this thesis will be using a 2-dimensional Euler-Bernoulli beam. In an effort to detect damage or update the FEM, a massless spring of variable stiffness or a lumped mass of variable value has been introduced into the system to provide new resonance frequencies and sensitivity matrices based on the theory of Synthesis and the Eigenvector Sensitivity method.

III. EXPERIMENTAL SETUP AND TESTING

A. EXPERIMENTAL SETUP

The structure used in this thesis was a 6061 Aluminum beam with the properties detailed in Table 1 and Figure 8:

Table 1. Properties of 6061 Aluminum Beam

Length cm (in)	182.88 (72)
Width cm (in)	4.9 (1.93)
Height cm (in)	0.947 (0.373)
Modulus of elasticity MPa (psi)	68947.5729 (10000000)
Node/Accerometer Locations mm(in)	1.27(0.5), 14.15(5.57), 27.03(10.64), 39.90(15.71), 52.78(20.78), 65.66(25.85), 78.54(30.92), 91.41(35.99), 104.29(41.06), 117.17(46.13), 130.05(51.20), 142.93(56.27), 155.80(61.34), 168.68(66.41), 181.56(71.48)

Figure 8. Experimental Beam Node Numbering

To reduce complications with joint modeling and to be consistent with theory developed in Chapter II, the beam was set up in a free-free condition by suspending the beam from the ceiling. To ensure the pendulum frequency would not be present in the harmonic response of the beam, the beam was suspended with an elasto-polymer cord at a length of approximately 270 cm (106.3 in). At this length, the idealized pendulum frequency ($\theta << 0$) is approximately 0.54Hz. Additionally, the elasto-polymer cord is made of a soft core material that is significantly less weight when compared to the beam to accommodate the heave rigid body motion of the cord.

The beam response was measured using Pulse Reflex software, version 21, as developed by the Brüel Kjaer company [Pulse]. Instrumentation secured onto the beam was a Piezotronics, Inc., model 336C04 ICP Accelerometer with the properties detailed in Table 2 and Table 3:

Table 2. Accelerometer Properties

Screw Weight g (lb)	0.5 (0.0011)
Accelerometer weight g (lb)	6.5 (0.0143)
Accelerometer height cm (in)	1.236 (0.487)
Accelerometer depth cm (in)	1.574 (0.620)

Table 3. Accelerometer Locations

Node	Serial Number	Calibration Date	Voltage sensitivity (mV/ g)
1	10867	9/10/1993	98.4
2	10875	9/10/1993	99.3
3	10857	9/10/1993	99.3
4	10851	9/10/1993	98.9
5	10858	9/10/1993	98.4
6	10859	9/10/1993	98.7
7	10856	9/10/1993	98.8
8	10854	9/10/1993	95.5
9	11798	2/17/1993	97.1
10	10877	9/10/1993	96.4
11	10226	7/27/1993	99.2
12	10847	9/10/1993	97.9
13	10860	9/10/1993	99.1
14	10868	9/10/1993	96.5
15	10866	9/10/1993	99.0

Piezotronics, Inc. also manufactured the load cells used in testing with the specifications detailed in Table 4:

Table 4. Load Cell Specifications

	MN	SN	Cal	mV/g (mV/lb)
Hammer	086B03	2195	5/22/1986	0.02089 (9.48)
Shaker	208A02	10875	2/16/1994	0.17809 (80.78)

Because we are collecting data specifically for the location of resonance peaks, the current calibration dates of the accelerometers and load cells are acceptable as long as measurements are repeatable. A more current calibration would be required if a study was being conducted on waveforms or effects on amplitudes of resonance peaks.

As identified in Figure 8, the Accelerometers are offset by 12.7mm (0.5in) from the ends of the beam. This was done to ensure the accelerometer remained flush during the measurement and is accounted for in Chapter IV

B. EXPERIMENTAL TESTING

The beam was excited using four different modes: Single Impact Hammer, Random Impact Hammer, Random Burst Shaker, Sine-Sweep Shaker

The single impact hammer measurement utilizes a calibrated impact hammer to excite the beam at a node and accelerometers measure the response over a given length of time with a single strike. This process is repeated several times per node and averaged, and repeated for each node.

The Random Impact Hammer test is conducted similarly to the single impact hammer, but has multiple strikes taken over time, providing a larger amount of excitation. Like the single impact hammer test, the random impact hammer measurement is taken for each node to formulate a full FRF matrix

The Burst Random Shaker test utilizes an electrodynamic shaker to excite the beam with a randomly generated burst of frequencies and measure the response. This test requires a stand to isolate the shaker from outside frequencies while it conducting the measurement and to be attached to the beam

with a sufficiently stiff “stinger” to reduce the loss of energy generated by the shaker. Similar to the hammer tests, this process is repeated for each node to formulate a full FRF matrix.

The Sine-Sweep shaker test also utilizes an electrodynamic shaker to excite the beam. However, instead of exciting the beam with a very short burst of random frequencies, the sine-sweep method excited the beam at every frequency given a specified bandwidth and step. This is done slowly as to ensure the beam is responding only to the given input forcing function and the accelerometers can accurately measure the response. Again, this process is repeated for each node to formulate a full FRF matrix

Ultimately, the single impact hammer test and random impact hammer test proved far more accurate and repeatable than the burst random shaker test and the sine-sweep shaker test. The shaker tests where not useable due to the mass ratio of the shaker to the beam significantly altering the location of the resonance frequencies as displayed in Figure 9.

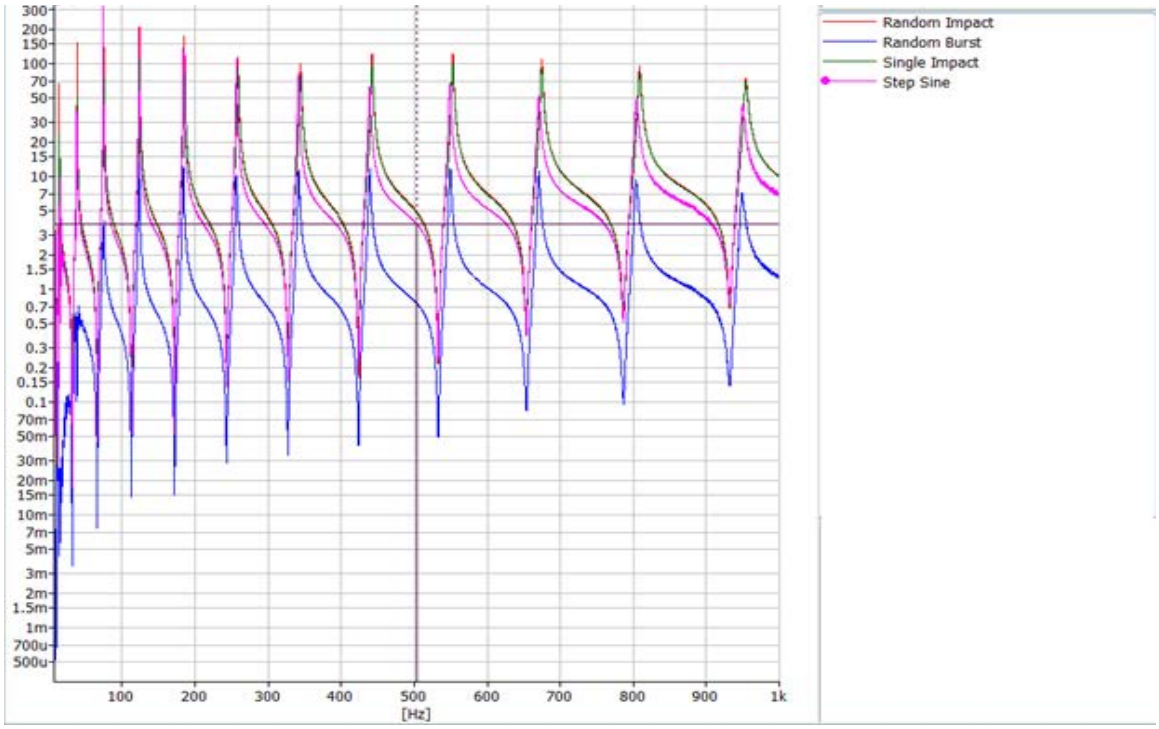

Graph developed using [7]

Figure 9. Testing Signal Comparison

Using the measurements from the single impact hammer, the measurement software [7] was able to determine the resonance frequencies of the beam using a rational fraction polynomial, parameter estimation method. The results of which are displayed in Figure 10.

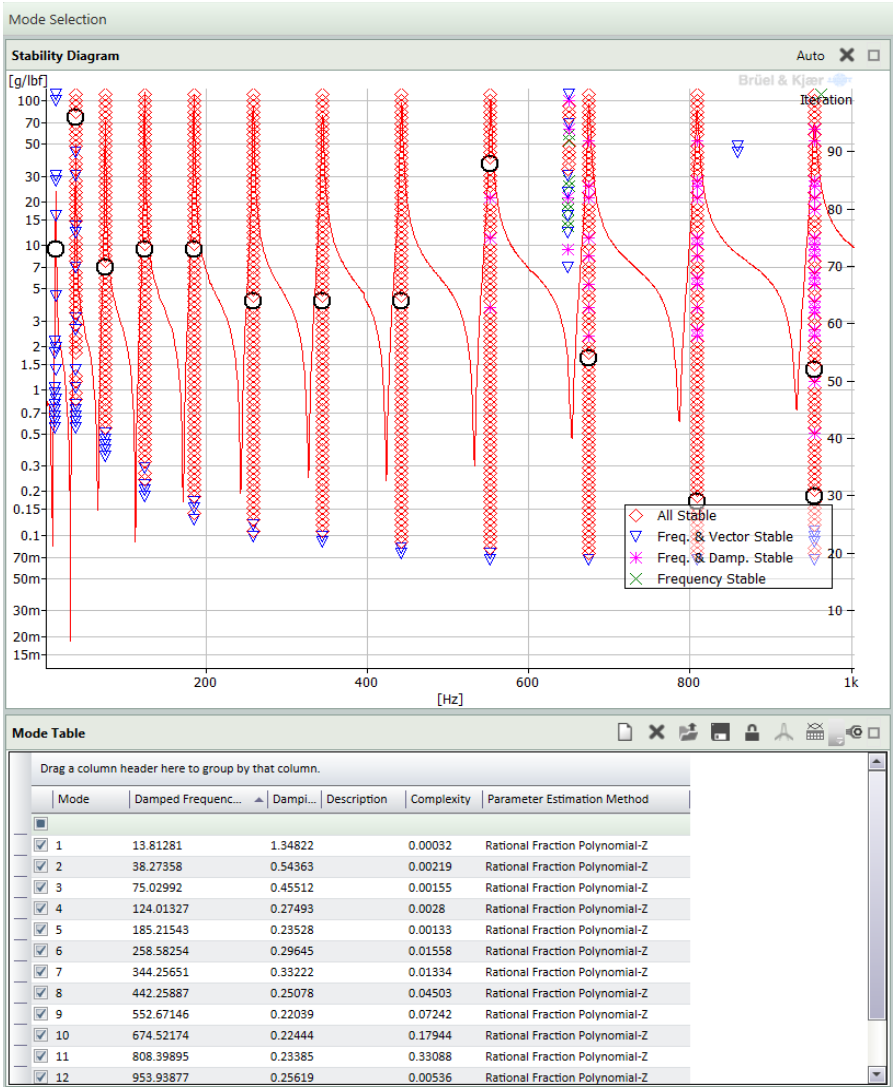

Graph created using [7].

Figure 10. Single Impact Hammer Testing Mode Selection

C. CONCLUDING REMARKS

Experimental testing using the impact hammer provided much clearer results in determining the modal response of the beam. Tests using the shaker setup did not provide a clear picture of the lower frequencies possibly due to the mass ratio. Investigations and research should be conducted to determine the limits of using the electro-dynamic shaker because it is capable of producing high quality results with a dramatic decrease in time given the correct setup.

IV. FINITE ELEMENT MODELING AND SIMULATION

A. FINITE ELEMENT MODELING

The Finite Element Model was constructed using 16, 2-D Euler-Bernoulli elements. The FEM had 17 nodes placed on either end of the bar and correlated to the placement of the accelerometers on the prototype beam. As such, the FEM had the properties displayed in Table 5 and Figure 11:

Table 5. Properties of Beam FEM

Length cm (in)	182.88 (72)
Width cm (in)	4.9 (1.93)
Height cm (in)	0.947 (0.373)
Modulus of elasticity MPa (psi)	68947.5729 (10000000)
Density Kg/m^3 (lbm/in^3)	2698.79 (0.0975)
Node Locations cm(in)	0(0), 1.27(0.5), 14.15(5.57), 27.03(10.64), 39.90(15.71), 52.78(20.78), 65.66(25.85), 78.54(30.92), 91.41(35.99), 104.29(41.06), 117.17(46.13), 130.05(51.20), 142.93(56.27), 155.80(61.34), 168.68(66.41), 181.56(71.48), 182.83(71.98)

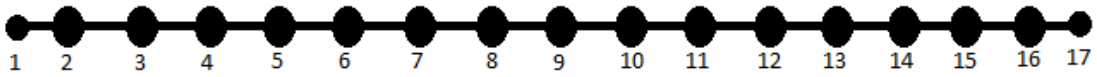

Figure 11. FEM Node Numbering

In total, the FEM has 34 DOF, where odd numbered DOF are related to translation and even numbered DOF are related to rotation as identified in Figure 12.

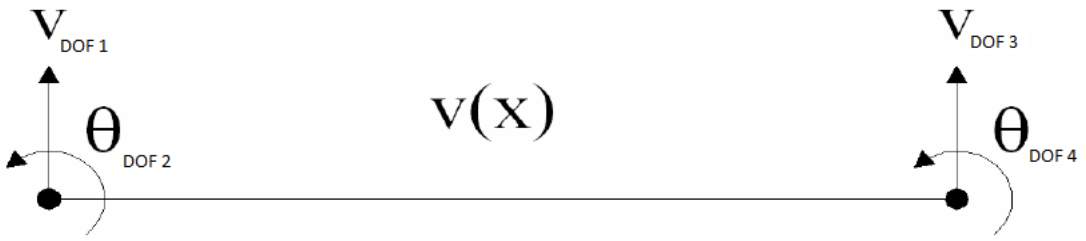

Figure 12. 2-D Euler-Bernoulli Element DOF Setup. Adapted from [25].

In addition to formulating the Mass and Stiffness properties for the beam with the data from Table 5, the instrumentation for the accelerometers where added to the mass matrix as a point load with inertial mass. As such, the nodes that are not on the ends have the instrumentation loads added to the diagonal.

In addition to the FEM, a second model was constructed using the same specifications in Table 2 and Table 5, but damaged. The damage was simulated by reducing the flexural rigidity (EI) in a single element.

Additional aspects for setting up the FEM are detailed in Appendix A.

B. FINITE ELEMENT MODEL TESTING

Following the theory in Chapter II, the FEM mass and stiffness matrices are constructed and used to solve the eigenvalue problem as described for equation (2.18). Using the “eig” function in MATLAB [17], we calculate a series of resonance frequencies and mass-normalized mode shapes. To confirm their accuracy, the frequencies are compared to an analytic solution using the roots to the characteristic equation for a uniform, cantilevered beam utilizing equation (4.1) from [4] :

$$\omega_i = \frac{\left(\lambda L_i\right)^2}{L}\frac{EI}{\sqrt{\rho A}}\ , \tag{4.1}$$

where (λL_i) is a tabulated value found in [26] for specific modes given specific boundary conditions. This thesis used the following values to predict the first 4 modes:

$$\begin{aligned} \lambda L_1 &= 1.8751 \\ \lambda L_2 &= 4.6941 \\ \lambda L_3 &= 7.8548 \\ \lambda L_4 &= 10.996 \end{aligned} \tag{4.2}$$

Table 6 displays the accuracy of the FEM to an analytical assessment:

Table 6. Analytical and FEM Frequency Comparison

	Analytical Frequency	FEM Frequency	% Rel Error
Mode 1	2.22641373	2.2276613	0.00163
Mode 2	13.9528099	13.960624	0.01021
Mode 3	39.0685476	39.092269	0.03098
Mode 4	76.5643263	76.618568	0.07084

Because the percent relative error is less than 0.1%, we can say the FEM has good correlation to analytical values. The FEM is capable of calculating 34 total natural frequencies, however, the equipment measuring the response of the beam is limited to 1000 Hz, which captures the first 12 modes of the beam. Additionally, because we are using a beam in a free-free boundary condition, the first two calculated modes are considered rigid body modes due to their proximity to zero Hz resonance and their mode shape. For the purposes of calculations, rigid body modes are removed. Table 7 compares the FEM resonance values to the measured values:

Table 7. FEM Resonance Frequencies

	FEM Frequency (Hz)	Measured Frequency (Hz)	Absolute Error (Hz)	% Rel Error
Mode 1	14.35143	13.81281	0.53862	3.8994
Mode 2	39.55544	38.27358	1.28186	3.3492
Mode 3	77.54409	75.02992	2.51417	3.3509
Mode 4	128.20934	124.01327	4.19607	3.3836
Mode 5	191.61915	185.21543	6.40372	3.4574
Mode 6	267.88319	258.58254	9.30065	3.5968
Mode 7	357.17924	344.25651	12.92273	3.7538
Mode 8	459.76188	442.25887	17.50301	3.9576
Mode 9	575.95281	552.67146	23.28135	4.2125
Mode 10	706.07569	674.52174	31.55395	4.678
Mode 11	850.20479	808.39895	41.80584	5.1714
Mode 12	1007.10225	953.93877	53.16348	5.573

To adjust for the discrepancies, a 3% correction factor used on the modulus of elasticity. The results of which are displayed in Table 8.

Table 8. FEM Resonance Frequencies with Correction Factor

	Corrected FEM Frequency(Hz)	Measured Frequency (Hz)	Absolute Error (Hz)	% Rel Error
Mode 1	14.13452	13.81281	0.32171	2.329
Mode 2	38.95759	38.27358	0.68401	1.7872
Mode 3	76.37207	75.02992	1.34215	1.7888
Mode 4	126.27156	124.01327	2.25829	1.821
Mode 5	188.72298	185.21543	3.50755	1.8938
Mode 6	263.83435	258.58254	5.25181	2.031
Mode 7	351.78075	344.25651	7.52424	2.1856
Mode 8	452.81294	442.25887	10.55407	2.3864
Mode 9	567.24773	552.67146	14.57627	2.6374
Mode 10	695.40391	674.52174	20.88217	3.0958
Mode 11	837.35461	808.39895	28.95566	3.5819
Mode 12	991.88069	953.93877	37.94192	3.9774

The new FEM values correlate to previous work [11] and prove consistency among the models.

C. FEM INITIAL SENSITIVITY MATRIX AND FRF

1. Initial Sensitivity Matrix

The initial sensitivity matrix is influence by the number of modes that are available for calculation. For this FEM, if we use all modes that can be calculated, then we will get an over determined sensitivity matrix of 34 by 14. However, because of the equipment bandwidth limitation of 1,000 hertz, we only use the first 12 flexural modes of the initial matrix for calculation. As such, the initial sensitivity matrix is:

$$\left[S^0\right]=\begin{bmatrix}
2.33E-05 & 0.0004 & 0.0021 & 0.0054 & 0.0098 & 0.0141 & 0.0168 & 0.0168 & 0.0141 & 0.0098 & 0.0054 & 0.0021 & 0.0004 & 0.0000\\
0.0011 & 0.0178 & 0.0631 & 0.1083 & 0.1088 & 0.0604 & 0.0105 & 0.0105 & 0.0604 & 0.1088 & 0.1083 & 0.0631 & 0.0178 & 0.0011\\
0.0144 & 0.1751 & 0.4148 & 0.3483 & 0.0709 & 0.0743 & 0.3244 & 0.3244 & 0.0743 & 0.0709 & 0.3483 & 0.4148 & 0.1751 & 0.0144\\
0.0900 & 0.8146 & 1.0697 & 0.2027 & 0.4223 & 0.9942 & 0.2939 & 0.2939 & 0.9942 & 0.4223 & 0.2027 & 1.0697 & 0.8146 & 0.0900\\
0.3710 & 2.3396 & 1.2645 & 0.6437 & 2.1226 & 0.3942 & 1.5482 & 1.5482 & 0.3942 & 2.1226 & 0.6437 & 1.2645 & 2.3396 & 0.3710\\
1.1525 & 4.7002 & 0.8986 & 3.6816 & 1.3456 & 3.0337 & 2.1594 & 2.1594 & 3.0337 & 1.3456 & 3.6816 & 0.8986 & 4.7002 & 1.1525\\
2.9140 & 7.0920 & 2.4919 & 5.5831 & 3.2166 & 4.8527 & 4.0214 & 4.0214 & 4.8527 & 3.2166 & 5.5831 & 2.4919 & 7.0920 & 2.9140\\
6.2837 & 8.6226 & 8.2602 & 4.0817 & 10.4211 & 4.2973 & 8.0243 & 8.0243 & 4.2973 & 10.4211 & 4.0817 & 8.2602 & 8.6226 & 6.2837\\
11.9021 & 9.7756 & 14.9724 & 8.9028 & 8.8994 & 15.1000 & 8.8989 & 8.8989 & 15.1000 & 8.8994 & 8.9028 & 14.9724 & 9.7756 & 11.9021\\
20.1484 & 13.1424 & 17.9452 & 20.1283 & 14.1650 & 13.1212 & 19.2531 & 19.2531 & 13.1212 & 14.1650 & 20.1283 & 17.9452 & 13.1424 & 20.1484\\
30.6023 & 21.6249 & 21.7209 & 24.8308 & 26.3369 & 24.3565 & 21.4784 & 21.4784 & 24.3565 & 26.3369 & 24.8308 & 21.7209 & 21.6249 & 30.6023\\
40.5225 & 33.6458 & 34.8236 & 34.8729 & 33.6127 & 31.8271 & 30.5621 & 30.5621 & 31.8271 & 33.6127 & 34.8729 & 34.8236 & 33.6458 & 40.5225
\end{bmatrix} \quad (4.3)$$

As detailed for equation (2.31), the sensitivity matrix is sized for the number of modes by the number of interested elements. Because we are limited to 12 modes, the initial sensitivity matrix is sized 14 elements by 12 modes. Additionally, because this sensitivity matrix is developed for a free-free boundary condition, the matrix is symmetric and thus only rank 6. The under-determined, rank deficient, initial matrix is not suitable for damage detection or model updating and will need additional modes and information before it can be used as such.

As a proof, equation (2.32) is used to check the sensitivity matrix for accuracy by using the sensitivity value to predict a new resonance frequency for

a given change in EI at a specified element, and compared the resonance frequency calculated from an FEM with the change installed.

$$[Check]=\begin{bmatrix}
0.0002 & 0.0043 & 0.0169 & 0.0341 & 0.0463 & 0.0450 & 0.0283 & 0.0014 & 0.0256 & 0.0428 & 0.0448 & 0.0334 & 0.0166 & 0.0042\\
0.0016 & 0.0225 & 0.0614 & 0.0618 & 0.0019 & 0.0643 & 0.0666 & 0.0001 & 0.0674 & 0.0661 & 0.0004 & 0.0598 & 0.0603 & 0.0223\\
0.0051 & 0.0566 & 0.0848 & 0.0222 & 0.0966 & 0.0014 & 0.0881 & 0.0008 & 0.0870 & 0.0010 & 0.0977 & 0.0242 & 0.0830 & 0.0559\\
0.0116 & 0.0933 & 0.0338 & 0.1105 & 0.0284 & 0.0740 & 0.0891 & 0.0003 & 0.0903 & 0.0726 & 0.0278 & 0.1117 & 0.0320 & 0.0921\\
0.0214 & 0.1136 & 0.0608 & 0.0353 & 0.0854 & 0.0987 & 0.0666 & 0.0006 & 0.0658 & 0.0997 & 0.0843 & 0.0360 & 0.0622 & 0.1122\\
0.0340 & 0.1048 & 0.1111 & 0.0822 & 0.0681 & 0.0500 & 0.0252 & 0.0004 & 0.0261 & 0.0491 & 0.0691 & 0.0812 & 0.1122 & 0.1036\\
0.0483 & 0.0697 & 0.0757 & 0.0516 & 0.0388 & 0.0275 & 0.0134 & 0.0004 & 0.0142 & 0.0267 & 0.0396 & 0.0508 & 0.0766 & 0.0687\\
0.0628 & 0.0240 & 0.0033 & 0.0412 & 0.0637 & 0.0607 & 0.0376 & 0.0004 & 0.0368 & 0.0616 & 0.0629 & 0.0421 & 0.0041 & 0.0231\\
0.0759 & 0.0128 & 0.0335 & 0.0383 & 0.0004 & 0.0399 & 0.0391 & 0.0004 & 0.0399 & 0.0391 & 0.0004 & 0.0391 & 0.0327 & 0.0139\\
0.0854 & 0.0290 & 0.0208 & 0.0095 & 0.0249 & 0.0039 & 0.0265 & 0.0003 & 0.0257 & 0.0049 & 0.0257 & 0.0089 & 0.0201 & 0.0302\\
0.0895 & 0.0257 & 0.0009 & 0.0096 & 0.0047 & 0.0056 & 0.0081 & 0.0006 & 0.0090 & 0.0061 & 0.0042 & 0.0088 & 0.0002 & 0.0268\\
0.0845 & 0.0139 & 0.0029 & 0.0007 & 0.0020 & 0.0032 & 0.0023 & 0.0002 & 0.0028 & 0.0040 & 0.0031 & 0.0006 & 0.0018 & 0.0148
\end{bmatrix} \quad (4.4)$$

The largest difference is 0.1136% relative error occurring at element 2, mode 5. As this error is less than 1%, we can infer the sensitivity matrix has good prediction qualities.

2. Initial Calculated FRF

Using the process detailed in Chapter II, the initial FEM FRF is calculated and plotted in Figure 13. The initial FEM FRF is then compared to the measured FRF in Figure 14.

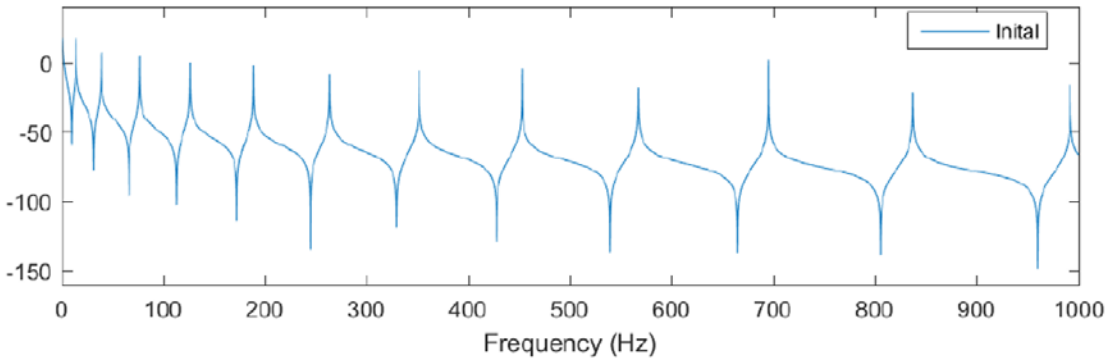

Figure 13. FEM Initial FRF Response, $H_{1,1}$

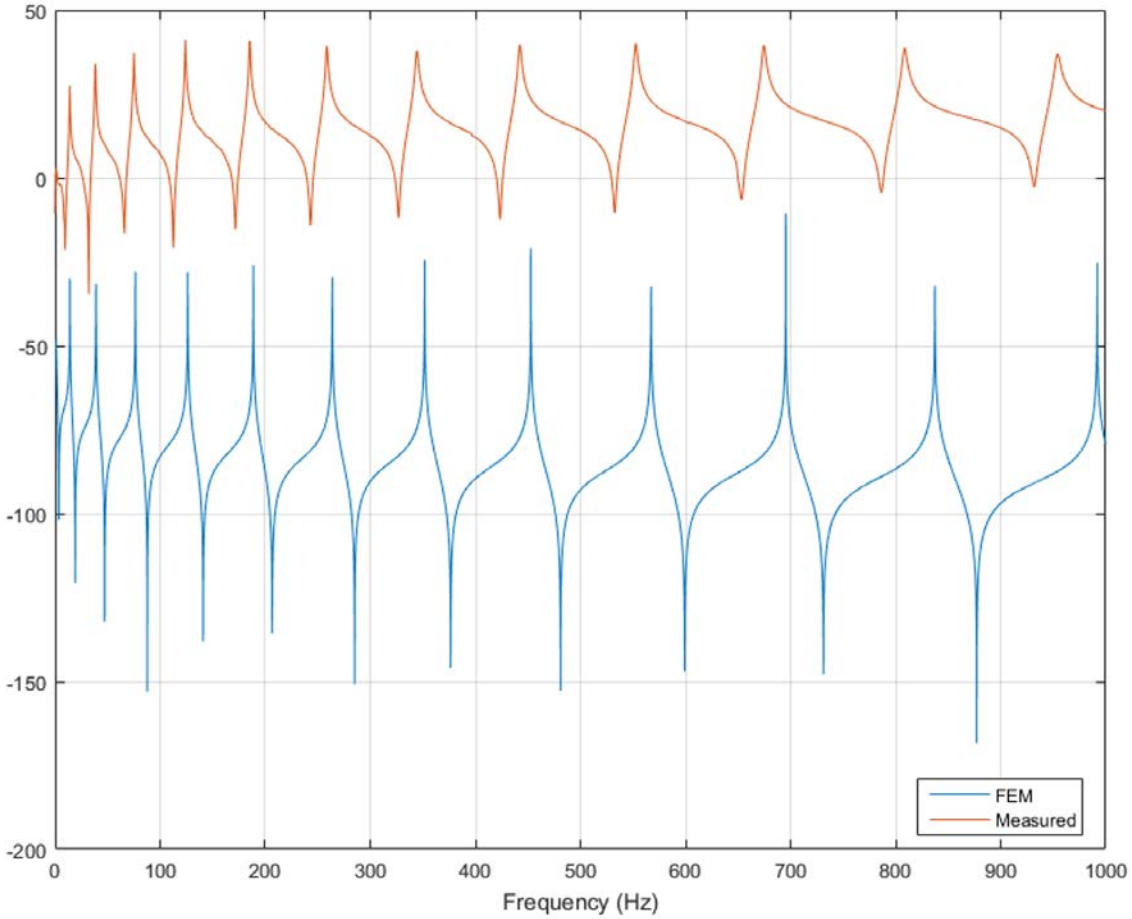

Figure 14. Initial FEM vs Measured FEM Response, $H_{1,1}$

In comparison with the measured response as detailed in Chapter III, the FEM and the model do not match up as displayed in Figure 14. This indicates that the model will need to undergo model updating to correctly reflect the prototype structure.

The proposed method for model updating and damage detection is to synthesize a massless spring or a lumped mass into the FEM to develop new sensitivity matrices that can be used to develop a composite sensitivity matrix for damage detection and model updating. The first step of this is to see if these variables can be synthesized into the new system

D. SINGLE SPRING DYNAMIC RESPONSE

As stated earlier, one of the benefits of synthesis is the capability to manipulate data without the tedious time and expense of actually installing the boundary conditions on the structure and performing another vibration test.

1. FRF Synthesis

Previous work [5, 11, 24] utilized a simulated pin to modify the structure response. For example, following the theory and procedure in Chapter II, if a pin was placed on node 13 of the beam, we would expect the response plotted in Figure 15.

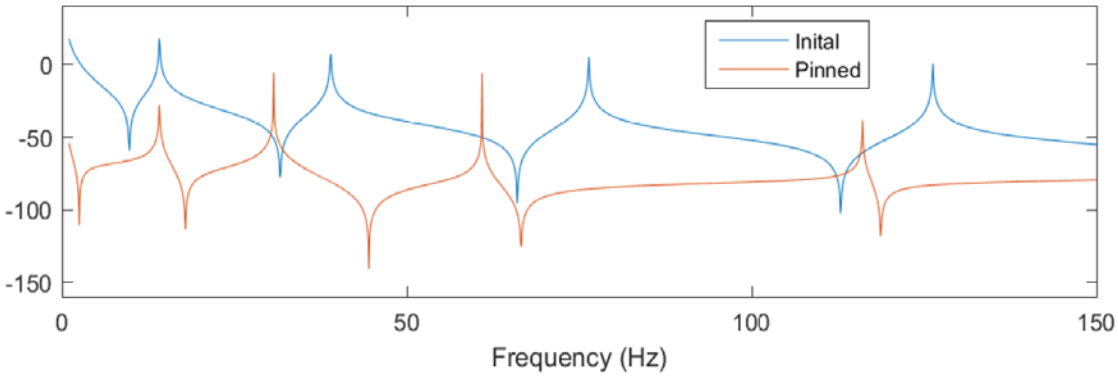

Figure 15. Initial FRF Response vs Synthesized Pin Located at Node 13, $H_{33,33}$

To ensure that the synthesis is accomplished correctly, a second FRF is calculated with the pin installed. This removes the associated row and column for the DOF the pin is attached to. The synthesis check is compared in Figure 16.

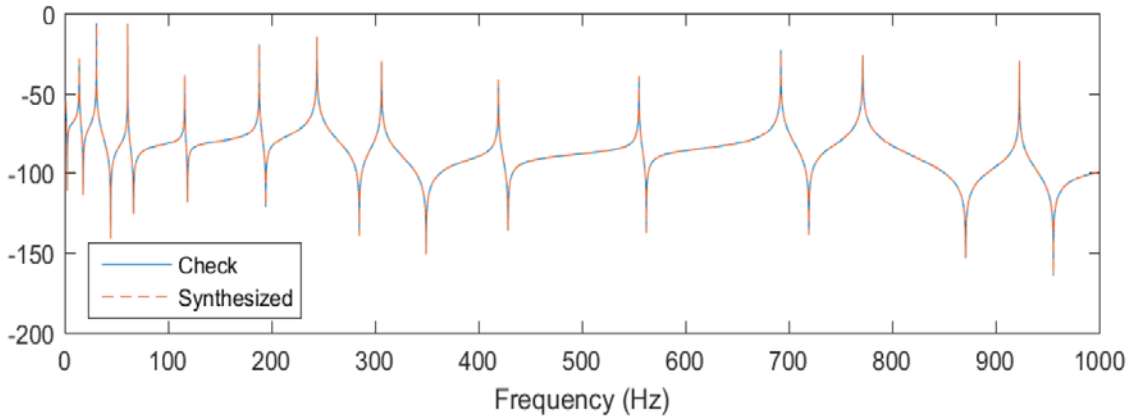

Figure 16. Pin FRF Response Check, Pin Located at Node 13, $H_{33,33}$

However, if this approach was unable to produce enough rows for a much larger structure, damage detection and model updating could not be reliably accomplished. As such, the synthesis of a variable quantity should provide more information

2. Single Spring FRF Synthesis

The introduction of a massless spring introduces the possibility of an infinite amount of new data as the spring can be any variable, and can be placed at any node.

To synthesize the spring, we follow the procedure detailed in Chapter II and identify the CSET as the translational DOF for the node the spring is placed on. Similar to the pin synthesis, we also perform a check of this synthesis to ensure an exact prediction as detailed in Figure 17.

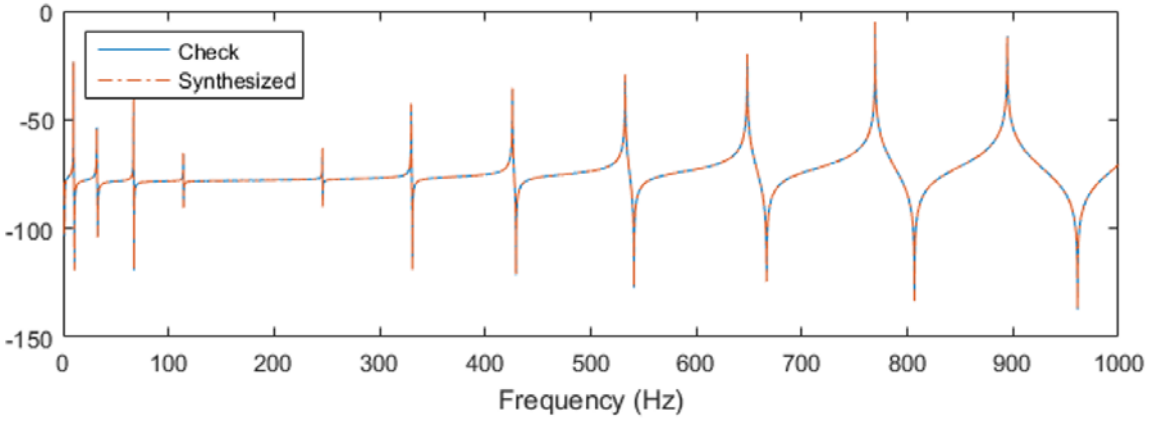

Figure 17. 178.579 kg/mm (10,000lb/in)Spring Synthesis at Node 2 Check, $H_{3,3}$

Using equation (2.64) and (2.65), we are able to predict the modal response of the beam with the spring installed as detailed in Figure 18 and Figure 19:

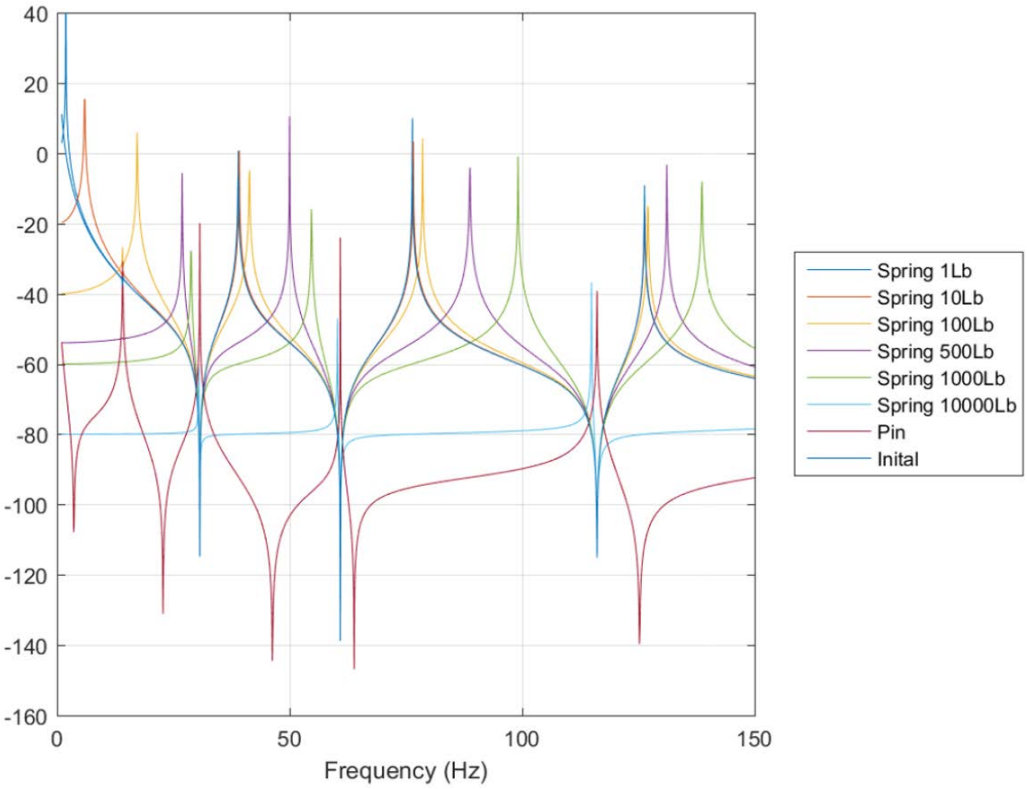

Figure 18. FRF Progression for Spring Synthesis at Node 13, $H_{25,25}$

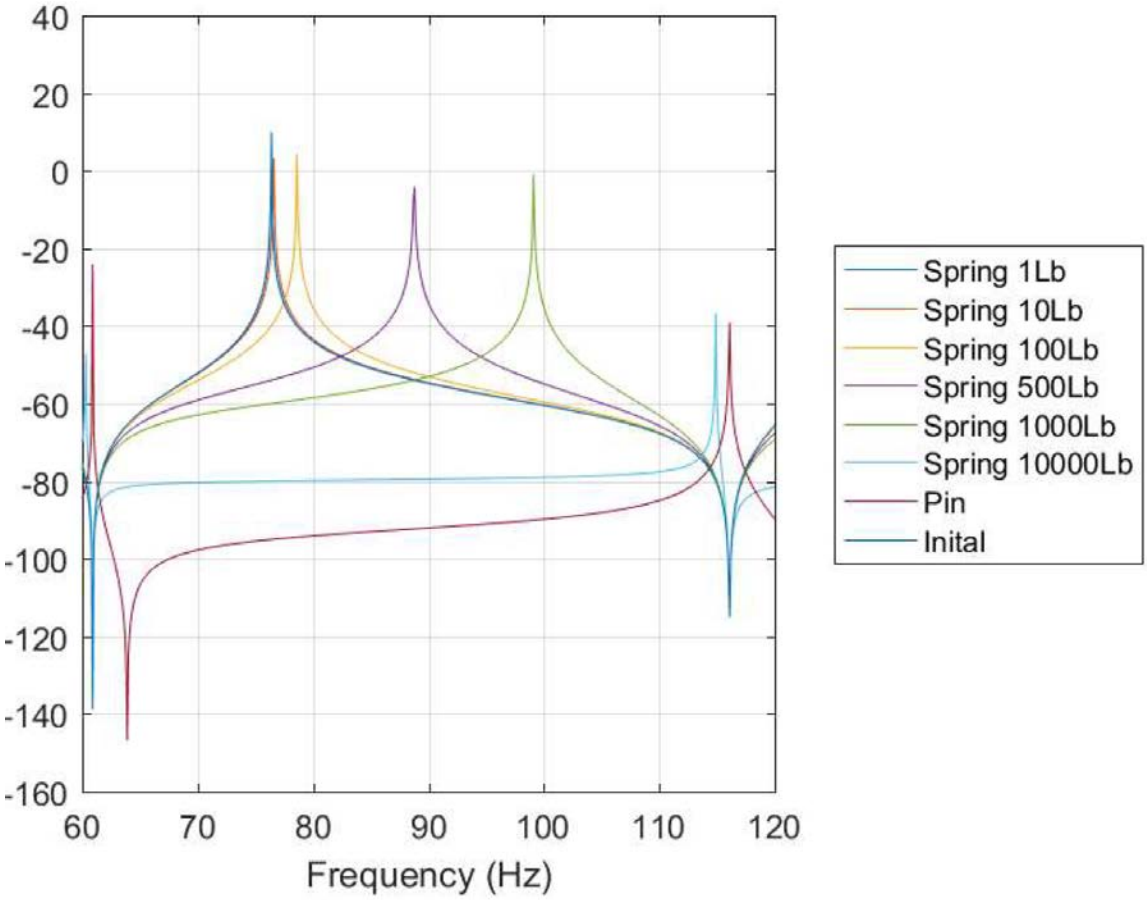

Figure 19. Magnification of FRF Progression for Spring Synthesis at Node 13, $H_{25,25}$

As can be seen in Figure 19, by increasing the strength of the spring, the dynamic beam response will gradually change to a response similar to that of pin connection. As such, we can see the progression of the modal resonance frequencies with the introduction of the spring in Figure 20 and Figure 21.

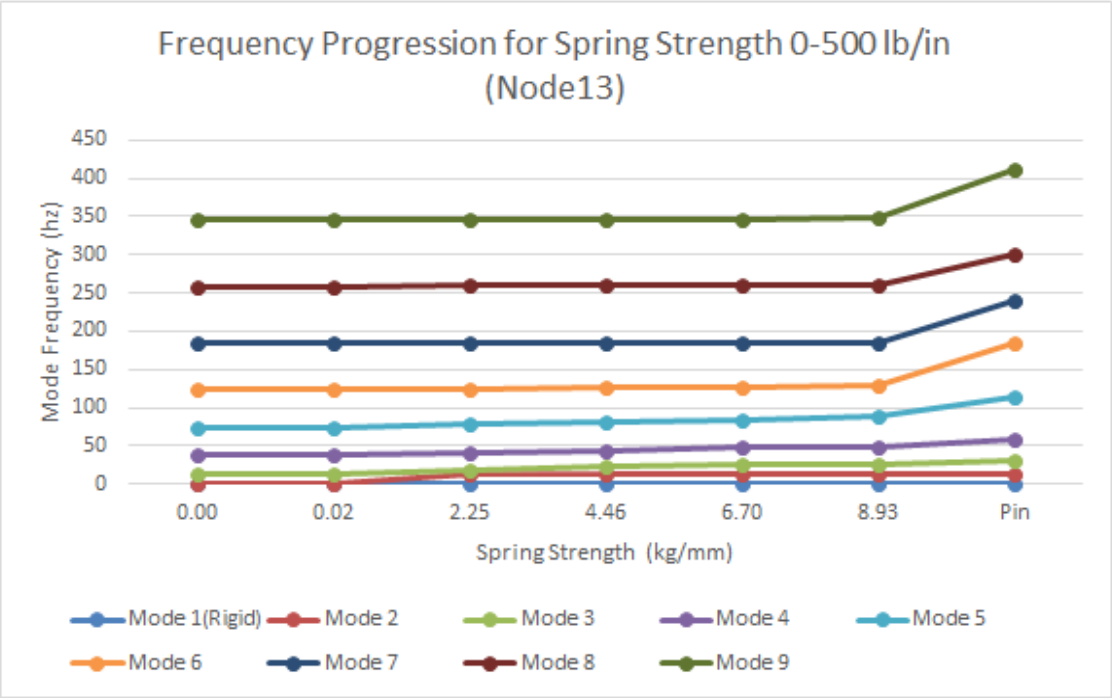

Figure 20. Modal Resonance Frequency Progression for Spring Strength 0–8.928 kg/mm (0–500lb/in) Located at Node 13

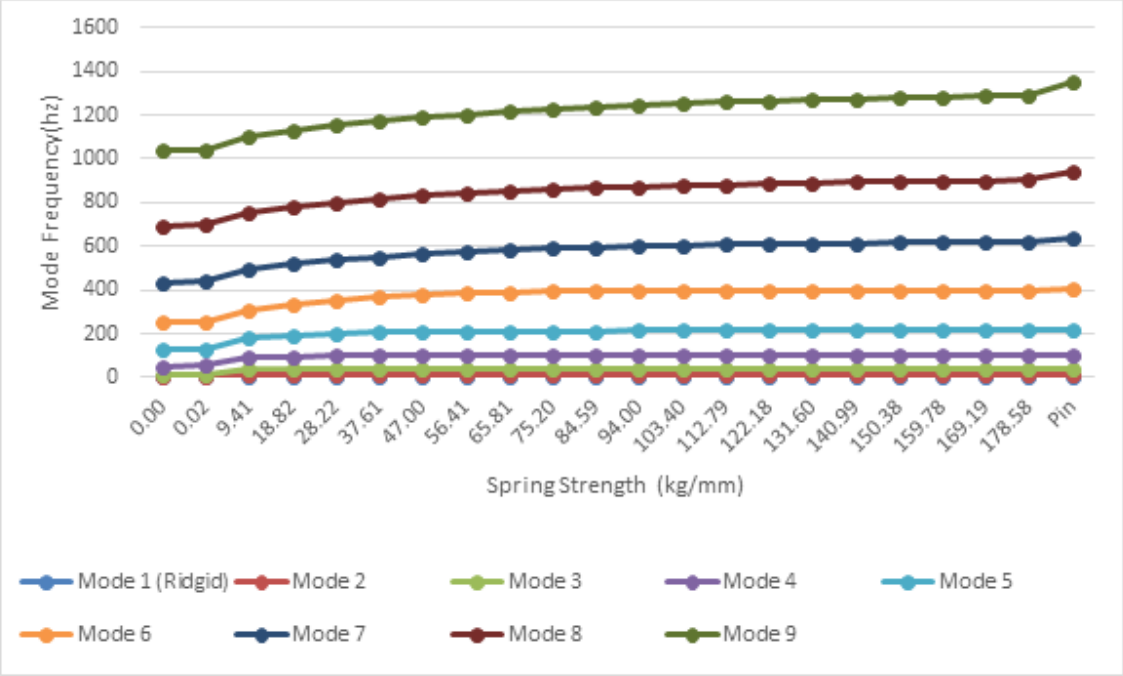

Figure 21. Modal Resonance Frequency Progression for Spring Strength 0–178.579 kg/mm (0–10,000lb/in) Located at Node 13

Even at low spring strengths, we see a loss of one of the two rigid body modes. To understand what the beam response is at these points, the mode shapes where mapped out in Figure 22 through Figure 31:

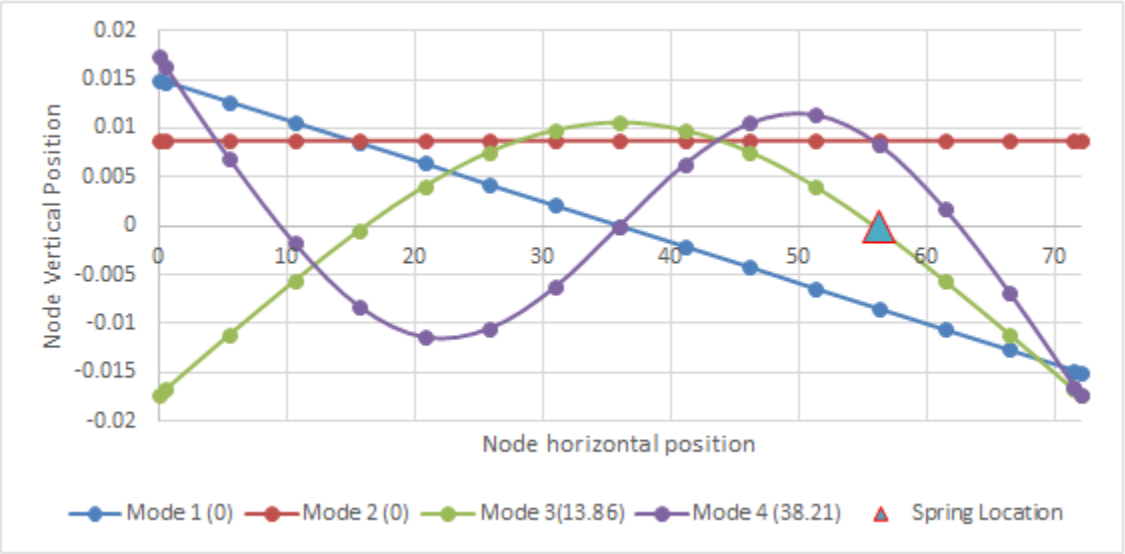

Figure 22. Mode Shapes with 0 kg/mm(0 lb/in) Spring Located at Node 13 (Resonance Frequency in Parentheses)

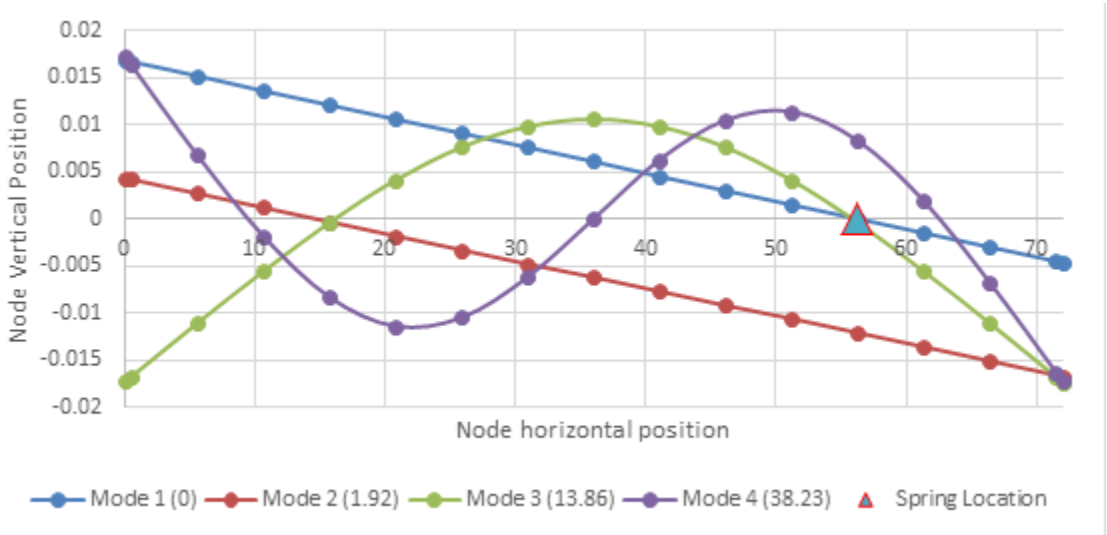

Figure 23. Mode Shapes with 0.017 kg/mm (1 lb/in) Spring Located at Node 13 (Resonance Frequency in Parentheses)

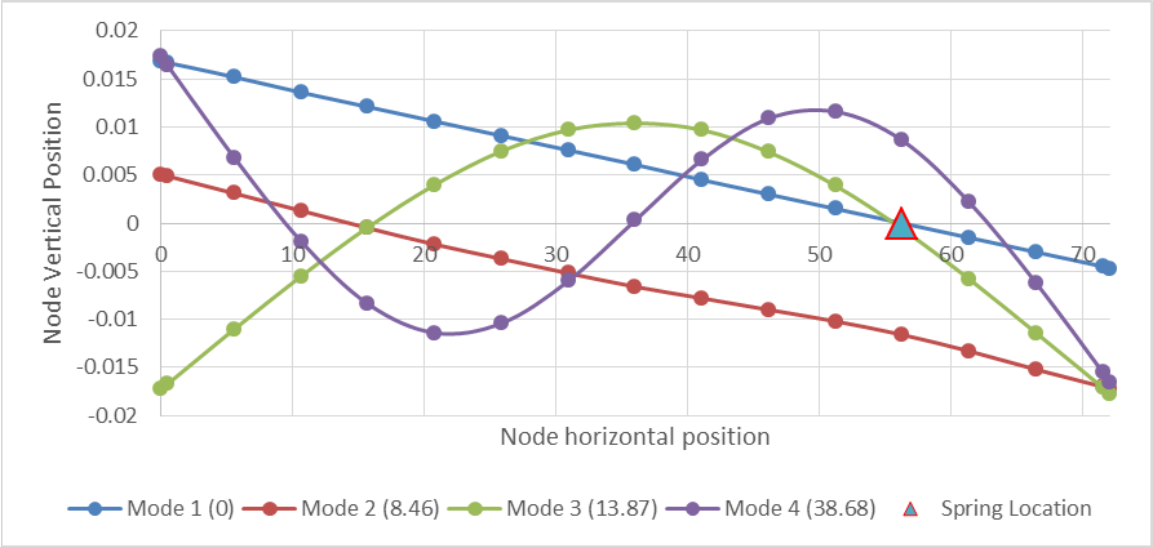

Figure 24. Mode Shapes with 0.357 kg/mm(20 lb/in) Spring Located at Node 13 (Resonance Frequency in Parentheses)

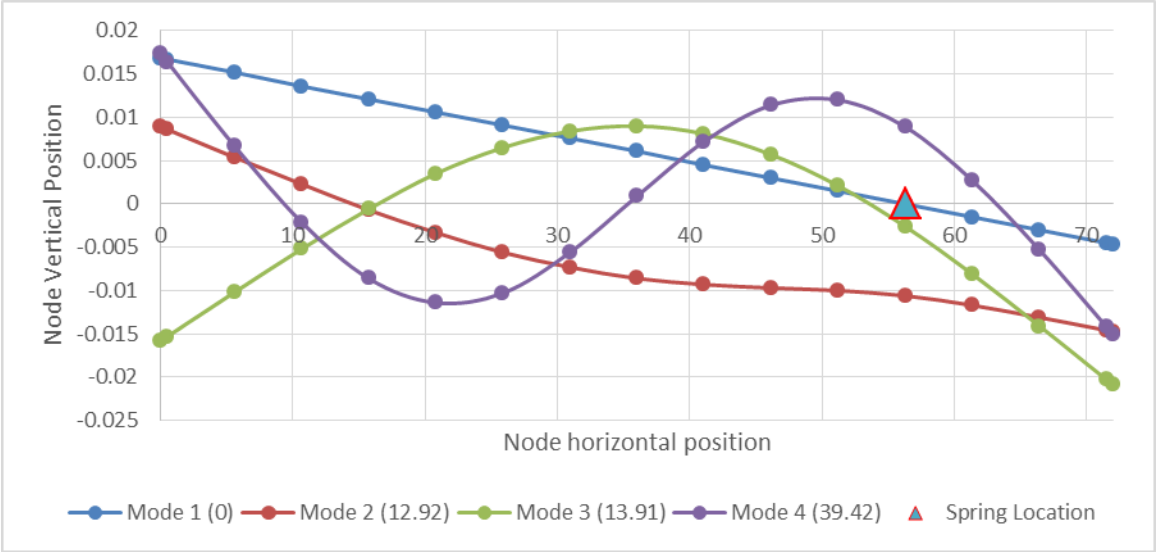

Figure 25. Mode Shapes with 0.892 kg/mm(50 lbf/in)Spring Located at Node 13 (Resonance Frequency in Parentheses)

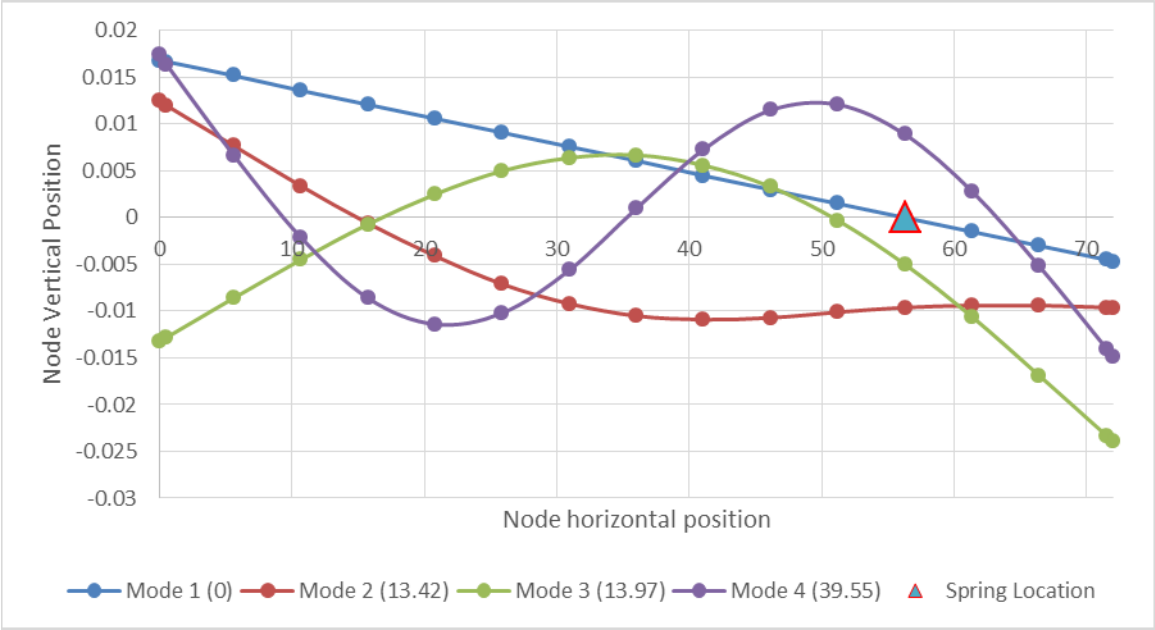

Figure 26. Mode Shapes with 0.982 kg/mm(55 lb/in) Spring Located at Node 13 (Resonance Frequency in Parentheses)

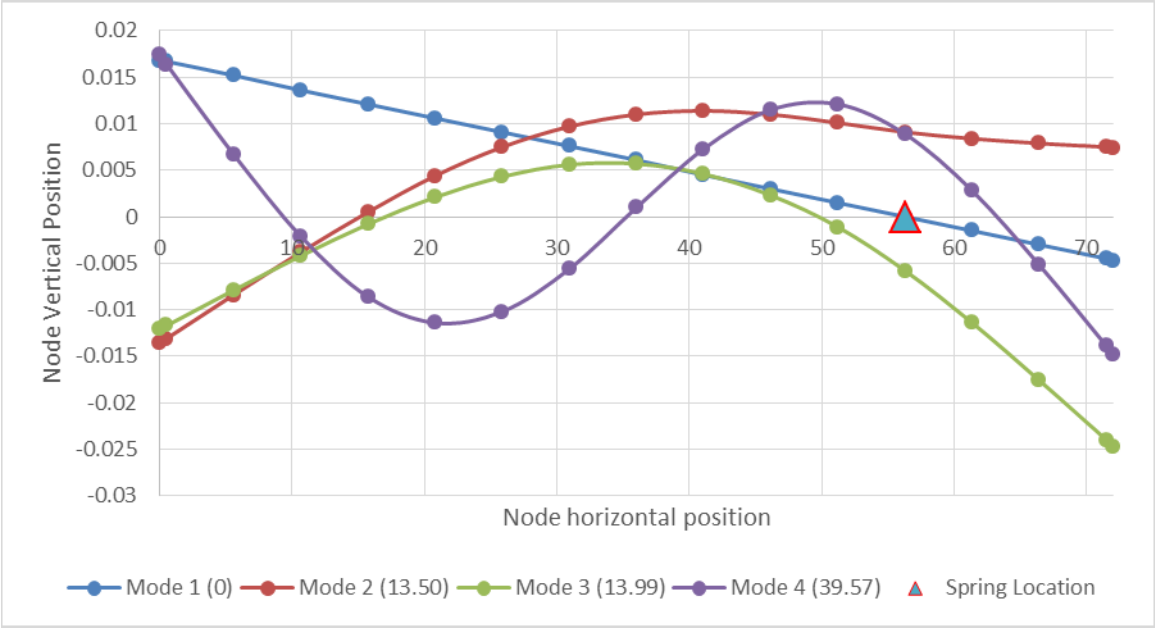

Figure 27. Mode Shapes with 1.00 kg/mm (56 lb/in) Spring Located at Node 13 (Resonance Frequency in Parentheses)

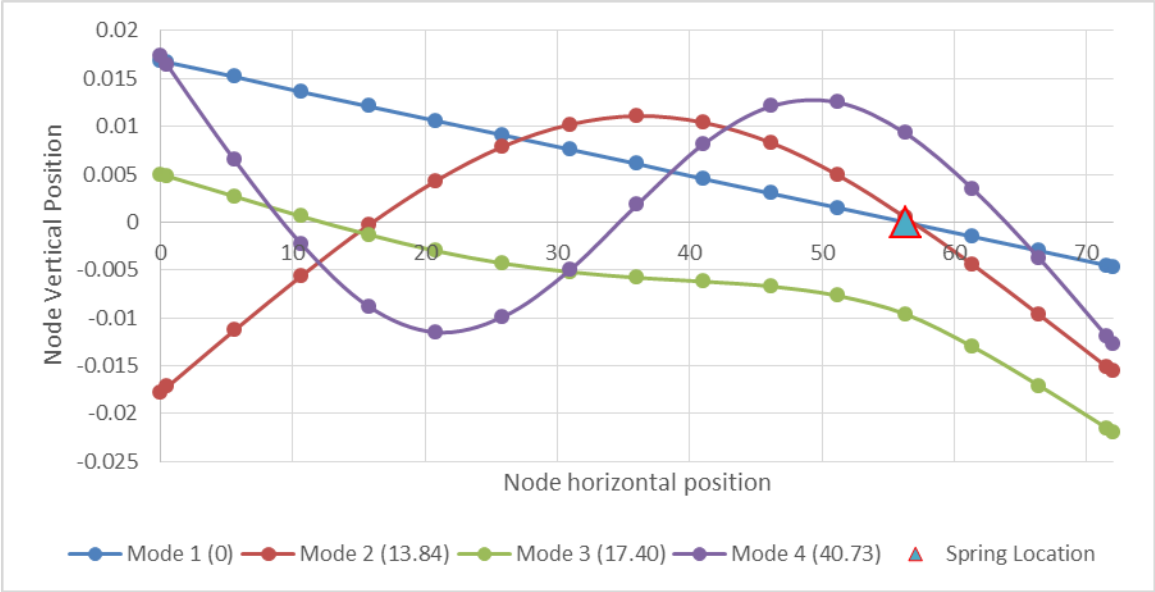

Figure 28. Mode Shapes with 1.79 kg/mm (100 lb/in) Spring Located at Node 13 (Resonance Frequency in Parentheses)

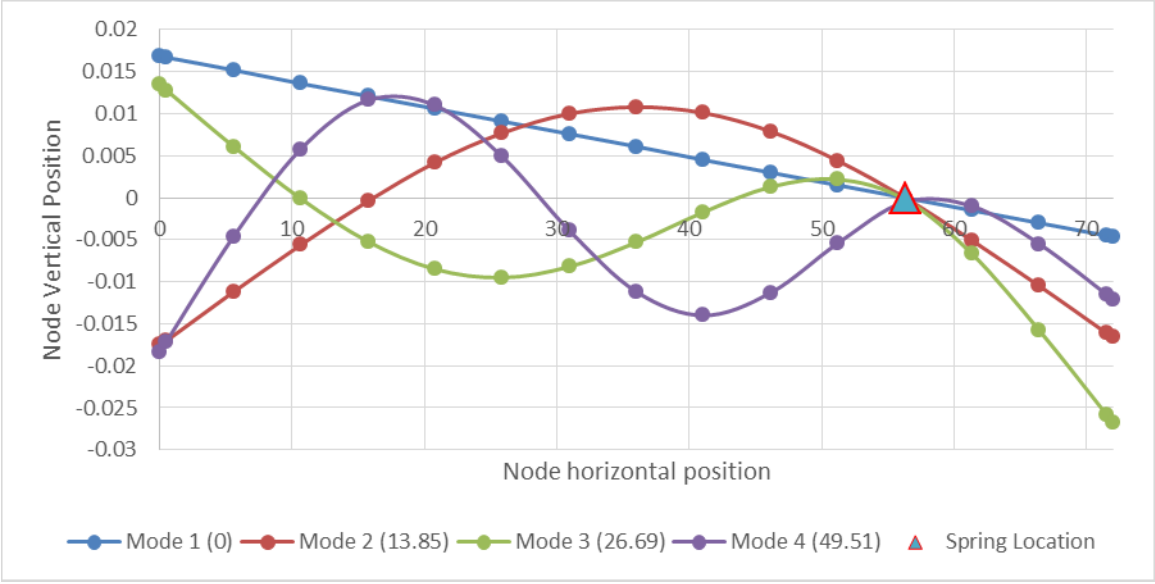

Figure 29. Mode Shapes with 8.93 kg/mm(500 lbf/in)Spring Located at Node 13 (Resonance Frequency in Parentheses)

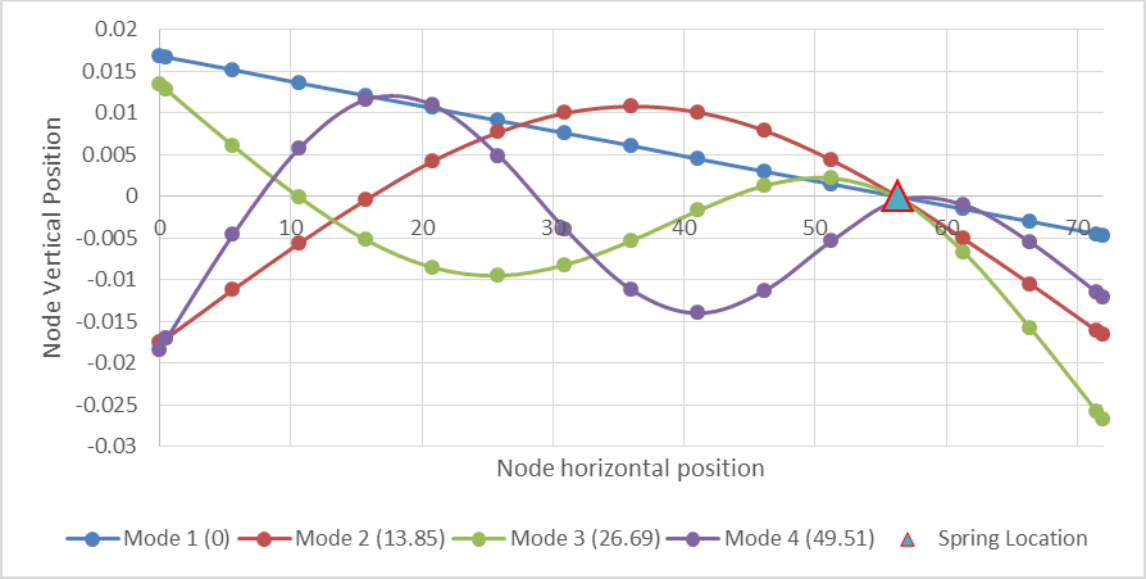

Figure 30. Mode Shapes with 178.579 kg/mm (10,000 lb/in) Spring Located at Node 13 (Resonance Frequency in Parentheses)

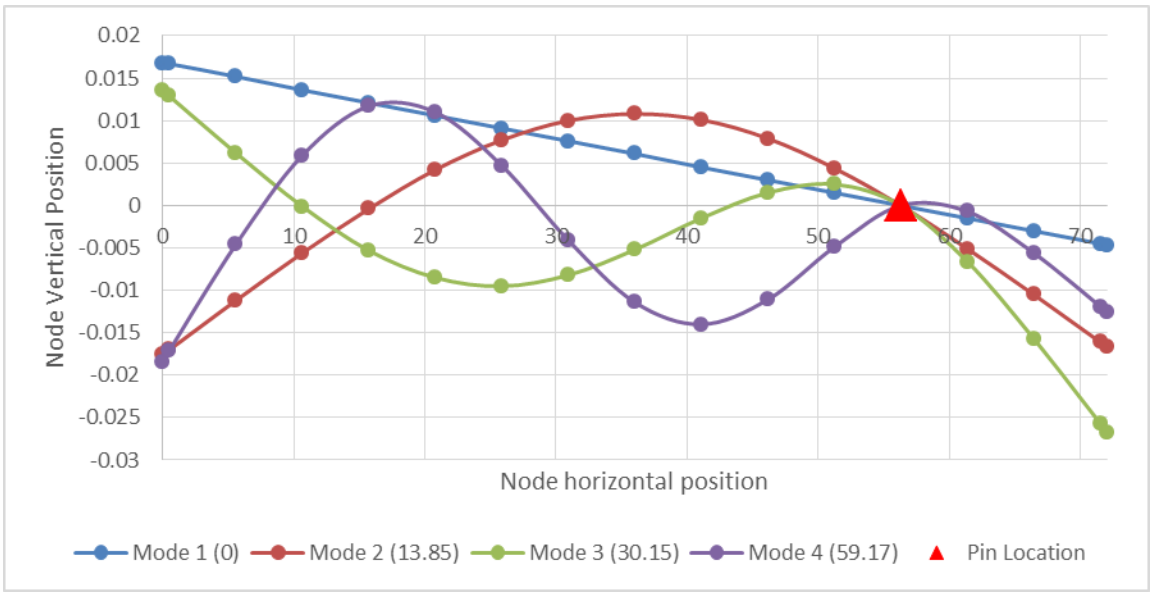

Figure 31. Mode Shapes with a Pin Connection Located at Node 13 (Resonance Frequency in Parentheses)

As Figure 22 through Figure 31 display, by adding a spring to the beam, even at small values, we transfer a rigid body mode into a flexural mode. As the spring increases in strength, the mode shapes gradually transform the next lower mode (mode 4 transforms to mode 3). As the spring approaches a near infinite

strength, the dynamic beam response resembles that of an artificial pin connection placed at the selected node. To see if this transformation ultimately provides new and relevant information for damage detection and model updating we looked at the values of the sensitivity matrix.

3. Single Spring Sensitivity Analysis

As discussed in Chapter II, the sensitivity matrix is what is ultimately used in damage detection and model updating. Previous thesis work [11] indicated higher sensitivity modes provide greater fidelity in damage detection. As such, we tracked the beam sensitivity values of the highest mode in the sensitivity matrix as the spring increased from 0–10,000 lbf/in.

$$\left[S^{K1}\right]=\begin{bmatrix} \left[Mode\left(1\right)\right] \\ \left[Mode\left(2\right)\right] \\ \vdots \\ \left[Mode\left(n-1\right)\right] \\ \left[Mode\left(n\right)\right] \end{bmatrix} \leftarrow HighestMode \tag{4.5}$$

It is important to note that, for a majority of these simulations, the resonance frequency for the highest mode goes above the 1,000 hertz limit at some point. When this happens, the sensitivity matrix no longer calculates the sensitivity to that mode, so the highest mode shifts to the next lower frequency. Ultimately, this will assist in damage detection and model updating. The results of the simulations are displayed in Figures 32 though Figure 46.

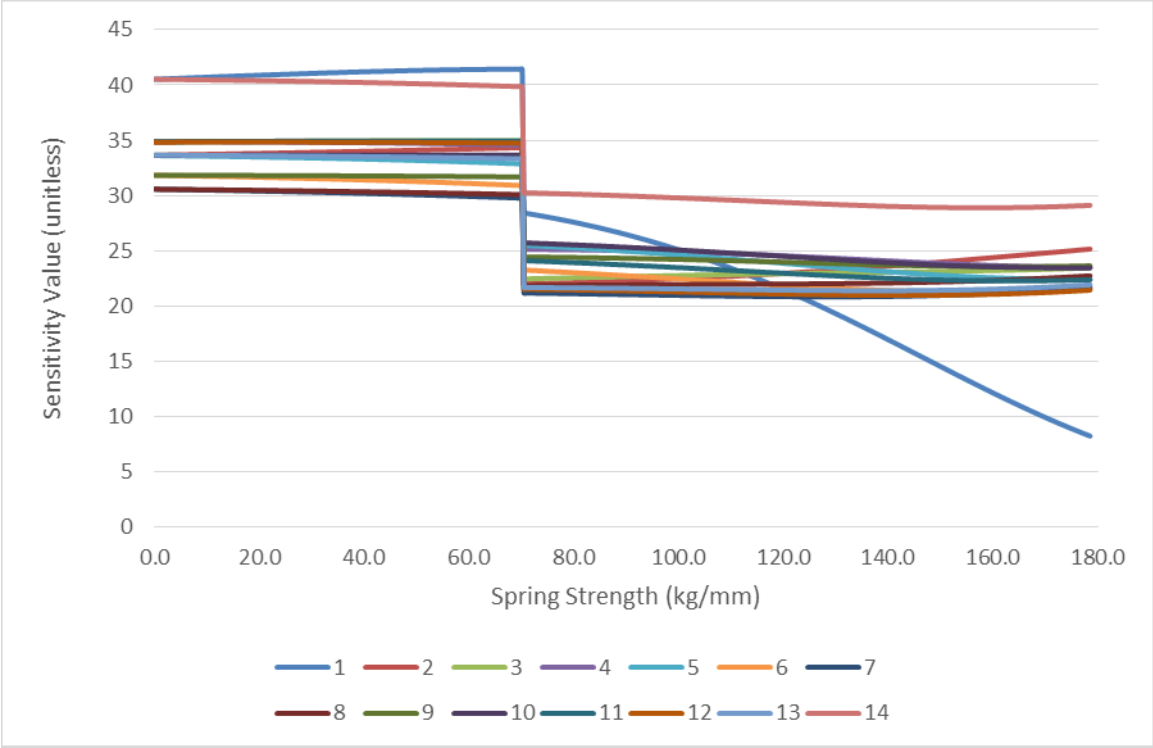

Figure 32. Effects of Spring Strength Variance on Sensitivity Value for Node 2

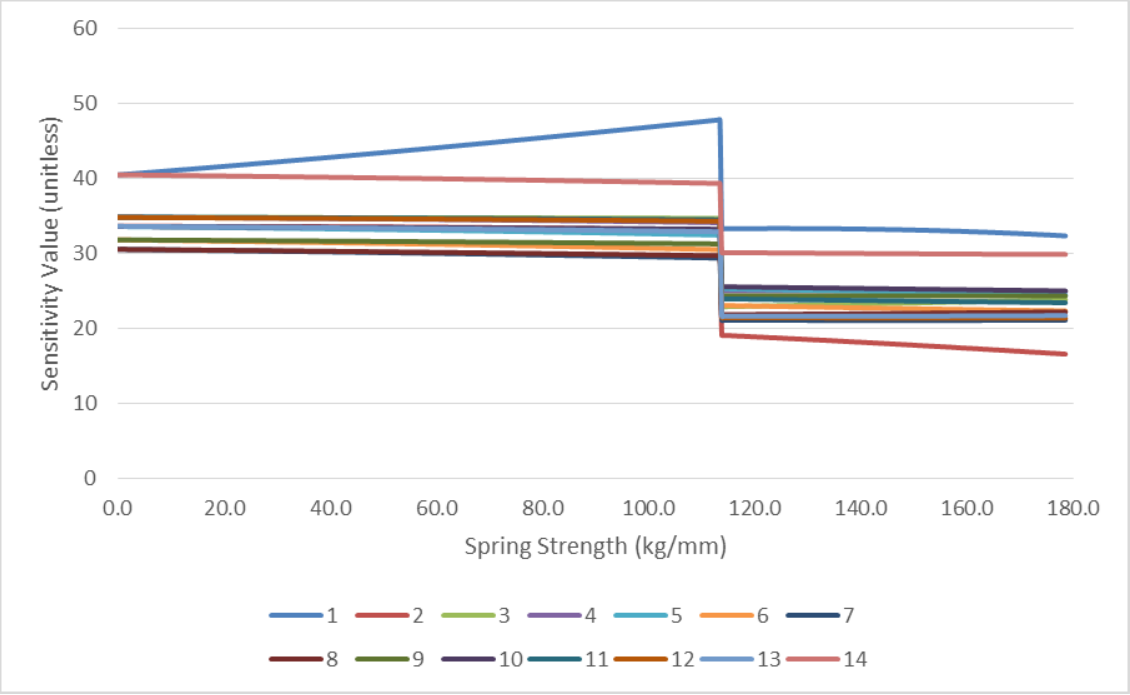

Figure 33. Effects of Spring Strength Variance on Sensitivity Value for Node 3

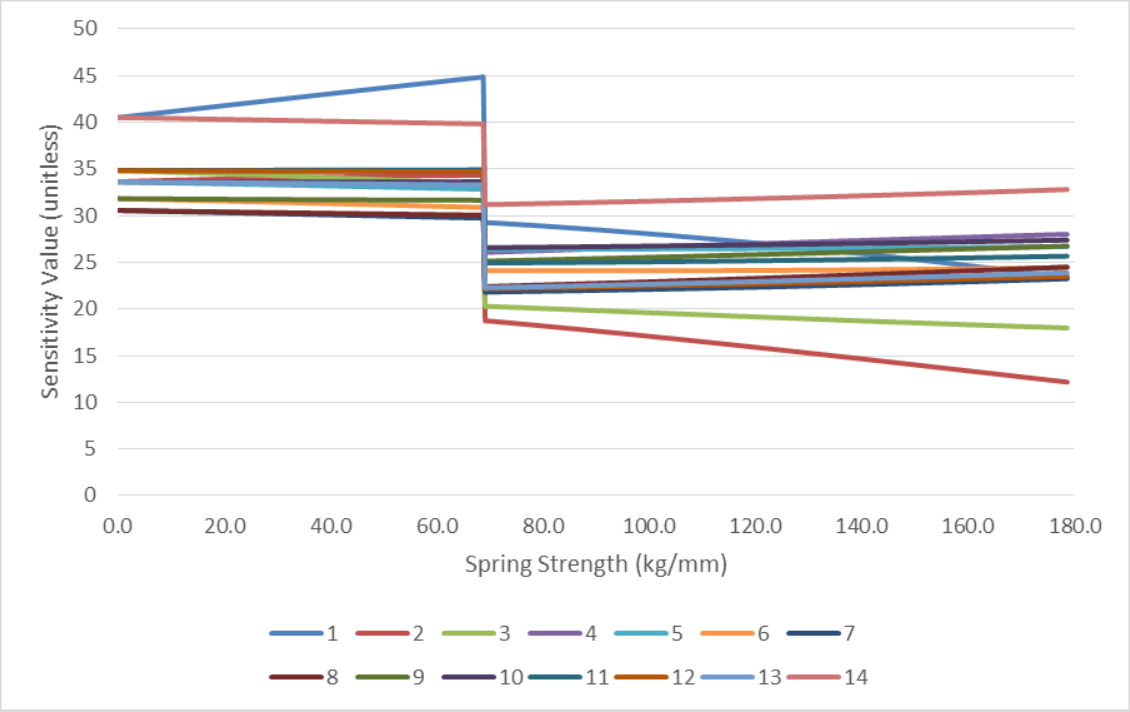

Figure 34. Effects of Spring Strength Variance on Sensitivity Value for Node 4

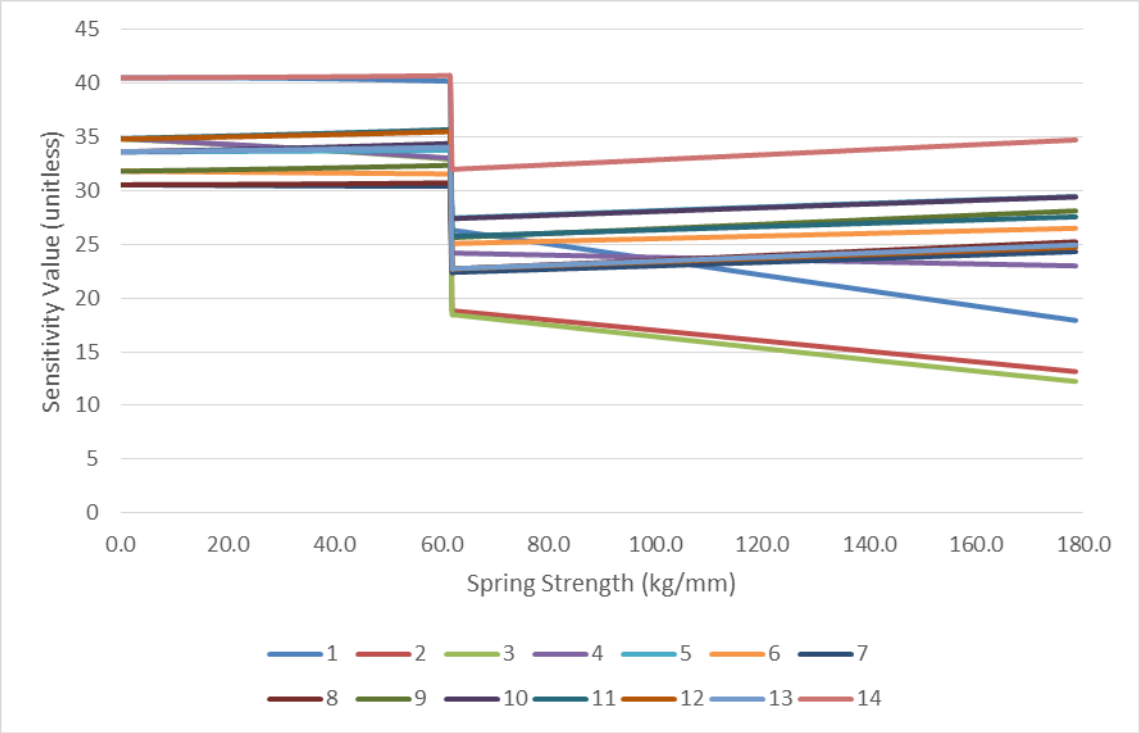

Figure 35. Effects of Spring Strength Variance on Sensitivity Value for Node 5

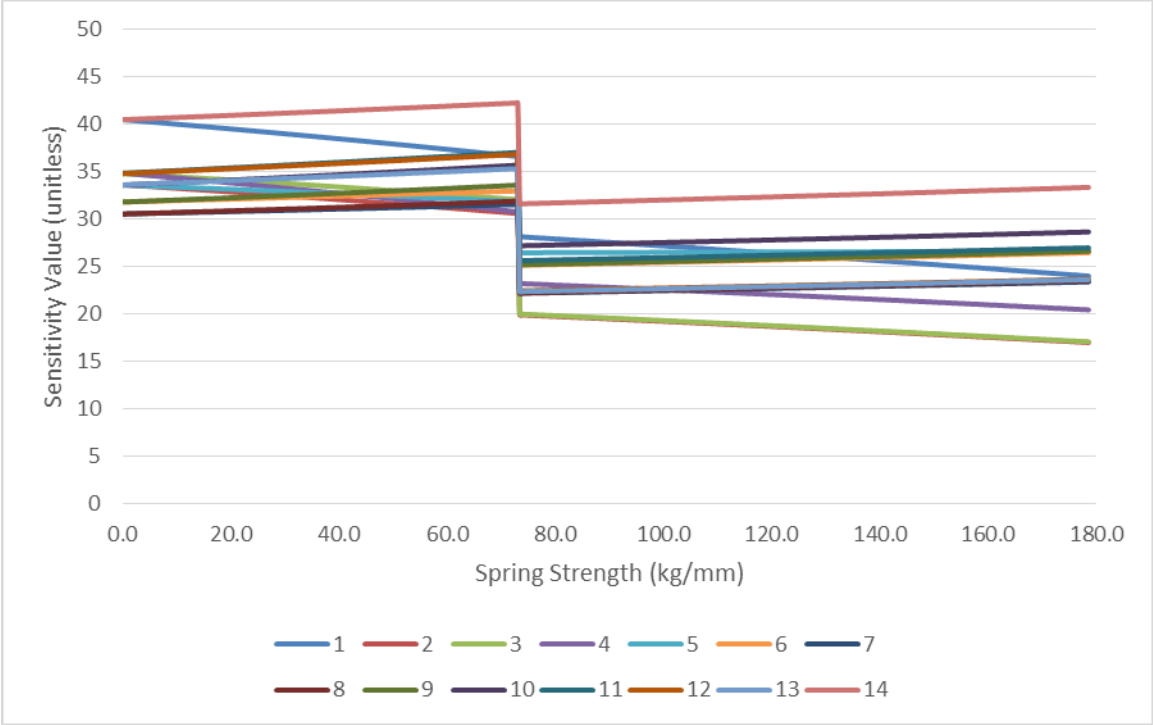

Figure 36. Effects of Spring Strength Variance on Sensitivity Value for Node 6

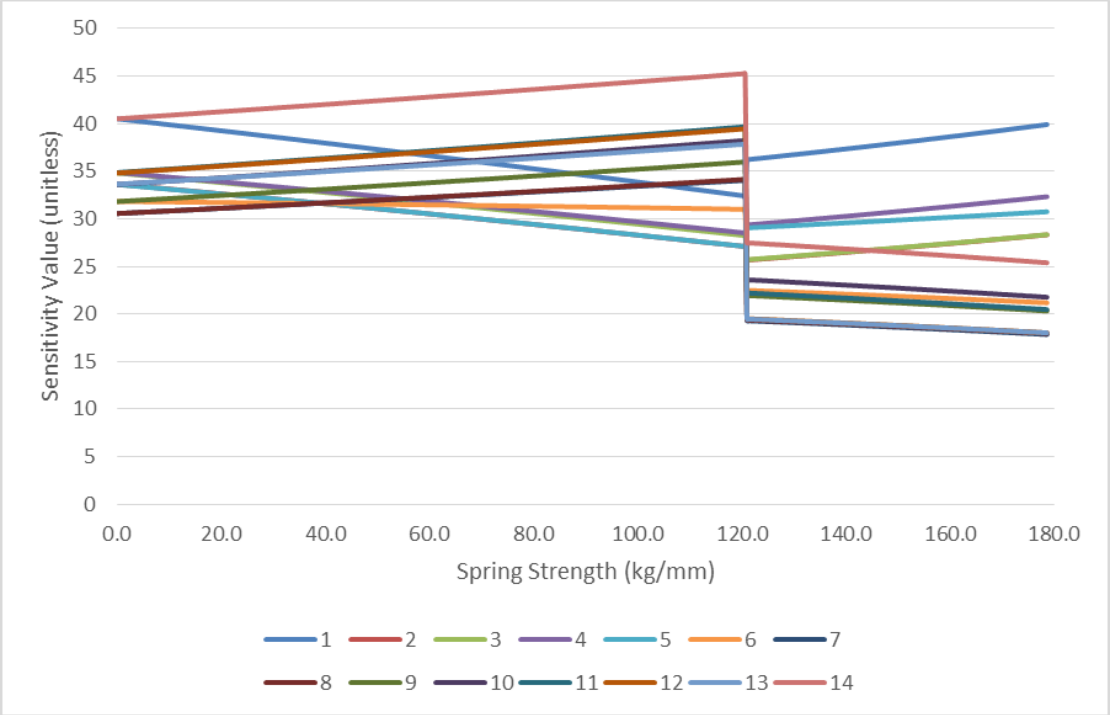

Figure 37. Effects of Spring Strength Variance on Sensitivity Value for Node 7

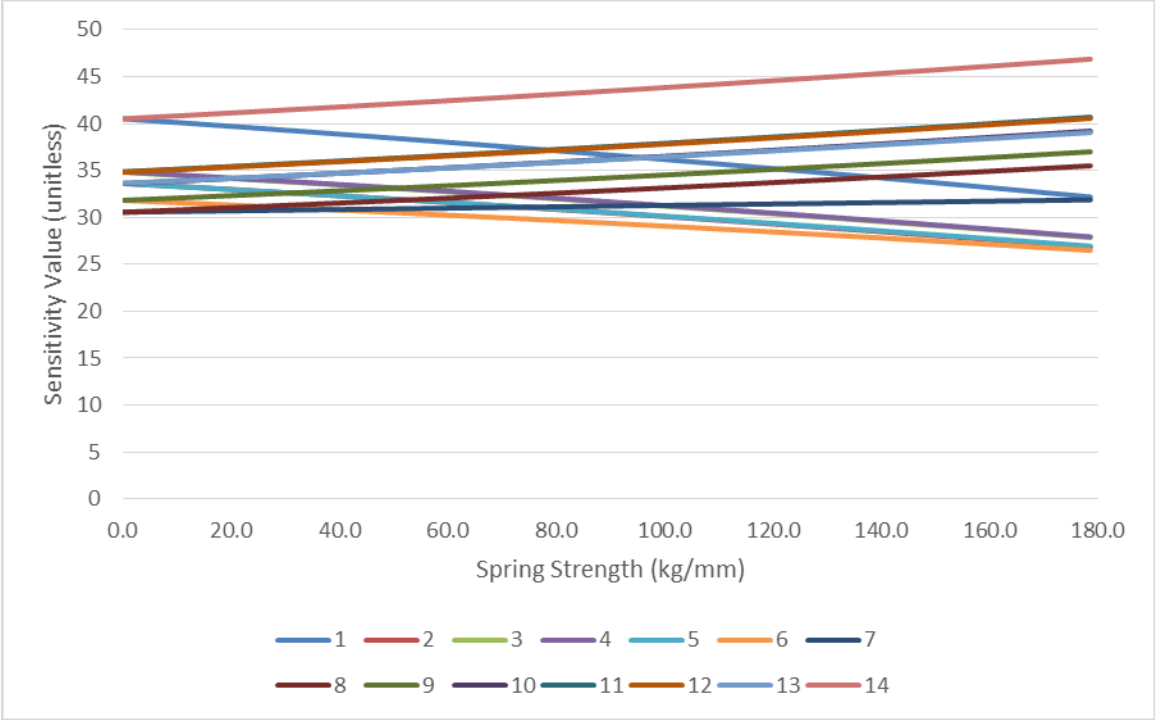

Figure 38. Effects of Spring Strength Variance on Sensitivity Value for Node 8

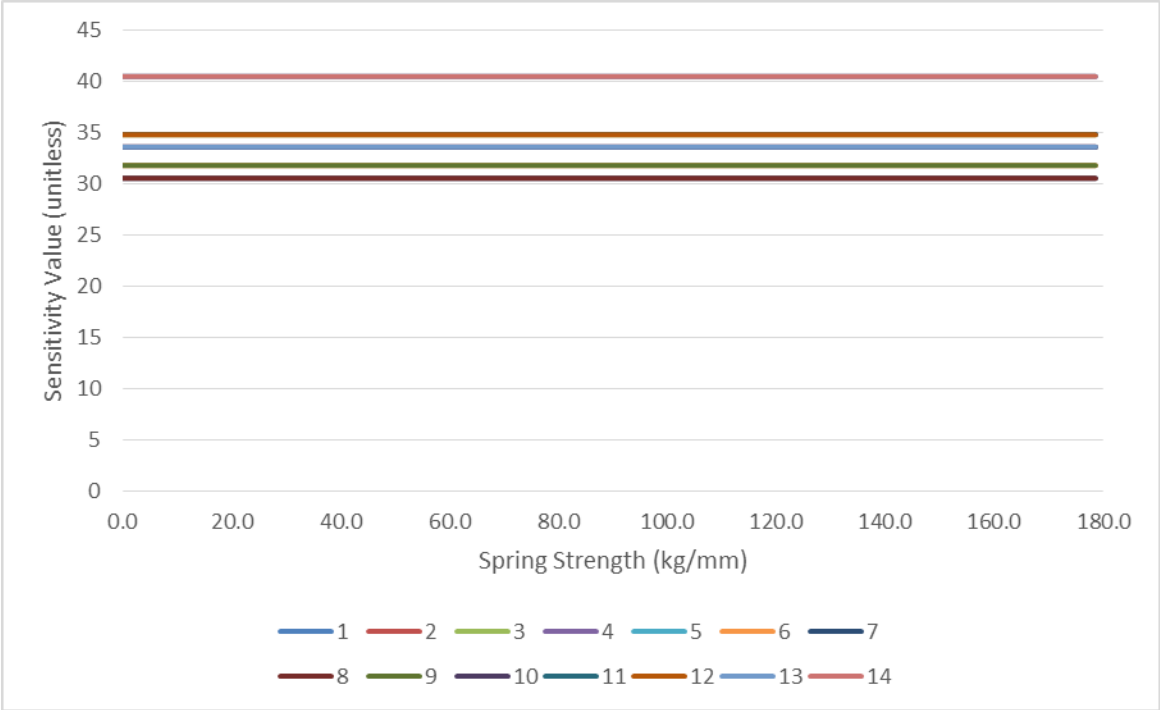

Figure 39. Effects of Spring Strength Variance on Sensitivity Value for Node 9

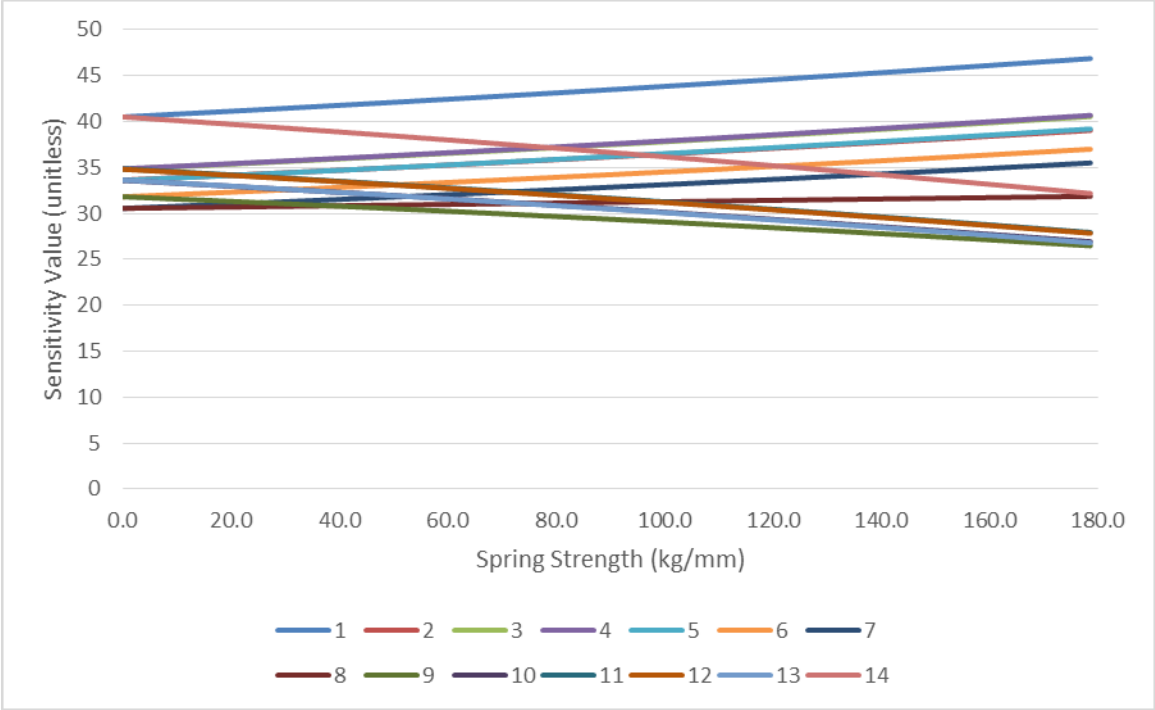

Figure 40. Effects of Spring Strength Variance on Sensitivity Value for Node 10

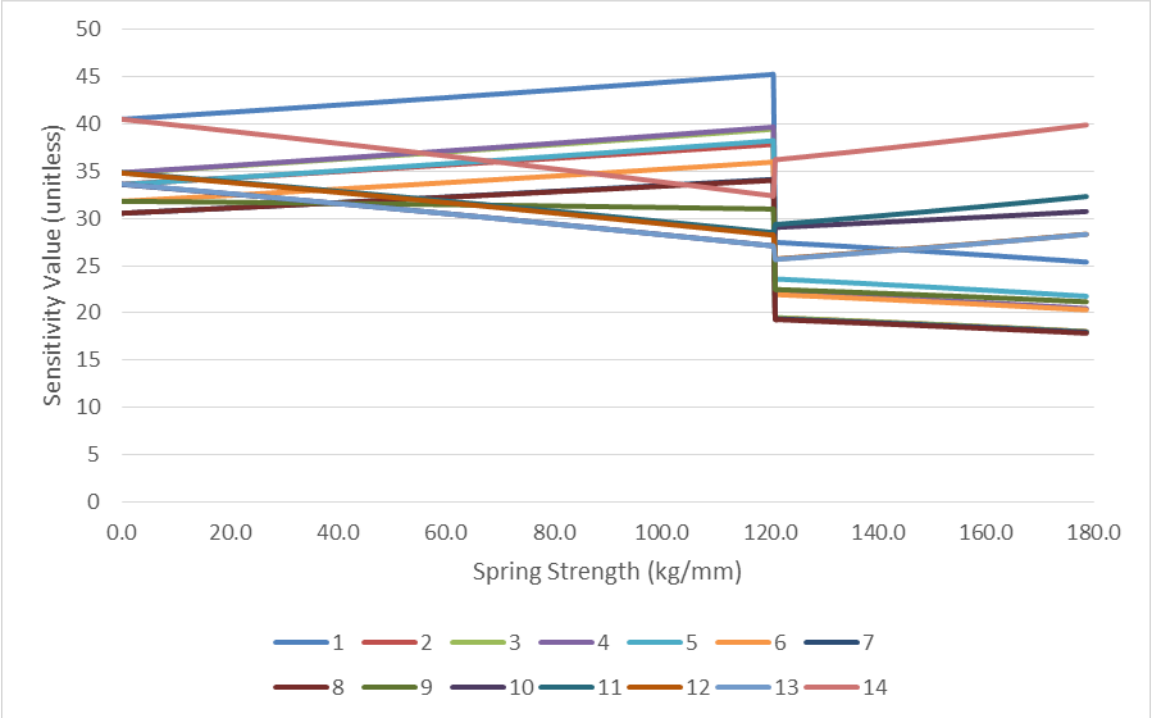

Figure 41. Effects of Spring Strength Variance on Sensitivity Value for Node 11

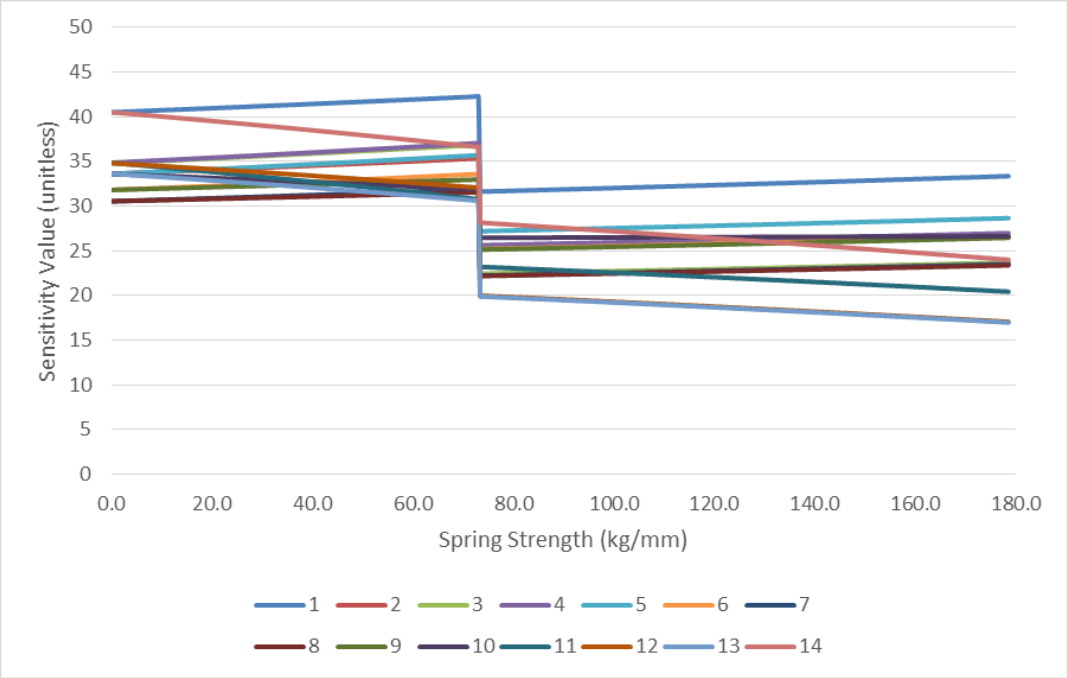

Figure 42. Effects of Spring Strength Variance on Sensitivity Value for Node 12

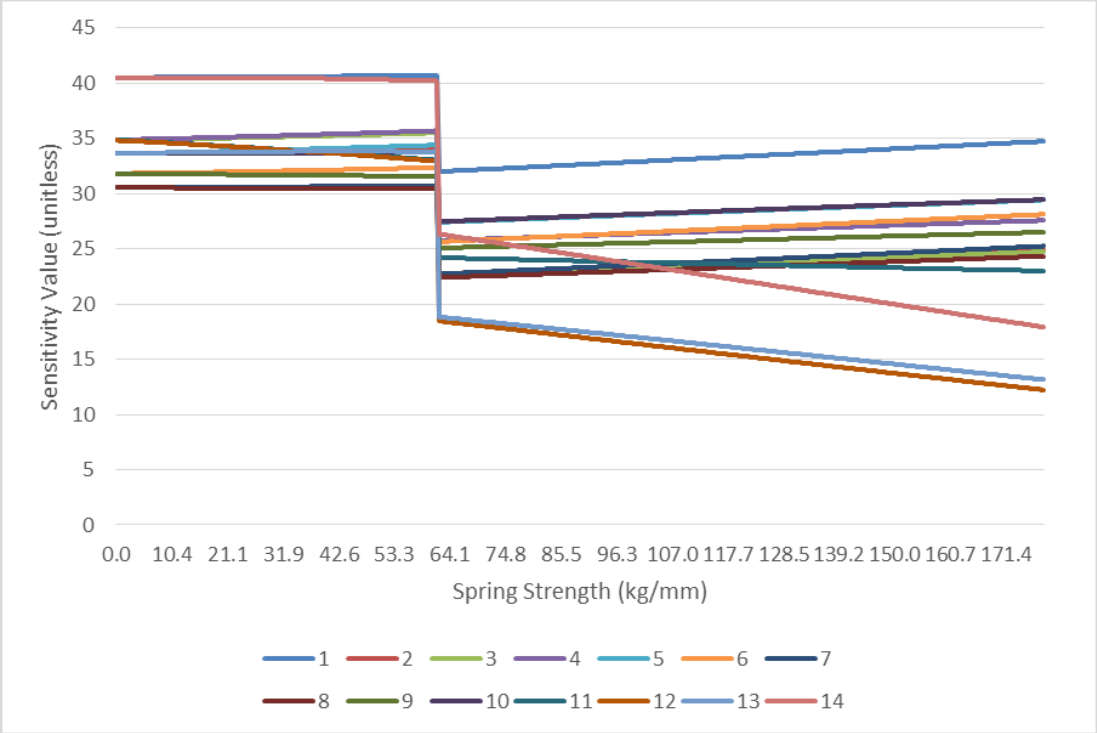

Figure 43. Effects of Spring Strength Variance on Sensitivity Value for Node 13

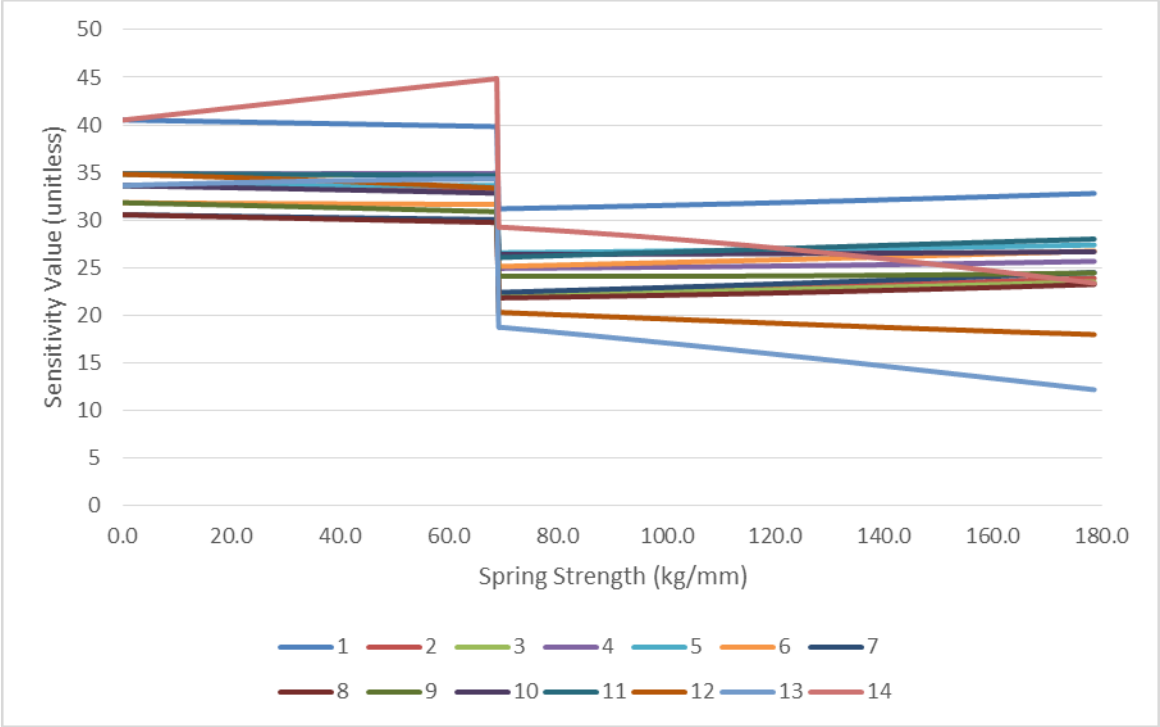

Figure 44. Effects of Spring Strength Variance on Sensitivity Value for Node 14

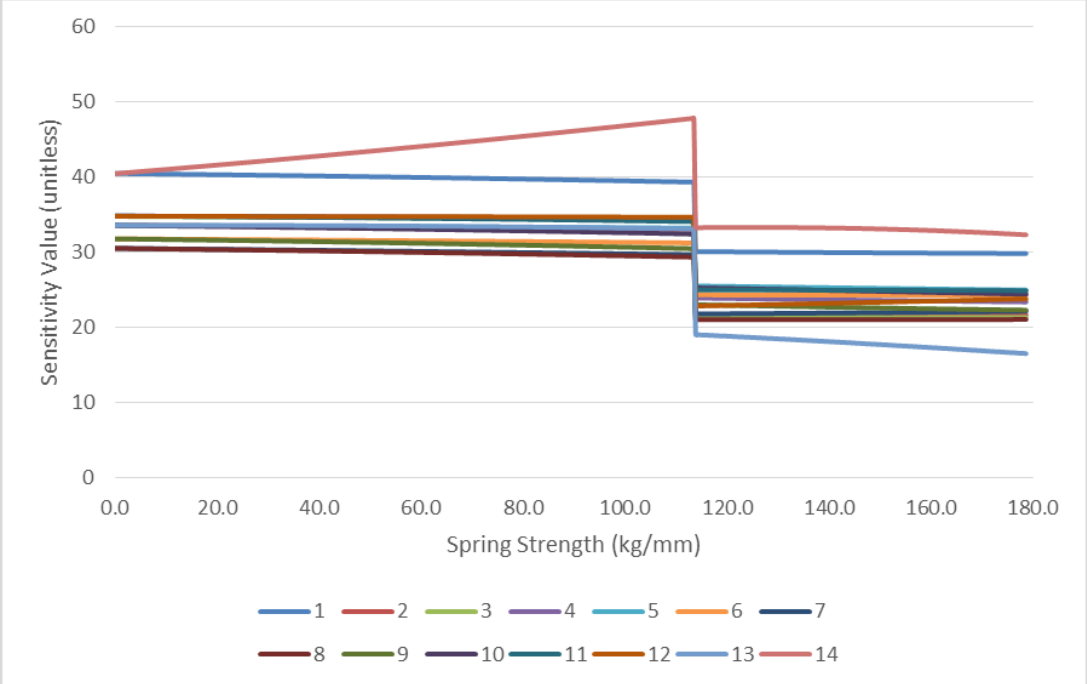

Figure 45. Effects of Spring Strength Variance on Sensitivity Value for Node 15

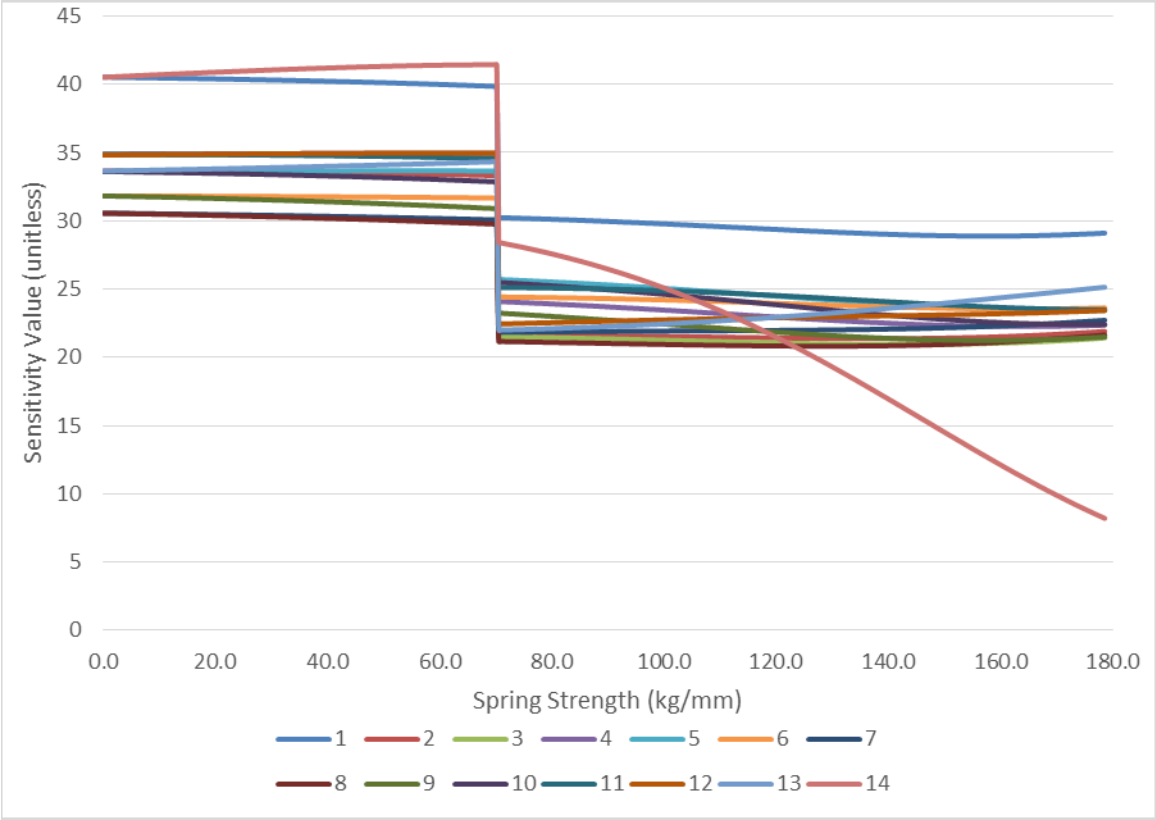

Figure 46. Effects of Spring Strength Variance on Sensitivity Value for Node 16

As was alluded to in Chapter II, one of the concerns of this method is matrix conditioning, otherwise known as the matrix condition number. For the purposes of this thesis, the condition number relates to the linear dependence of the rows and columns in the matrix. An example of how this effects our capability to locate damage is as follows:

If we use the all of the baseline sensitivity matrix and supplement two additional modes from a sensitivity matrix that has an 8.928 kg/mm (500lb/in) spring installed at node 9, we get a square, full rank matrix that has a matrix condition number of 6.7441e+11. This high of a condition number indicates a poorly conditioned matrix that most likely will not produce accurate results. For example, Figure 47 is the result of using this sensitivity matrix to find 5% damage at node 6

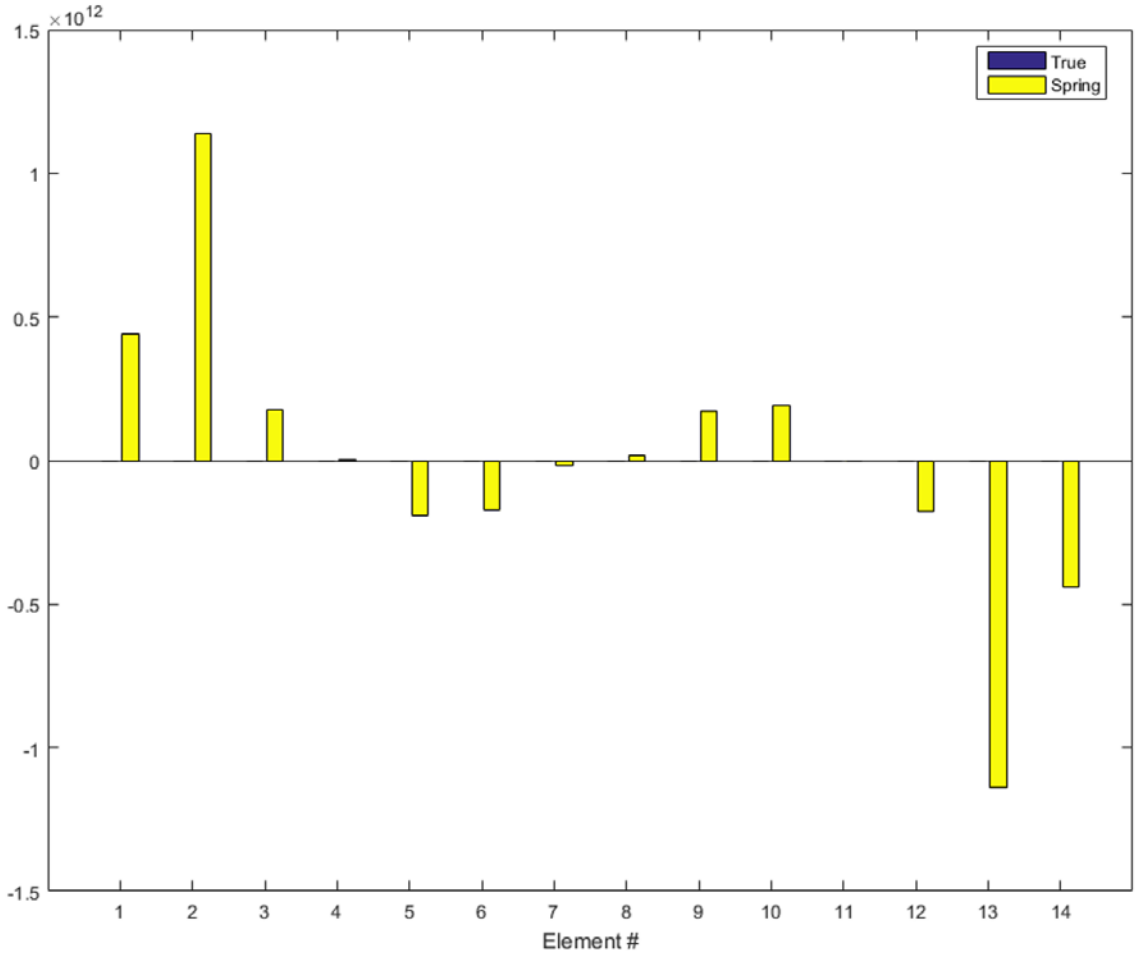

Figure 47. Model Error vs True Error Using Poorly Conditioned Sensitivity Matrix

However, sensitivity matrix that has two baseline modes and twelve modes from a sensitivity matrix that has a 178.579 kg/mm (10000lb/in) spring installed at node 2, we also have a square, full rank matrix with a matrix condition number of 1.7671e+04. This condition number indicates a better conditioned matrix that most likely will produce accurate results. For example, Figure 48 is the result of using this matrix to find the same 5% damage at node 6.

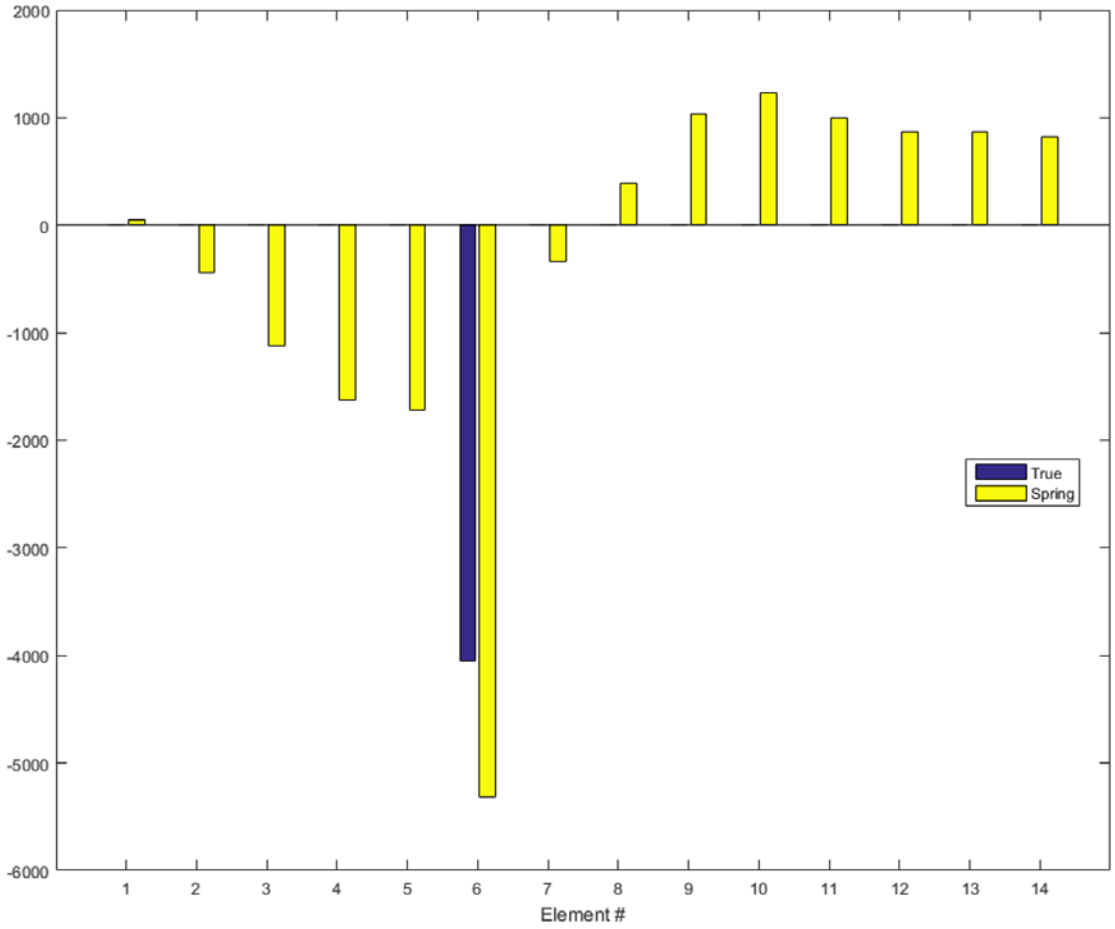

Figure 48. Model Error vs True Error Using a Well Conditioned Sensitivity Matrix

Because of this, we identified spring stiffness values from Figures 32 through Figure 46 that varied greatly from baseline, and from each other. These spring strengths are identified in Table 9.

Table 9. Useable Single Spring Strengths

Node	Spring Strength kg/mm (lb/mm)	
2	71.43(4000)	178.58(10000)
3	107.15(6000)	178.58(10000)
4	64.29(3600)	178.58(10000)
5	71.43(4000)	178.58(10000)
6	67.86(3800)	178.58(10000)
7	116.08(6500)	178.58(10000)
8	71.43(4000)	178.58(10000)
9	Not useable	
10	71.43(4000)	178.58(10000)
11	116.08(6500)	178.58(10000)
12	67.86(3800)	178.58(10000)
13	71.43(4000)	178.58(10000)
14	64.29(3600)	178.58(10000)
15	107.15(6000)	178.58(10000)
16	71.43(4000)	178.58(10000)

As noted in Table 9, Node 9 was determined to be unusable due to no variance in the sensitivity. This lack of variance may be due to its location in the middle of the beam and the symmetric characteristics a free-free beam exhibits.

Because the baseline sensitivity matrix is both under-determined and not full rank, we used the sensitivity matrices from the baseline and those developed from the spring strengths detailed in Table 9 to build an overall composite sensitivity matrix.

$$\left[S_{comp}\right] = \begin{bmatrix} \left[S^{0}\right] \\ \left[S^{N13-4,000}\right] \\ \left[S^{N13-10,000}\right] \end{bmatrix} \tag{4.6}$$

Equation (4.6) is an example of how a composite sensitivity matrix could be developed where $\left[S^{0}\right]$ is the baseline sensitivity matrix and $\left[S^{N13-10,000}\right]$ is the

sensitivity matrix as developed from using a 10,000 lbf/in spring on node 13. To make a square composite matrix, we take a selected number of rows separate from each configurations. An easily repeatable method is to extract a fixed set series of rows from either the top or bottom of a sensitivity matrix and determining the overall matrix condition number. A high condition number indicates poor matrix conditioning and likely will have large errors when used in calculations, whereas a low condition number indicates linear independence between the rows and columns of the matrix. A matrix with a condition number of 1 will be perfectly accurate in solving a system of equations.

As there are many different possible combinations of the sensitivity matrices that would still get a square, full-rank matrix for damage detection, we calculated the condition number for several different scenarios. The first series of calculations determine how many baseline modes should be used in the development of the composite sensitivity matrix, and whether to use higher frequency modes, or to use lower frequency modes. The composite matrix was built under the following system where the variable “r” indicates the number of rows from either the top (for low modes) or bottom (for high modes) of that matrix. Using equation (4.7), Figure 49 and Figure 50 show the effects the number of baseline modes has on the sensitivity matrix condition number.

$$\left[S_{comp}\right]_{14x14} = \begin{bmatrix} \left[S^{0}\right]_{r\times 14} \\ \left[S^{N7-6,500}\right]_{(14-\mathrm{r})x14} \end{bmatrix} \tag{4.7}$$

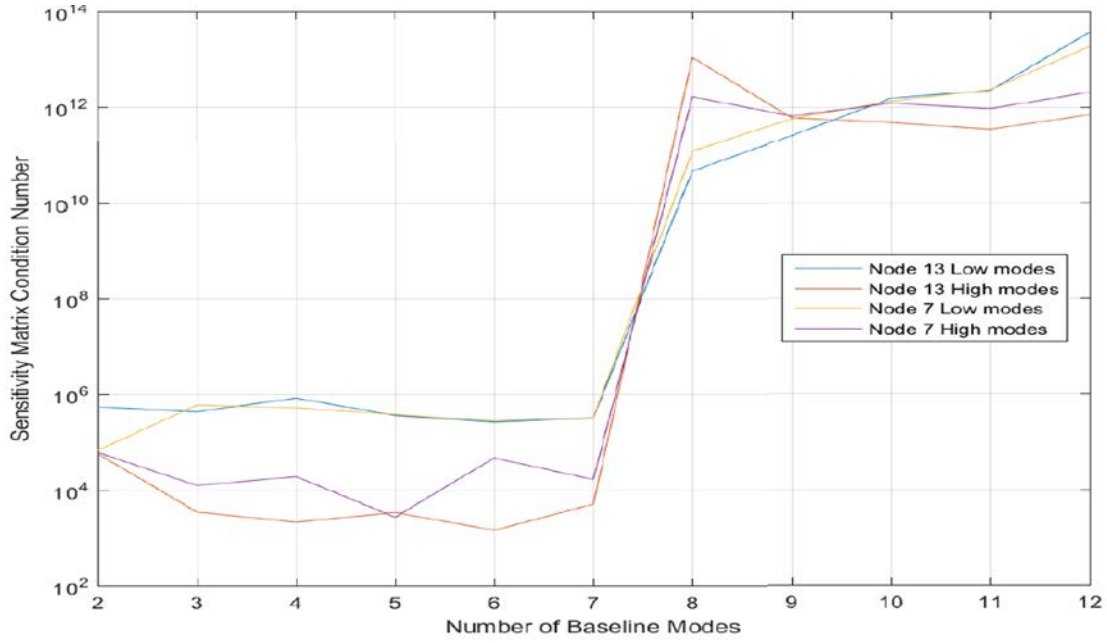

Figure 49. Effect of Number of Baseline Modes Used in Sensitivity Matrix on Condition Number, Single Node, 178.579 kg/mm (10,000 lb/in) Artificial Spring

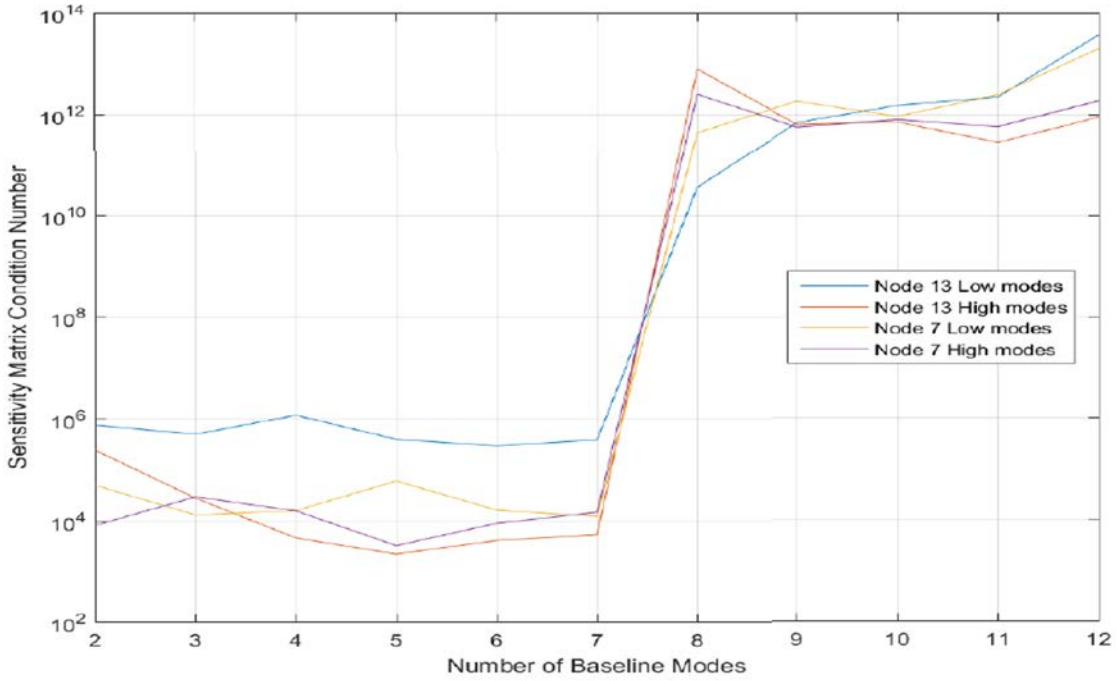

Figure 50. Effect of Number of Baseline Modes Used in Sensitivity Matrix on Condition Number, 71.431kg/mm (4000lb/in) (Node 13) 116.076 kg/mm (6500lb/in) (Node 7)

For the development of Figure 51, the sensitivity matrix comprised of values from three matrices: Baseline, Single-Spring Mid-Strength, and Single-Spring High Strength. Using the same rules developing equation (4.7), the sensitivity matrix was developed using equation (4.8)

$$\left[S_{comp}\right]_{14x14} = \begin{bmatrix} \left[S^{0}\right]_{\mathrm{r}\times 14} \\ \left[S^{N7-6,500}\right]_{\frac{(14-\mathrm{r})}{2}x14} \\ \left[S^{N7-10,00}\right]_{\frac{(14-\mathrm{r})}{2}x14} \end{bmatrix} \tag{4.8}$$

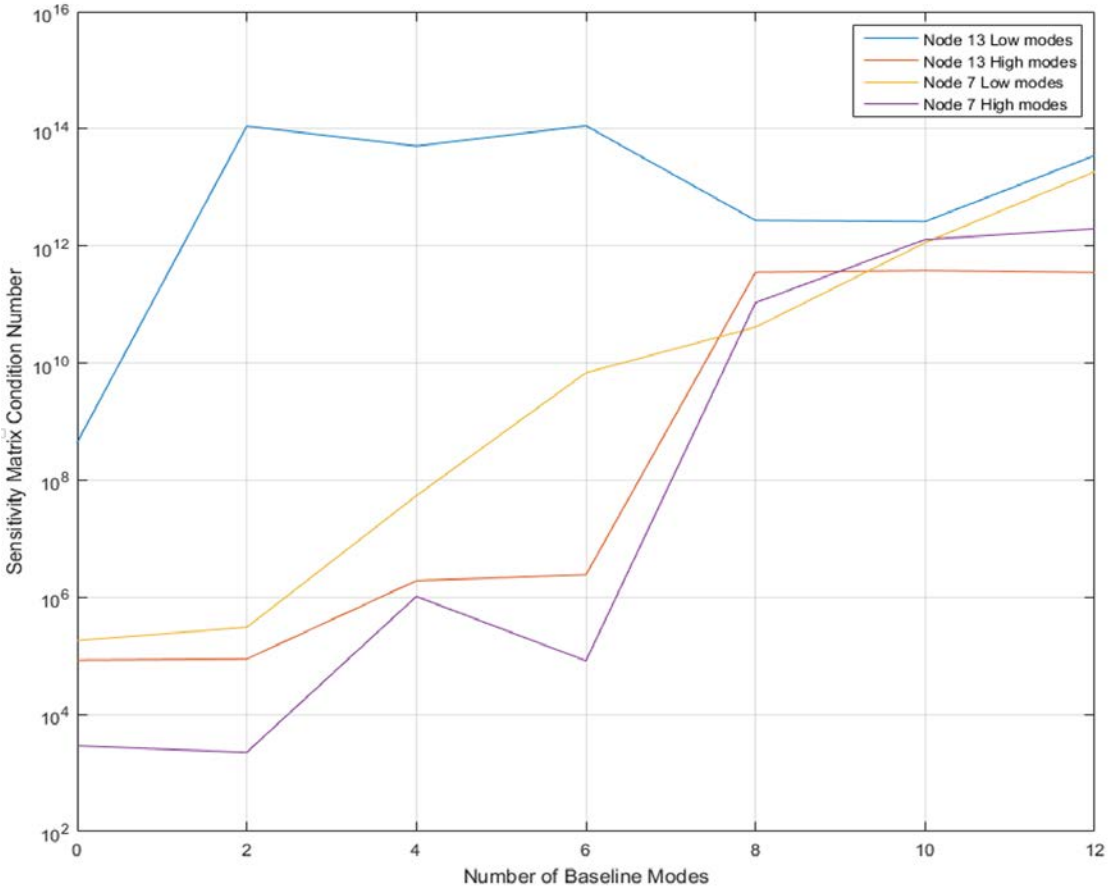

Figure 51. Effect of Number of Baseline Modes Used in Sensitivity Matrix on Condition Number, 71.431 & 178.579kg/mm (4,000&10,000lb/in) on Node 13, 116.076 & 178.579kg/mm (6,500&10,000lb/in) on Node 7

Figure 49 through Figure 51 indicate to us that the best-conditioned composite sensitivity matrices (lowest matrix condition number) are found when we use two or less modes from the baseline sensitivity matrix and when using at least two modified matrices. Additionally, these figures confirm previous thesis work [11] in that the use of higher order modes will provide a more accurate solution in damage detection as opposed to using low order modes.

Using the identified useable conditions noted in Table 9, we can combine modes from different spring strengths and different nodes. We can combine these different conditions into a composite sensitivity matrix, and then evaluate the matrix condition number. From this, we developed a map of possible combinations for spring strengths and nodes based on an index system, as displayed in Table 10.

Table 10. Single Spring Index for Evaluating Condition Number

Index Number	Node	Spring kg/mm (lb/in)
1	2	71.43(4000)
2	2	178.58(10000)
3	3	107.15(6000)
4	3	178.58(10000)
5	4	64.29(3600)
6	4	178.58(10000)
7	5	71.43(4000)
8	5	178.58(10000)
9	6	67.86(3800)
10	6	178.58(10000)
11	7	116.08(6500)
12	7	178.58(10000)
13	8	71.43(4000)
14	8	178.58(10000)

Index Number	Node	Spring kg/mm (lb/in)
15	10	71.43(4000)
16	10	178.58(10000)
17	11	116.08(6500)
18	11	178.58(10000)
19	12	67.86(3800)
20	12	178.58(10000)
21	13	71.43(4000)
22	13	178.58(10000)
23	14	64.29(3600)
24	14	178.58(10000)
25	15	107.15(6000)
26	15	178.58(10000)
27	16	71.43(4000)
28	16	178.58(10000)

Using equation (4.8), two modes where used from baseline and six modes where used from two different indexes identified in Table 10 to form a square, full rank sensitivity matrix.

$$\left[S^{(K1)}\right]=\left[\begin{array}{c}\left[Mode(1)\right]\\ \left[Mode(2)\right]\\ \vdots\\ \left[Mode(n-5)\right]\\ \vdots\\ \left[Mode(n)\right]\end{array}\right]\leftarrow ModesUtilized$$

$$\left[S^{(K2)}\right]=\left[\begin{array}{c}\left[Mode(1)\right]\\ \left[Mode(2)\right]\\ \vdots\\ \left[Mode(n-5)\right]\\ \vdots\\ \left[Mode(n)\right]\end{array}\right]\leftarrow ModesUtilized$$

$$\rightarrow\left[S_{comp}\right]=\left[\begin{array}{c}\left[S^{(0)}\right]_{2\times 14}\\ \left[S^{(K1)}\right]_{6\times 14}\\ \left[S^{(K2)}\right]_{6\times 14}\end{array}\right] \qquad (4.9)$$

This composite sensitivity matrix was then evaluated for its condition number and compared to the remaining possible combinations. In total, there are 784 different combinations, all with different condition numbers indicating the accuracy of that matrix's capability to evaluate damage. To assist in determining what combination worked best, the index of Table 10 was used to develop Figure 52 and Figure 53.

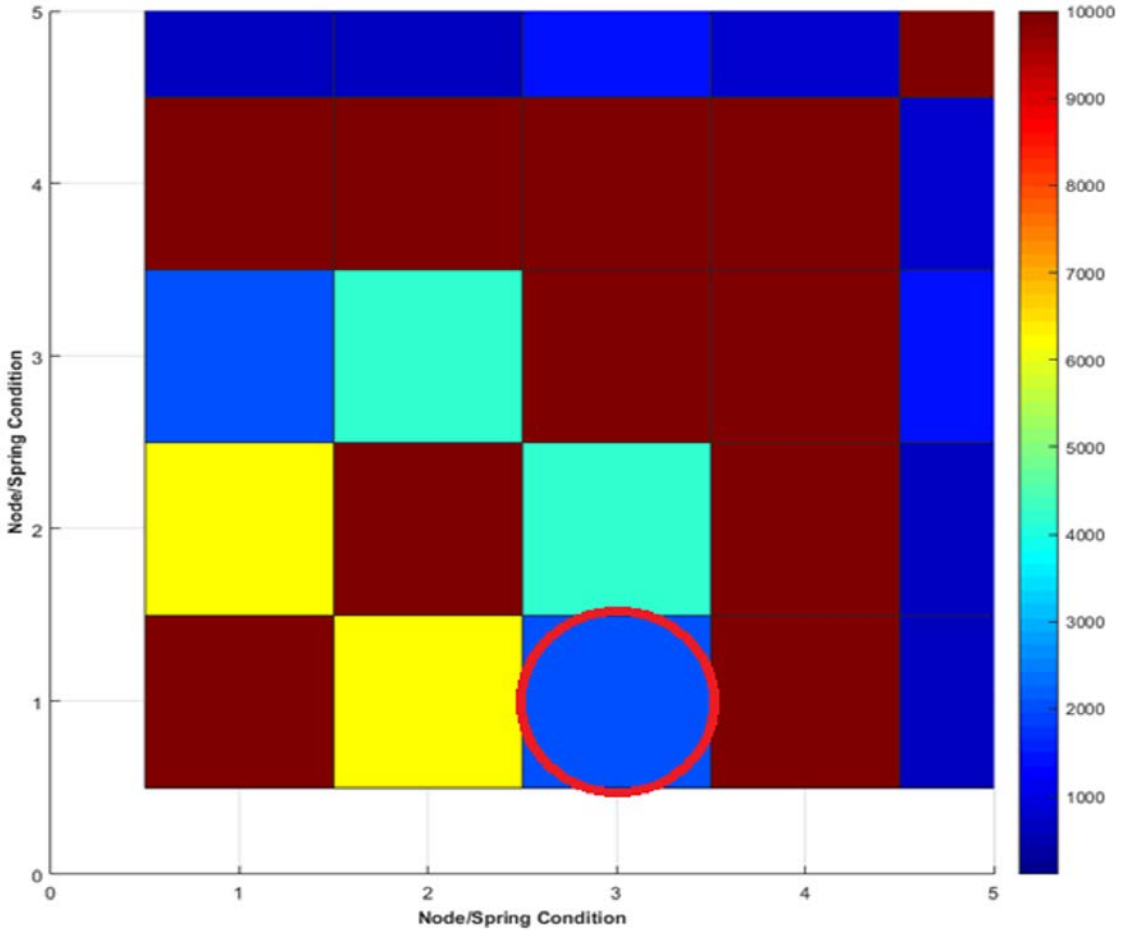

Figure 52. Sensitivity Matrix Condition Number Index Example

Figure 52 is a magnified view of all possible combinations using the index provided in Table 10. The color of the identified box indicates the condition number of a composite sensitivity matrix consisting of the two highest baseline modes and of six highest modes from the sensitivity matrix from index 1 and index 3 as explained in equation (4.10). In this instance, the corresponding condition number is approximately 2600

$$\left[S_{comp}\right]_{14x14} = \begin{bmatrix} \left[S^{0}\right]_{2\times14} \\ \left[S^{N3-6,000}\right]_{6\times14} \\ \left[S^{N2-4,000}\right]_{6\times14} \end{bmatrix} \tag{4.10}$$

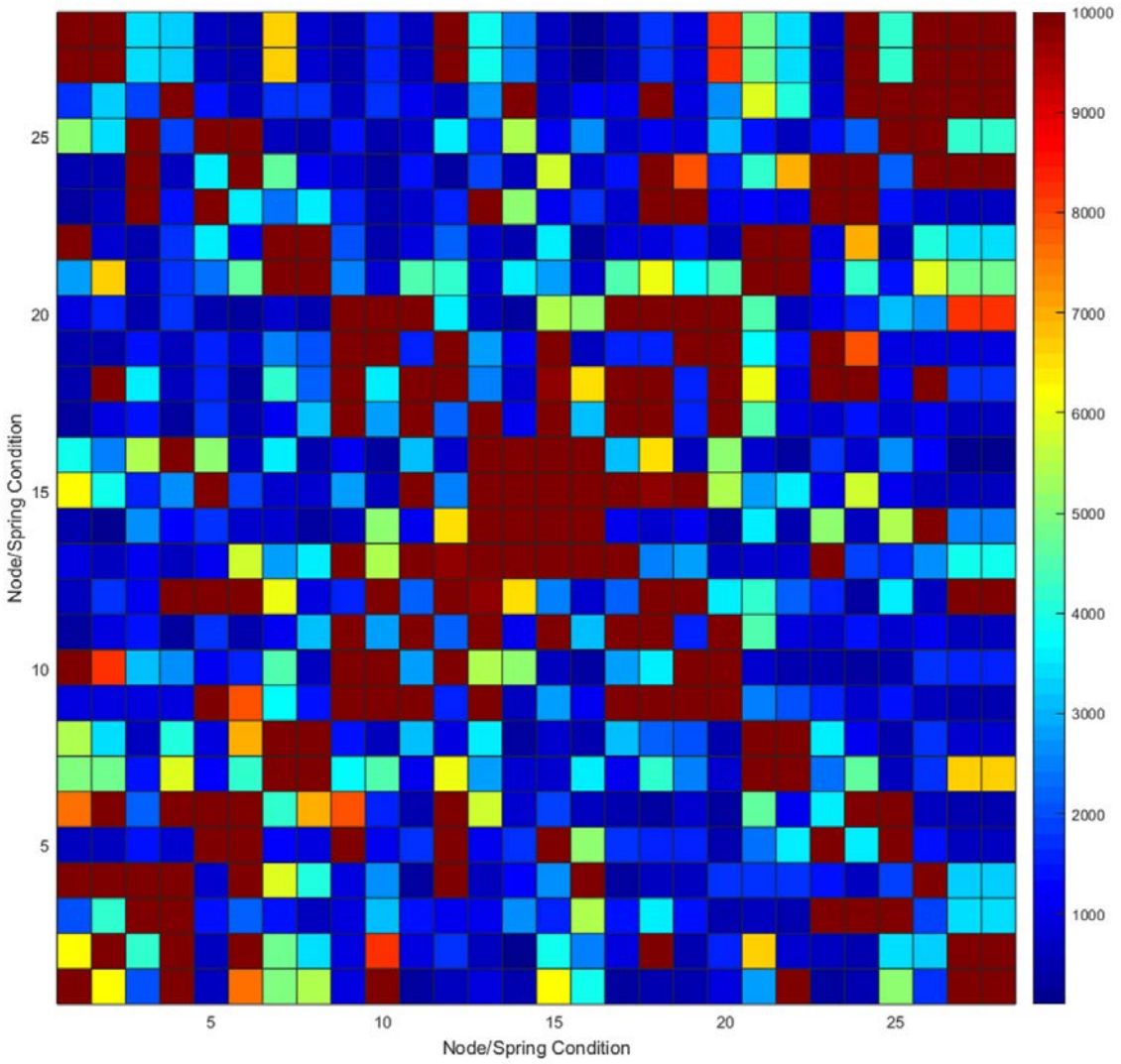

Figure 53. Sensitivity Matrix Combination Condition Number Indicator, Single Spring

We want to minimize the matrix condition number to get the most accurate damage detection solution. By analyzing Figure 53, the combination of index 2 combined with index 17 will provide the most accurate solution since it has the lowest condition number of 237.9826. thus, the composite sensitivity matrix is displayed in equation (4.11) and equation (4.12)

$$\left[S_{comp}\right]_{14x14} = \begin{bmatrix} \left[S^{0}\right]_{2\times14} \\ \left[S^{N2-10,000}\right]_{6\times14} \\ \left[S^{N8-10,000}\right]_{6\times14} \end{bmatrix} \tag{4.11}$$

$$\left[S_{comp}\right] = \begin{bmatrix} 30.602 & 21.625 & 21.721 & 24.831 & 26.337 & 24.357 & 21.478 & 21.478 & 24.357 & 26.337 & 24.831 & 21.721 & 21.625 & 30.602 \\ 40.523 & 33.646 & 34.824 & 34.873 & 33.613 & 31.827 & 30.562 & 30.562 & 31.827 & 33.613 & 34.873 & 34.824 & 33.646 & 40.523 \\ 3.753 & 2.661 & 4.691 & 2.557 & 4.908 & 2.313 & 5.137 & 2.096 & 5.343 & 1.906 & 5.487 & 1.733 & 6.492 & 2.346 \\ 6.363 & 2.939 & 9.173 & 3.534 & 7.342 & 6.214 & 4.394 & 8.727 & 2.922 & 8.808 & 4.241 & 6.295 & 8.107 & 5.097 \\ 8.552 & 6.003 & 9.608 & 12.014 & 5.496 & 10.907 & 10.873 & 5.504 & 12.049 & 9.482 & 6.050 & 12.661 & 8.916 & 9.529 \\ 7.669 & 13.961 & 9.272 & 14.572 & 16.229 & 10.066 & 11.366 & 16.908 & 12.962 & 9.304 & 15.003 & 15.823 & 10.497 & 15.475 \\ 3.037 & 22.123 & 17.293 & 14.183 & 16.335 & 20.123 & 19.095 & 15.003 & 14.825 & 18.864 & 20.241 & 16.512 & 14.620 & 22.025 \\ 8.209 & 25.143 & 23.434 & 23.485 & 22.415 & 21.495 & 21.650 & 22.723 & 23.626 & 23.443 & 22.367 & 21.424 & 21.908 & 29.105 \\ 5.666 & 13.570 & 4.953 & 10.697 & 5.804 & 6.615 & 2.092 & 1.214 & 0.995 & 0.731 & 1.209 & 0.564 & 1.551 & 0.647 \\ 2.513 & 2.697 & 3.402 & 1.472 & 3.651 & 0.214 & 9.187 & 7.016 & 12.142 & 13.910 & 6.252 & 14.829 & 11.714 & 10.918 \\ 20.275 & 15.918 & 24.749 & 16.239 & 13.801 & 19.067 & 4.231 & 5.373 & 7.116 & 3.983 & 4.676 & 7.167 & 4.607 & 5.869 \\ 11.231 & 7.302 & 9.489 & 11.072 & 8.875 & 6.187 & 20.493 & 24.326 & 17.290 & 20.812 & 27.366 & 23.359 & 17.978 & 27.651 \\ 41.616 & 30.100 & 29.711 & 32.768 & 35.585 & 25.396 & 13.627 & 17.296 & 18.541 & 19.231 & 18.006 & 16.318 & 16.531 & 22.855 \\ 32.193 & 26.820 & 27.857 & 27.942 & 26.946 & 26.488 & 31.874 & 35.510 & 37.005 & 39.210 & 40.693 & 40.560 & 39.051 & 46.874 \end{bmatrix} \tag{4.12}$$

To test the capability of this matrix, an identical FEM was made that included damage in one of the elements. Because we made the sensitivity matrix for the flexural rigidity (EI), damage was simulated by decreasing the EI value in one element by 5%, and tested for the length of the beam, thus including all 15 elements. As detailed in Chapter II, this is accomplished by solving equation (2.46), which has been adapted and displayed here as equation (4.13) and equation(4.14):

$$\begin{bmatrix} \left[S^{0}\right]_{2\times14} \\ \left[S^{N2-10,000}\right]_{6\times14} \\ \left[S^{N8-10,000}\right]_{6\times14} \end{bmatrix}^{-1} \begin{Bmatrix} \left\{\Delta\lambda^{0}\right\}_{2\times1} \\ \left\{\Delta\lambda^{N2-10,000}\right\}_{6\times1} \\ \left\{\Delta\lambda^{N8-10,000}\right\}_{6\times1} \end{Bmatrix} = \begin{Bmatrix} \Delta EI_{1} \\ \Delta EI_{2} \\ \vdots \\ \Delta EI_{14} \end{Bmatrix} \tag{4.13}$$

$$\left[S_{comp}\right]^{-1}_{14\times14} \left\{\Delta\lambda_{comp}\right\}_{14\times1} = \left\{\Delta EI\right\}_{14\times1} \tag{4.14}$$

Figures 54 through Figure 67 show the results of testing for simulated damage in every possible location. The simulated error is identified as the blue line, and solution provided using equation (4.13) and (4.14) is in yellow.

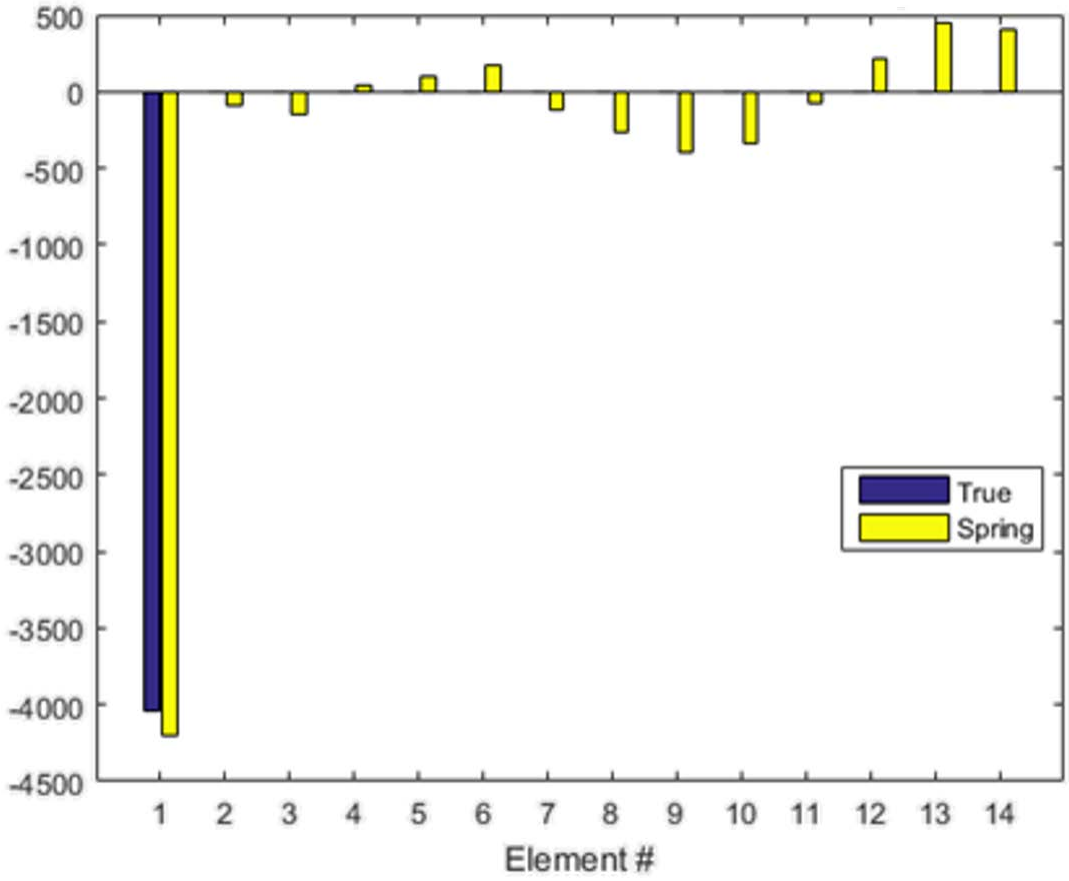

Figure 54. Single Spring Error Identification with Damage at Element 1

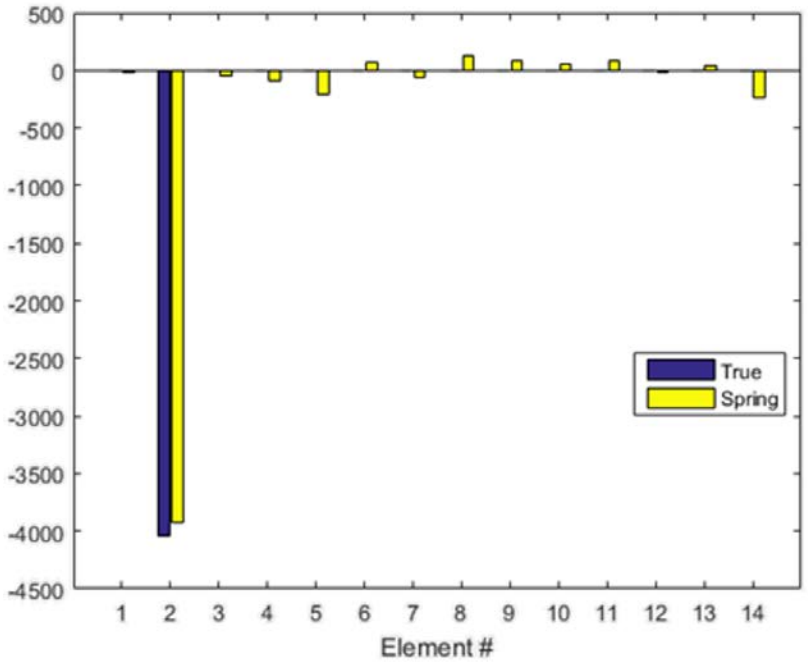

Figure 55. Single Spring Error Identification with Damage at Element 2

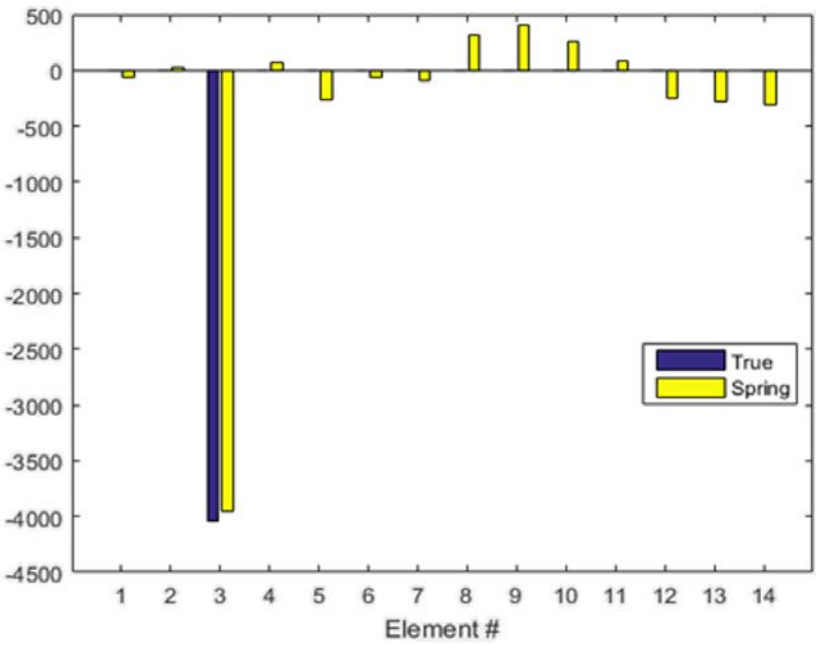

Figure 56. Single Spring Error Identification with Damage at Element 3

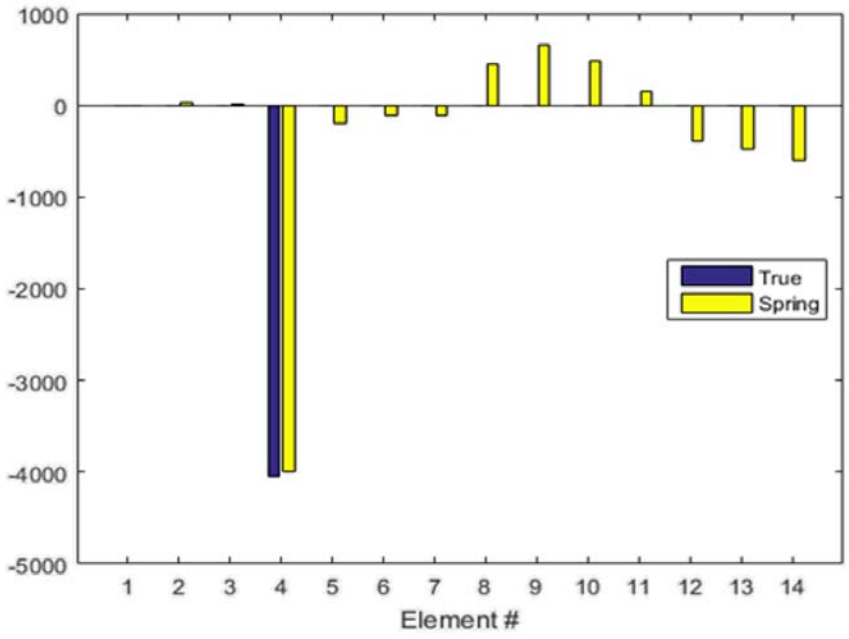

Figure 57. Single Spring Error Identification with Damage at Element 4

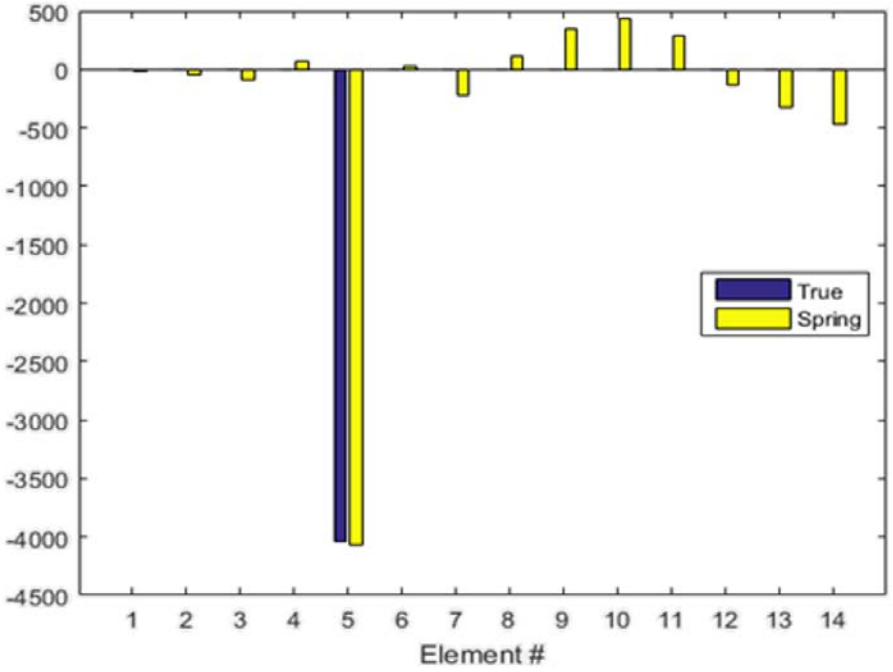

Figure 58. Single Spring Error Identification with Damage at Element 5

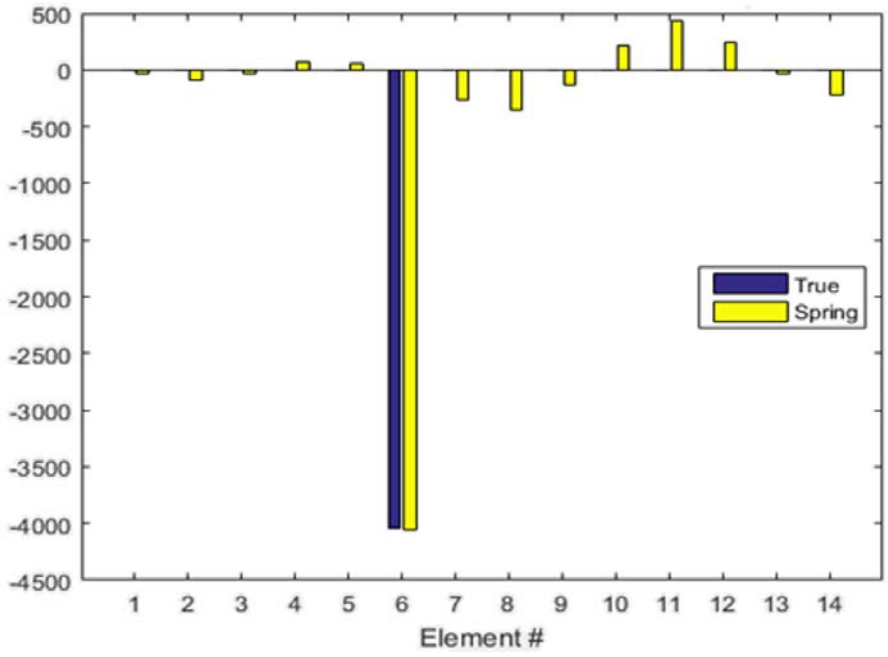

Figure 59. Single Spring Error Identification with Damage at Element 6

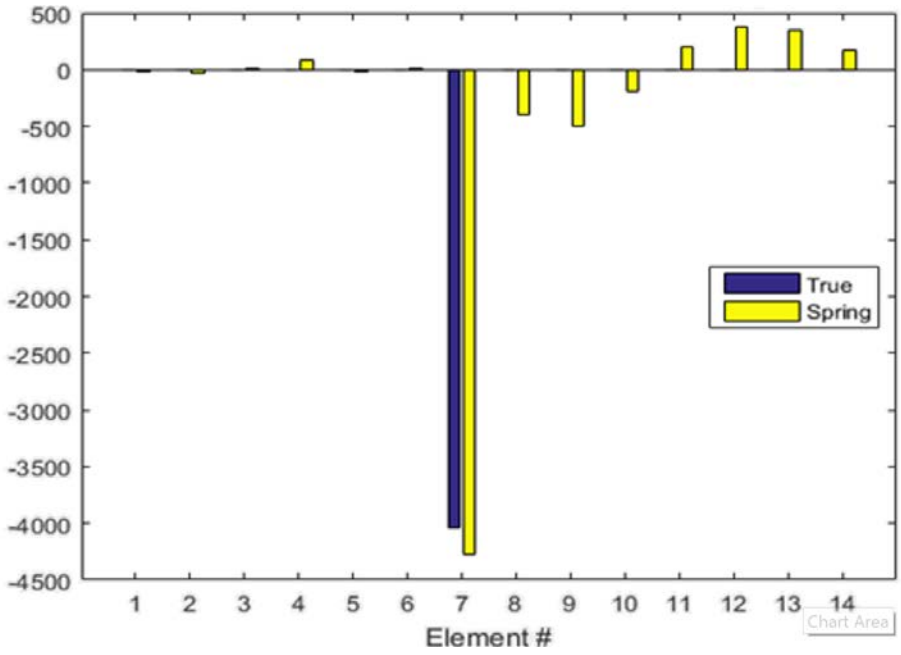

Figure 60. Single Spring Error Identification with Damage at Element 7

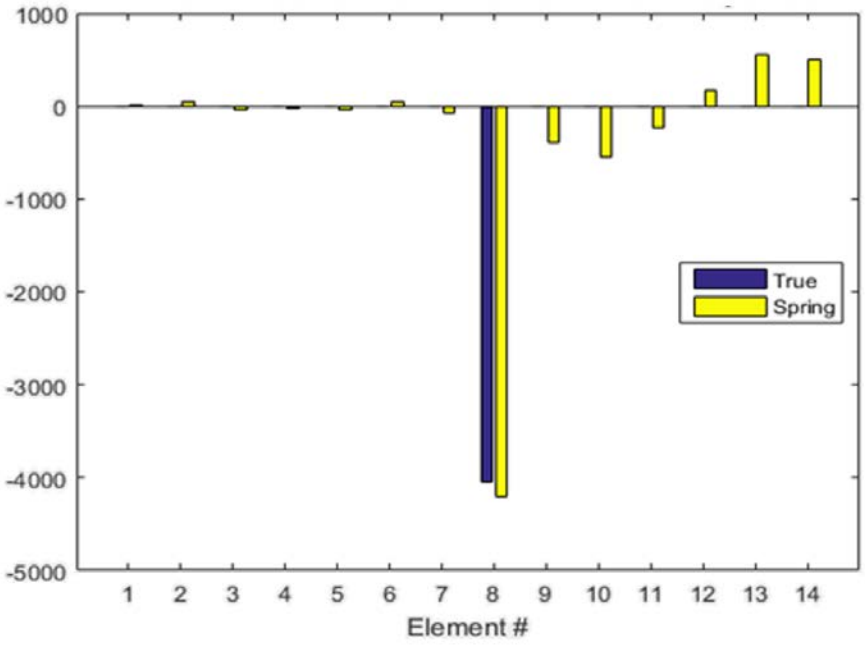

Figure 61. Single Spring Error Identification with Damage at Element 8

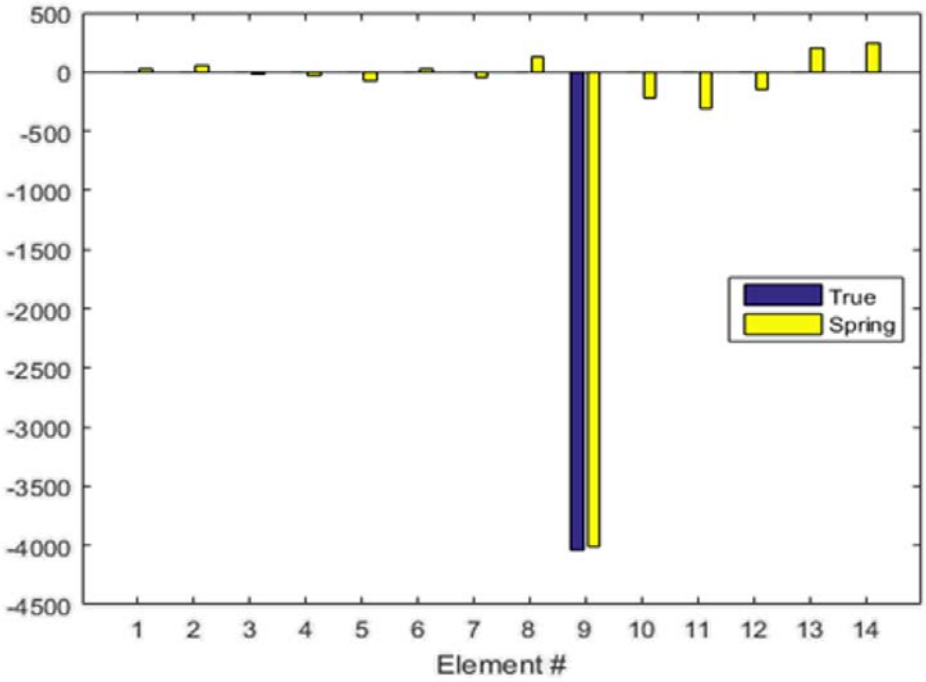

Figure 62. Single Spring Error Identification with Damage at Element 9

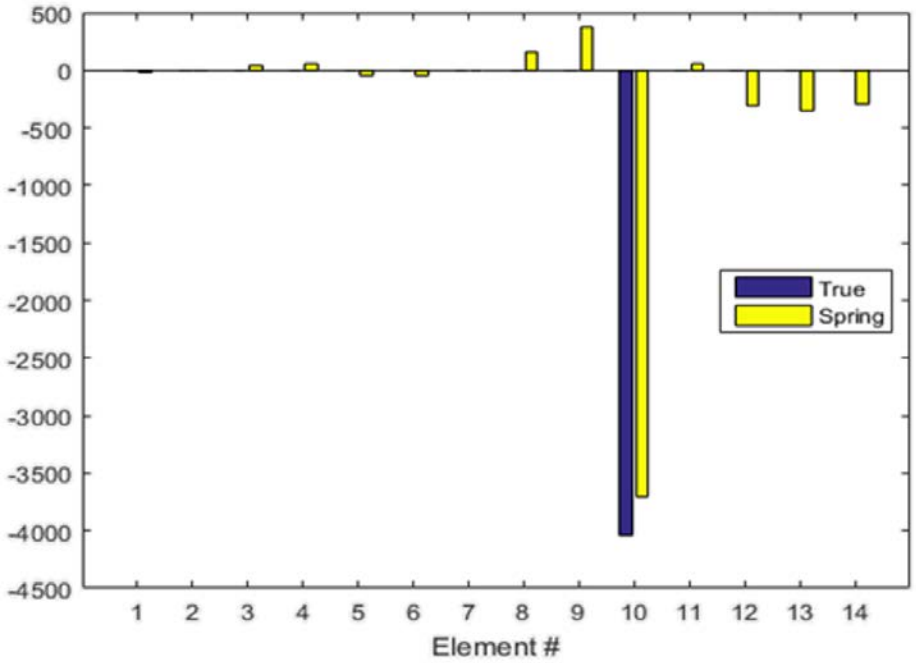

Figure 63. Single Spring Error Identification with Damage at Element 10

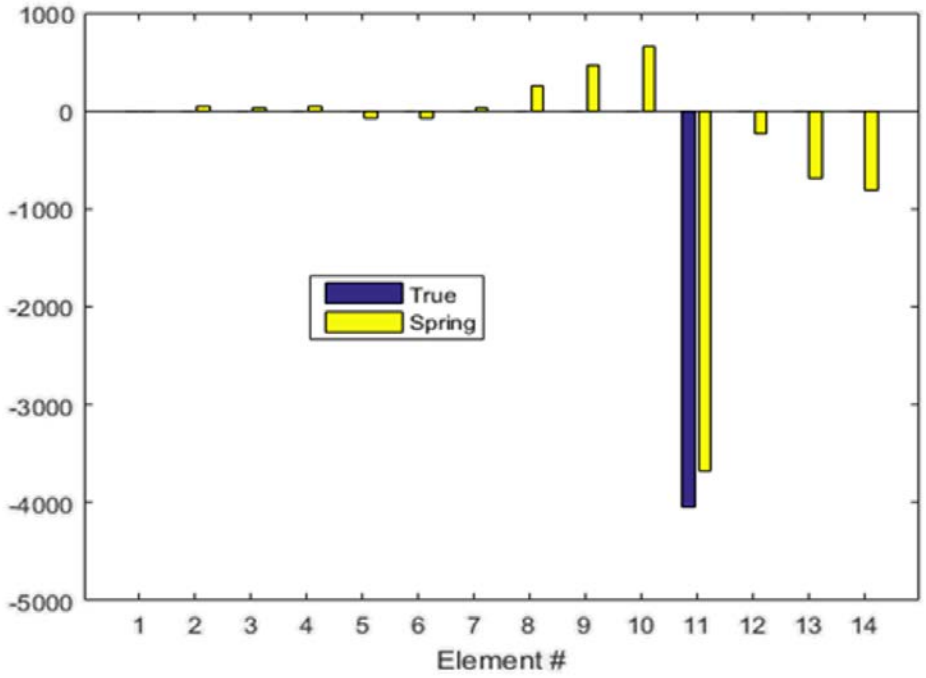

Figure 64. Single Spring Error Identification with Damage at Element 11

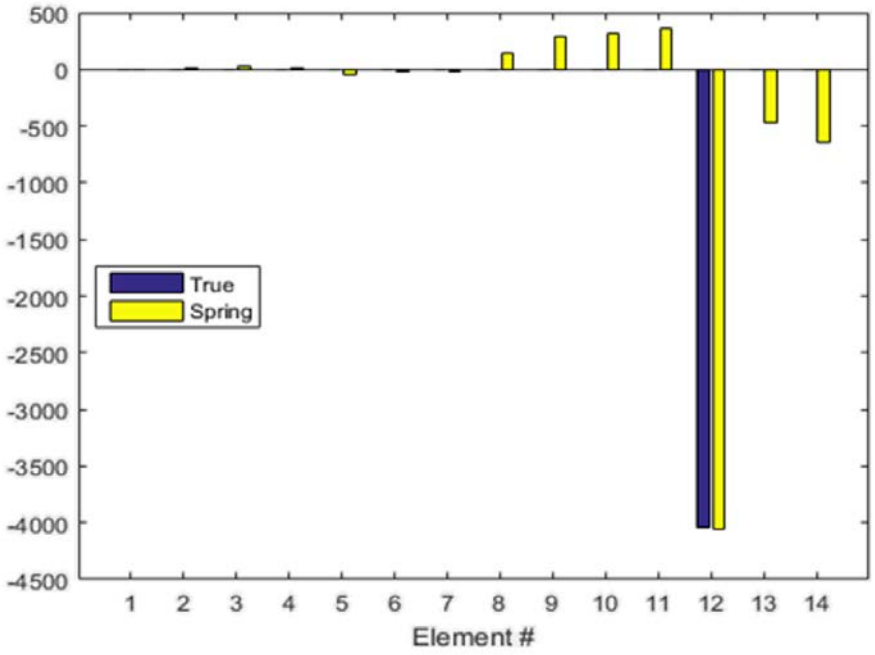

Figure 65. Single Spring Error Identification with Damage at Element 12

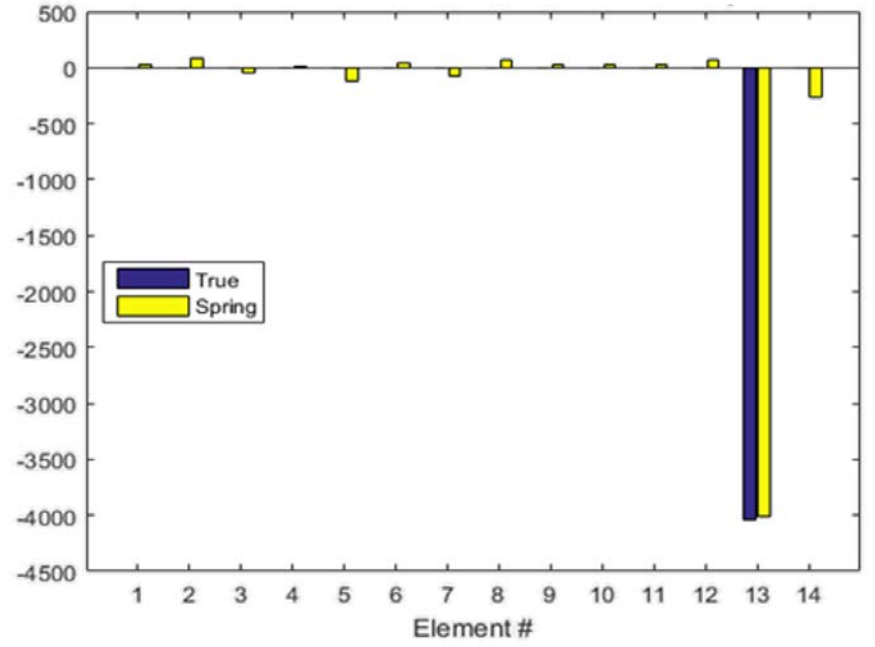

Figure 66. Single Spring Error Identification with Damage at Element 13

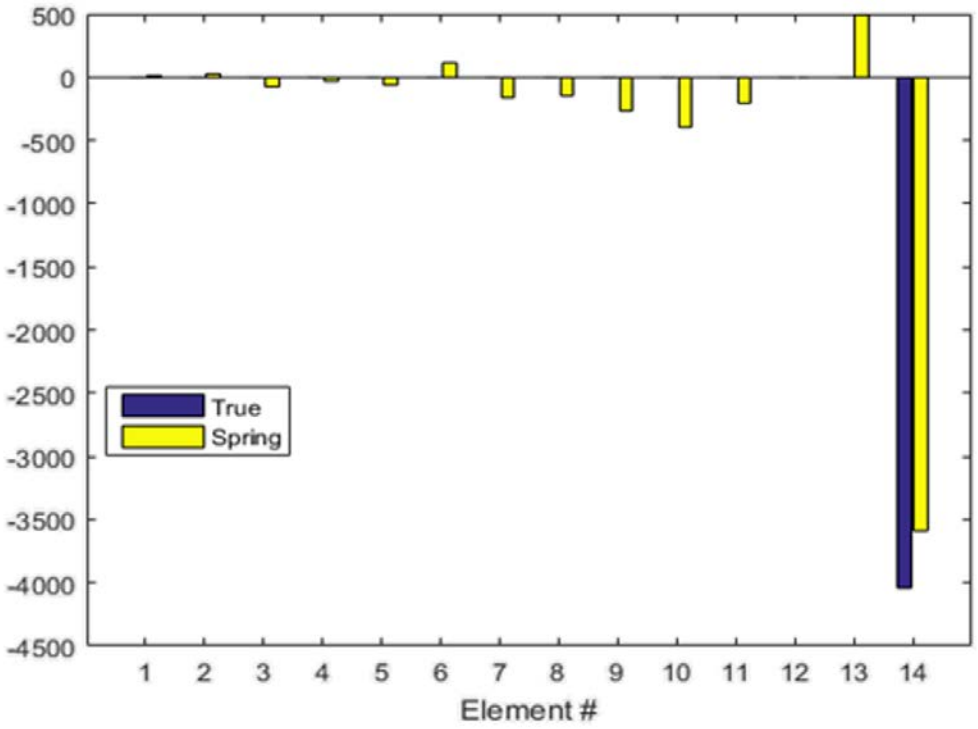

Figure 67. Single Spring Error Identification with Damage at Element 14

What Figures 54 through Figure 67 tell us is the use of the sensitivity matrix identified in equation (4.13) will accurately find error in all places with minimal false readings.

E. SINGLE MASS SYSTEM DYNAMIC RESPONSE

Similar to the development of the single spring system, a single lumped mass can be synthesized into the initial FRF of the beam to provide new and relevant information for damage detection and/or model updating. As discussed before, the concept of the idealized, lumped mass allows us to apply a numeric value directly to the translational DOF of the system without having to add a corresponding inertial force.

1. Single Mass FRF Synthesis

Following the same procedure as with the single spring and the process detailed in Chapter II, a lumped mass was synthesized into the FRF and checked

against a physical modification of the same structure. This check is plotted in Figure 68.

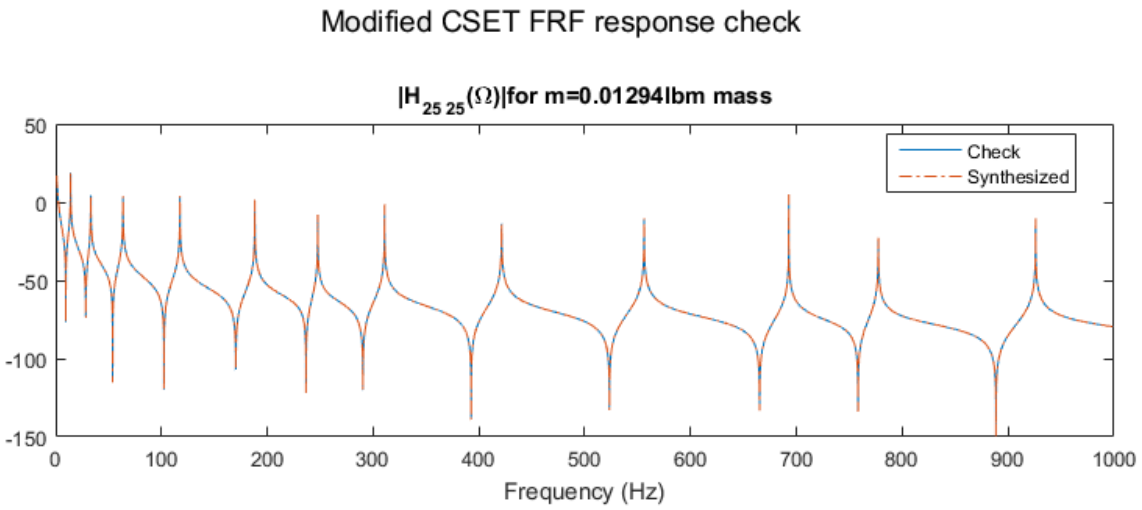

Figure 68. 0.227 kg (0.5 lb) Lumped Mass on Node 13 FRF Synthesis Check, $H_{25,25}$

Since the FRF synthesis and modified model check lay directly on top of each other as displayed in Figure 68, we can infer that synthesis has been correctly calculated. Figure 69 shows the results for a progressively increasing amount of mass.

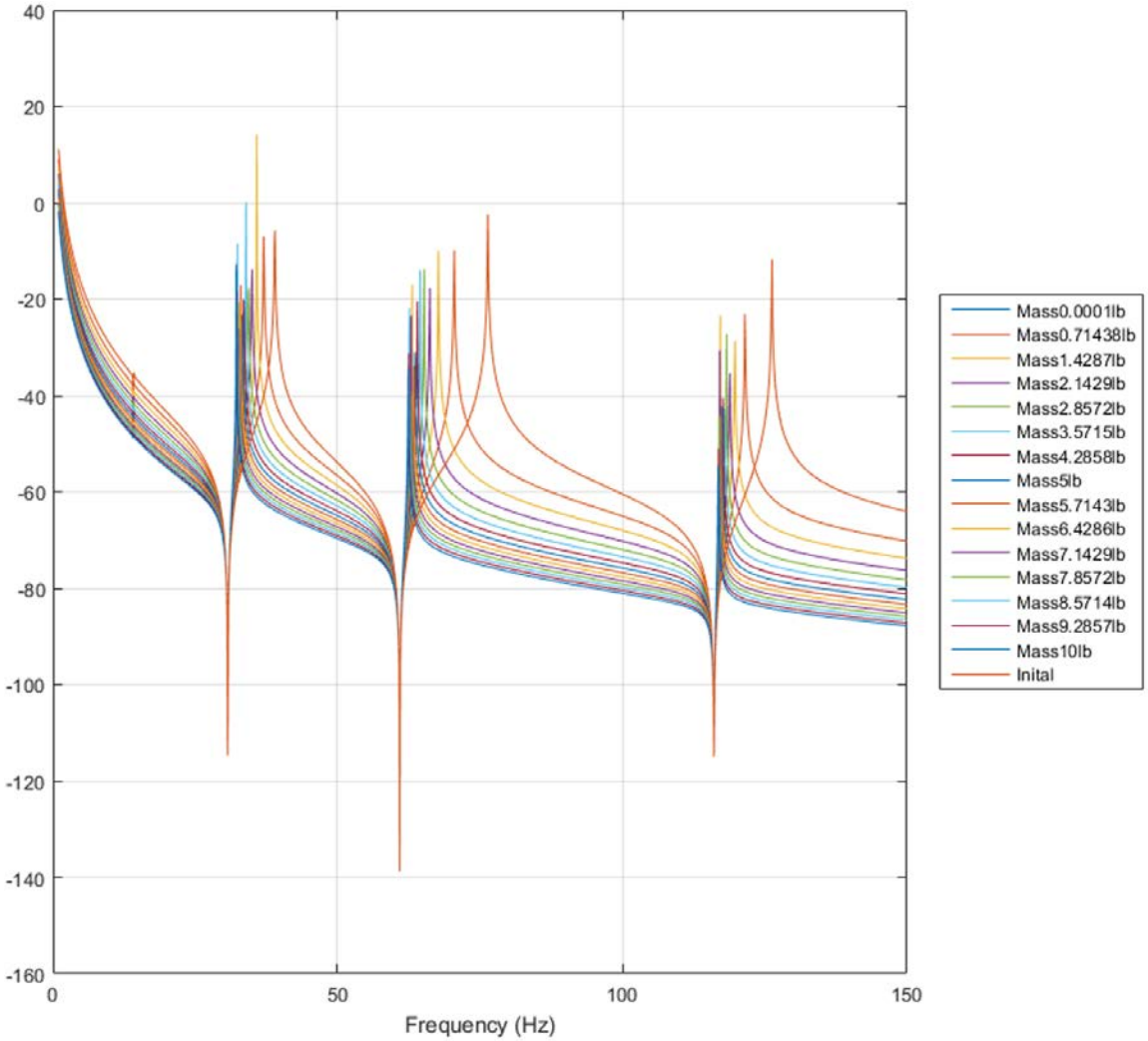

Figure 69. Lumped Mass on Node 13 FRF Synthesis Progression, $H_{25,25}$

As identified earlier, Figure 69 gives a detailed progression of the FRF with the addition of mass. Unlike the synthesis of a spring, the beam maintains two rigid body modes. Additionally, for the point of which the mass is applied, the resonance peaks move down in frequency, with a limit of the anti-resonance point from the initial FRF. Figure 70 displays the effects of the added mass on the resonance frequency for the first nine modes.

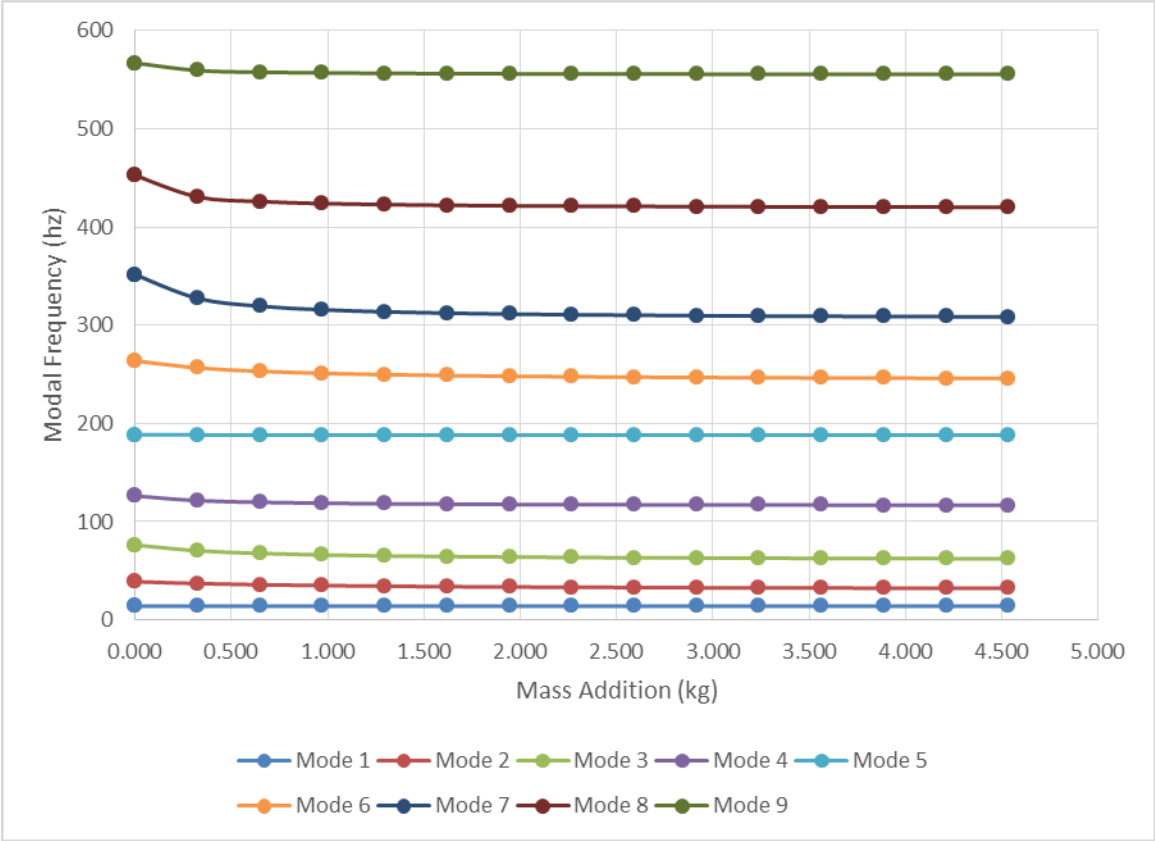

Figure 70. Modal Frequency Variance Due to Mass Addition at Node 13

Figure 70 displays the amount of change the resonance frequencies experience for each mode as the lumped mass increases which correlates to the trend displayed in Figure 69. From this graph, it appears there is minimal change in frequency after 1.81 kgs (4 lbs) of added mass.

2. Single Mass Sensitivity Analysis

Following the same process for a single spring, to find the values of mass that will provide that will minimize the condition number, the values of the highest mode of the of the sensitivity matrix where graphed as the amount of mass changed. Equation (4.15) graphically displays which row is used, and Figures 71 through Figure 85 display the corresponding results.

$$\left[S^{(K1)}\right]=\begin{bmatrix}\left[Mode\left(1\right)\right]\\\left[Mode\left(2\right)\right]\\\vdots\\\left[Mode\left(n-1\right)\right]\\\left[Mode\left(n\right)\right]\end{bmatrix}\leftarrow HighestMode \tag{4.15}$$

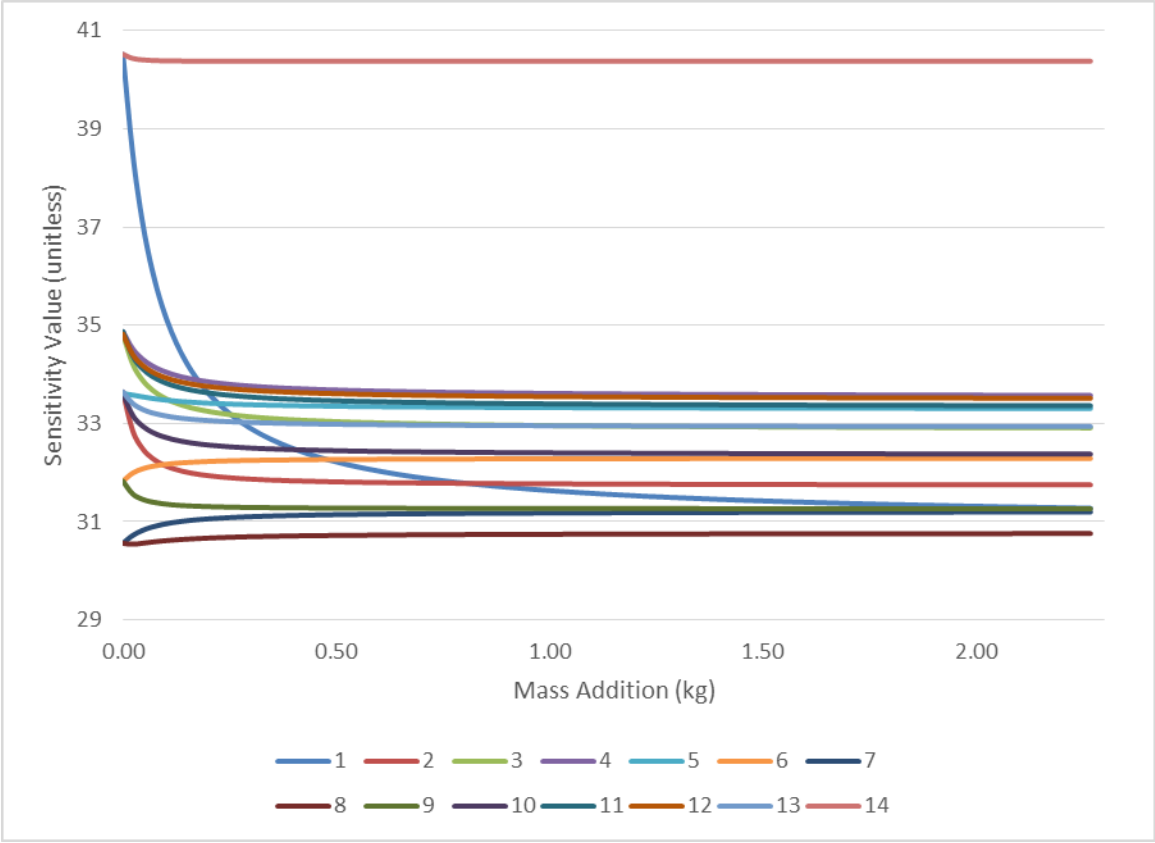

Figure 71. Effects on Sensitivity Value for Mass Addition Variance on Node 2

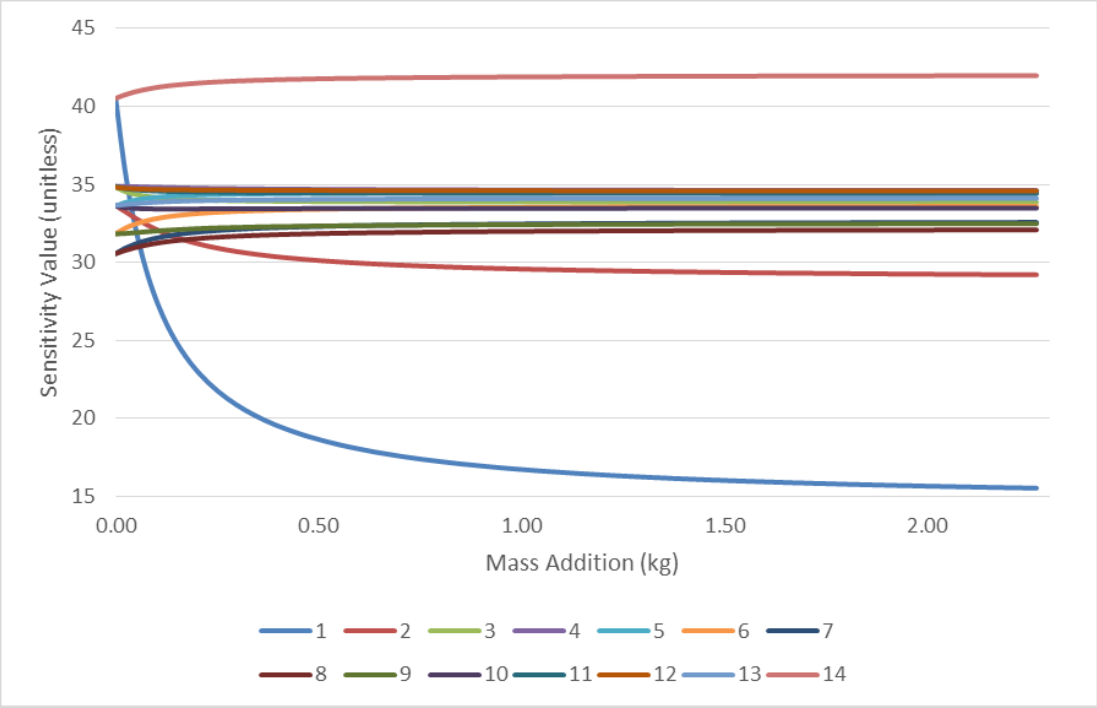

Figure 72. Effects on Sensitivity Value for Mass Addition Variance on Node 3

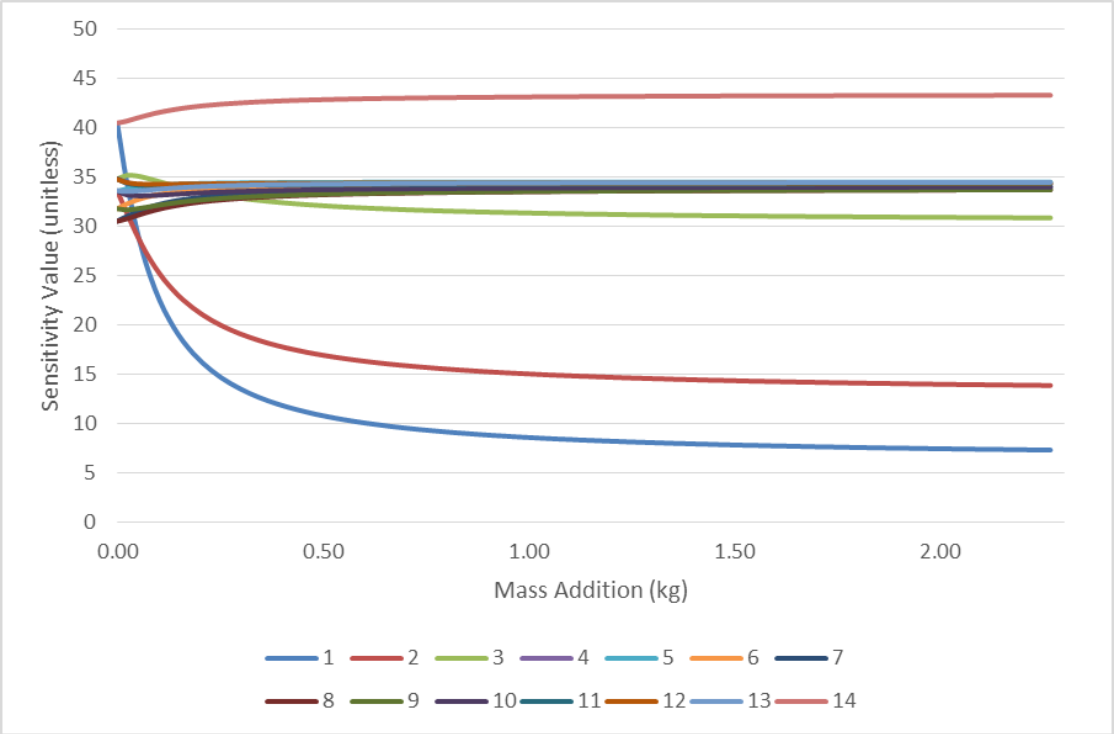

Figure 73. Effects on Sensitivity Value for Mass Addition Variance on Node 4

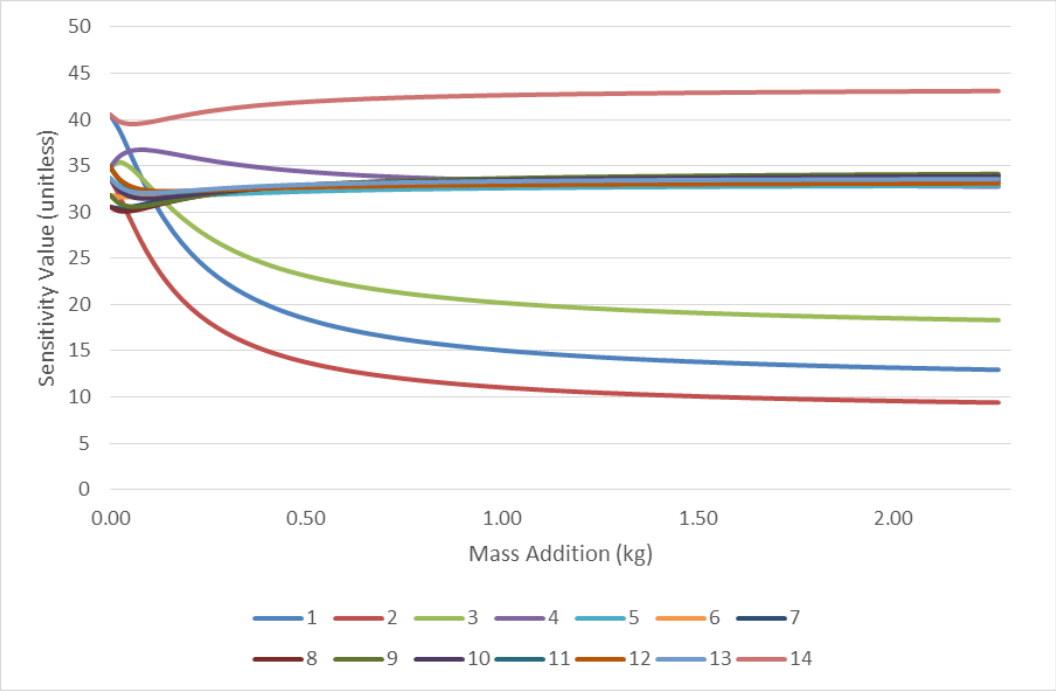

Figure 74. Effects on Sensitivity Value for Mass Addition Variance on Node 5

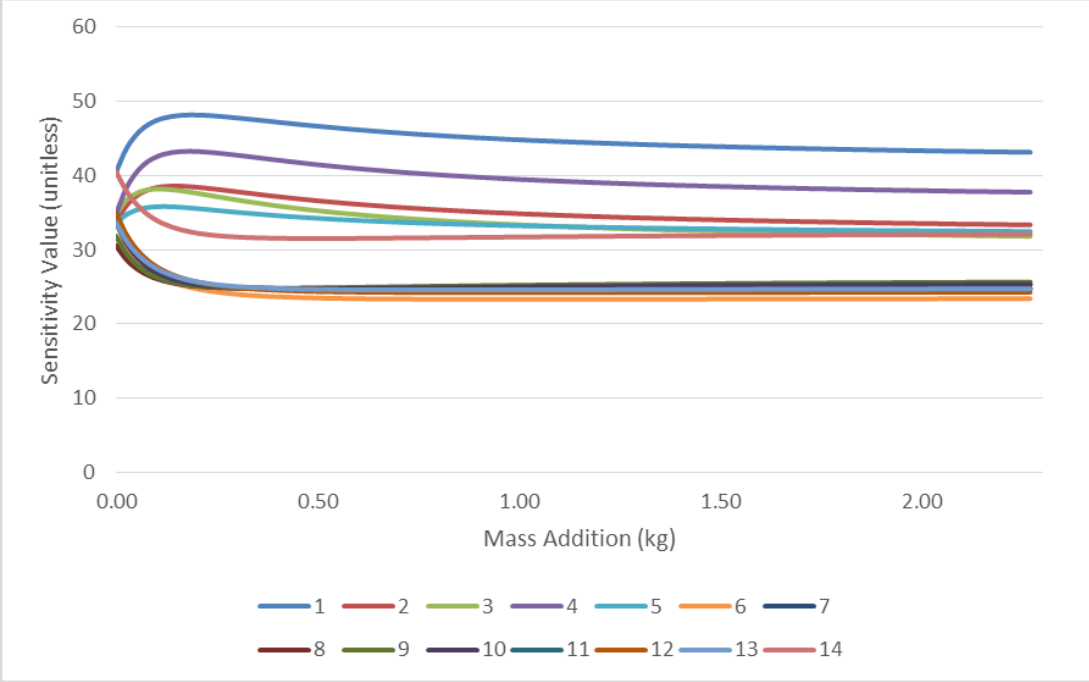

Figure 75. Effects on Sensitivity Value for Mass Addition Variance on Node 6

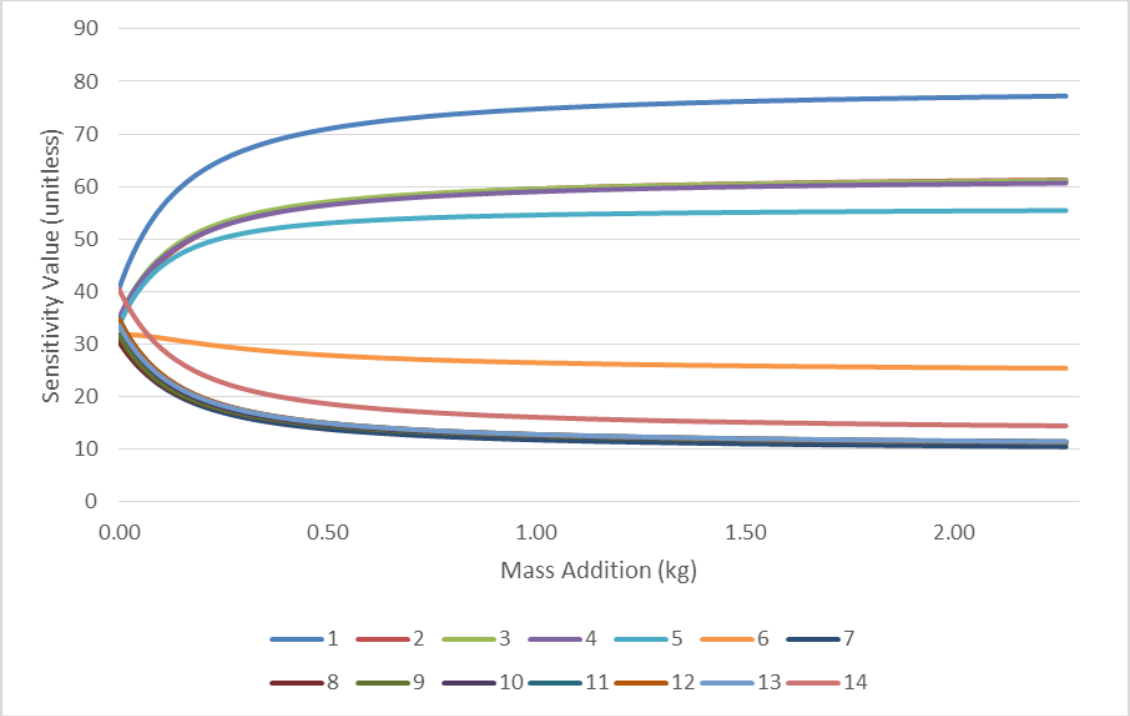

Figure 76. Effects on Sensitivity Value for Mass Addition Variance on Node 7

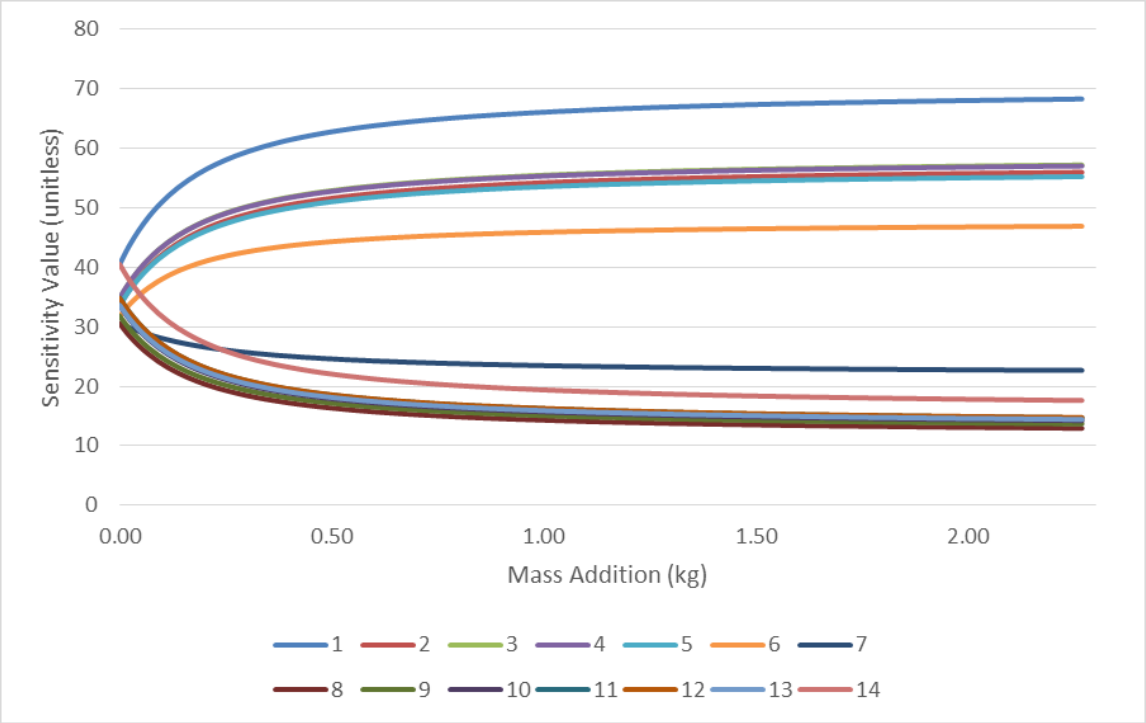

Figure 77. Effects on Sensitivity Value for Mass Addition Variance on Node 8

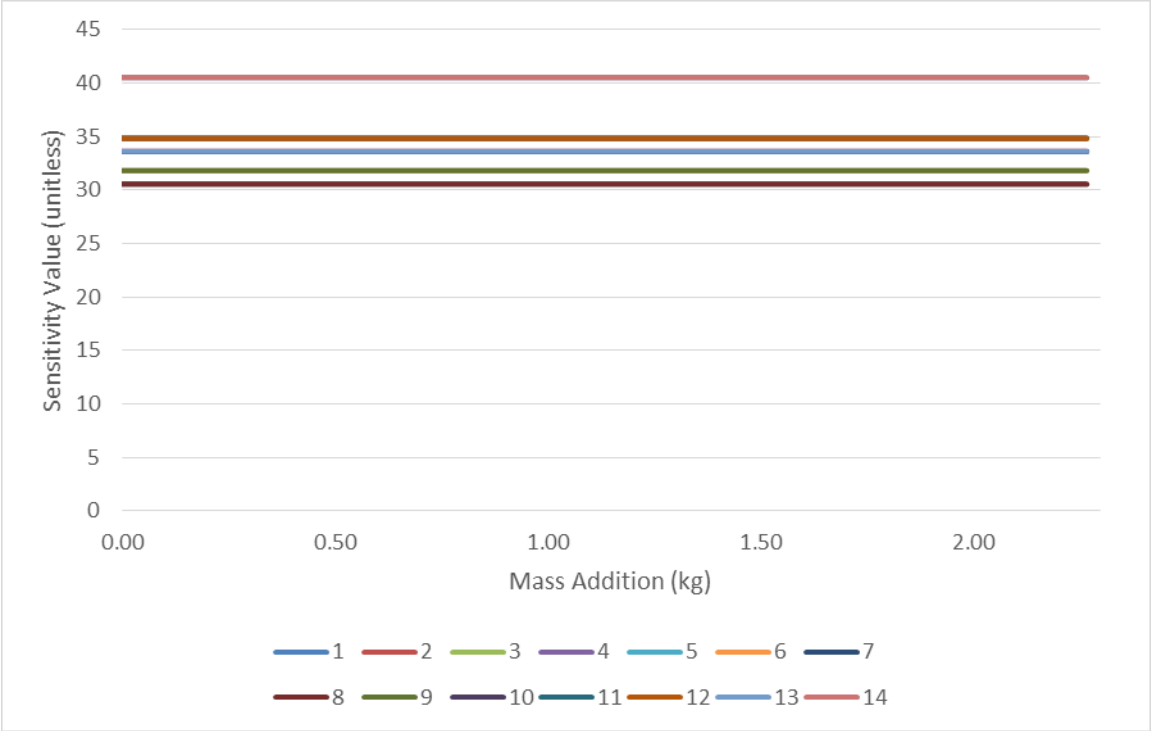

Figure 78. Effects on Sensitivity Value for Mass Addition Variance on Node 9

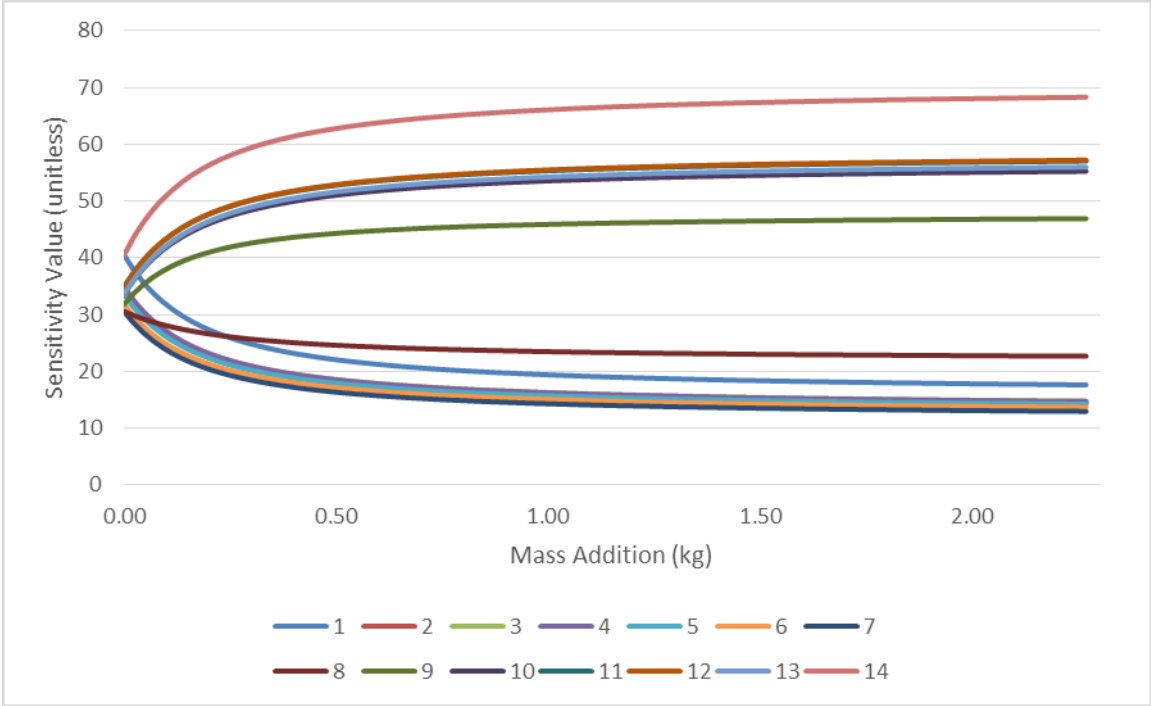

Figure 79. Effects on Sensitivity Value for Mass Addition Variance on Node 10

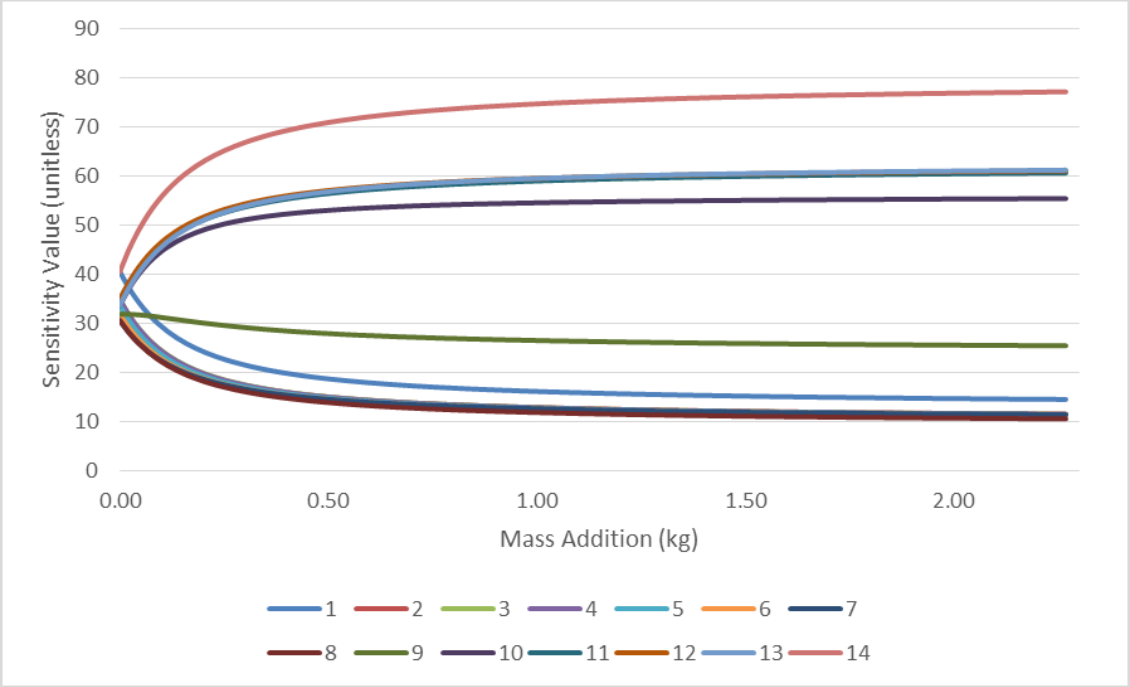

Figure 80. Effects on Sensitivity Value for Mass Addition Variance on Node 11

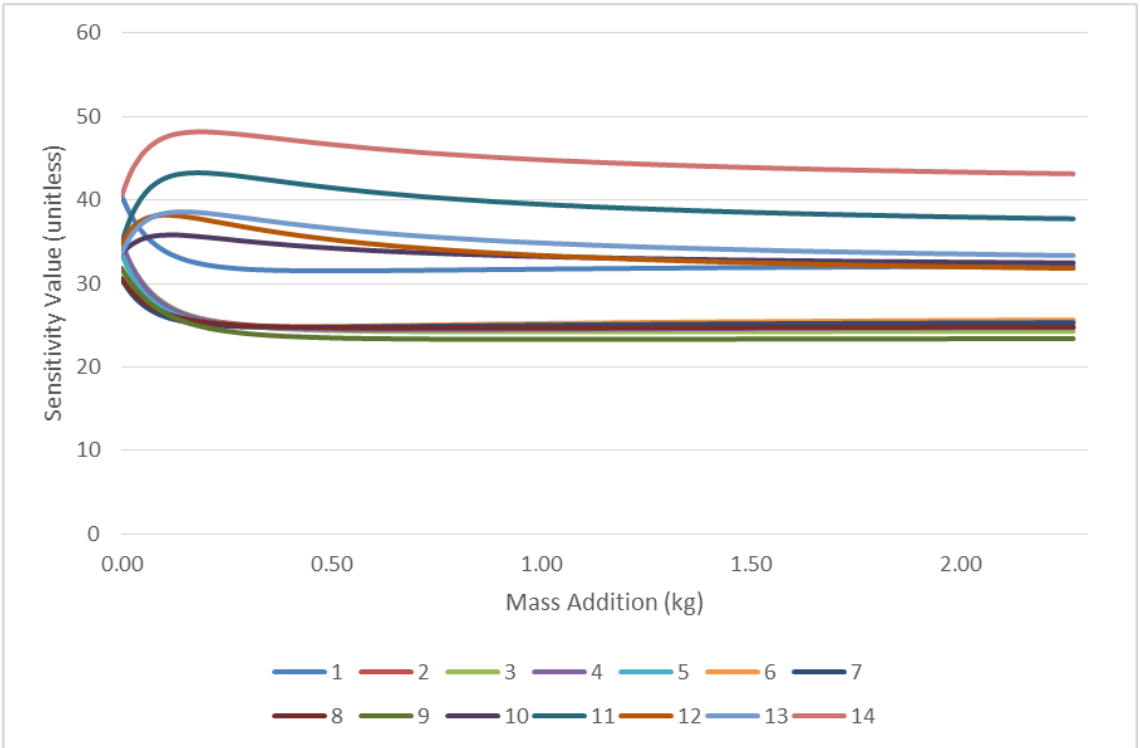

Figure 81. Effects on Sensitivity Value for Mass Addition Variance on Node 12

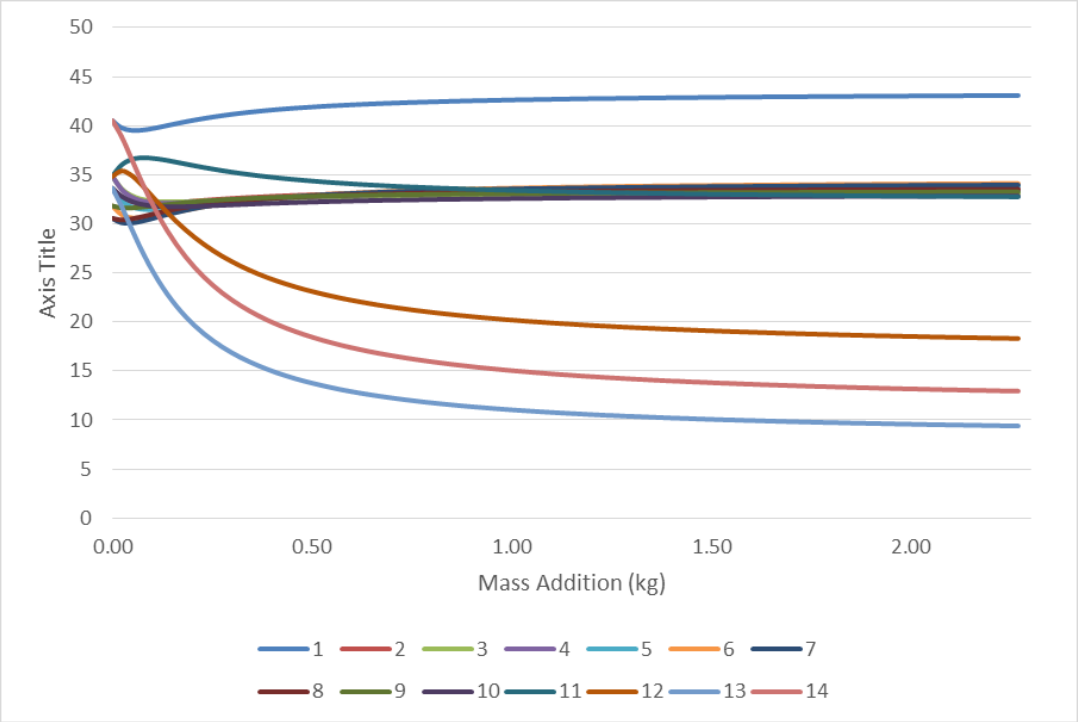

Figure 82. Effects on Sensitivity Value for Mass Addition Variance on Node 13

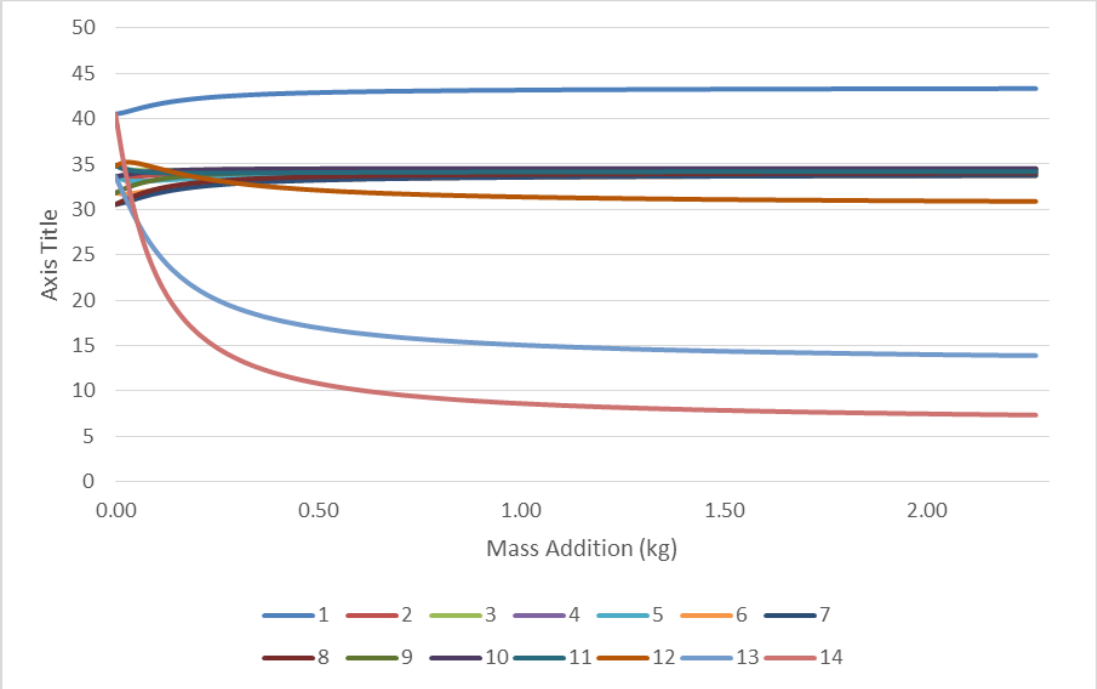

Figure 83. Effects on Sensitivity Value for Mass Addition Variance on Node 14

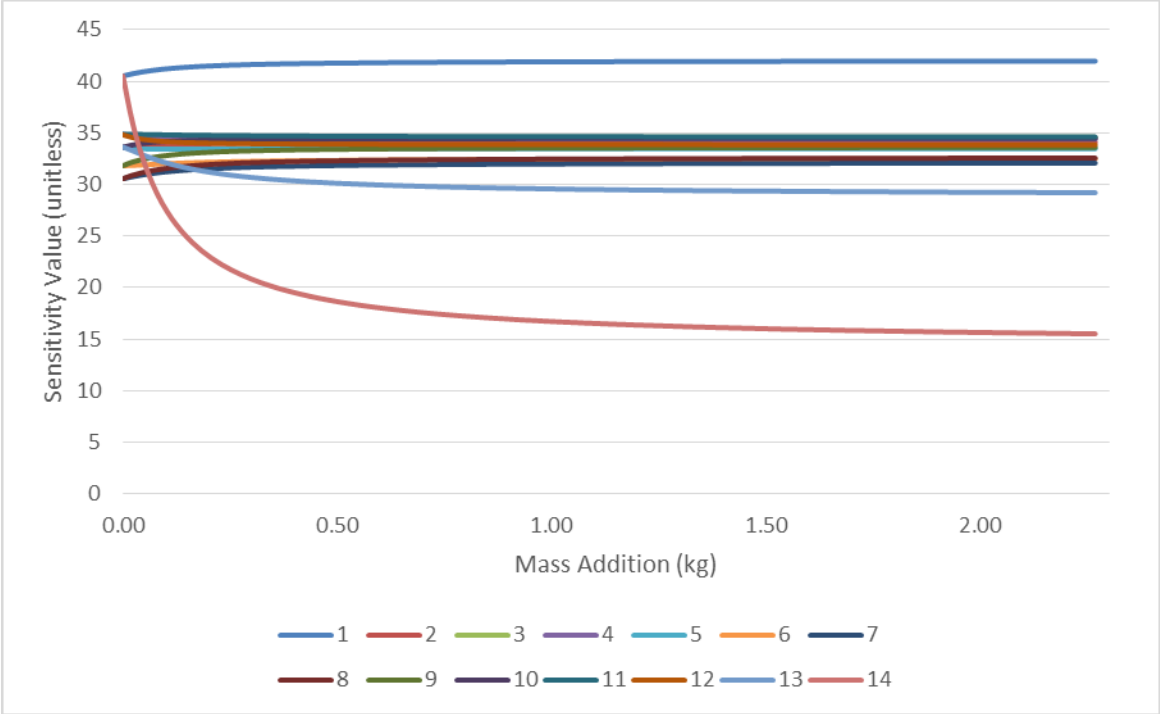

Figure 84. Effects on Sensitivity Value for Mass Addition Variance on Node 15

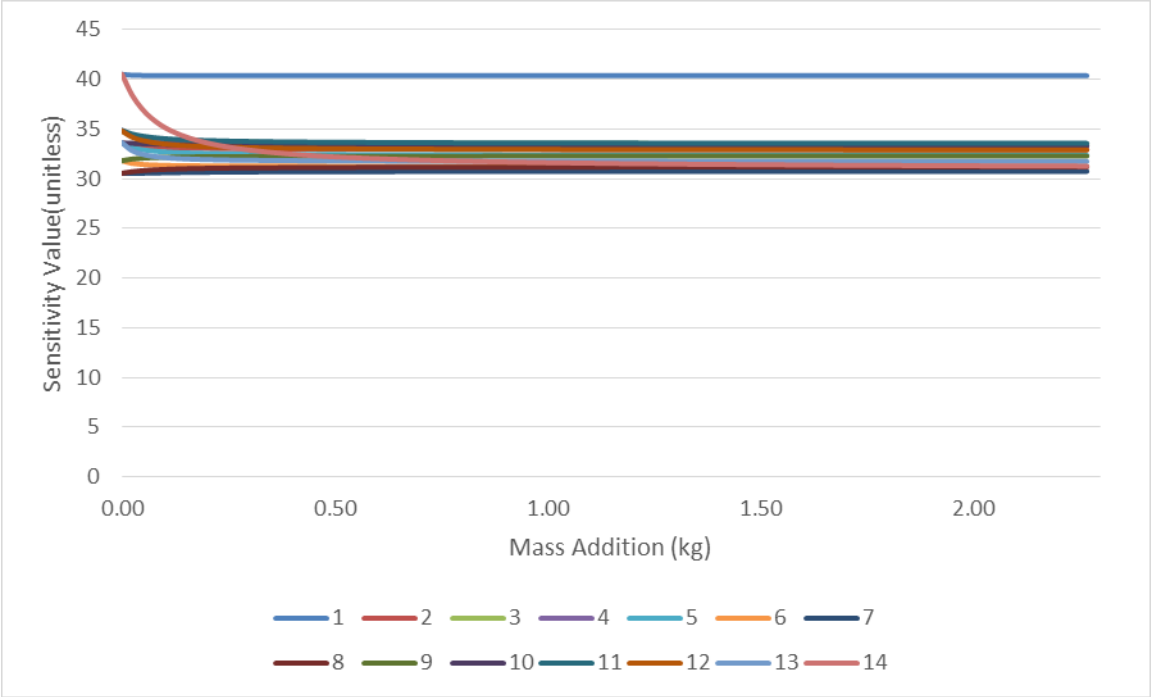

Figure 85. Effects on Sensitivity Value for Mass Addition Variance on Node 16

Figure 71 through Figure 85 show the effects of adding a lumped mass at their respective nodes. Similar to the single spring, individual masses were identified to maximize the condition number and tabulated in Table 11.

Table 11. Useable Single Mass Additions

Node	Added Mass kg(lbm)	
2	0.113(0.25)	1.814(4.0)
3	0.113(0.25)	1.814(4.0)
4	0.113(0.25)	1.814(4.0)
5	0.113(0.25)	1.814(4.0)
6	0.159(0.35)	1.814(4.0)
7	0.113(0.25)	1.814(4.0)
8	0.113(0.25)	1.814(4.0)
9	Not useable	
10	0.113(0.25)	1.814(4.0)
11	0.113(0.25)	1.814(4.0)
12	0.159(0.35)	1.814(4.0)
13	0.113(0.25)	1.814(4.0)
14	0.113(0.25)	1.814(4.0)
15	0.113(0.25)	1.814(4.0)
16	0.113(0.25)	1.814(4.0)

To evaluate the best combination of sensitivity matrices, the useable single mass additions where placed into an index as tabulated in Table 12.

Table 12. Single Mass Addition Index for Evaluating Condition Number

Index Number	Node	Mass kg(lbm)
1	2	0.113(0.25)
2	2	1.814(4.0)
3	3	0.113(0.25)
4	3	1.814(4.0)
5	4	0.113(0.25)
6	4	1.814(4.0)
7	5	0.113(0.25)
8	5	1.814(4.0)
9	6	0.159(0.35)
10	6	1.814(4.0)
11	7	0.113(0.25)
12	7	1.814(4.0)
13	8	0.113(0.25)
14	8	1.814(4.0)

Index Number	Node	Mass kg(lbm)
15	10	0.113(0.25)
16	10	1.814(4.0)
17	11	0.113(0.25)
18	11	1.814(4.0)
19	12	0.159(0.35)
20	12	1.814(4.0)
21	13	0.113(0.25)
22	13	1.814(4.0)
23	14	0.113(0.25)
24	14	1.814(4.0)
25	15	0.113(0.25)
26	15	1.814(4.0)
27	16	0.113(0.25)
28	16	1.814(4.0)

Following the same procedure as the single spring, the two highest baseline modes are combined with six highest modes from two different indexes and evaluated for the overall sensitivity matrix condition number. The result is another matrix of 784 different combinations. Using the same method as described for Figure 52, a graphic was developed for the different matrix condition numbers and displayed in Figure 86.

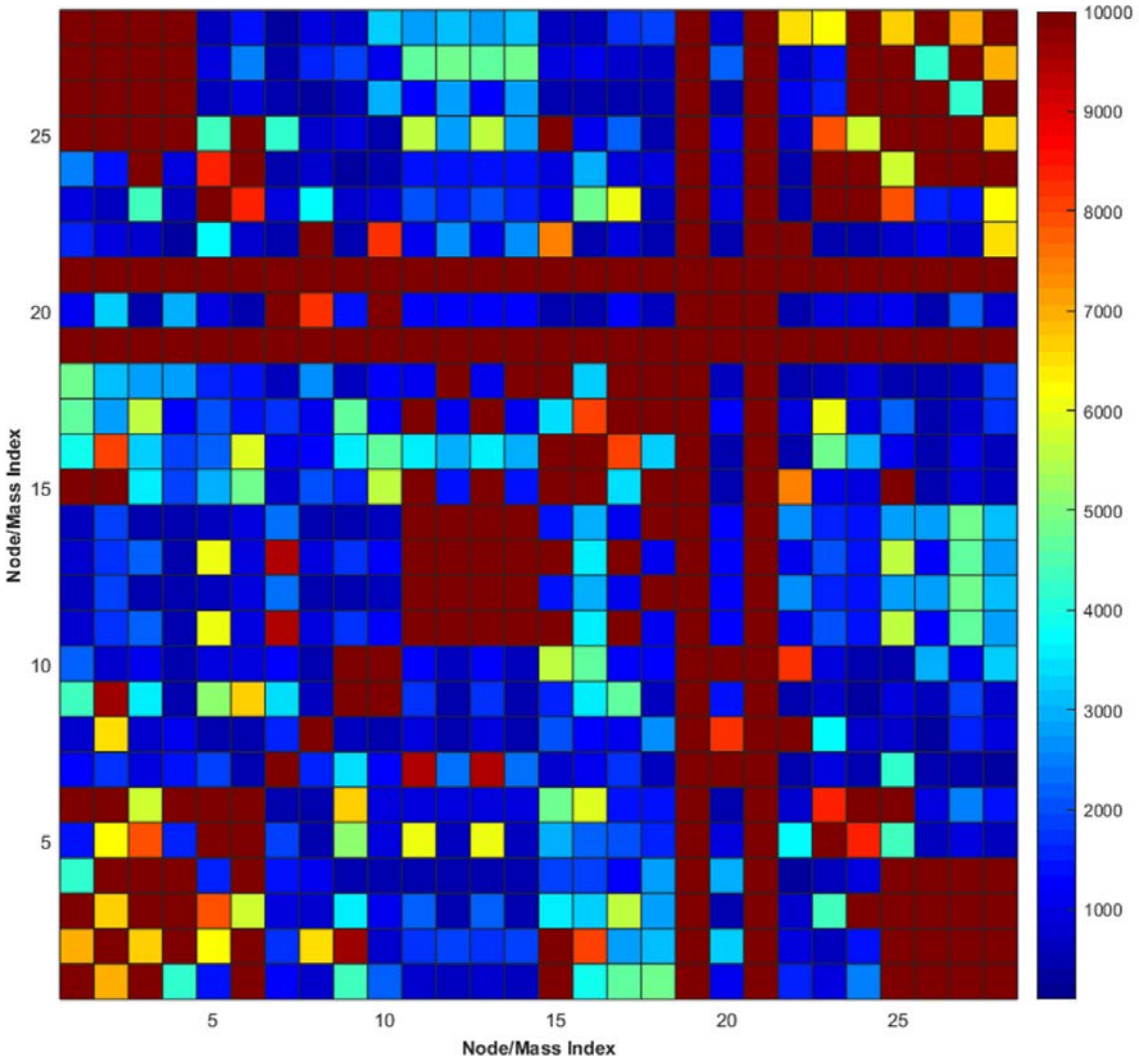

Figure 86. Sensitivity Matrix Combination Condition Number Indicator, Single Mass

In this instance, the lowest sensitivity matrix condition number displayed in Figure 86 occurs at index 9,24 with a value of 354.71. Using Table 12, the composite sensitivity matrix for a single lumped mass should be:

$$\left[S_{comp}\right]_{14x14} = \begin{bmatrix} \left[S^{(0)}\right]_{2\times14} \\ \left[S^{(N6-0.35)}\right]_{6\times14} \\ \left[S^{(N14-4.00)}\right]_{6\times14} \end{bmatrix} \tag{4.16}$$

$$\left[S_{comp}\right]=\begin{bmatrix}
30.602 & 21.625 & 21.721 & 24.831 & 26.337 & 24.357 & 21.478 & 21.478 & 24.357 & 26.337 & 24.831 & 21.721 & 21.625 & 30.602\\
40.523 & 33.646 & 34.824 & 34.873 & 33.613 & 31.827 & 30.562 & 30.562 & 31.827 & 33.613 & 34.873 & 34.824 & 33.646 & 40.523\\
2.373 & 5.797 & 2.068 & 4.947 & 3.356 & 4.978 & 4.387 & 4.205 & 5.237 & 3.372 & 5.987 & 2.628 & 7.574 & 3.094\\
8.671 & 12.506 & 10.805 & 6.018 & 10.048 & 3.816 & 5.427 & 6.783 & 2.986 & 8.060 & 3.307 & 6.144 & 6.833 & 4.751\\
9.186 & 8.249 & 11.494 & 9.376 & 8.778 & 12.799 & 11.057 & 6.674 & 14.046 & 9.923 & 7.282 & 14.310 & 9.789 & 10.919\\
11.537 & 7.549 & 10.393 & 14.866 & 16.520 & 13.728 & 20.894 & 22.518 & 15.264 & 15.292 & 22.553 & 20.679 & 14.785 & 22.568\\
39.780 & 28.048 & 28.203 & 30.772 & 25.515 & 21.130 & 18.606 & 18.458 & 20.972 & 22.820 & 21.557 & 18.777 & 18.641 & 26.454\\
48.128 & 38.595 & 37.976 & 43.247 & 35.749 & 25.291 & 25.715 & 25.359 & 25.411 & 25.764 & 26.163 & 26.262 & 26.204 & 32.735\\
3.064 & 7.684 & 2.531 & 6.171 & 3.162 & 5.541 & 3.873 & 4.790 & 4.652 & 4.053 & 5.079 & 2.842 & 3.922 & 1.232\\
6.038 & 8.298 & 7.934 & 3.930 & 10.022 & 4.118 & 7.739 & 7.689 & 4.150 & 10.004 & 3.957 & 8.417 & 10.021 & 7.544\\
6.595 & 5.984 & 8.680 & 4.335 & 6.151 & 8.455 & 3.949 & 6.903 & 7.977 & 3.726 & 7.011 & 16.233 & 26.028 & 30.231\\
15.351 & 10.625 & 16.313 & 14.528 & 9.038 & 14.043 & 16.703 & 10.195 & 11.205 & 17.280 & 11.530 & 14.781 & 17.061 & 17.943\\
28.987 & 19.365 & 21.442 & 26.217 & 25.068 & 20.014 & 19.396 & 24.236 & 26.526 & 22.601 & 18.144 & 21.547 & 12.878 & 8.853\\
43.303 & 34.479 & 34.430 & 34.350 & 33.999 & 33.712 & 33.703 & 33.979 & 34.324 & 34.524 & 34.176 & 30.995 & 14.119 & 7.581
\end{bmatrix} \quad (4.17)$$

To test the capability of this matrix, an identical FEM was made that included damage in one of the elements. Because we made the sensitivity matrix for the flexural rigidity (EI), damage was simulated by decreasing the EI value in one element by 5 percent, and tested for the length of the beam, thus including all 15 elements. As detailed in Chapter II, this is accomplished by solving equation (2.46), which has been adapted and displayed here as equation (4.18) and equation (4.19):

$$\begin{bmatrix} \left[S^{(0)}\right]_{2\times 14} \\ \left[S^{(N6-0.35)}\right]_{6\times 14} \\ \left[S^{(N14-4.00)}\right]_{6\times 14} \end{bmatrix}^{-1} \begin{Bmatrix} \left\{\Delta\lambda^{(0)}\right\}_{2\times 1} \\ \left\{\Delta\lambda^{(N6-0.35)}\right\}_{6\times 1} \\ \left\{\Delta\lambda^{(N14-4.00)}\right\}_{6\times 1} \end{Bmatrix} = \begin{Bmatrix} \Delta EI_1 \\ \Delta EI_2 \\ \vdots \\ \Delta EI_{14} \end{Bmatrix} \quad (4.18)$$

$$\left[S_{comp}\right]^{-1}_{14\times 14} \left\{\Delta\lambda_{comp}\right\}_{14\times 1} = \left\{\Delta EI\right\}_{14\times 1} \quad (4.19)$$

Figure 87 through Figure 100 show the results for testing for damage in every possible location. As with the testing for a single spring synthesis, the blue line indicates the actual damage of a five percent reduction in EI, and the yellow is the indicated damage from solving equation (4.19).

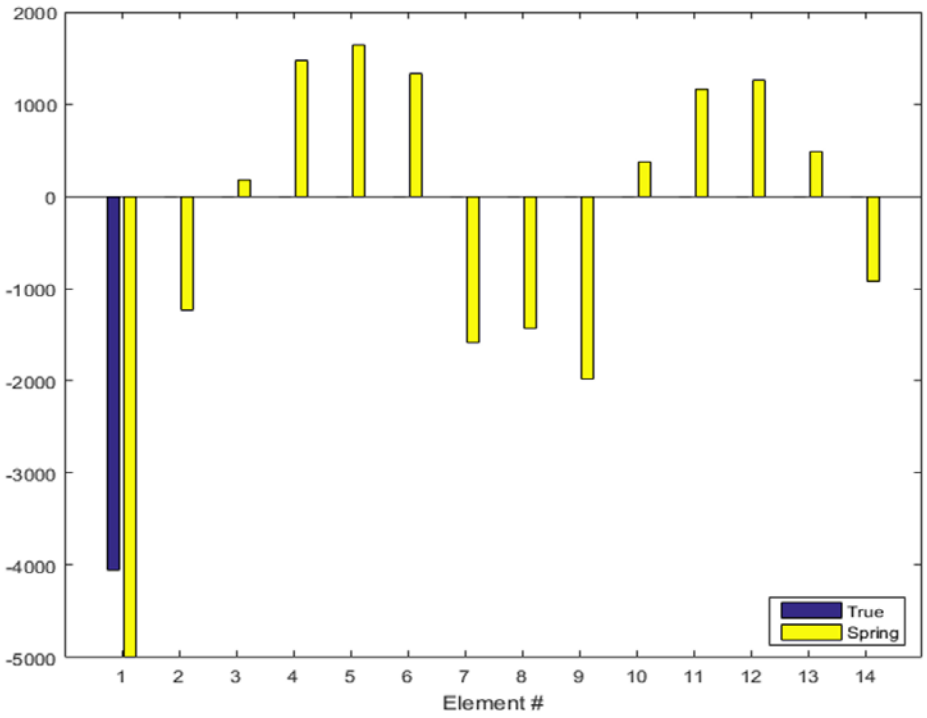

Figure 87. Single Mass Error Identification with Damage at Element 1

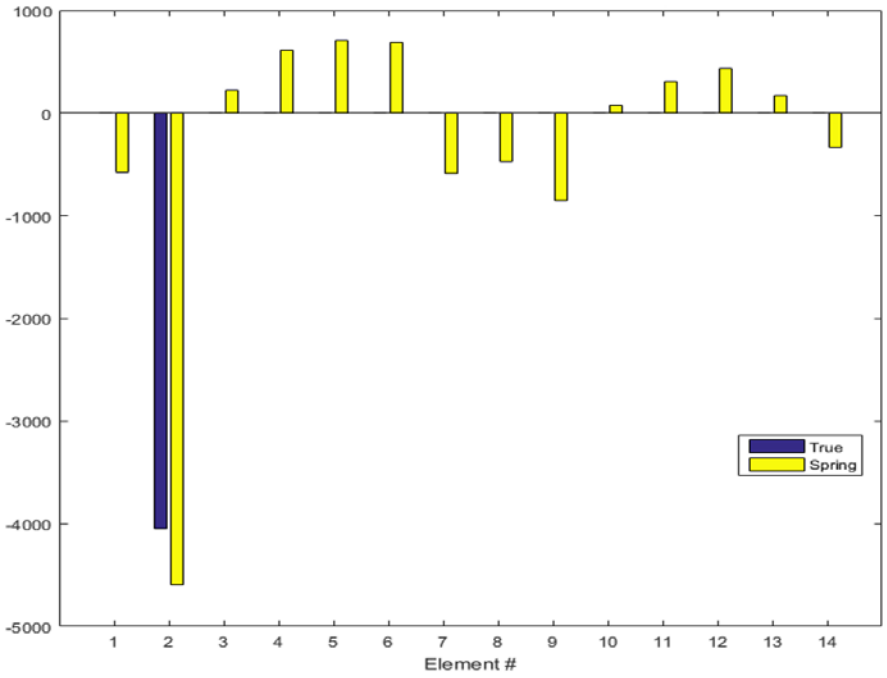

Figure 88. Single Mass Error Identification with Damage at Element 2

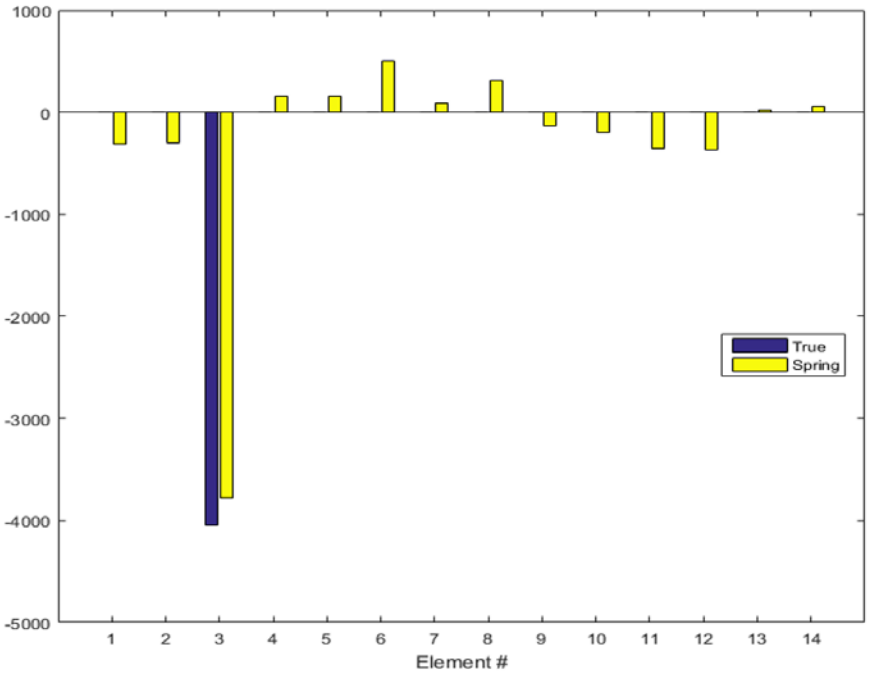

Figure 89. Single Mass Error Identification with Damage at Element 3

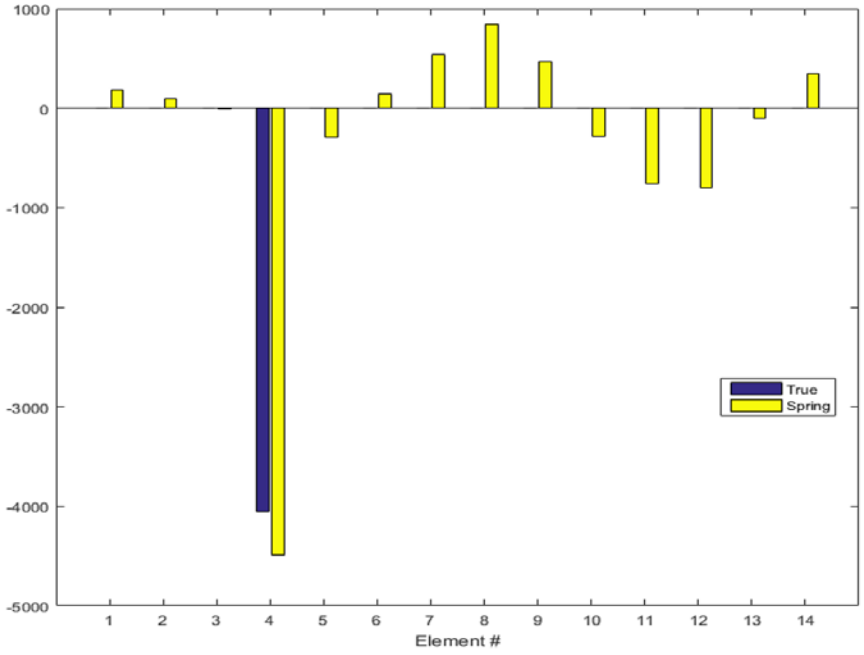

Figure 90. Single Mass Error Identification with Damage at Element 4

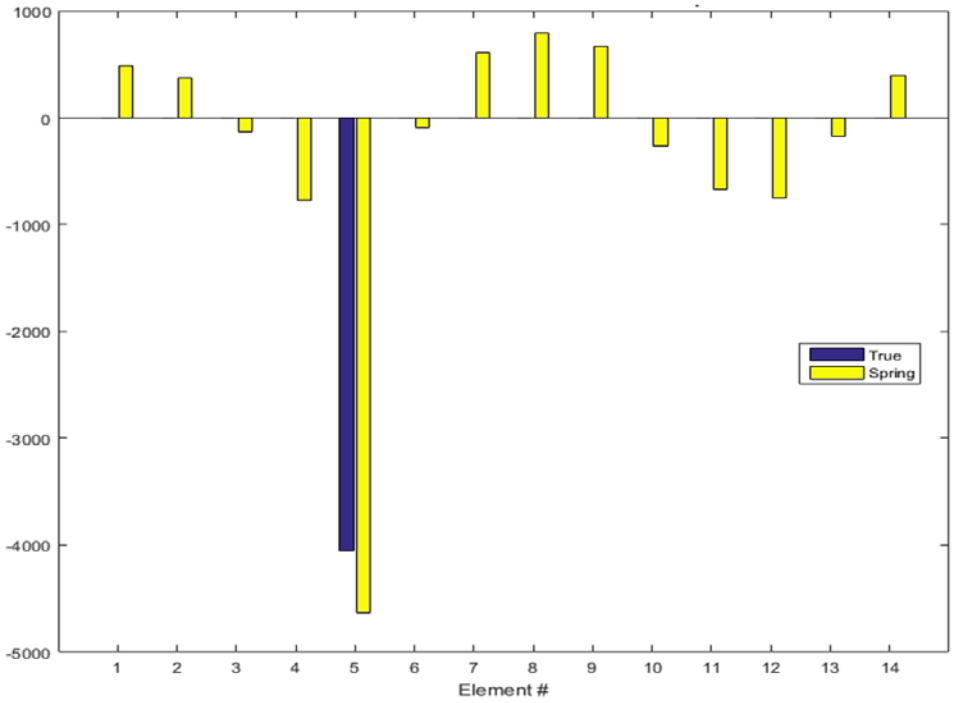

Figure 91. Single Mass Error Identification with Damage at Element 5

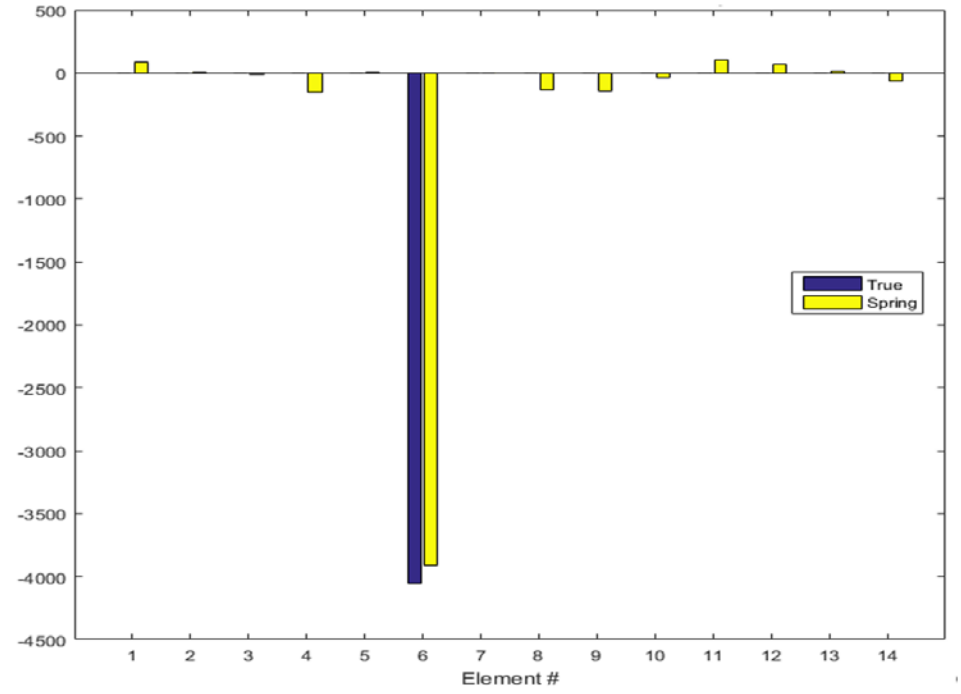

Figure 92. Single Mass Error Identification with Damage at Element 6

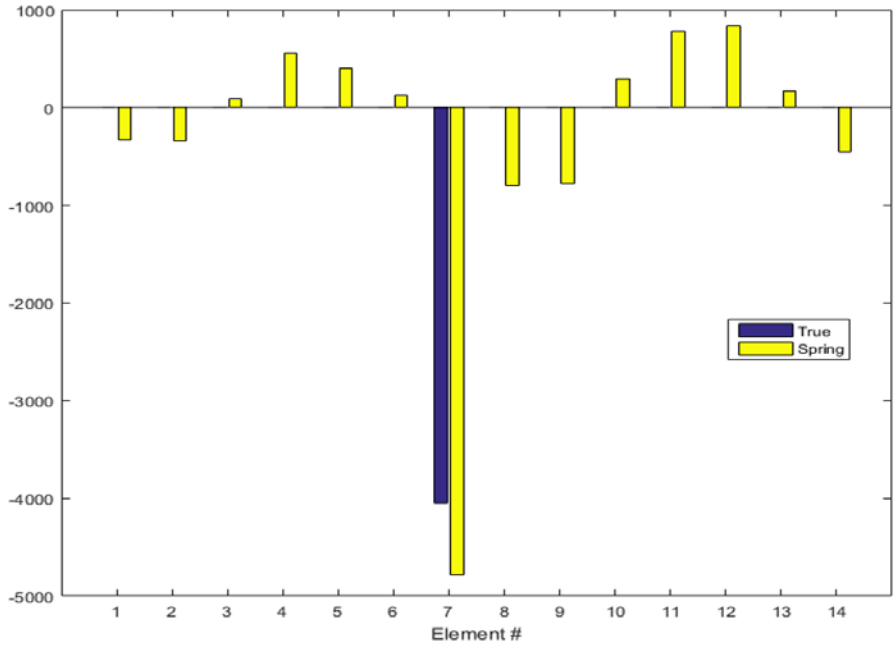

Figure 93. Single Mass Error Identification with Damage at Element 7

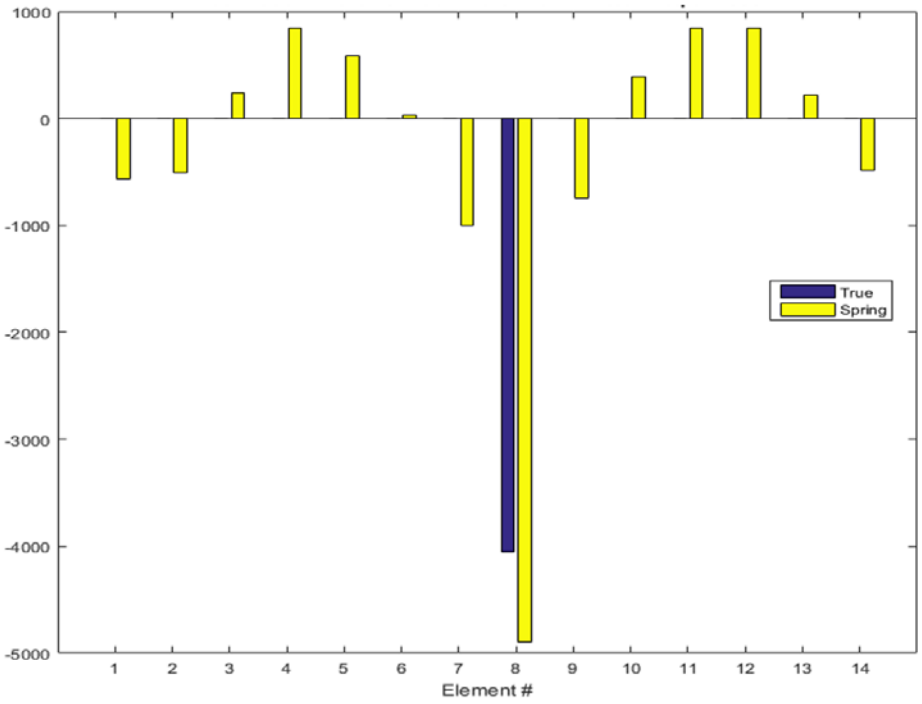

Figure 94. Single Mass Error Identification with Damage at Element 8

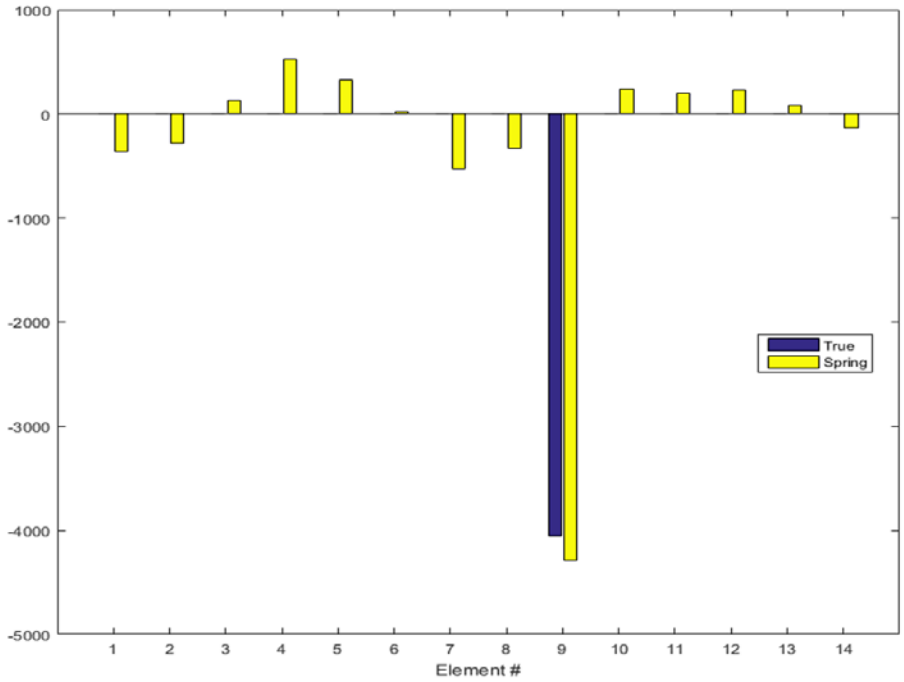

Figure 95. Single Mass Error Identification with Damage at Element 9

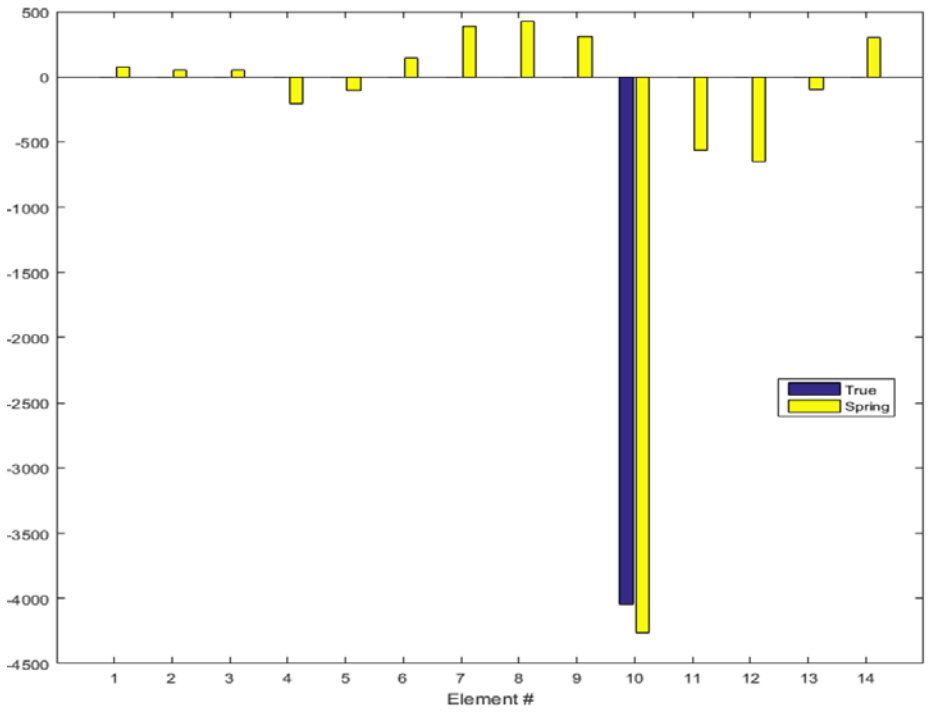

Figure 96. Single Mass Error Identification with Damage at Element 10

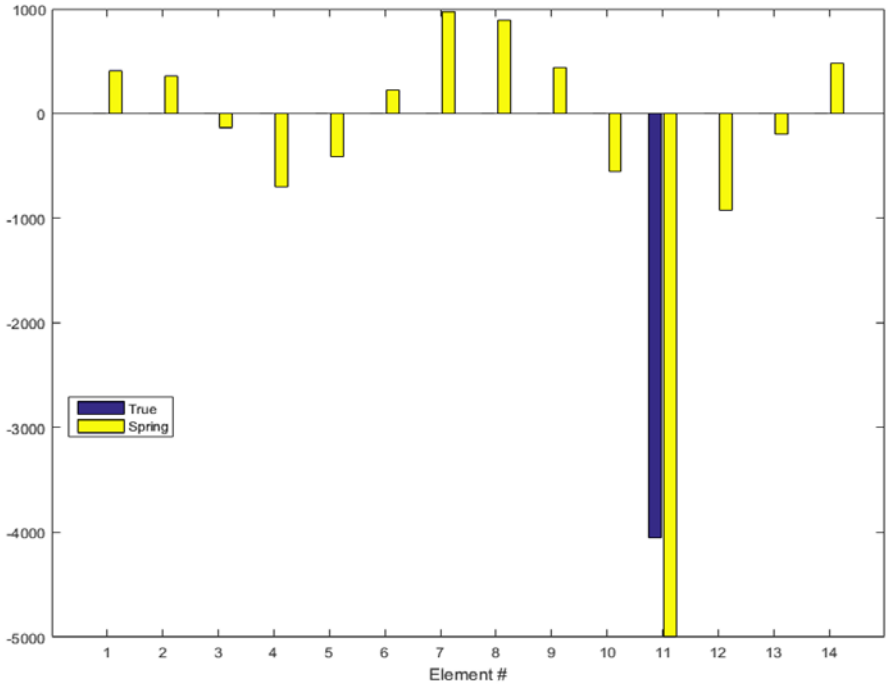

Figure 97. Single Mass Error Identification with Damage at Element 11

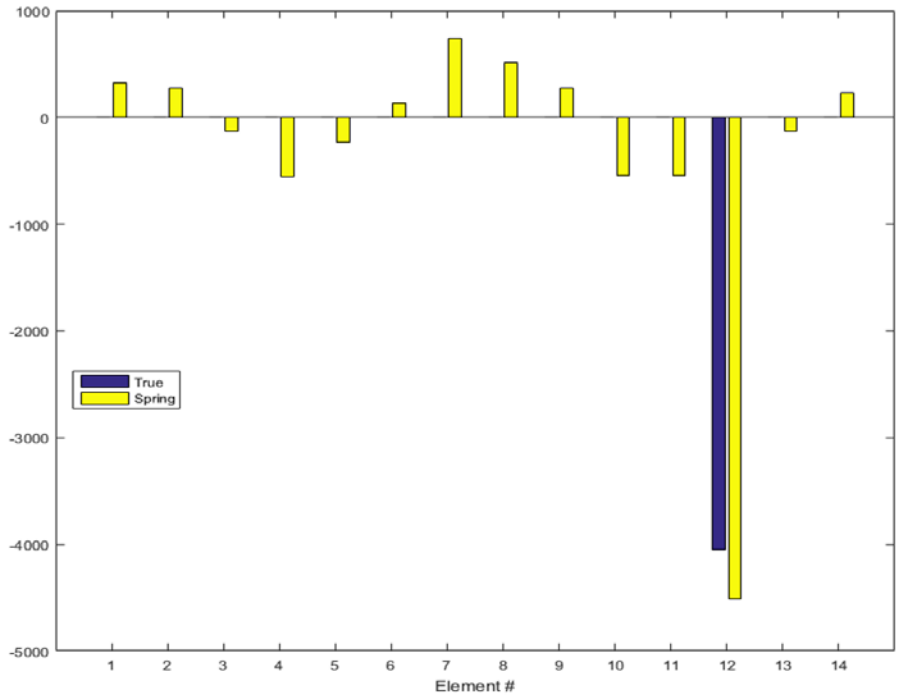

Figure 98. Single Mass Error Identification with Damage at Element 12

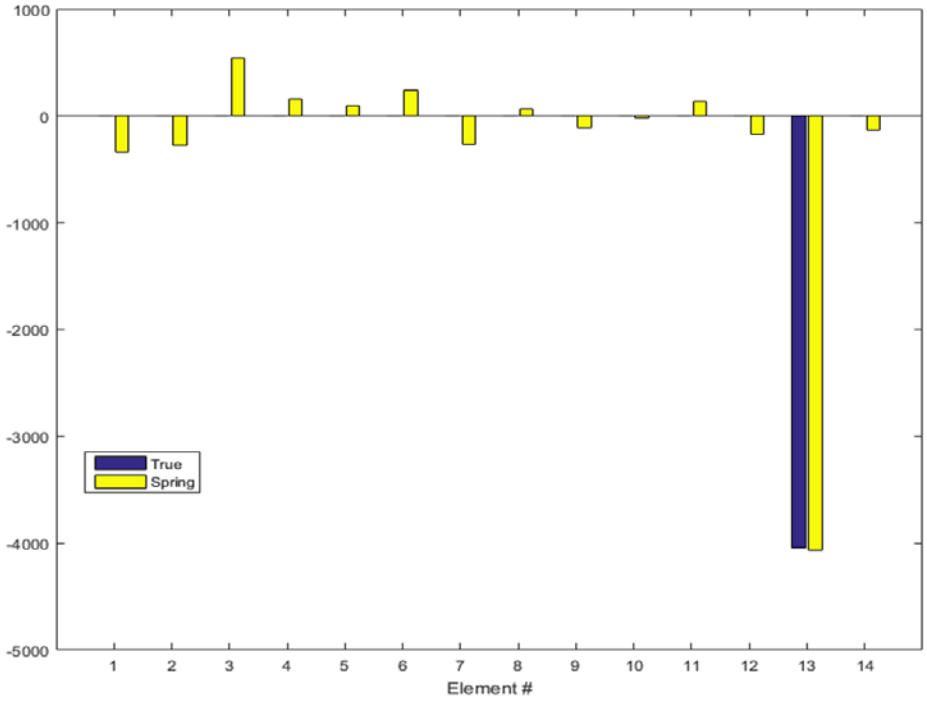

Figure 99. Single Mass Error Identification with Damage at Element 13

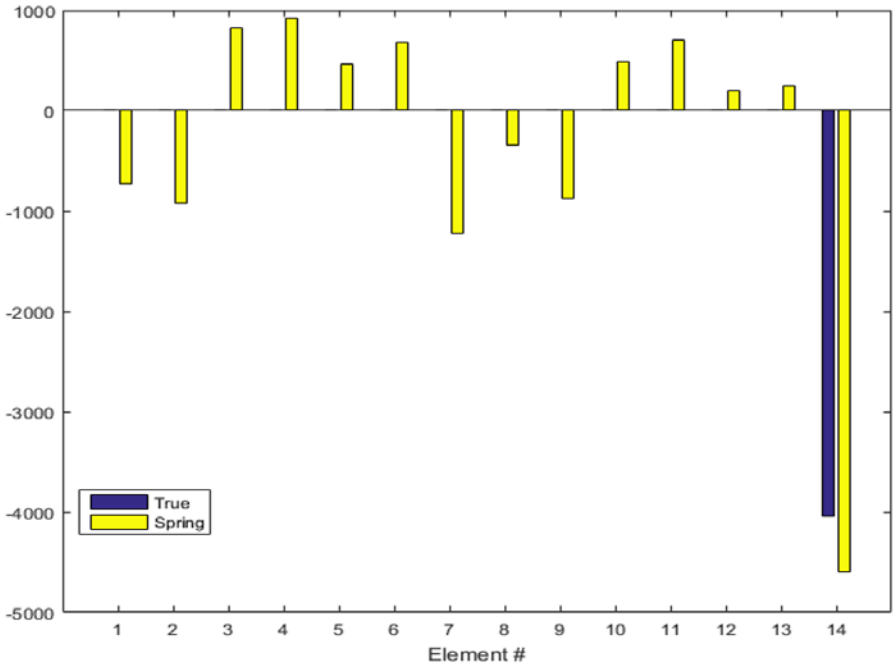

Figure 100. Single Mass Error Identification with Damage at Element 14

Figure 87 through Figure 100 indicate the use of the sensitivity matrix identified in equation (4.18) will accurately find error in all places with minimal false readings.

F. TWO SPRING SYSTEM

In previous thesis work, as described in [11], a two pin solution was developed concurrently with a single pin solution. For example, a pin was synthesized onto nodes 4 and 10 to provide new sensitivity matrices and new resonance frequencies. In some instances, this setup would provide better damage detection capability than a single pin solution. As such, this thesis also explored this capability using a two spring solution as a proof of concept.

Because this thesis is exploring this concept as a proof of concept, springs being synthesized onto the beam are of equal value. Additionally, this thesis will continue to use the same process described for single spring with a 178.579 kg/ mm (10,000 lb/in) spring as the upper bound of the spring.

1. Two Spring FRF Analysis

The process for synthesizing a second spring onto the beam follows the same procedure described in Chapter II and demonstrated earlier in this chapter. The primary difference is expanding the CSET to include the two translational DOFs, and expanding equation (2.65) into a 2x2 matrix with the spring values on the diagonal so it can be used in equation (2.64). As such, equation (2.65) is displayed here as equation (4.20):

$$\left[\Delta Z(\omega)\right] = \begin{bmatrix} \Delta k_{spring} & 0 \\ 0 & \Delta k_{spring} \end{bmatrix} \tag{4.20}$$

Figure 101 checks the synthesis of two springs against a FEM that would have the springs physically installed.

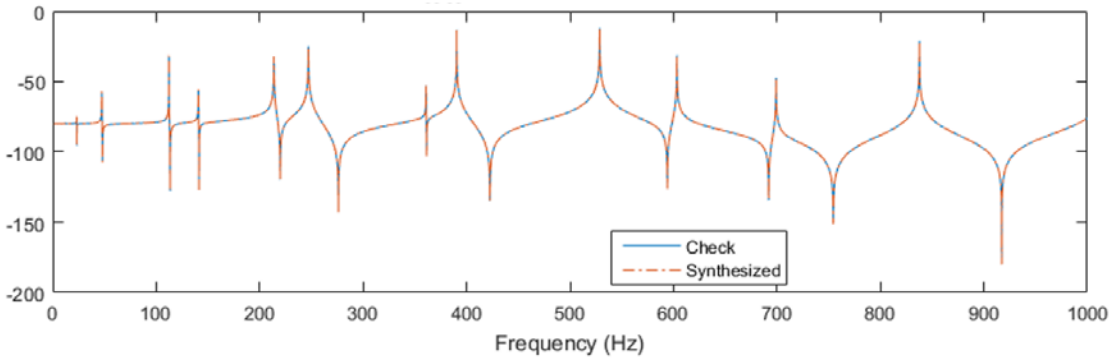

Figure 101. Two Springs at Nodes 5 and 12 FRF Synthesis Check, $H_{33,33}$, 178.579 kg/mm (10,000 lb/in) Springs

Following the procedure in Chapter II with the modification presented in equation (4.15), we can synthesize two springs onto the beam and check the synthesis by creating a second beam with the new stiffness installed. Using two springs at 178.579 kg/mm (10,000 lb/in) on nodes 5 and 12, Figure 101 confirms that the springs are being synthesized correctly.

As displayed in Figure 102, when we vary the strength of the spring on these nodes, similar to the single spring, the resonance frequencies change, confirming that useful information can be used from this process. Additionally, we see that the addition of the springs transfers both rigid body modes into elastic modes

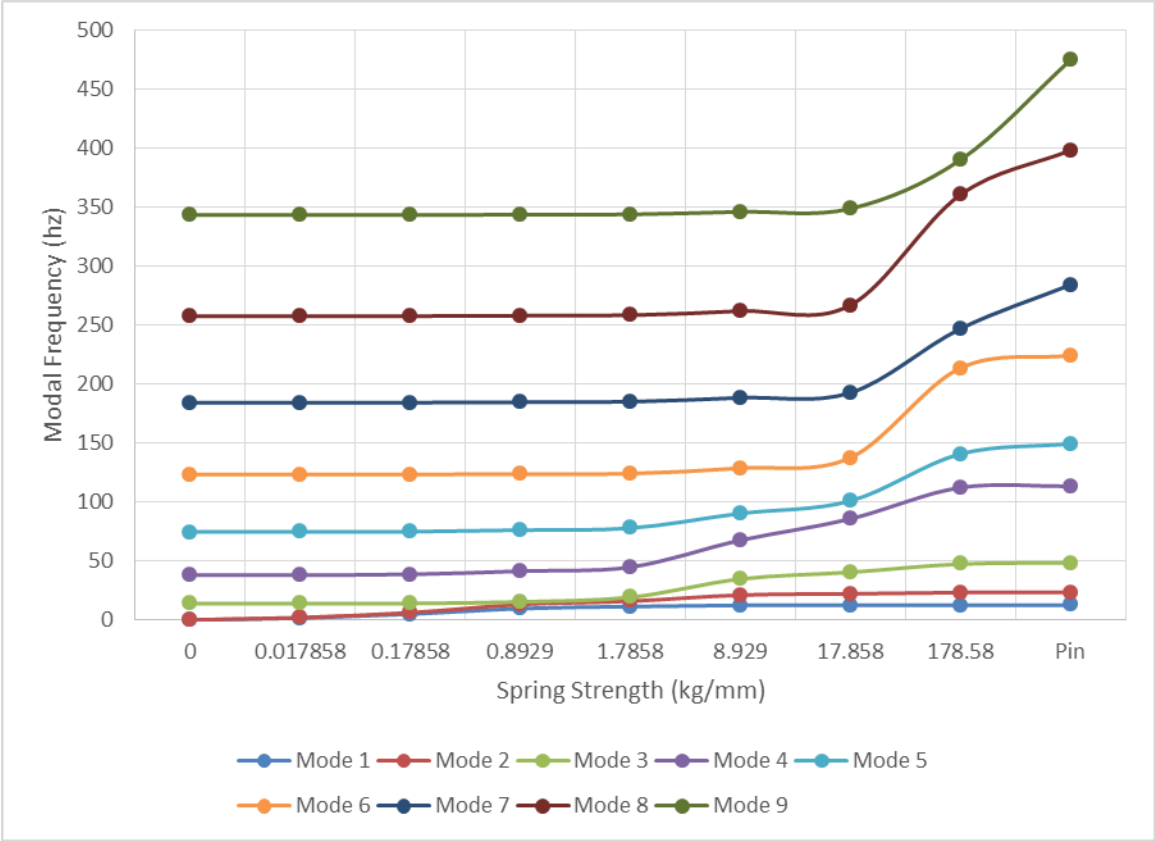

Figure 102. Frequency Progression with Springs Installed at Nodes 5 and 12, Varying strength from 0–178.579 kg/mm (0-10,000 lb/in) Equally

Using equation (2.64) and (2.65), we are able to predict the modal response of the beam with the spring installed as detailed in Figure 103 and Figure 104.

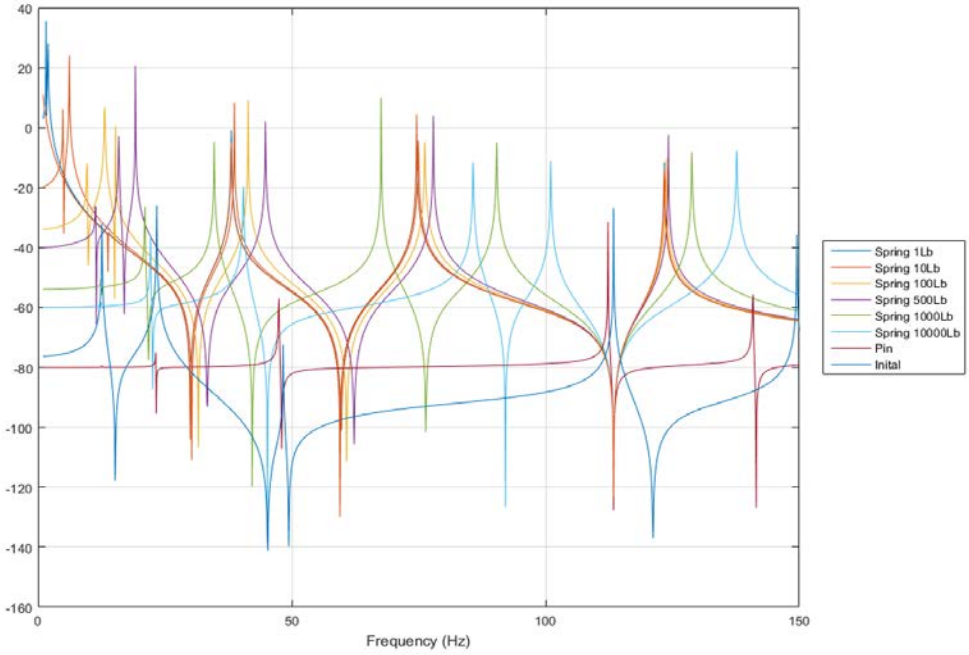

Figure 103. FRF Progression with Springs Installed at Nodes 5 and 12, Varying strength from 0–178.579 kg/mm (0-10,000 lb/in) Equally, $H_{9,9}$

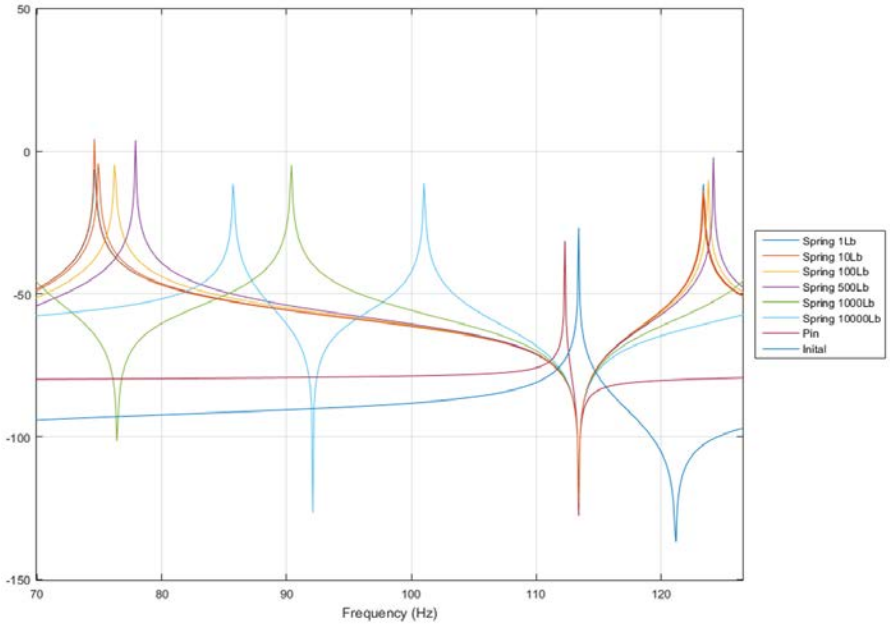

Figure 104. Magnified FRF Variance with Springs Installed at Nodes 5 and 12, Varying strength from 0–178.579 kg/mm (0-10,000 lb/in) Equally,$H_{9,9}$

2. Two Spring Sensitivity Analysis

Following the procedure described in the single spring synthesis analysis, this thesis explored the variance of the highest mode of the sensitivity matrix as spring strength increased. A two-spring synthesis can be installed in 105 different locations; however, as a proof of concept, this thesis will not be exploring every possible combination of sensitivity matrices. As such, 14 different locations where chosen at random. These locations and the subsequent results are displayed in Figure 105 through Figure 118.

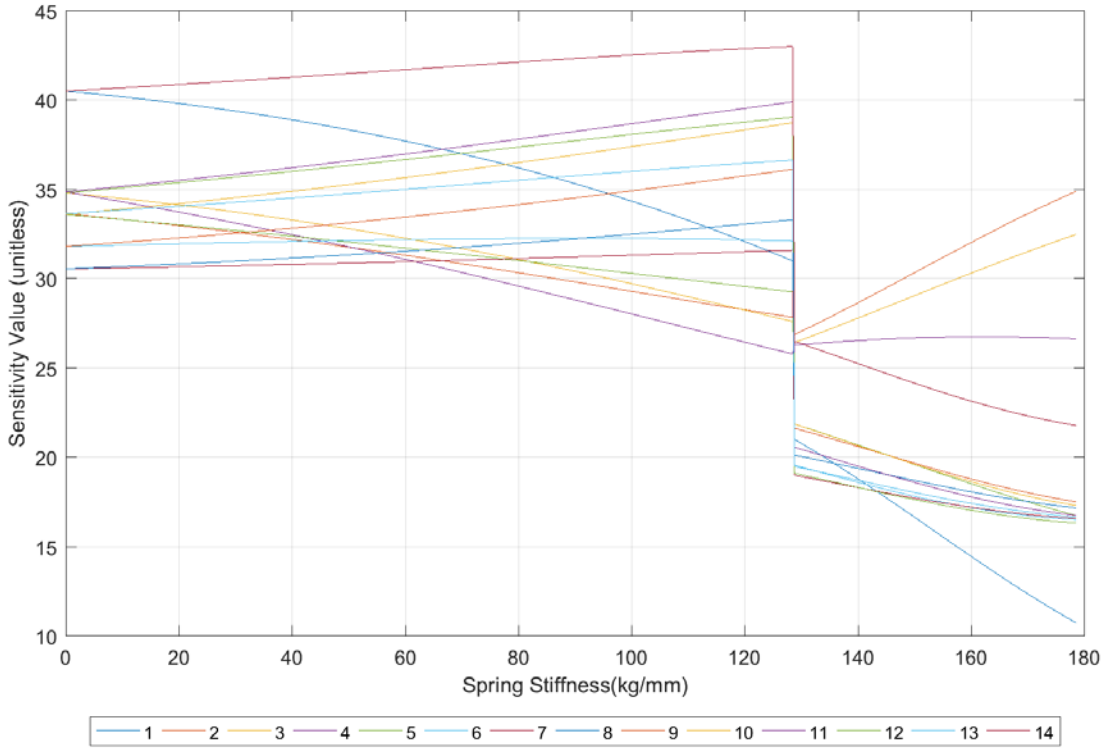

Figure 105. Effects on Sensitivity Value with Increasing Spring Strength for Springs Located on Nodes 2 and 6 from 0–178.579 kg/mm (0-10,000 lb/in) Equally

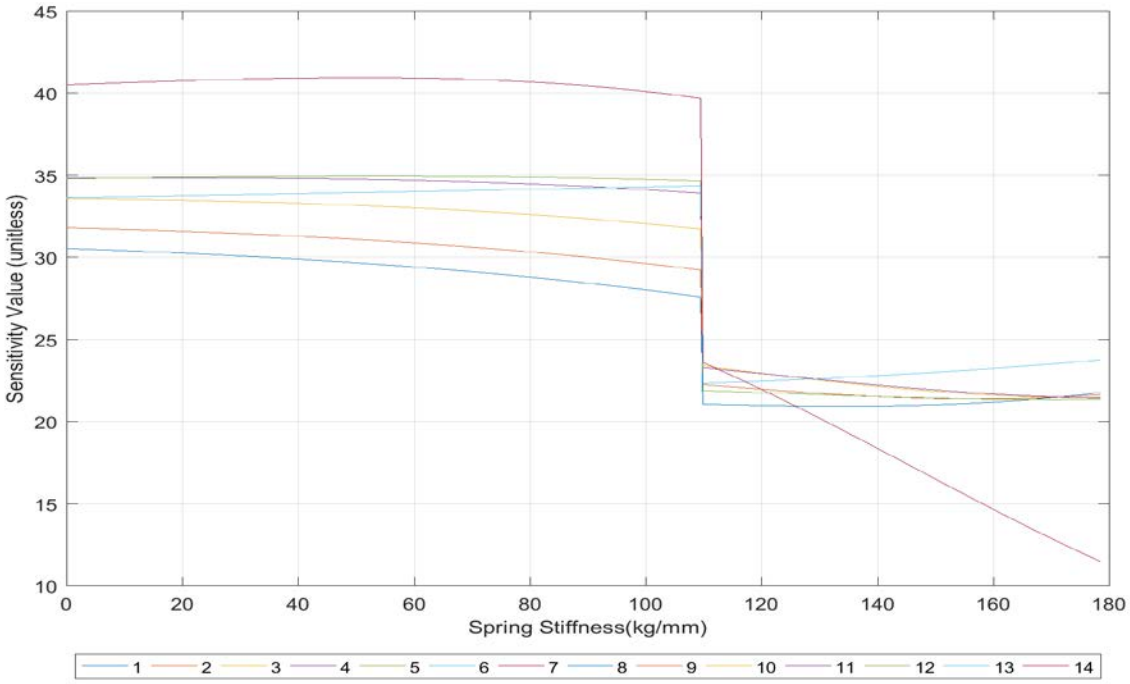

Figure 106. Effects on Sensitivity Value with Increasing Spring Strength for Springs Located on Nodes 2 and 16 from 0–178.579 kg/mm (0-10,000 lb/in) Equally

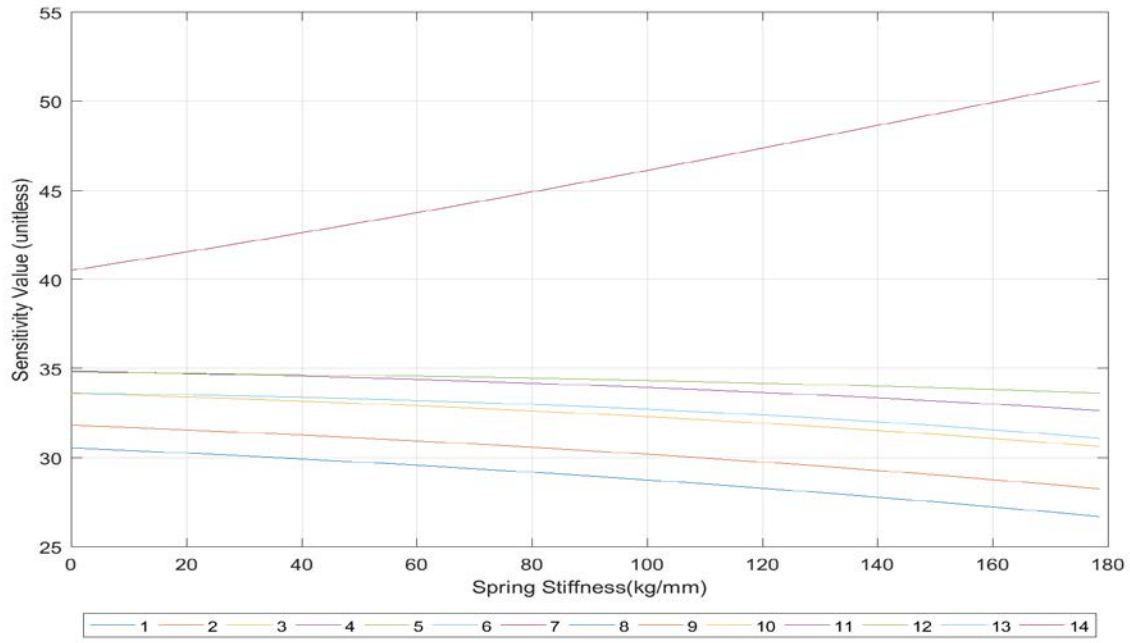

Figure 107. Effects on Sensitivity Value with Increasing Spring Strength for Springs Located on Nodes 3 and 15 from 0–178.579 kg/mm (0-10,000 lb/in) Equally

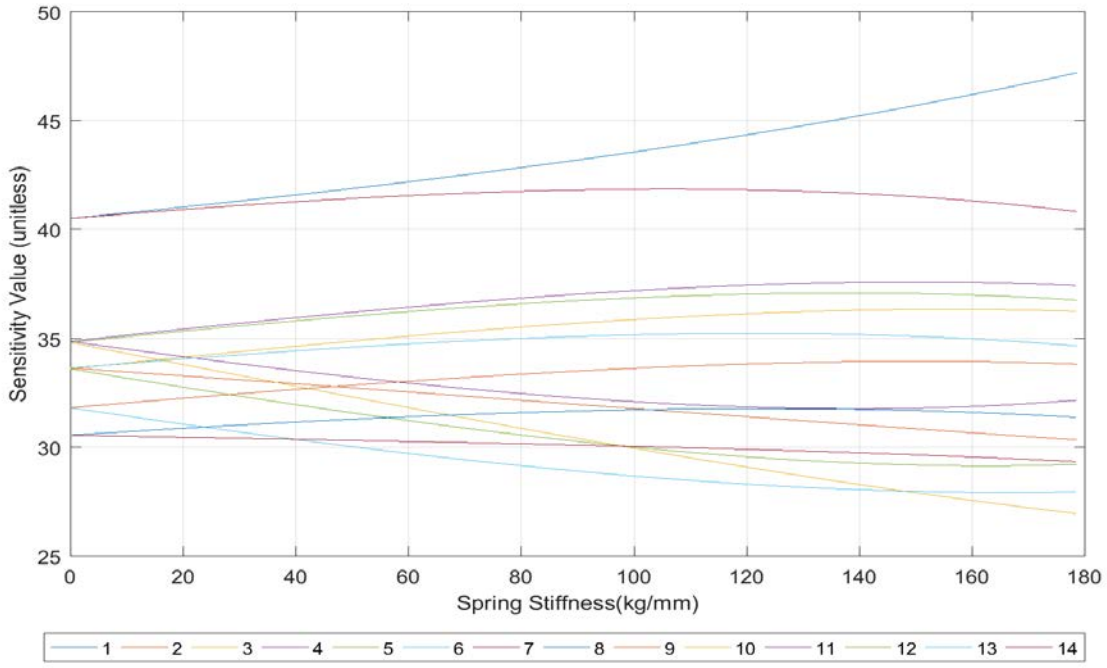

Figure 108. Effects on Sensitivity Value with Increasing Spring Strength for Springs Located on Nodes 4 and 8 from 0–178.579 kg/mm (0-10,000 lb/in) Equally

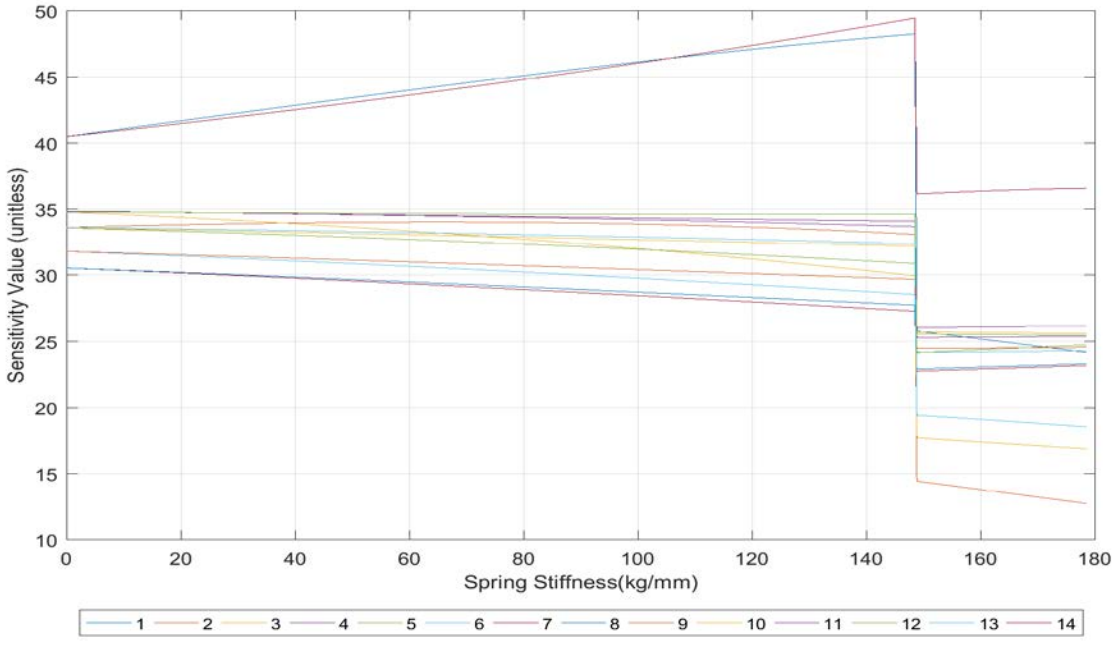

Figure 109. Effects on Sensitivity Value with Increasing Spring Strength for Springs Located on Nodes 4 and 15 from 0–178.579 kg/mm (0-10,000 lb/in) Equally

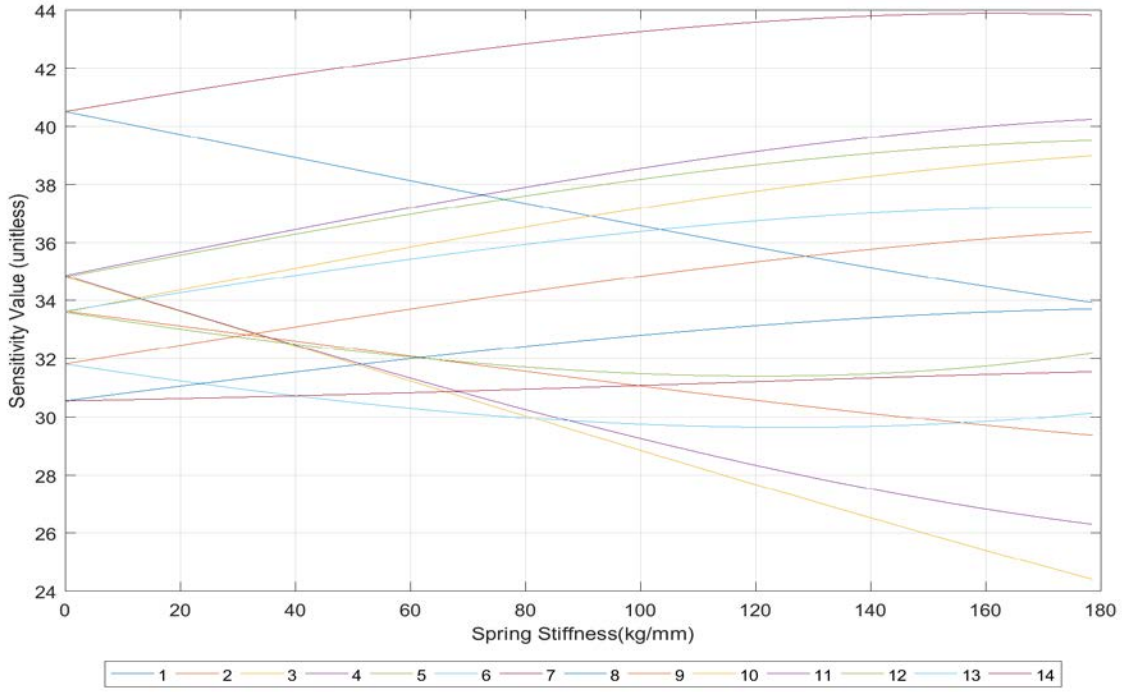

Figure 110. Effects on Sensitivity Value with Increasing Spring Strength for Springs Located on Nodes 5 and 8 from 0–178.579 kg/mm (0-10,000 lb/in) Equally

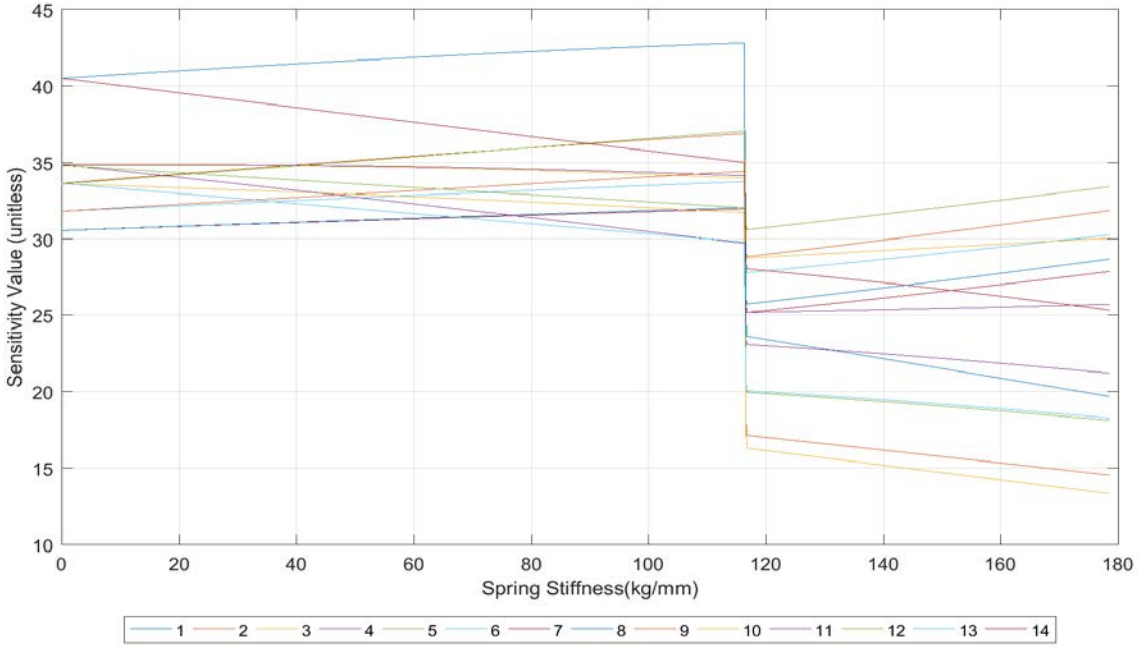

Figure 111. Effects on Sensitivity Value with Increasing Spring Strength for Springs Located on Nodes 5 and 12 from 0–178.579 kg/mm (0-10,000 lb/in) Equally

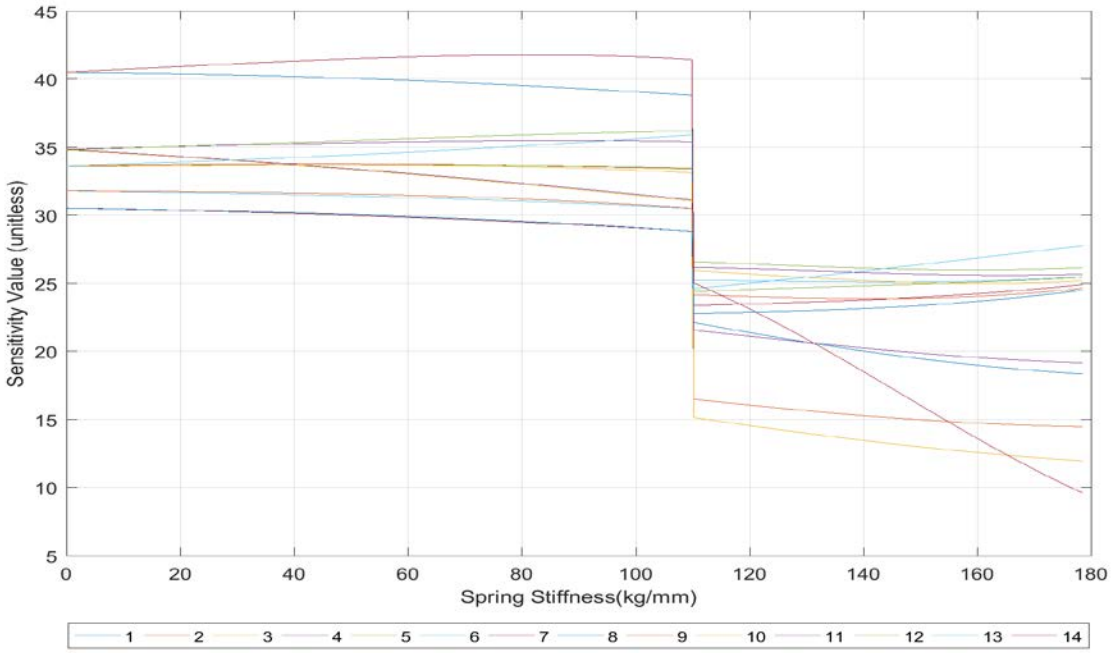

Figure 112. Effects on Sensitivity Value with Increasing Spring Strength for Springs Located on Nodes 5 and 16 from 0–178.579 kg/mm (0-10,000 lb/in) Equally

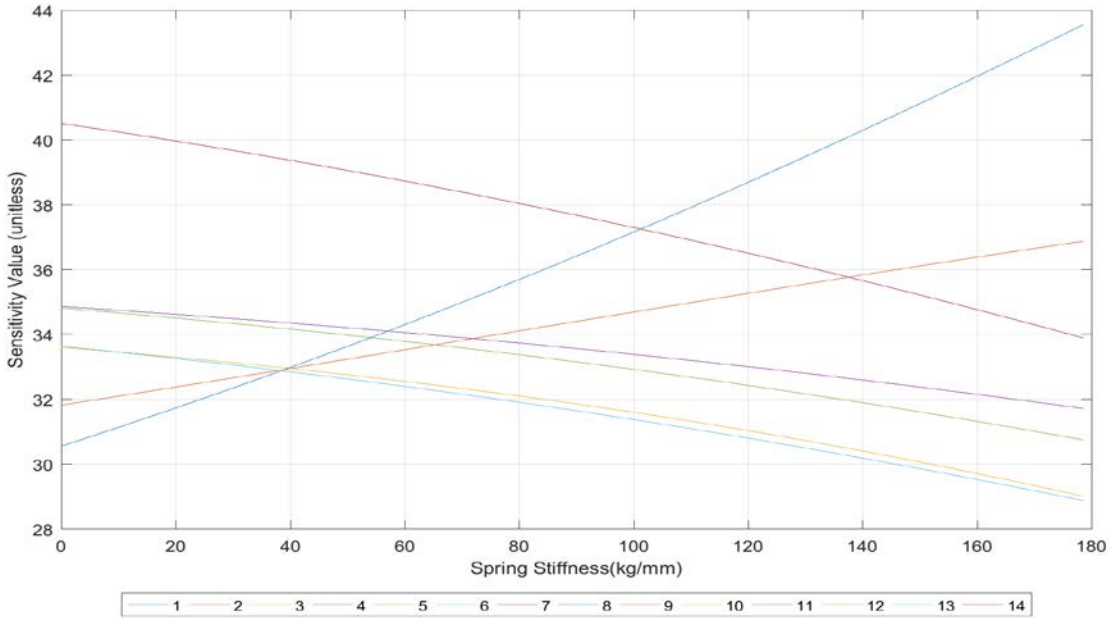

Figure 113. Effects on Sensitivity Value with Increasing Spring Strength for Springs Located on Nodes 7 and 11 from 0–178.579 kg/mm (0-10,000 lb/in) Equally

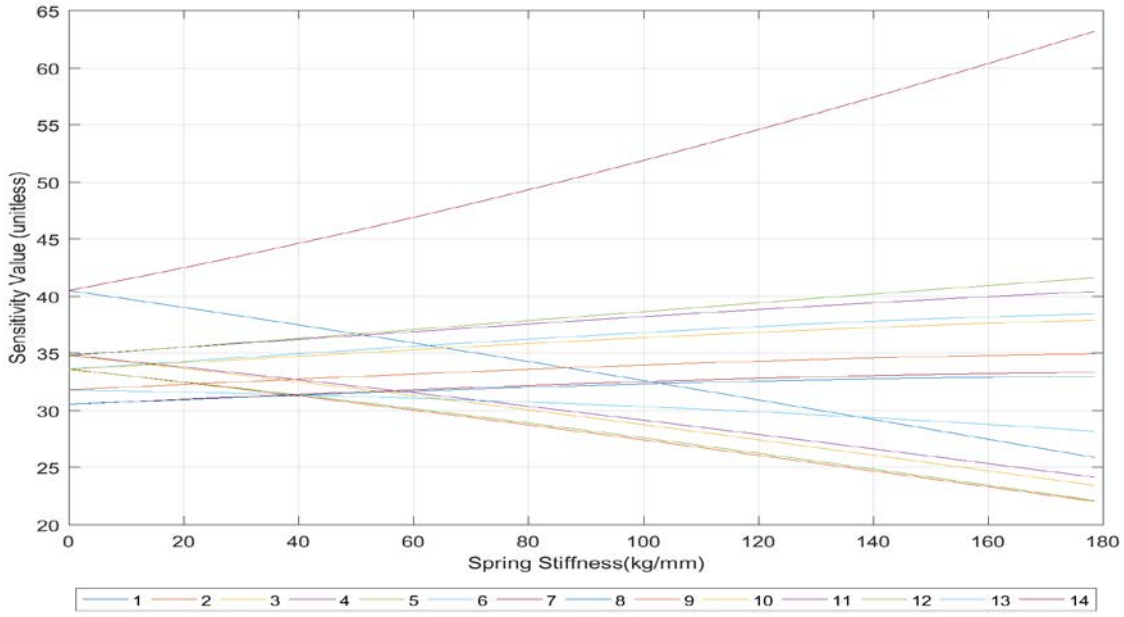

Figure 114. Effects on Sensitivity Value with Increasing Spring Strength for Springs Located on Nodes 7 and 15 from 0–178.579 kg/mm (0-10,000 lb/in) Equally

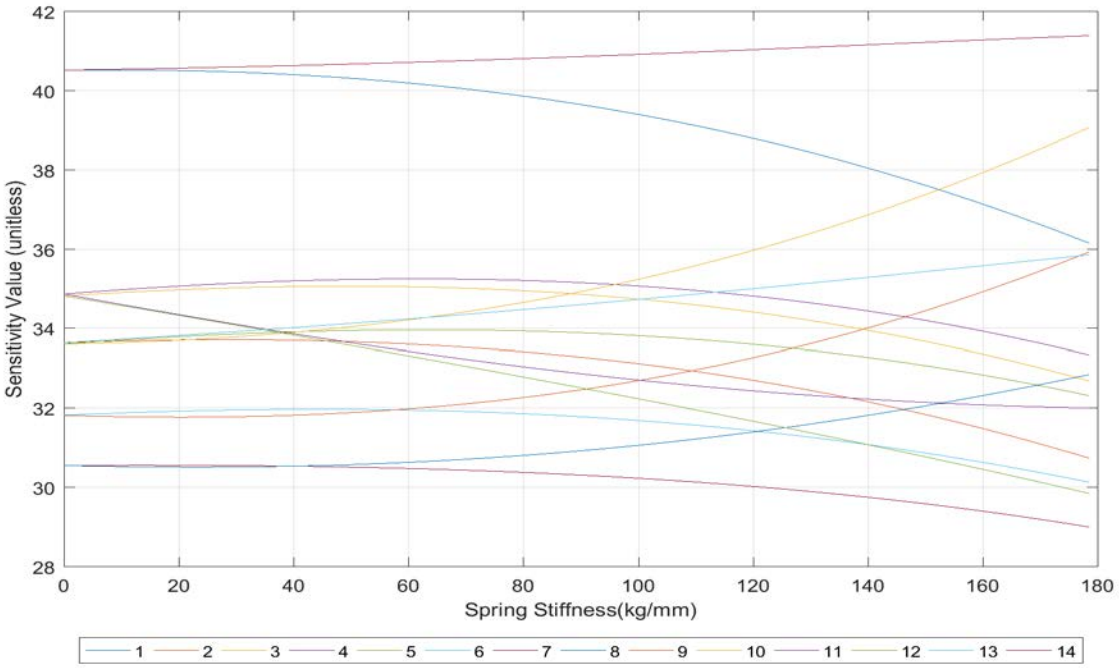

Figure 115. Effects on Sensitivity Value with Increasing Spring Strength for Springs Located on Nodes 9 and 13 from 0–178.579 kg/mm (0-10,000 lb/in) Equally

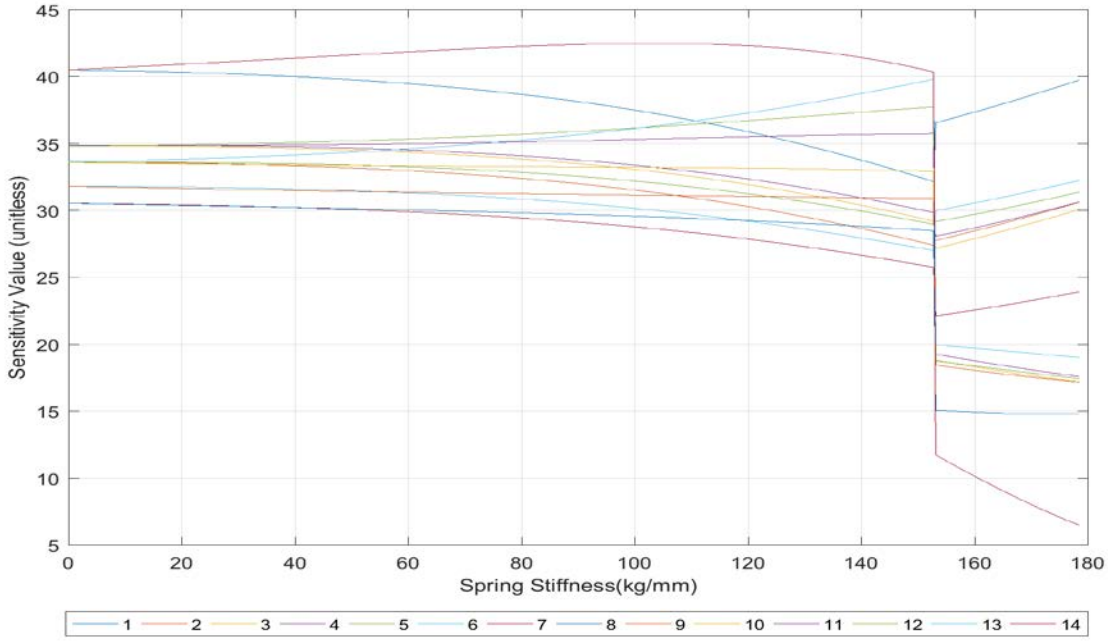

Figure 116. Effects on Sensitivity Value with Increasing Spring Strength for Springs Located on Nodes 9 and 16 from 0–178.579 kg/mm (0-10,000 lb/in) Equally

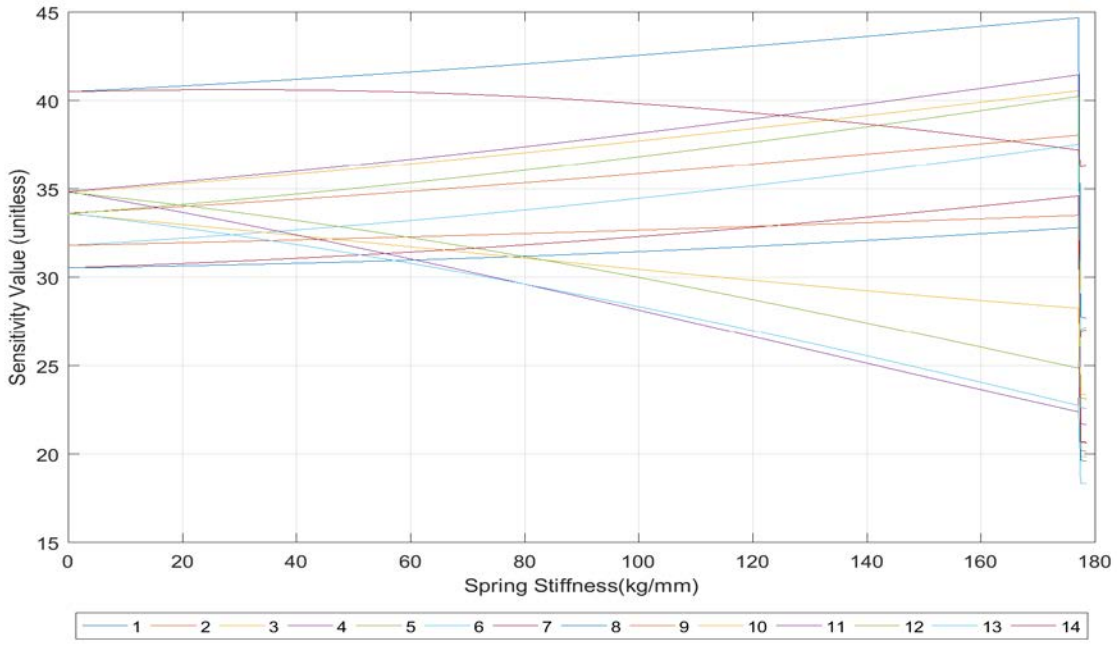

Figure 117. Effects on Sensitivity Value with Increasing Spring Strength for Springs Located on Nodes 12 and 15 from 0–178.579 kg/mm (0-10,000 lb/in) Equally

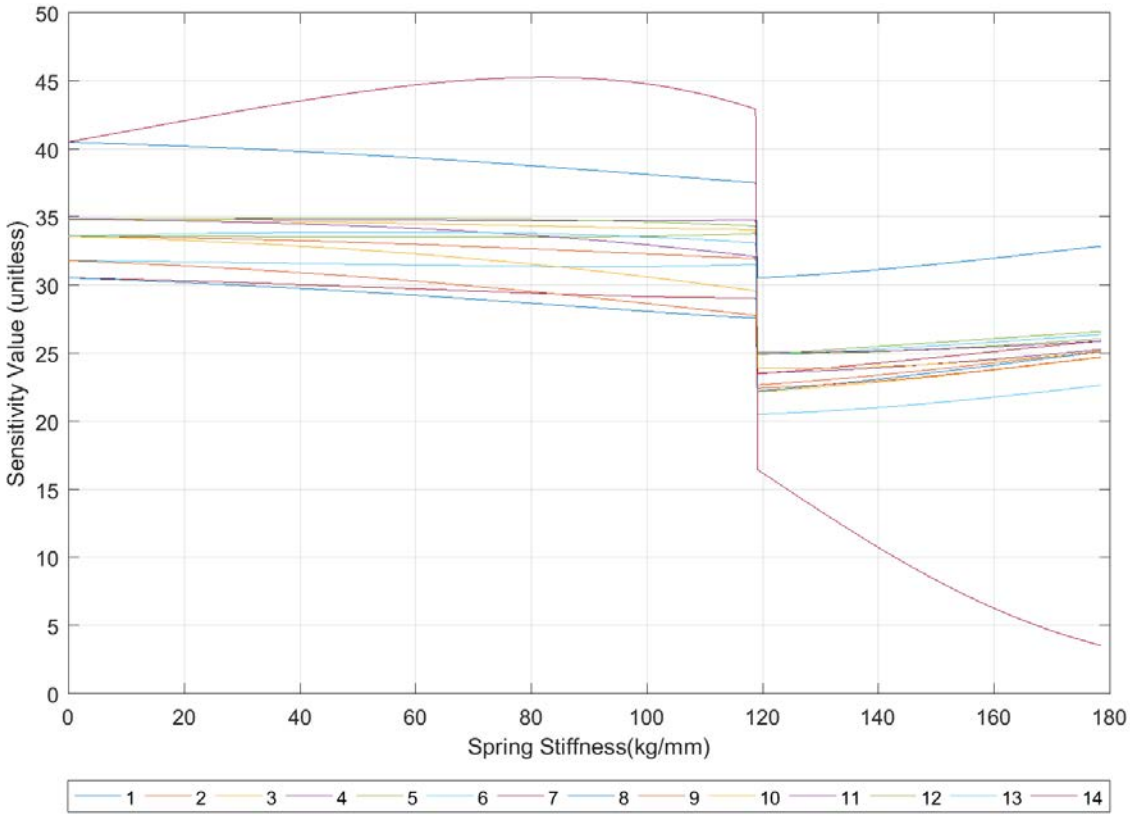

Figure 118. Effects on Sensitivity Value with Increasing Spring Strength for Springs Located on Nodes 15 and 16 from 0–178.579 kg/mm (0-10,000 lb/in) Equally

Using the 14 different spring locations chosen at random as displayed in Figure 105 through Figure 118 we can generate multiple sensitivity matrices from each set of locations. These are identified in Table 13.

Table 13. Useable Two Spring Sensitivity Matrices

Nodes	Spring Value (kg/mm)	Spring Value (lb/in)
2,6	71.43, 125.01, 178.58	4000, 7000, 10000
2,16	116.08, 178.58	6500, 10000
3,15	53.57, 125.01, 178.58	3000, 7000, 10000
4,8	53.57, 125.01, 178.58	3000, 7000, 10000
4,15	71.43, 142.86, 178.58	4000, 8000, 10000
5,8	53.57, 178.58	3000, 10000
5,12	53.57, 107.15, 125.01, 178.58	3000, 6000, 7000, 10000
5,16	80.36, 178.58	4500, 1000
7,11	53.57, 89.29, 178.58	3000, 5000, 10000
7,15	71.43, 178.58	4000, 10000
9,13	116.08, 160.72	6500, 9000
9,16	125.01, 178.58	7000, 10000
12,15	71.43, 107.15, 160.72, 178.58	4000, 6000, 9000, 10000
15,16	80.36, 178.58	4500, 1000

To minimize the sensitivity matrix condition number, thus maximizing matrix accuracy, the conditions identified in Table 13 are indexed and placed in Table 14. Following the procedures detailed for Figure 52 two baseline modes are concatenated with six of the highest modes from two different indexes. The resulting sensitivity matrix condition numbers are displayed in Figure 119.

Table 14. Index of Two Spring Sensitivity Matrices for Evaluating Condition Number

Index Number	Nodes	Spring Value kg/mm (lb/in)
1	2,6	71.43(4000)
2	2,6	125.01(7000)
3	2,6	178.58(10000)
4	2,16	116.08(6500)
5	2,16	178.58(10000)
6	3,15	53.57(3000)
7	3,15	125.01(7000)
8	3,15	178.58(10000)
9	4,8	53.57(3000)
10	4,8	125.01(7000)
11	4,8	178.58(10000)
12	4,15	71.43(4000)
13	4,15	142.86(8000)
14	4,15	178.58(10000)
15	5,8	53.57(3000)
16	5,8	178.58(10000)
17	5,12	53.57(3000)
18	5,12	107.15(6000)

Index Number	Nodes	Spring Value kg/mm (lb/in)
19	5,12	125.01(7000)
20	5,12	178.58(10000)
21	5,16	80.36(4500)
22	5,16	178.58(10000)
23	7,11	53.57(3000)
24	7,11	89.29(5000)
25	7,11	178.58(10000)
26	7,15	71.43(4000)
27	7,15	178.58(10000)
28	9,13	116.08(6500)
29	9,13	160.72(9000)
30	9,16	125.01(7000)
31	9,16	178.58(10000)
32	12,15	71.43(4000)
33	12,15	107.15(6000)
34	12,15	160.72(9000)
35	12,15	178.58(10000)
36	15,16	80.36(4500)
37	15,16	178.58(10000)

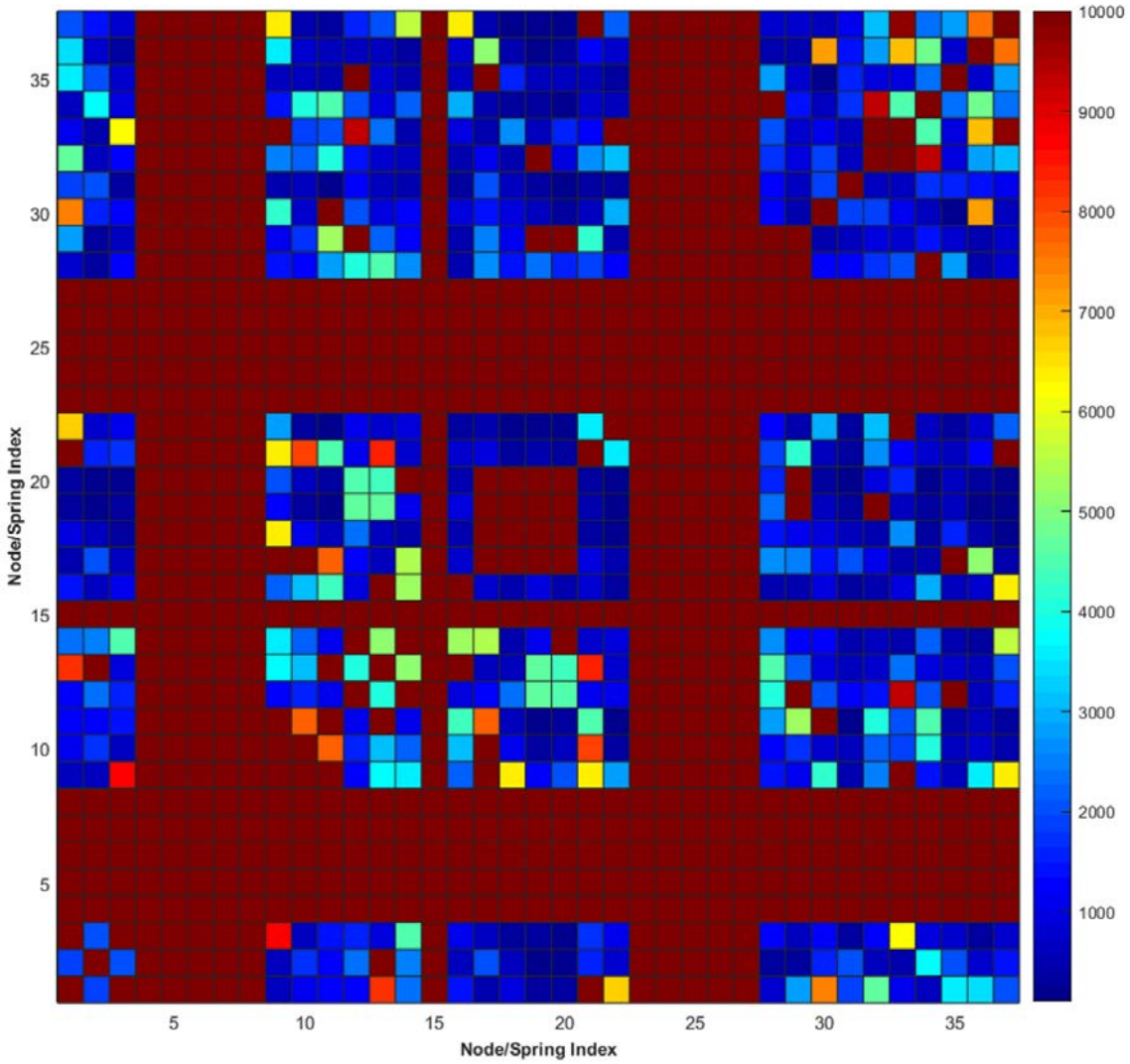

Figure 119. Sensitivity Matrix Condition Number Evaluation, Two Springs

With 37 identified possibilities, 1,369 sensitivity matrix combinations where evaluated for their matrix condition number in Figure 119. The lowest condition number occurred at index 22,30 with a condition number of 112.55. Using Table 14, the equation (4.16) should provide the most accurate combination of conditions for solving for damage detection:

$$\left[S_{comp}\right]_{14x14} = \begin{bmatrix} \left[S^{(0)}\right]_{2\times14} \\ \left[S^{(N5,12-10,000)}\right]_{6\times14} \\ \left[S^{(N5,16-10,000)}\right]_{6\times14} \end{bmatrix} \tag{4.21}$$

$$\left[S_{comp}\right] = \begin{bmatrix} 30.602 & 21.625 & 21.721 & 24.831 & 26.337 & 24.357 & 21.478 & 21.478 & 24.357 & 26.337 & 24.831 & 21.721 & 21.625 & 30.602 \\ 40.523 & 33.646 & 34.824 & 34.873 & 33.613 & 31.827 & 30.562 & 30.562 & 31.827 & 33.613 & 34.873 & 34.824 & 33.646 & 40.523 \\ 0.001 & 0.006 & 0.024 & 0.184 & 0.151 & 0.349 & 0.127 & 0.441 & 0.112 & 0.894 & 8.477 & 6.933 & 19.455 & 8.739 \\ 0.159 & 0.433 & 0.453 & 6.686 & 4.264 & 12.904 & 3.867 & 12.608 & 4.889 & 7.708 & 2.520 & 1.666 & 2.273 & 1.250 \\ 14.357 & 13.342 & 8.767 & 2.968 & 9.293 & 5.183 & 10.795 & 7.761 & 5.624 & 7.309 & 0.291 & 2.309 & 1.384 & 1.539 \\ 25.431 & 18.162 & 24.307 & 11.328 & 7.439 & 12.584 & 11.584 & 6.903 & 11.534 & 6.879 & 2.064 & 8.072 & 4.845 & 6.766 \\ 9.239 & 6.057 & 8.434 & 13.133 & 10.829 & 9.297 & 12.989 & 14.299 & 11.124 & 8.846 & 28.775 & 32.559 & 24.815 & 38.110 \\ 19.713 & 14.569 & 13.363 & 25.734 & 33.431 & 30.279 & 27.885 & 28.695 & 31.873 & 30.058 & 21.234 & 18.141 & 18.294 & 25.347 \\ 0.028 & 0.128 & 0.529 & 3.963 & 3.289 & 7.551 & 2.793 & 8.229 & 2.287 & 8.378 & 2.500 & 7.878 & 3.167 & 5.630 \\ 1.808 & 2.354 & 0.219 & 6.306 & 4.494 & 9.898 & 8.953 & 4.982 & 11.713 & 5.644 & 7.974 & 10.640 & 4.235 & 8.254 \\ 24.344 & 20.064 & 19.234 & 0.987 & 8.194 & 4.627 & 4.080 & 7.356 & 4.693 & 4.056 & 7.341 & 4.778 & 4.055 & 4.701 \\ 17.957 & 12.132 & 17.648 & 15.181 & 9.161 & 12.557 & 16.526 & 11.262 & 9.743 & 15.712 & 14.448 & 9.135 & 13.276 & 8.111 \\ 12.466 & 8.491 & 9.829 & 19.273 & 20.682 & 16.570 & 17.473 & 21.764 & 22.392 & 18.330 & 16.235 & 19.501 & 24.628 & 3.834 \\ 18.360 & 14.491 & 11.983 & 19.181 & 26.173 & 25.506 & 24.941 & 24.530 & 24.665 & 25.223 & 25.708 & 25.480 & 27.797 & 9.620 \end{bmatrix} \tag{4.22}$$

To test the capability of this matrix, an identical FEM was made that included damage in one of the elements. Because we made the sensitivity matrix for the flexural rigidity (EI), damage was simulated by decreasing the EI value in one element by 5%, and evaluated all elements of the beam, i.e., including all 15 elements. As detailed in Chapter II, this is accomplished by solving equation (2.46), which has been adapted and displayed here as equation (4.23) and equation (4.24):

$$\begin{bmatrix} \left[S^{(0)}\right]_{2\times14} \\ \left[S^{(N5,12-10,000)}\right]_{6\times14} \\ \left[S^{(N5,16-10,000)}\right]_{6\times14} \end{bmatrix}^{-1} \begin{Bmatrix} \left\{\Delta\lambda^{(0)}\right\}_{2\times1} \\ \left\{\Delta\lambda^{(N5,12-10,000)}\right\}_{6\times1} \\ \left\{\Delta\lambda^{(N5,16-10,000)}\right\}_{6\times1} \end{Bmatrix} = \begin{Bmatrix} \Delta EI_1 \\ \Delta EI_2 \\ \vdots \\ \Delta EI_{14} \end{Bmatrix} \tag{4.23}$$

$$\left[S_{comp}\right]^{-1}_{14\times14} \left\{\Delta\lambda_{comp}\right\}_{14\times1} = \left\{\Delta EI\right\}_{14\times1} \tag{4.24}$$

Figure 120 through Figure 133 show the results of testing for damage in every possible location. As with the testing for a single spring synthesis, the blue line indicates the actual damage of a five percent reduction in EI, and the yellow is the indicated damage from solving equation (4.24).

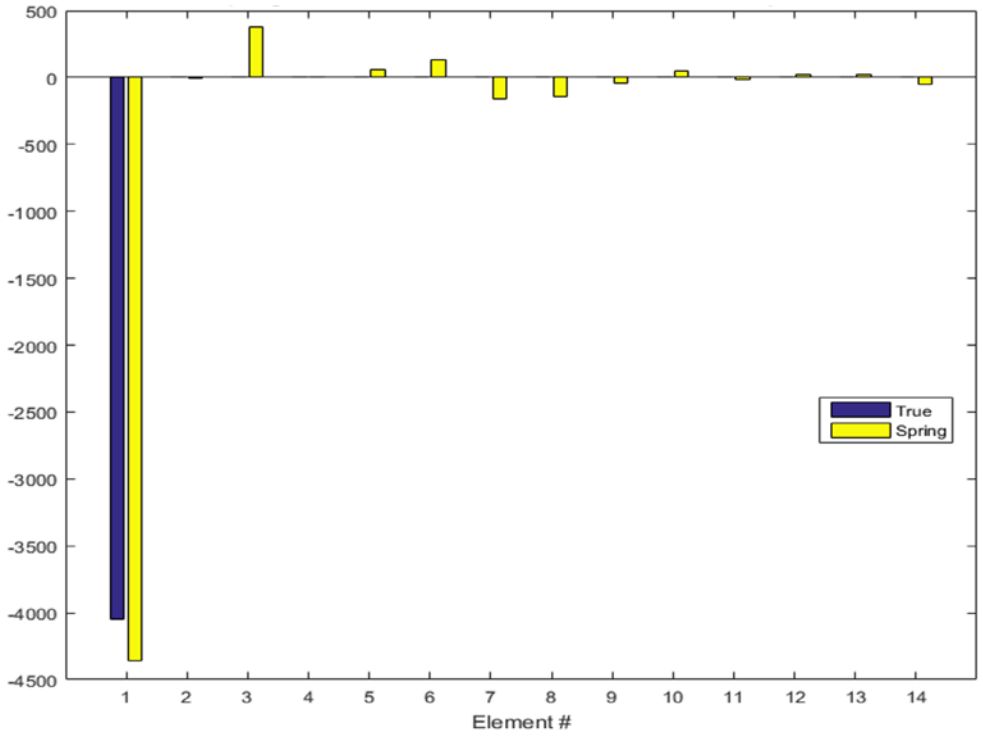

Figure 120. Two Spring Error Identification at Element 1

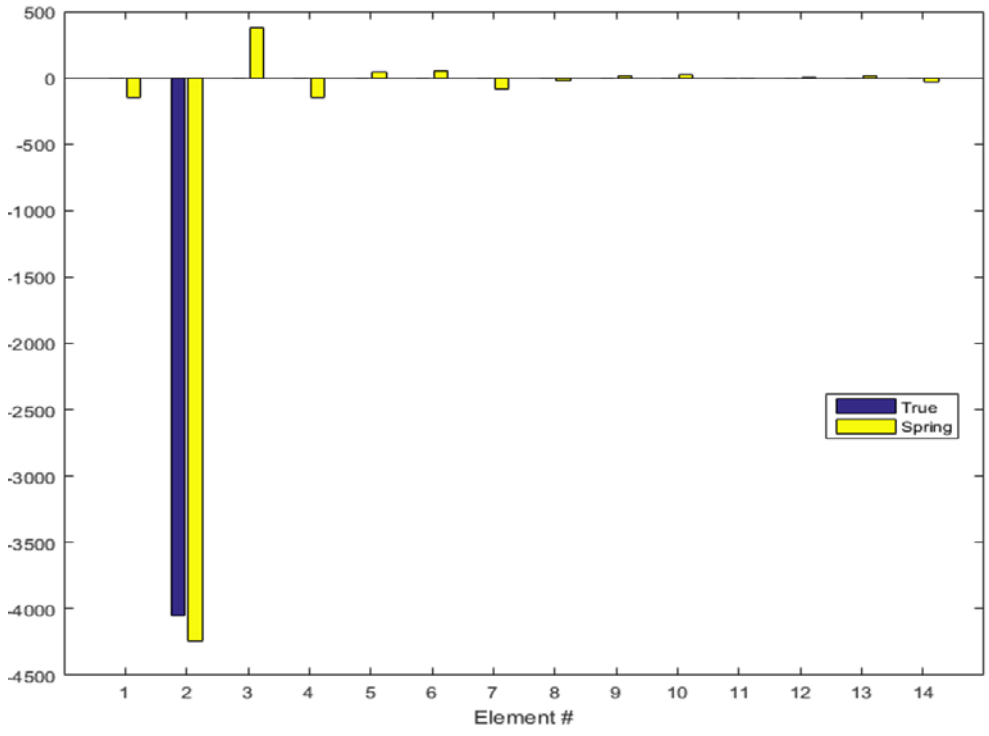

Figure 121. Two Spring Error Identification at Element 2

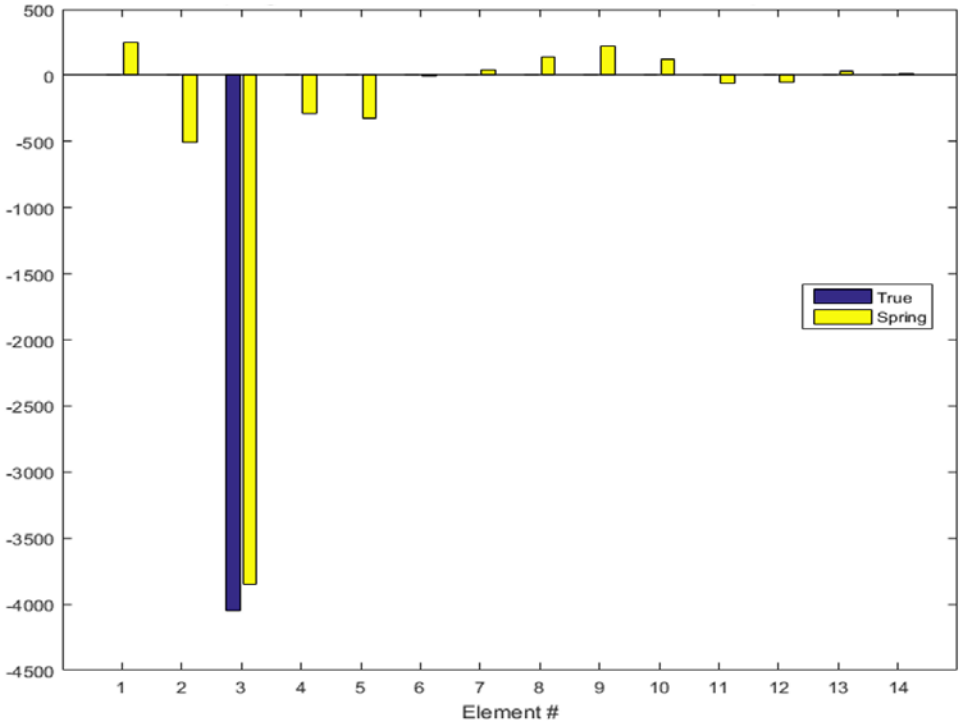

Figure 122. Two Spring Error Identification at Element 3

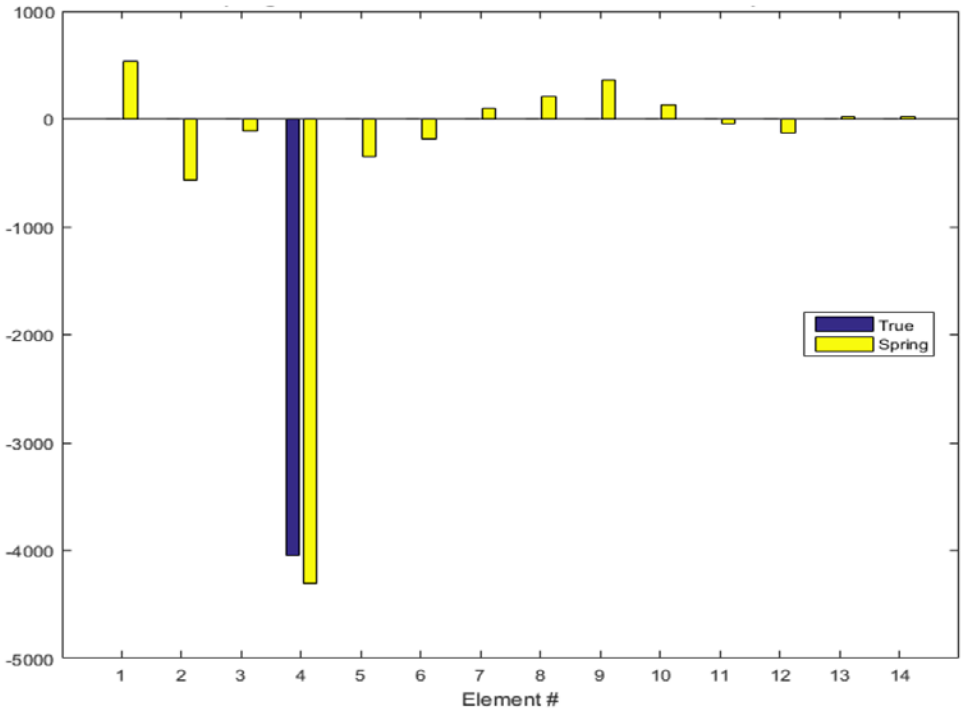

Figure 123. Two Spring Error Identification at Element 4

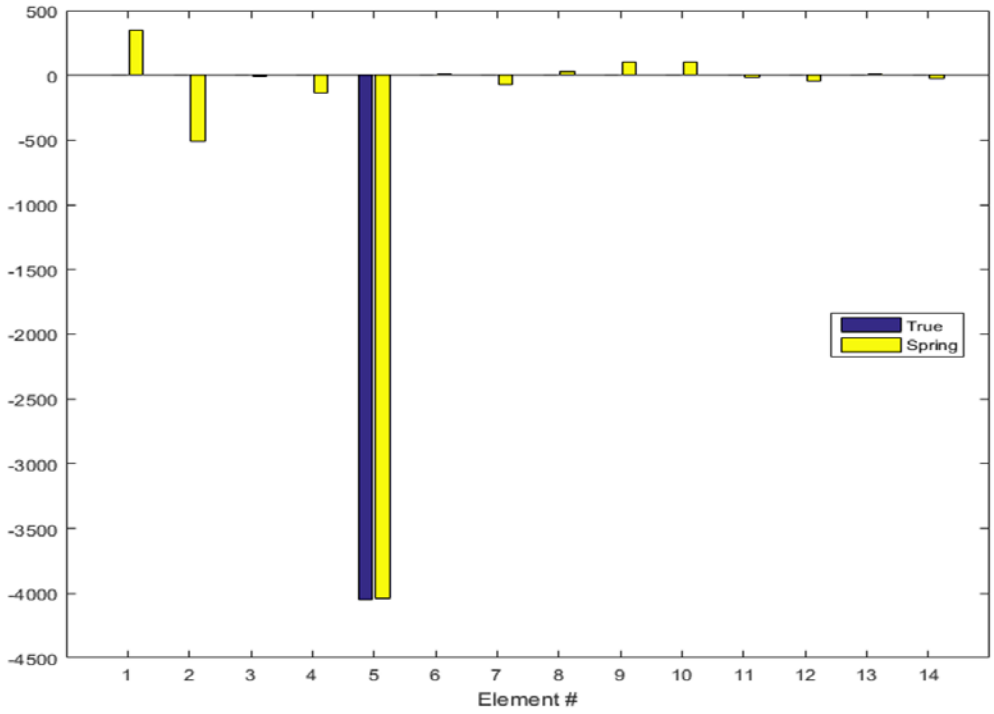

Figure 124. Two Spring Error Identification at Element 5

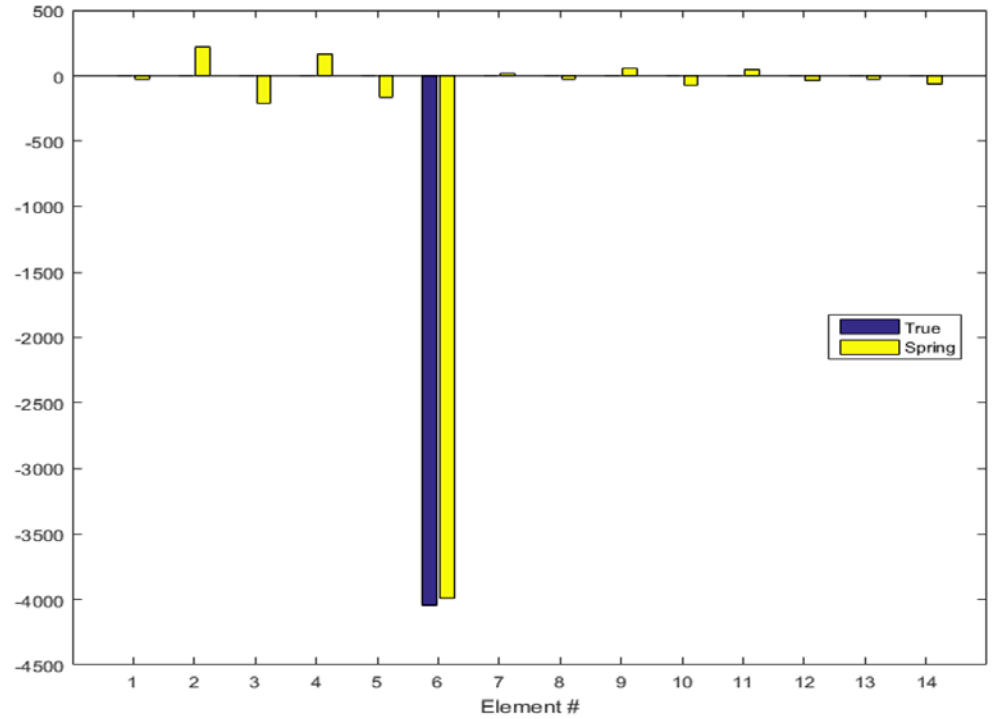

Figure 125. Two Spring Error Identification at Element 6

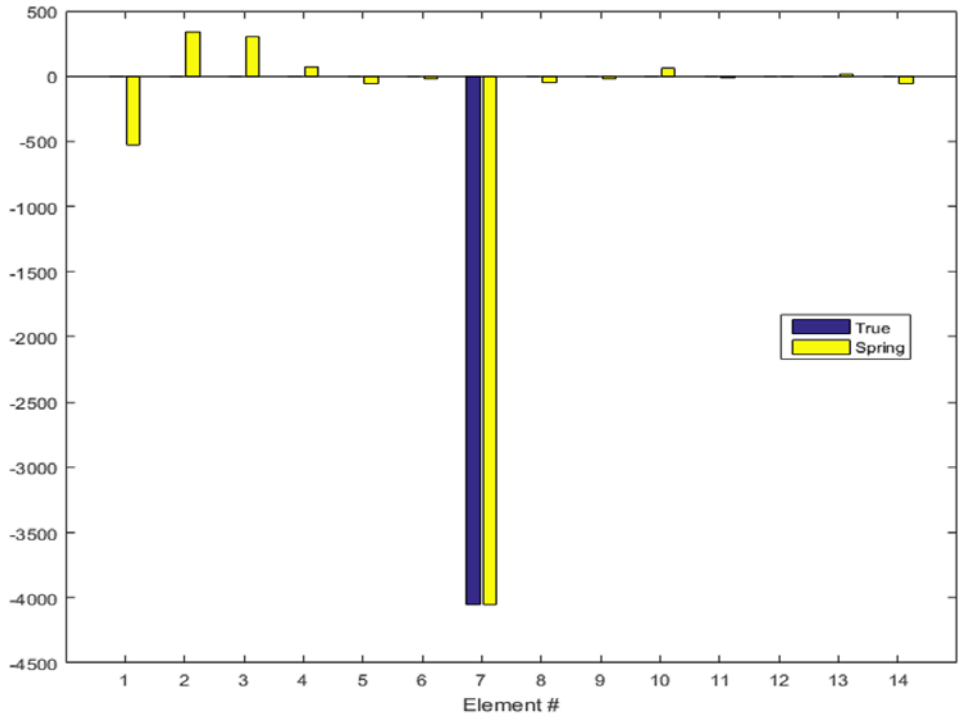

Figure 126. Two Spring Error Identification at Element 7

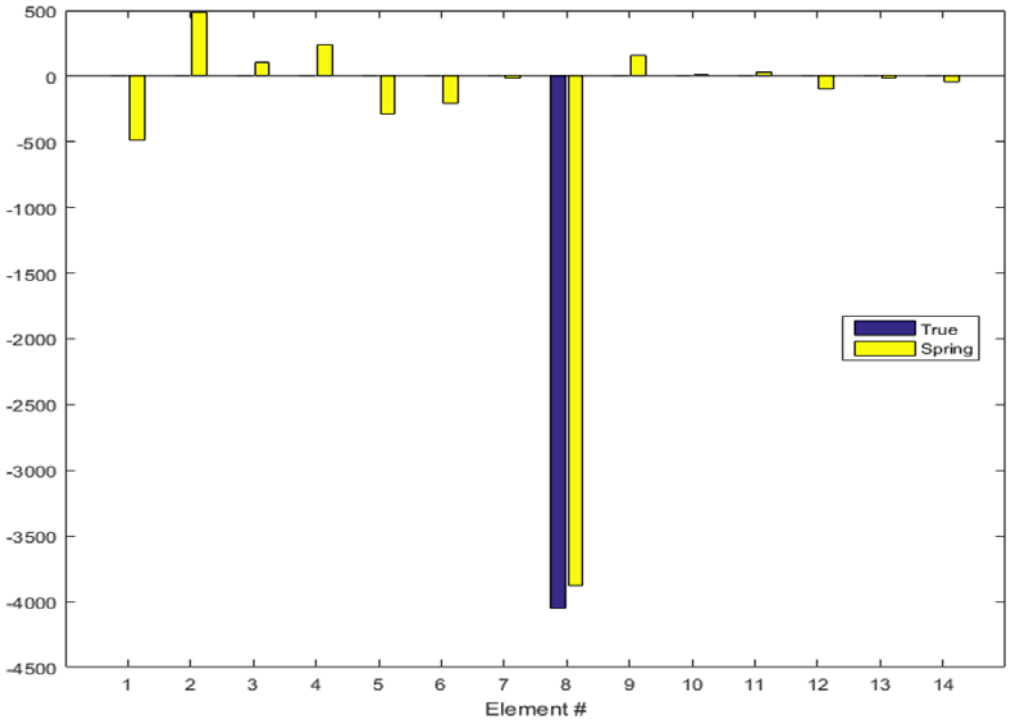

Figure 127. Two Spring Error Identification at Element 8

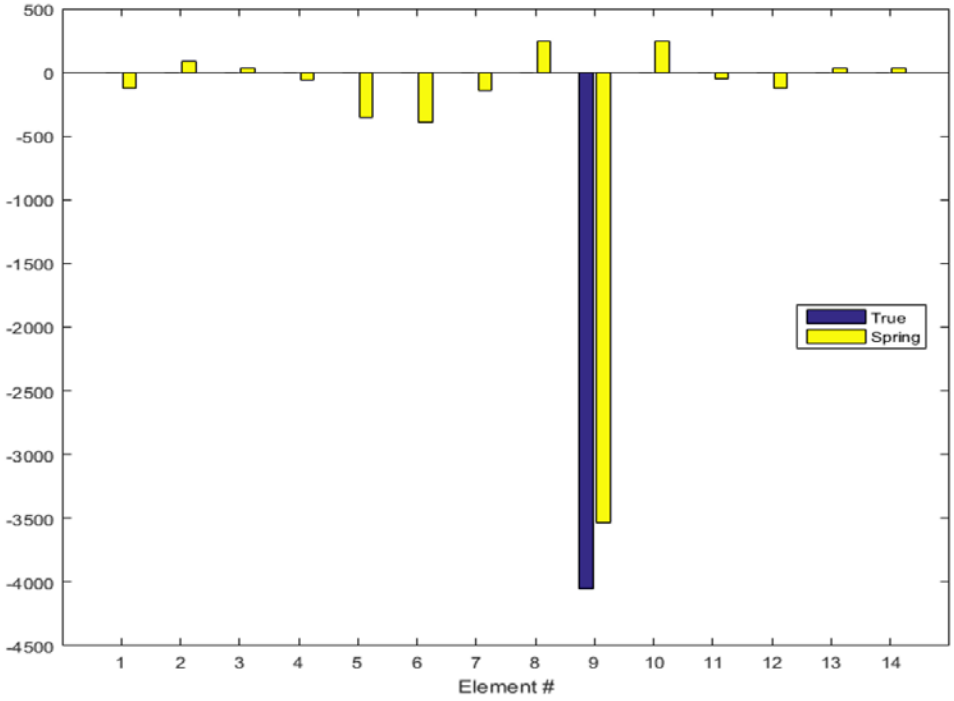

Figure 128. Two Spring Error Identification at Element 9

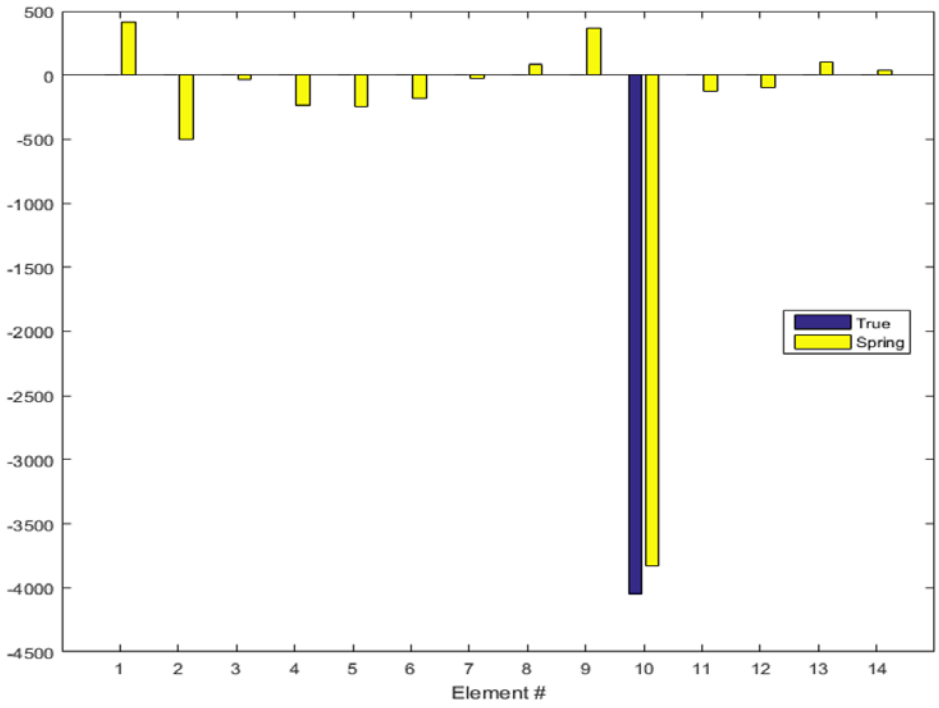

Figure 129. Two Spring Error Identification at Element 10

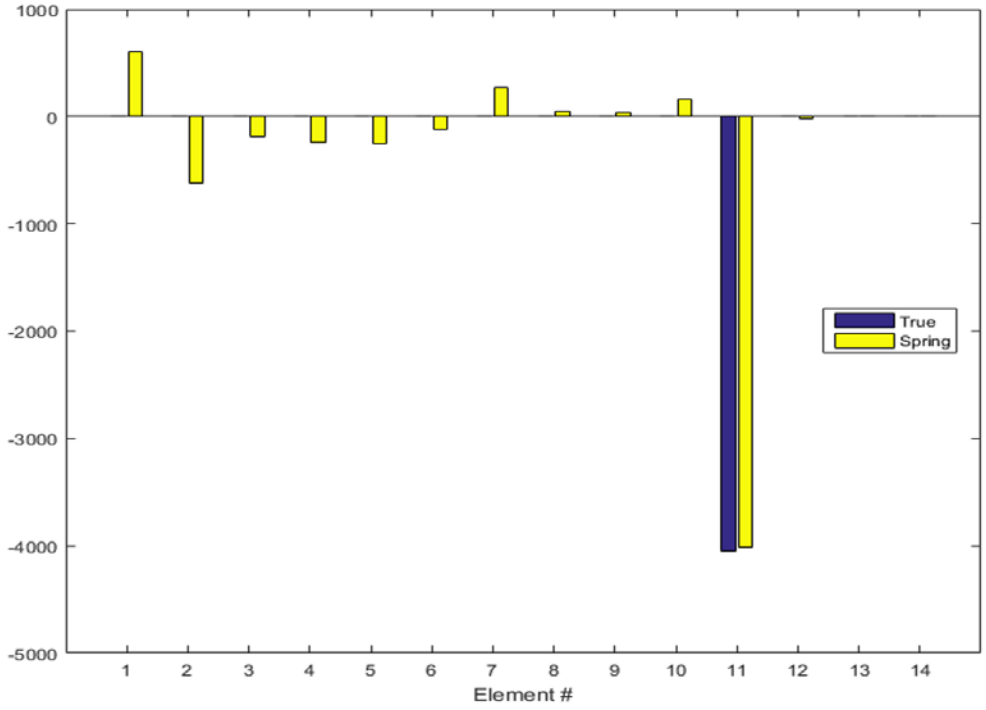

Figure 130. Two Spring Error Identification at Element 11

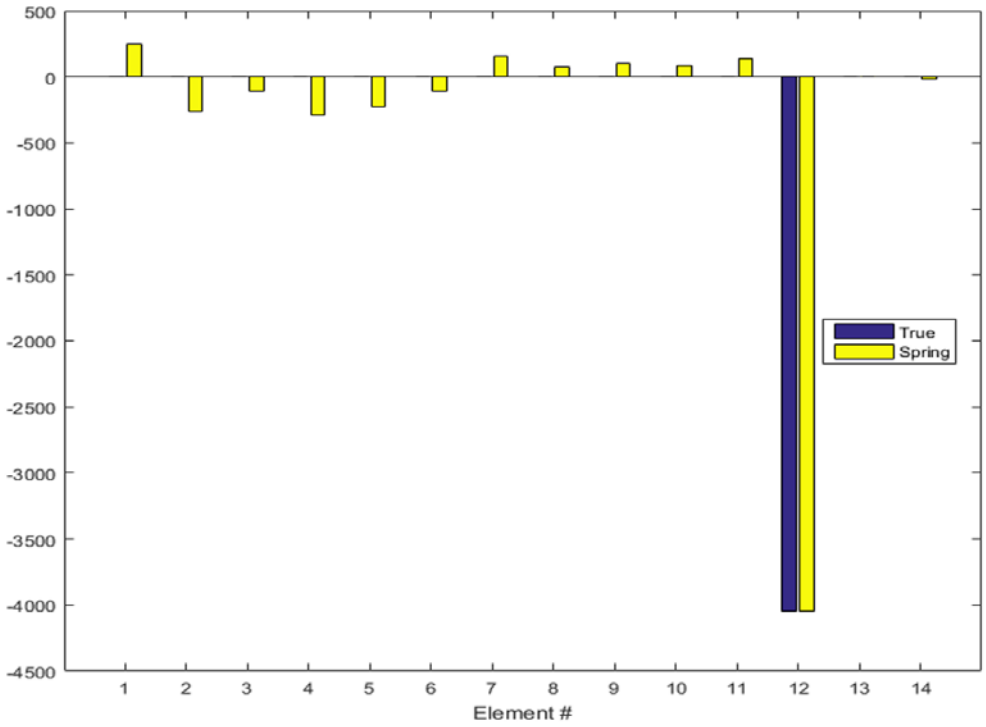

Figure 131. Two Spring Error Identification at Element 12

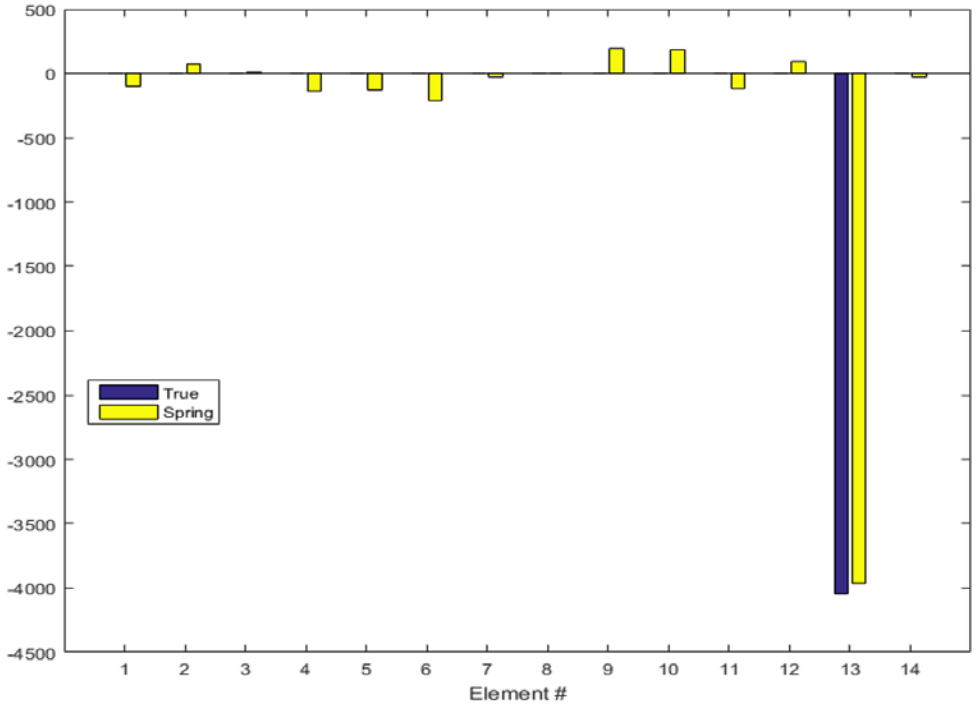

Figure 132. Two Spring Error Identification at Element 13

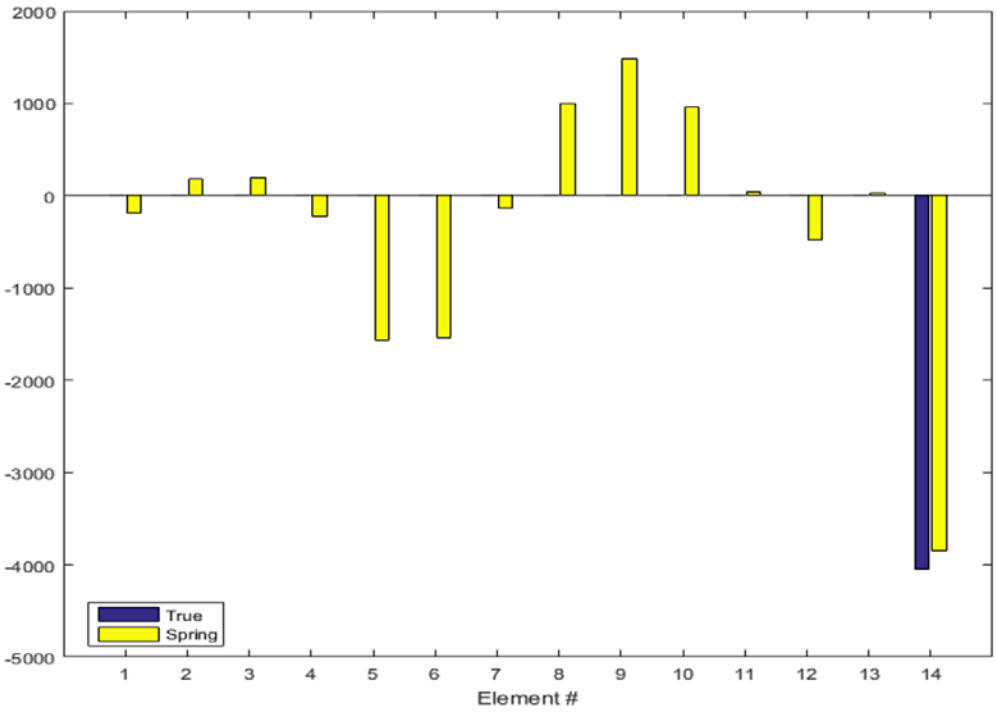

Figure 133. Two Spring Error Identification at Element 14

Figure 120 through Figure 133 confirm that the use of the sensitivity matrix identified in equation (4.23) will accurately identify damage in all locations with minimal errors

G. CONCLUDING REMARKS

For each scenario of synthesis of a single, dimensionless spring to ground, a single lumped mass, and two nodes, two springs, a combination of conditions was identified that could accurately detect simulated damage in all elements. The matrix condition number indicates the two spring solution should provide the most accurate solution when solving for model updating and damage detection

Based on the plots of the sensitivity value variance, there does not appear to be any more information provided by adding a single lumped mass. However, further exploration should be conducted in the exploration of the single spring and two spring scenarios to discover their limitations and capability to add more information to the sensitivity matrix.

THIS PAGE INTENTIONALLY LEFT BLANK

V. MODEL UPDATING AND DAMAGE DETECTION

A. INTRODUCTION

As described in Chapter II, The purpose of FRF synthesis is to manipulate test data to determine the exact dynamic response of the beam due to the integration of a boundary condition or beam modification. The advantage of which is the ability to determine the new resonance frequencies without the tedious implications of physically modifying the beam. These new resonance frequencies can then be compared against the correlating FEM frequencies and used in damage detection and model updating.

Experimental data will yield FRFs, and by using MATLAB's internal findpeaks function [17], the FRFs will provide resonance frequencies of the prototype structure. Additionally, by following the procedure for FRF synthesis detailed in Chapter II, we can synthesize the beam modifications demonstrated in Chapter IV on measured data to update the FEM and perform damage detection

It is important to note that node numbering for the FEM are not an exact match for the nodes on the measured beam. For example, node 2 on the FEM is physical node 1 on the measured beam. Additionally, the data captured from the measured beam captures the translational movement only. As such, the DOF number for the measured beam reflects the node number directly.

B. VERIFICATION OF DATA IMPORT

All experimental data gathered in Chapter III using the Single Impact Hammer test was exported to Microsoft Excel .xlsx files and imported into Matlab using the Matlab proprietary xlsread function [17]. By plotting the driving points, we can confirm the data was successfully transferred by ensuring the resonance peak frequencies line up as displayed in Figure 134. If the peaks did not occur at the same frequency, we would suspect an issue with either the measurement or data import.

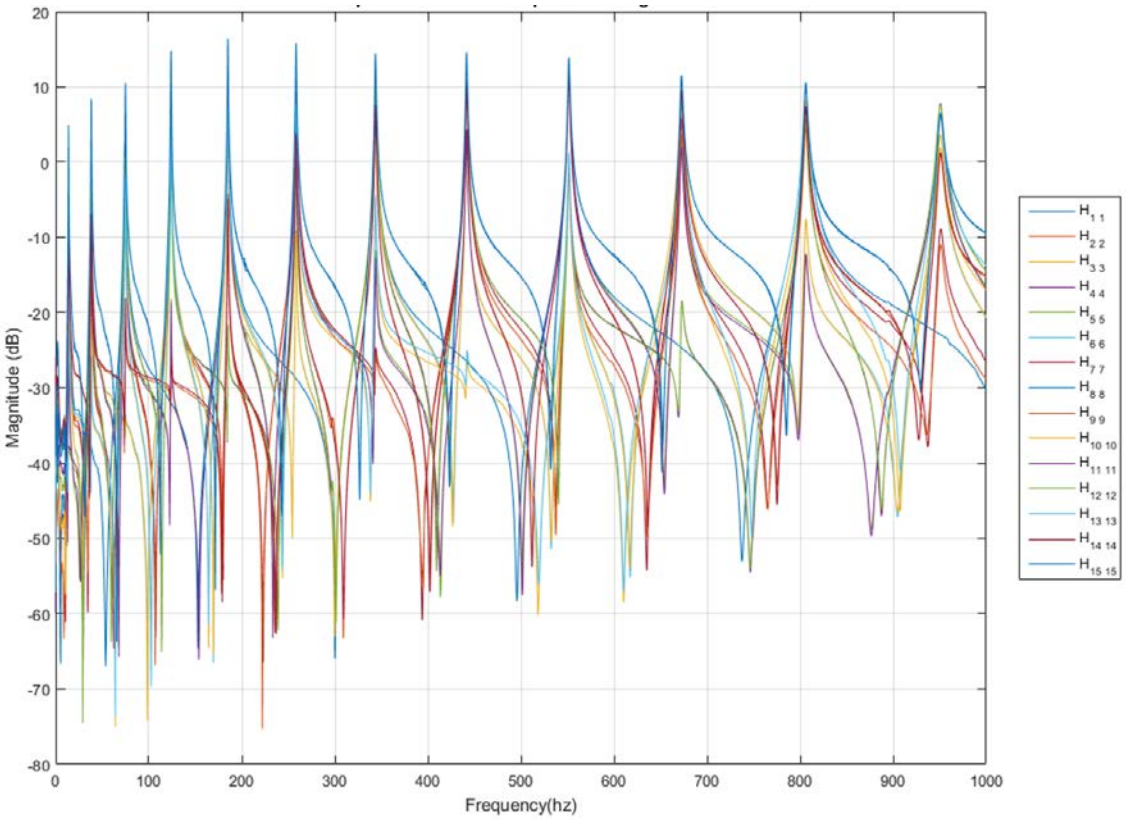

Figure 134. Experimental Beam Response Driving Point Data Verification

C. MODEL UPDATING USING SINGLE SPRING

Following the procedure detailed in Chapter II and demonstrated in Chapter IV, the conditions detailed in equation (4.13) were synthesized into the experimental data. First, a 178.579 kg/mm (10,000 lb/in) spring was synthesized onto node 1 using equation (2.64) and provides the dynamic response detailed in Figure 135.

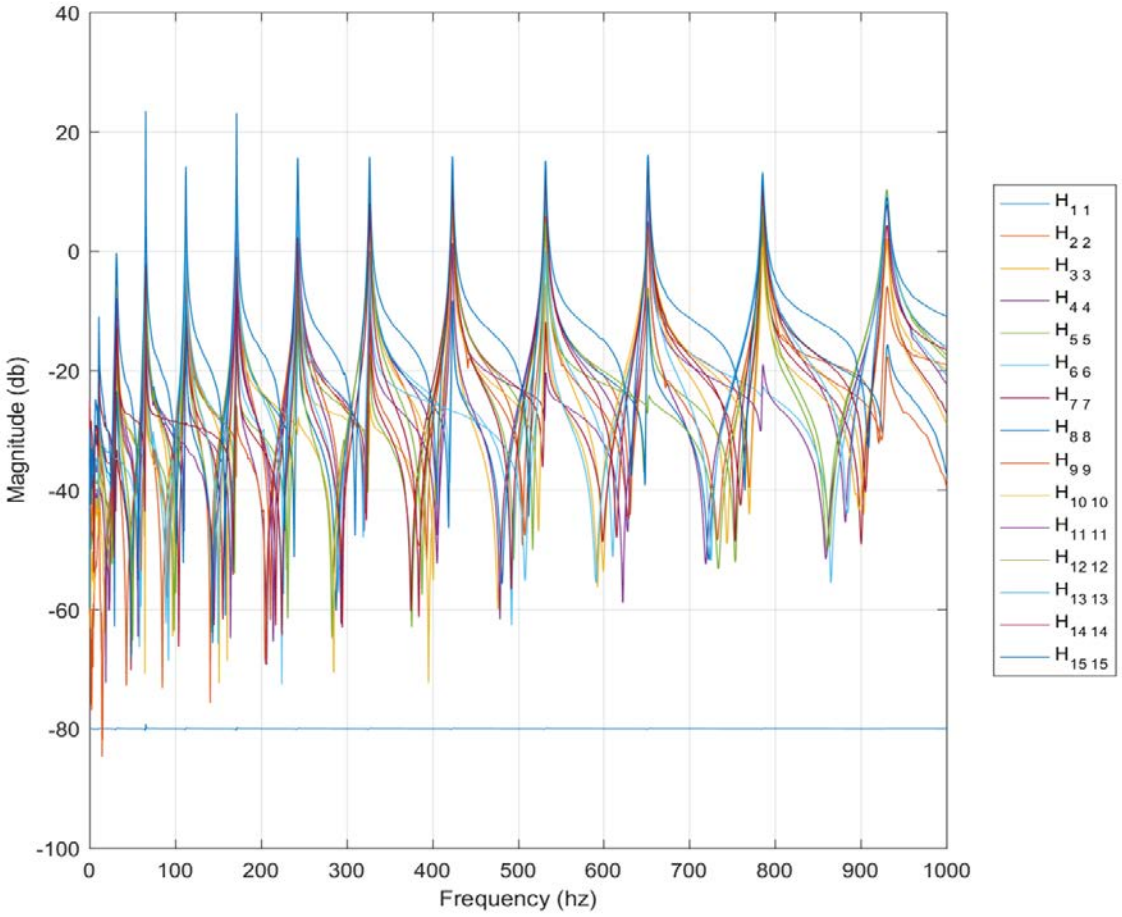

Figure 135. Synthesized Measured Data, 178.579 kg/mm (10,000 lb/in) Spring Synthesized on Node 1

In order to solve equation (4.13), we need to determine the new resonance frequencies of the beam. To do so, all driving point FRFs are averaged, providing a single FRF as displayed in Figure 136. Additionally, this minimizes false positives in identifying resonance frequencies and provides a clear comparison to the averaged FRFs of the FEM.

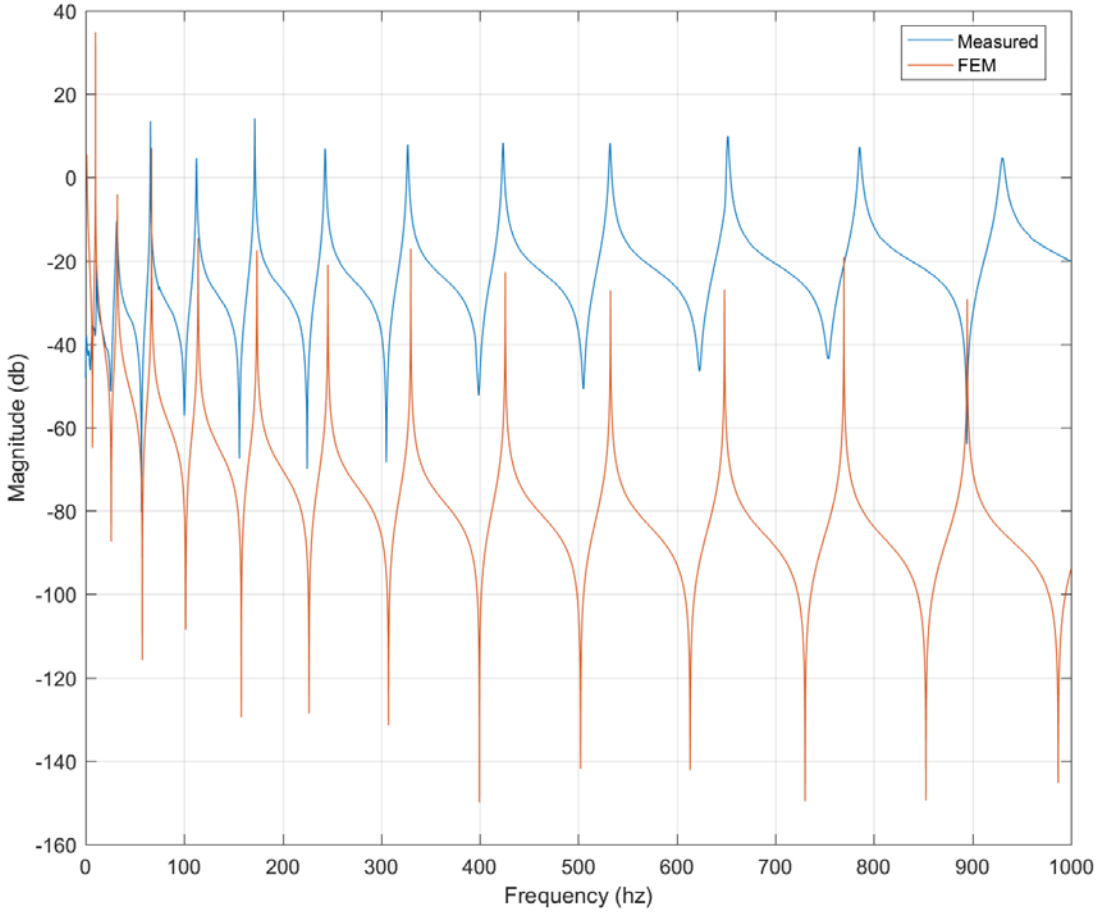

Figure 136. Synthesized Measured Data, 178.579 kg/mm (10,000 lb/in) on Node 1, Averaged Driving Points compared against FEM

Using the MATLAB findpeaks function [17], we can determine the resonance frequencies of the synthesized measured data and, as determined in the development of equation (4.13), use the six highest modes in damage detection.

To get the remaining modes, we synthesize a 178.579 kg/mm (10,000 lb/in) spring onto the baseline FRFs at node 7 using equation (2.64).

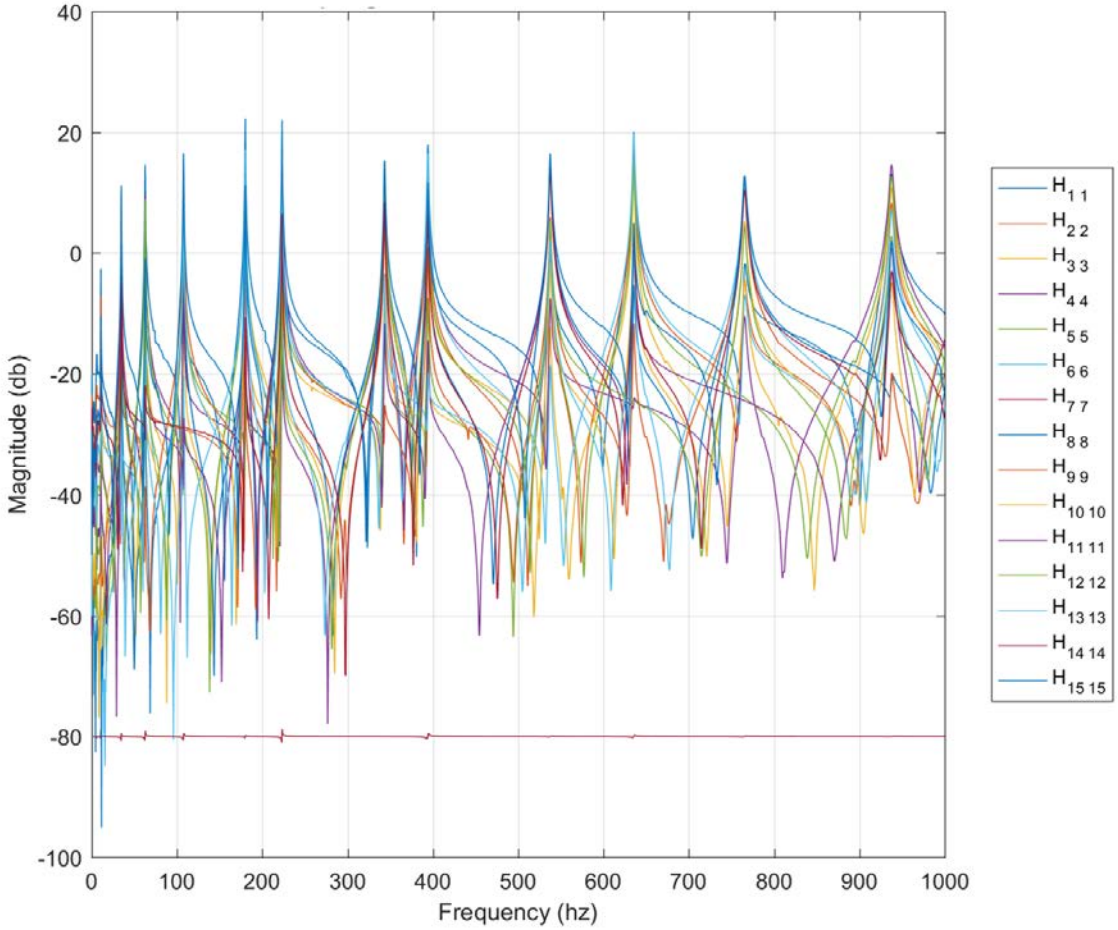

Figure 137. Synthesized Measured Data, 178.579 kg/mm (10,000 lb/in) Spring Synthesized on Node 7

Synthesis of a 178.579 kg/mm (10,000 lb/in) spring onto the baseline FRFs at node 7 produces 0, when looking at the driving points. Following the same procedure as the single spring, all driving point FRFs are averaged, providing a single FRF as displayed in Figure 138.

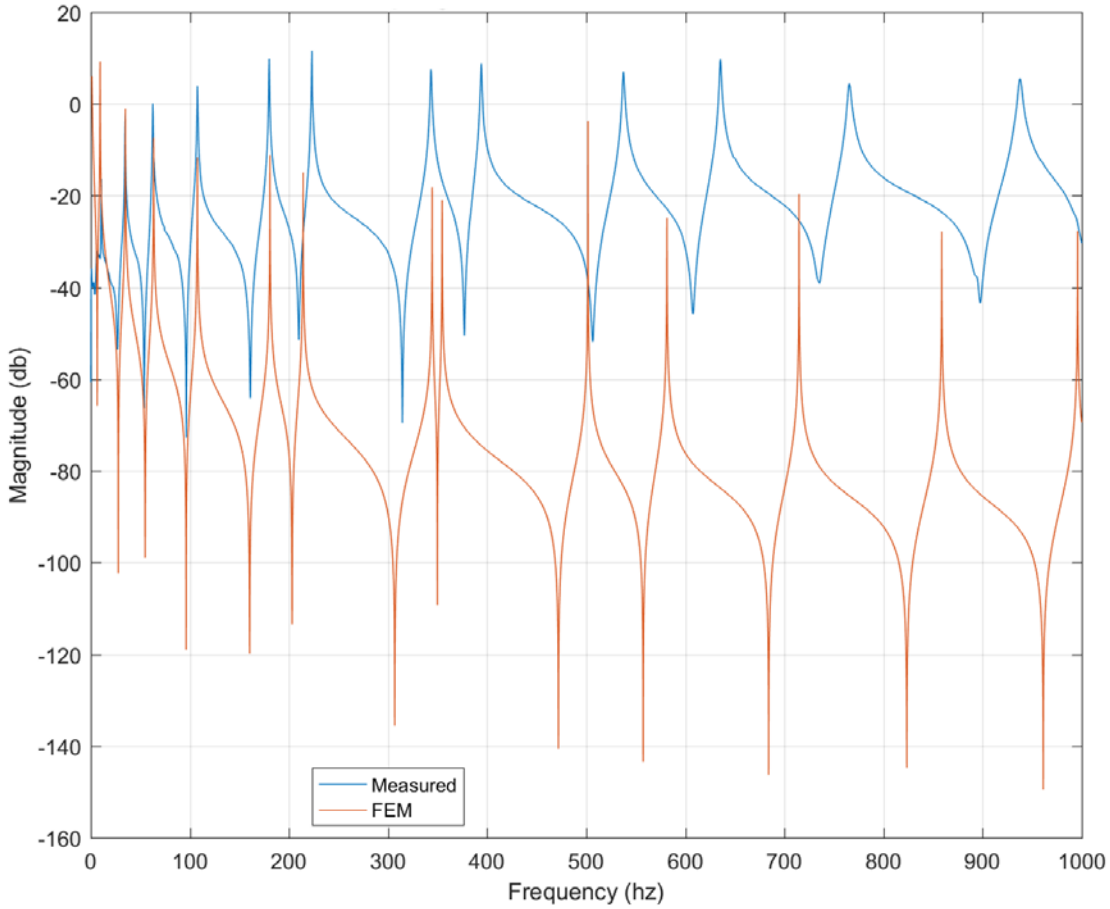

Figure 138. Synthesized Measured Data, 178.579 kg/mm (10,000 lb/in) on Node 7, Averaged Driving Points compared against FEM

Again, using the MATLAB findpeaks function [17], we can determine the resonance frequencies of the synthesized measured data and, as determined in the development of equation (4.8), use the six highest modes in damage detection. Understanding that $\{\Delta\omega^2\} = \{\Delta\lambda\}$ where ω is the resonance frequency, the difference in resonance frequencies between the six modes identified in the measured data and the synthesized FEM are then concatenated to the six identified with the previous synthesis and two of the baseline modes to create the $\{\Delta\lambda\}$ vector identified in equation (4.13) and reflected here as equation (5.1), modified to reflect the synthesized nodes for the measured data.

$$\begin{bmatrix} [S^0]_{2\times14} \\ [S^{N1-10,000}]_{6\times14} \\ [S^{N7-10,000}]_{6\times14} \end{bmatrix}^{-1} \begin{Bmatrix} \{\Delta\lambda^0\}_{2\times1} \\ \{\Delta\lambda^{N1-10,000}\}_{6\times1} \\ \{\Delta\lambda^{N7-10,000}\}_{6\times1} \end{Bmatrix} = \begin{Bmatrix} \Delta EI_1 \\ \Delta EI_2 \\ \vdots \\ \Delta EI_{14} \end{Bmatrix} \tag{5.1}$$

Using the sensitivity matrix identified for a single spring in Chapter IV and the difference in resonance frequencies developed using synthesis, the solution to equation(5.1) is displayed in Figure 139.

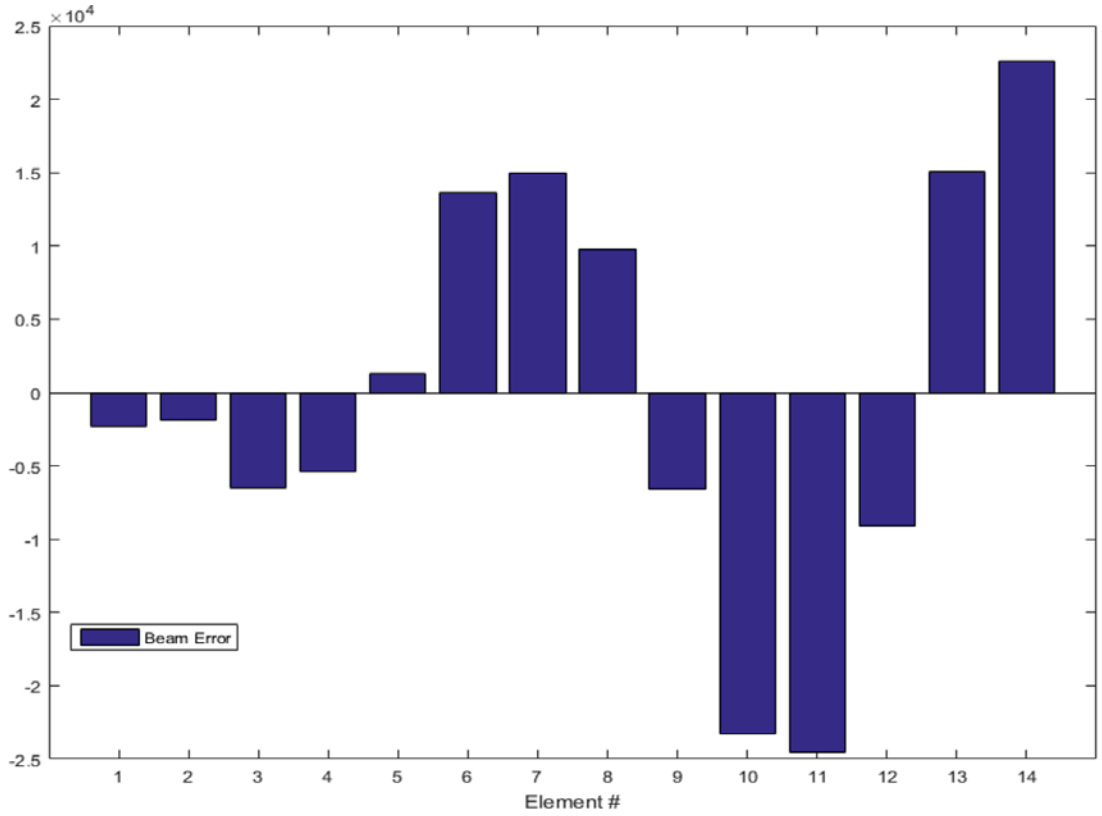

Figure 139. Identified Error in FEM Flexural Rigidity Using Single Spring Synthesis

$$\{\Delta EI\} = \begin{Bmatrix} -2186.557 \\ -1777.846 \\ -6410.194 \\ -5349.396 \\ 1239.977 \\ 13426.793 \\ 14609.369 \\ 9306.104 \\ -6999.914 \\ -23154.799 \\ -24016.903 \\ -8673.072 \\ 15371.071 \\ 22842.511 \end{Bmatrix} \tag{5.2}$$

$$\{\Delta EI\}_{AVERAGE} = -126.63 \tag{5.3}$$

The results of equation (5.1), displayed as Figure 139, equations (5.2) and equations (5.3), provide the necessary corrections to the FEM elements to better reflect the prototype's dynamic response. Using these corrections, the FRF for the FEM was recalculated using the element specific correction identified in equation (5.2), displayed in Figure 140 with Table 15. Separately, the FEM was recalculated using the average element correction identified in equation (5.3) and displayed in Figure 141 with Table 16.

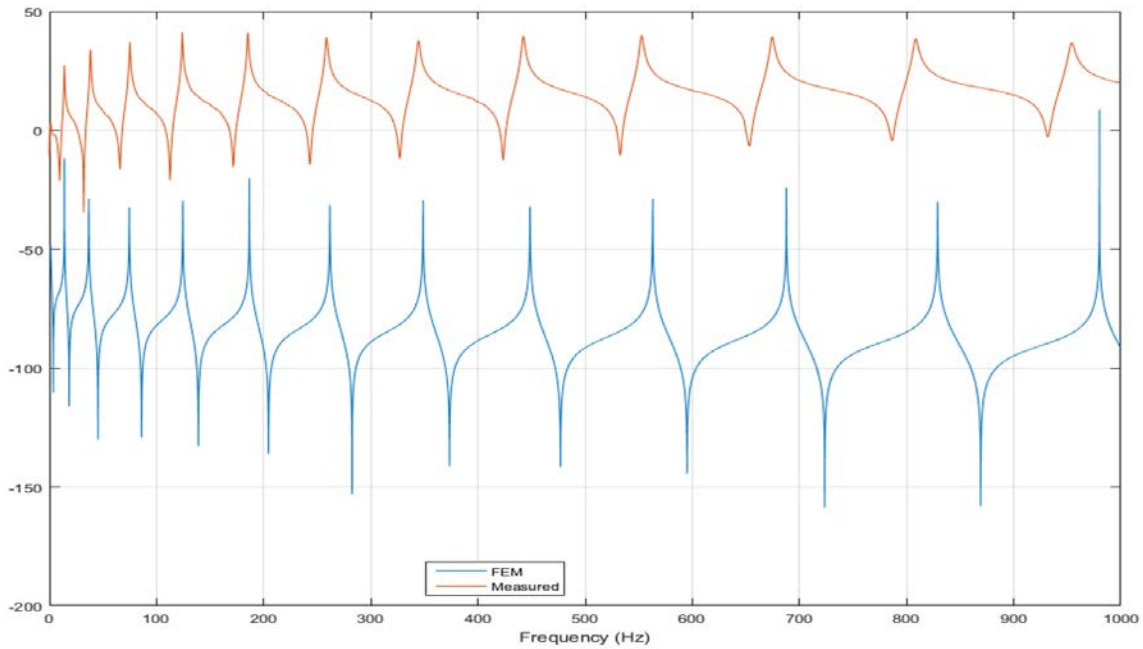

Figure 140. Updated FEM FRF compared to Prototype FRF Using Element Specific Correction, $H_{1,1}$

Table 15. Updated FEM Resonance Frequencies Using Single Spring Synthesis Element Specific Correction

Previous FEM Frequency(Hz)	Previous % Rel Error	Updated FEM Freq (Hz)	Measured Freq (Hz)	Absolute Error	% Relative Error	% Error Corrected
14.13452	2.7965	13.996	13.75	0.246	1.7891	1.00742
38.95759	2.1838	36.7333	38.125	-1.3917	-3.6504	-1.46652
76.37207	1.8294	74.5518	75	-0.4482	-0.5976	1.23183
126.27156	1.7806	124.5348	124.0625	0.4723	0.3807	1.39991
188.72298	2.0124	186.5883	185	1.5883	0.8585	1.15388
263.83435	2.0883	261.7421	258.4375	3.3046	1.2787	0.80958
351.78075	2.3362	348.7656	343.75	5.0156	1.4591	0.87713
452.81294	2.5479	448.5534	441.5625	6.9909	1.5832	0.96465
567.24773	2.8438	563.0675	551.5625	11.505	2.0859	0.75789
695.40391	3.4058	687.8183	672.5	15.3183	2.2778	1.12797
837.35461	3.8982	828.9641	805.9375	23.0266	2.8571	1.04109
991.88069	4.3056	980.0004	950.9375	29.0629	3.0562	1.24932

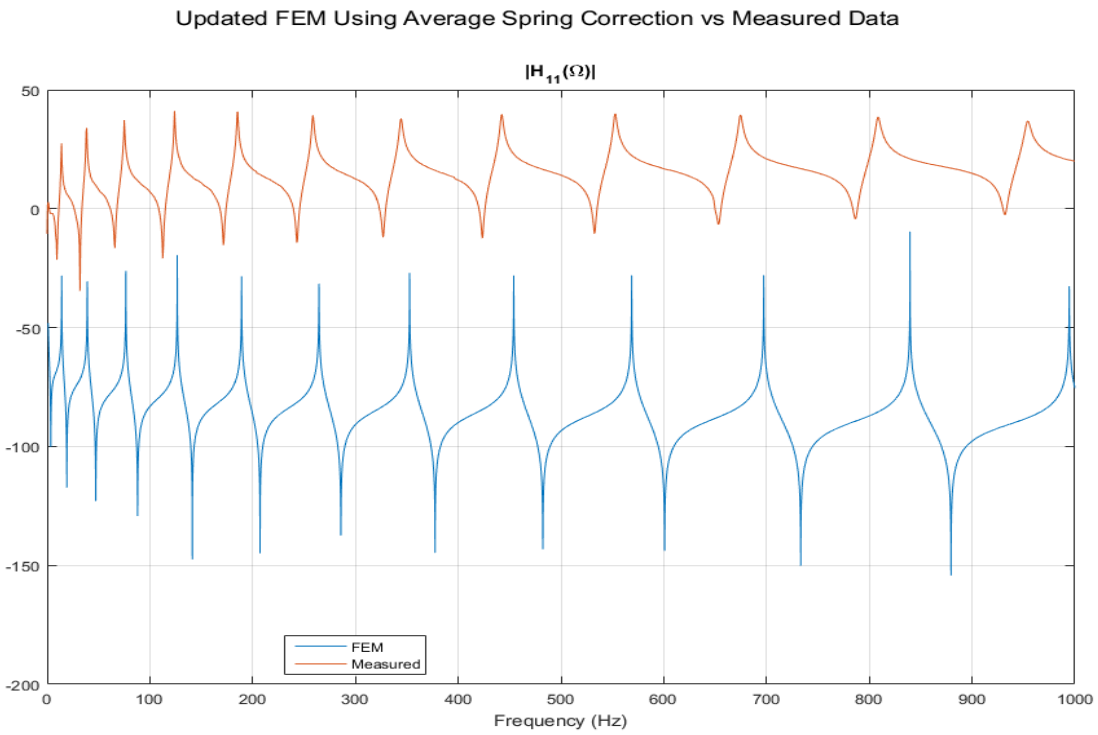

Figure 141. Updated FEM FRF Compared to Prototype FRF Using Average Element Correction

Table 16. Updated FEM Resonance Frequencies Using Single Spring Synthesis Average Element Correction

Previous FEM Frequency(Hz)	Previous % Rel Error	Updated FEM Freq (Hz)	Measured Freq (Hz)	Absolute Error	% Relative Error	% Error Corrected
14.13452	2.7965	14.1235	13.75	0.3735	2.7164	0.08015
38.95759	2.1838	38.9271	38.125	0.8021	2.1039	0.07997
76.37207	1.8294	76.3123	75	1.3123	1.7497	0.07969
126.27156	1.7806	126.1728	124.0625	2.1103	1.7010	0.07961
188.72298	2.0124	188.5753	185	3.5753	1.9326	0.07983
263.83435	2.0883	263.6279	258.4375	5.1904	2.0084	0.07988
351.78075	2.3362	351.5055	343.75	7.7555	2.2561	0.08007
452.81294	2.5479	452.4587	441.5625	10.8962	2.4676	0.08022
567.24773	2.8438	566.8039	551.5625	15.2414	2.7633	0.08047
695.40391	3.4058	694.8599	672.5	22.3599	3.3249	0.08089
837.35461	3.8982	836.6995	805.9375	30.762	3.8169	0.08129
991.88069	4.3056	991.1047	950.9375	40.1672	4.2240	0.08160

D. MODEL UPDATING USING SINGLE MASS

Following the same procedures described for the synthesis of a single spring, the conditions of the lumped mass identified in equation (4.17) where synthesized into the Measured, baseline FRF. Equation (4.19) is restated here with the modification to node locations to reflect placement on the beam.

$$\begin{bmatrix} \left[S^{(0)}\right]_{2\times14} \\ \left[S^{(N5-0.35)}\right]_{6\times14} \\ \left[\left[S^{(N13-4.00)}\right]_{6\times14}\right] \end{bmatrix}^{-1} \begin{Bmatrix} \left\{\Delta\lambda^{(0)}\right\}_{2\times1} \\ \left\{\Delta\lambda^{(N5-0.35)}\right\}_{6\times1} \\ \left\{\Delta\lambda^{(N13-4.00)}\right\}_{6\times1} \end{Bmatrix} = \begin{Bmatrix} \Delta EI_1 \\ \Delta EI_2 \\ \vdots \\ \Delta EI_{14} \end{Bmatrix} \tag{5.4}$$

First, a mass of 0.1588 kg (0.35 lb) was synthesized onto node 5. The resulting synthesized FRFs generated are displayed in Figure 142.

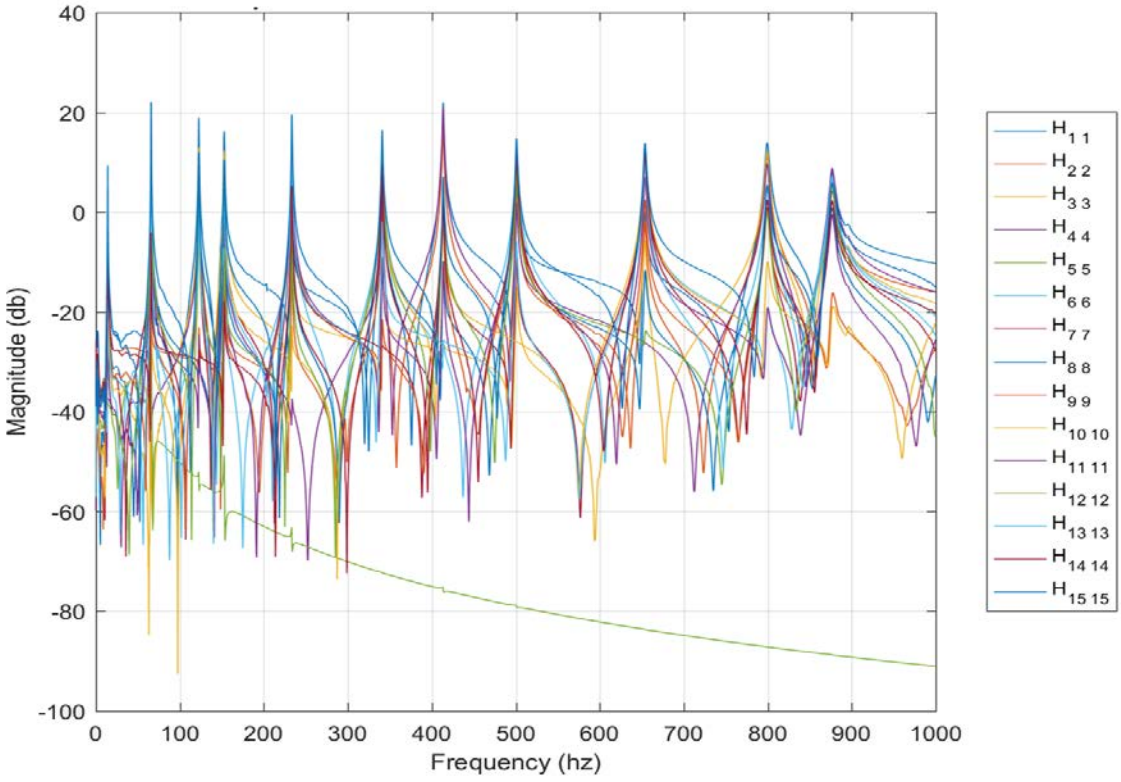

Figure 142. Synthesized Measured Data, 0.1588 kg (0.35 lb) on Node 5

By averaging the driving points identified in Figure 142, we can once again identify the resonance frequencies required in both the synthesized measured data and synthesized FEM FRFs, as displayed in Figure 143, for inclusion in equation (5.4).

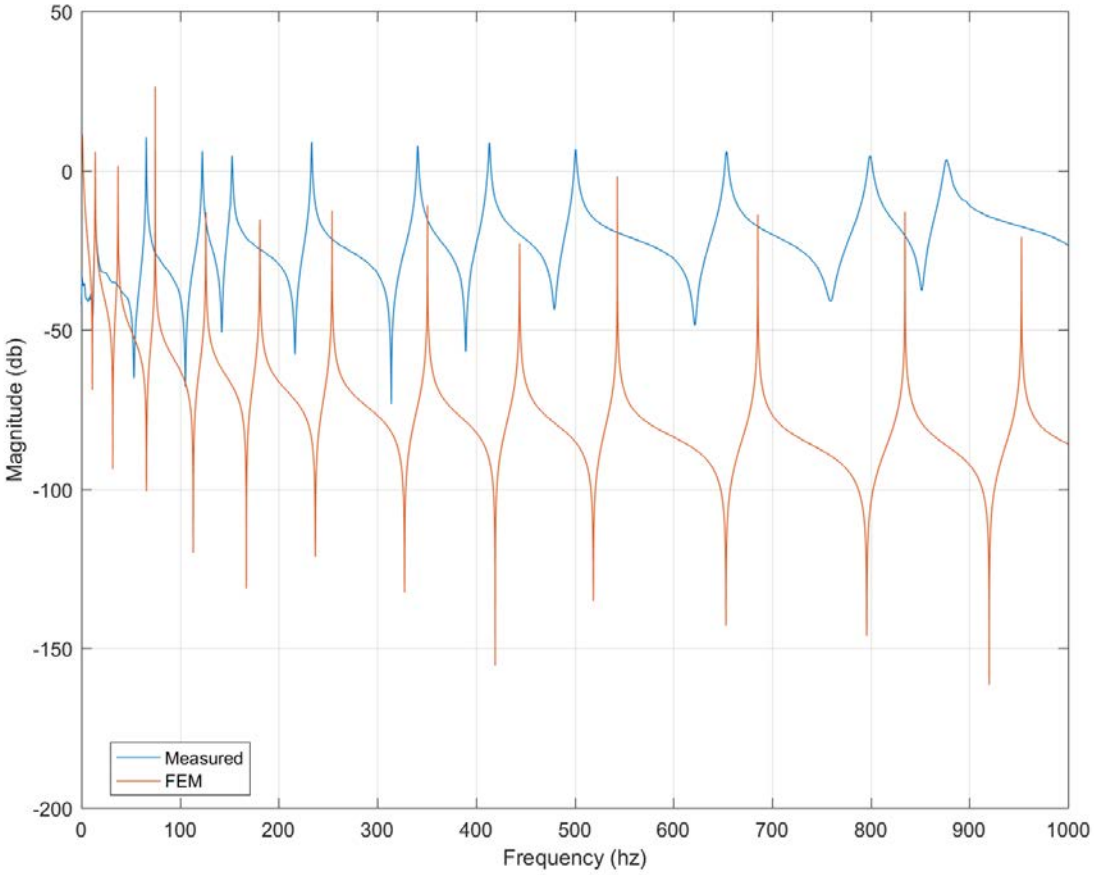

Figure 143. Synthesized Measured Data, Averaged Driving Points 0.1588 kg (0.35 lb) on Node 5

Next, a mass of 1.81437kg (4lb) is synthesized into the measured data on node 13. The resulting synthesized FRFs are displayed as Figure 144 With driving point averages displayed as Figure 145.

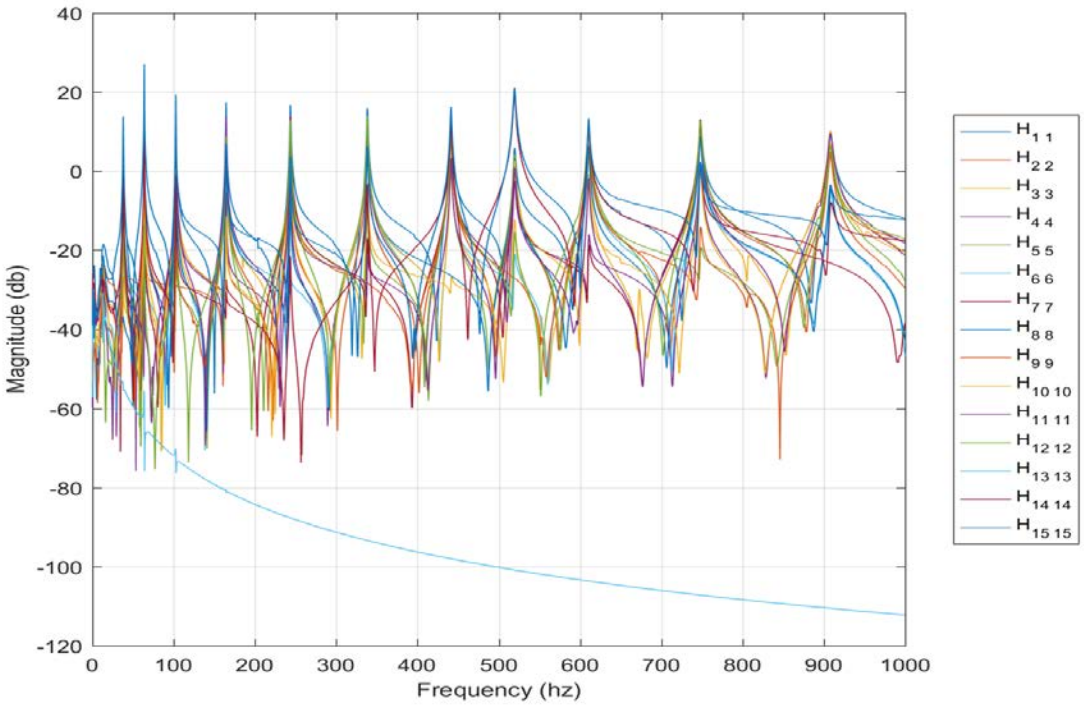

Figure 144. Synthesized Measured Data, 1.81437kg (4lb) on Node 13

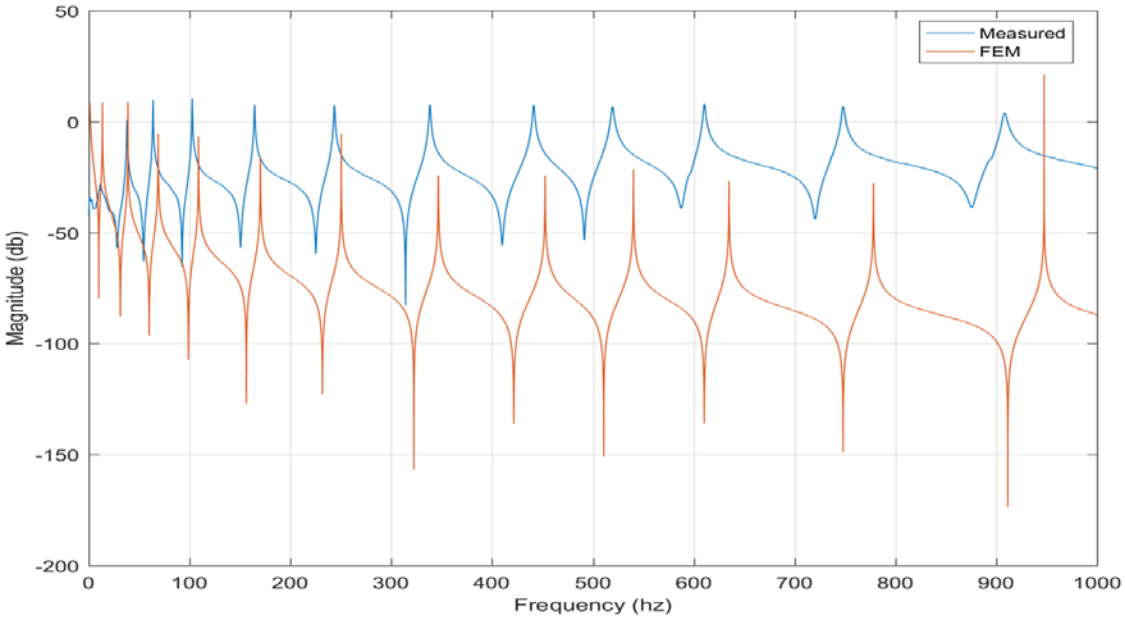

Figure 145. Synthesized Measured Data, Average Driving Points, 1.81437kg (4lb) on Node 13

Again, using the MATLAB findpeaks function [17] on Figure 145 as averaged from Figure 144 we can determine the resonance frequencies of the synthesized measured data and the synthesized FEM. As determined in the development of equation (5.4) the differences in the six highest modes are used in damage detection.

In using the sensitivity matrix identified in equation (4.19) and finding the differences in resonance frequencies of the required modes as identified by equation (5.4), Figure 143, and Figure 145, we can solve for the errors in the FEM flexural rigidity vector as displayed in Figure 146.

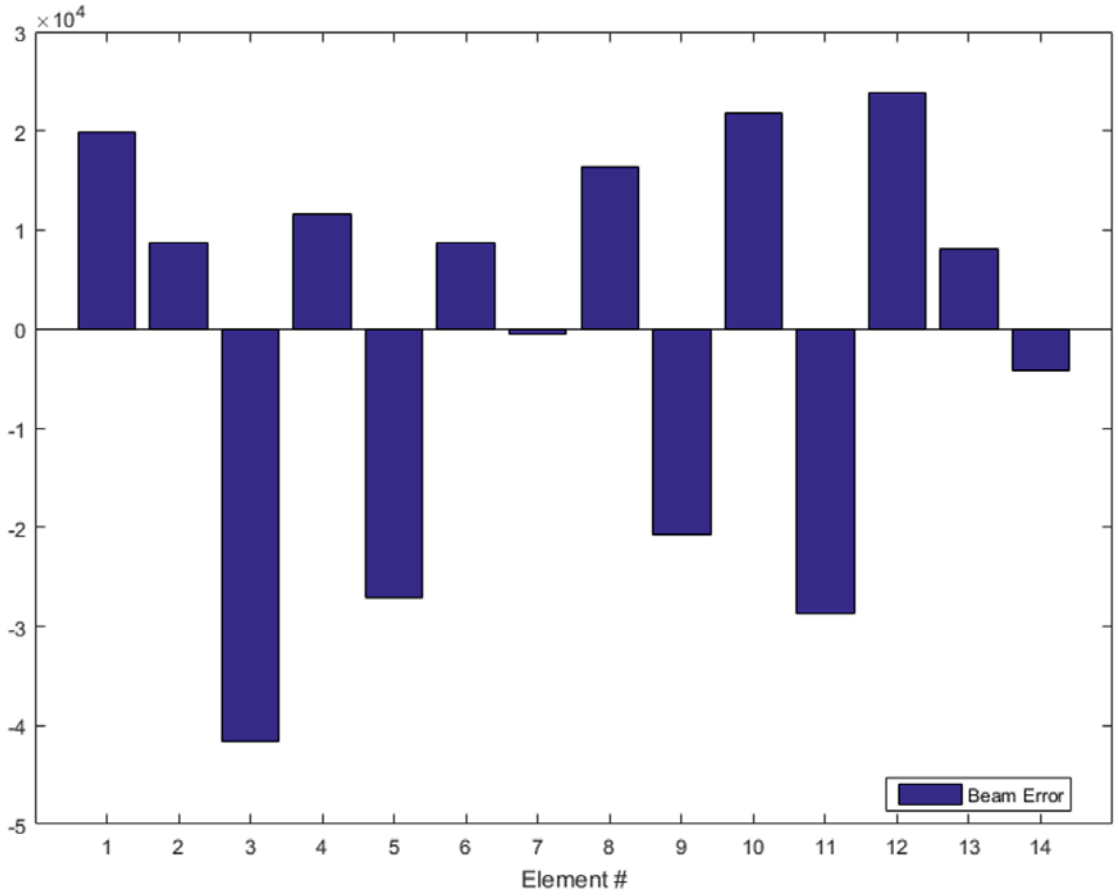

Figure 146. Identified Error in FEM Flexural Rigidity using Single Mass Synthesis

$$\{\Delta EI\} = \begin{Bmatrix} 19912.833 \\ 8767.437 \\ -41555.903 \\ 11521.216 \\ -27142.816 \\ 8750.094 \\ -536.109 \\ 16421.640 \\ -20753.952 \\ 21827.711 \\ -28668.482 \\ 23890.626 \\ 8121.619 \\ -4106.214 \end{Bmatrix} \tag{5.5}$$

$$\{\Delta EI\}_{AVERAGE} = -253.59 \tag{5.6}$$

The results of equation (5.4), displayed in Figure 146, equation (5.5), and equation (5.6), provide the necessary corrections to the FEM elements to better reflect the prototype's dynamic response. Using these corrections, the FRF for the FEM was recalculated using the element specific correction identified in equation (5.5), displayed in Figure 147 with Table 17. Separately, the FEM was recalculated using the average element correction identified in equation (5.6) and displayed in Figure 148 with Table 18.

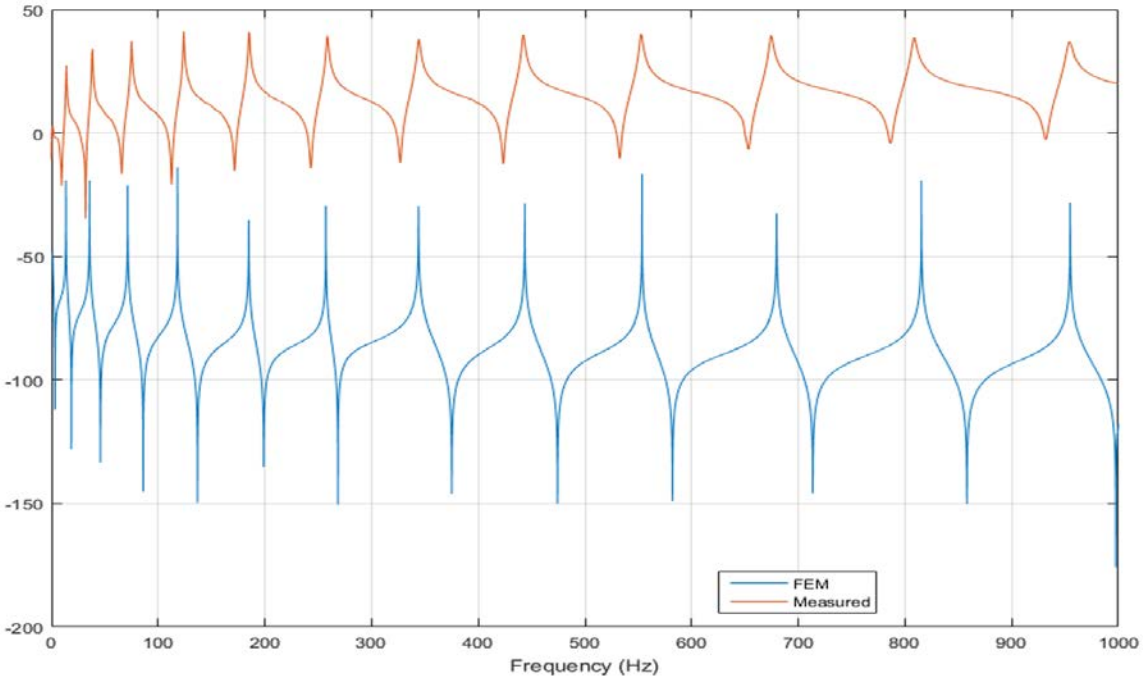

Figure 147. Updated FEM FRF compared to Prototype FRF Using Mass Synthesis Element Specific Correction, $H_{1,1}$

Table 17. Updated FEM Resonance Frequencies Using Mass Synthesis Element Specific Correction

Previous FEM Frequency(Hz)	Previous % Rel Error	Updated FEM Freq (Hz)	Measured Freq (Hz)	Absolute Error	% Relative Error	% Error Corrected
14.13452	2.3291	13.6115	13.81281	-0.20127	-1.4571	0.87196
38.95759	1.7872	35.7128	38.27358	-2.56082	-6.6908	-4.90367
76.37207	1.7888	71.4144	75.02992	-3.61556	-4.8188	-3.03000
126.27156	1.8210	118.0948	124.01327	-5.91842	-4.7724	-2.95141
188.72298	1.8938	184.9390	185.21543	-0.2764	-0.1492	1.74454
263.83435	2.0310	257.2172	258.58254	-1.36536	-0.5280	1.50298
351.78075	2.1856	344.0446	344.25651	-0.2119	-0.0616	2.12410
452.81294	2.3864	443.6277	442.25887	1.368806	0.3095	2.07690
567.24773	2.6374	553.5058	552.67146	0.834297	0.1510	2.48646
695.40391	3.0958	679.6416	674.52174	5.119838	0.7590	2.33682
837.35461	3.5819	815.3904	808.39895	6.991492	0.8649	2.71700
991.88069	3.9774	954.7796	953.93877	0.840799	0.0881	3.88926

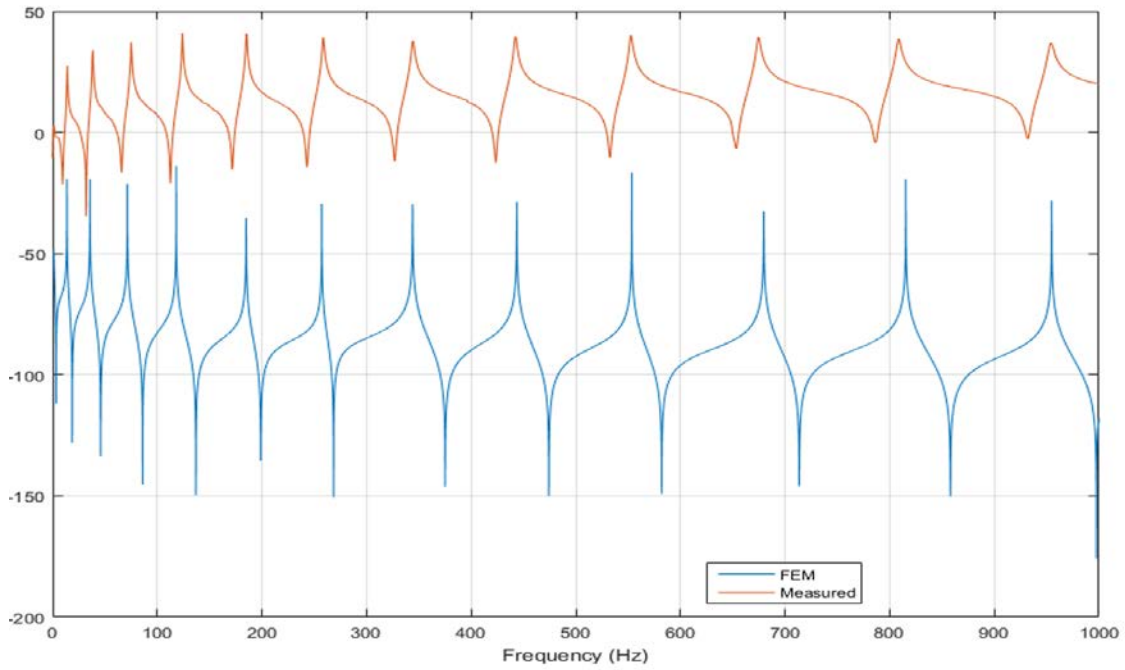

Figure 148. Updated FEM FRF compared to Prototype FRF Using Mass Synthesis Average Element Correction, $H_{1,1}$

Table 18. Updated FEM Resonance Frequencies Using Mass Synthesis Average Element Correction

Previous FEM Frequency(Hz)	Previous % Rel Error	Updated FEM Freq (Hz)	Measured Freq (Hz)	Absolute Error	% Relative Error	% Error Corrected
14.13452	2.3291	14.1124	13.81281	0.299551	2.1686	0.16042
38.95759	1.7872	38.8965	38.27358	0.622948	1.6276	0.15954
76.37207	1.7888	76.2524	75.02992	1.222447	1.6293	0.15954
126.27156	1.8210	126.0736	124.01327	2.060375	1.6614	0.15959
188.72298	1.8938	188.4272	185.21543	3.211751	1.7341	0.15971
263.83435	2.0310	263.4208	258.58254	4.838285	1.8711	0.15992
351.78075	2.1856	351.2294	344.25651	6.972875	2.0255	0.16016
452.81294	2.3864	452.1032	442.25887	9.844347	2.2259	0.16048
567.24773	2.6374	566.3587	552.67146	13.6872	2.4766	0.16087
695.40391	3.0958	694.3140	674.52174	19.79222	2.9343	0.16159
837.35461	3.5819	836.0422	808.39895	27.64324	3.4195	0.16235
991.88069	3.9774	990.3261	953.93877	36.3873	3.8144	0.16297

E. MODEL UPDATING USING TWO SPRINGS

Following the same procedures described for the synthesis of a single spring, two springs of equal strength, as identified in equation (4.21), were synthesized into the measured, baseline FRF. Equation (4.23) is restated here with the modification to node locations to reflect placement on the beam.

$$\begin{bmatrix} \left[S^{(0)}\right]_{2\times14} \\ \left[S^{(N\,4,11-10,000)}\right]_{6\times14} \\ \left[S^{(N\,4,15-10,000)}\right]_{6\times14} \end{bmatrix}^{-1} \begin{Bmatrix} \left\{\Delta\lambda^{(0)}\right\}_{2\times1} \\ \left\{\Delta\lambda^{(N\,4,11-10,000)}\right\}_{6\times1} \\ \left\{\Delta\lambda^{(N\,4,15-10,000)}\right\}_{6\times1} \end{Bmatrix} = \begin{Bmatrix} \Delta EI_1 \\ \Delta EI_2 \\ \vdots \\ \Delta EI_{14} \end{Bmatrix} \tag{5.7}$$

First, two springs, each of strength 178.579 kg/mm (10,000 lb/in) were synthesized onto node 4 and 11:

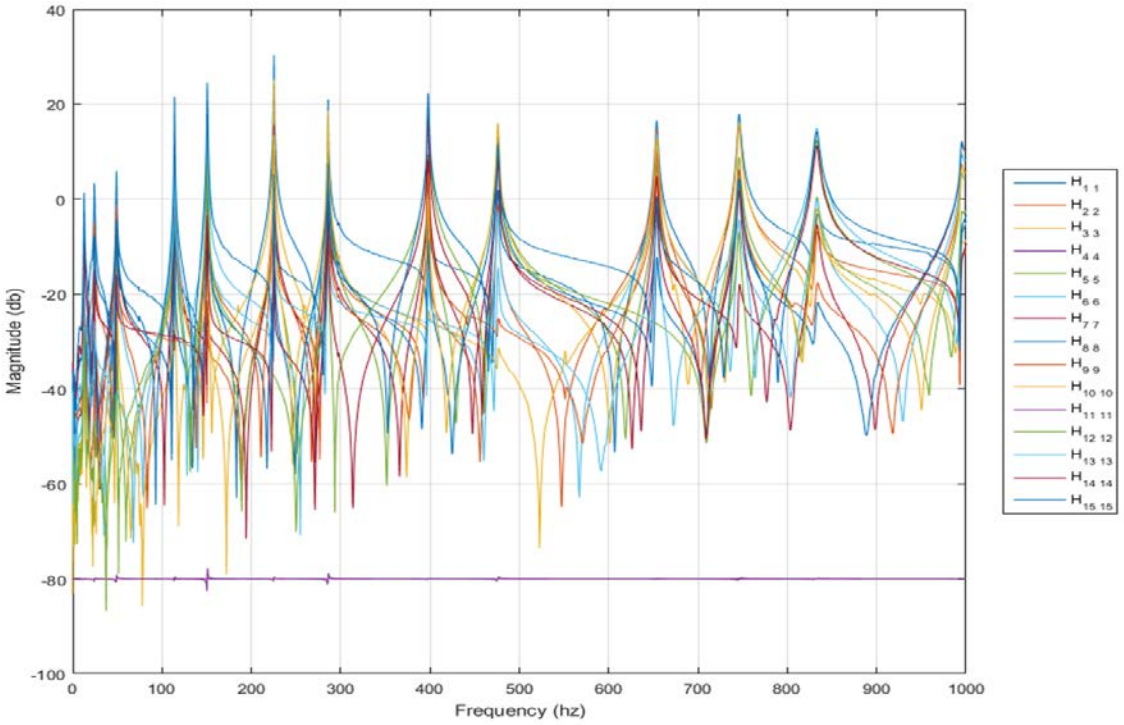

Figure 149. Synthesized Measured Data, 178.579 kg/mm (10,000 lb/in) on Nodes 4 and 11

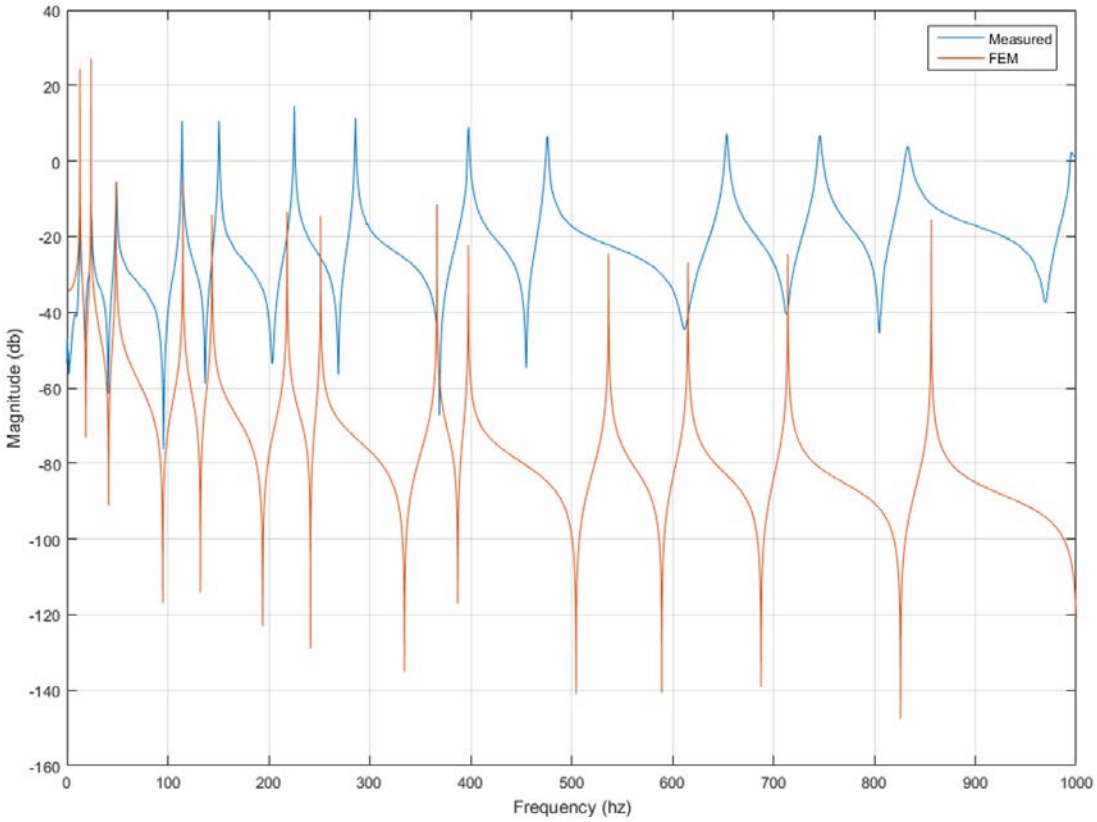

Figure 150. Synthesized Measured Data, Averaged Driving Points 178.579 kg/mm (10,000 lb/in) on Nodes 4 and 11

By averaging the driving points identified in Figure 149, we can once again identify the resonance frequencies required in both the synthesized measured data and synthesized FEM FRFs, as displayed in Figure 150, for inclusion in equation (5.7).

Next two springs, each of strength 178.579 kg/mm (10,000 lb/in) were synthesized onto node 4 and 15:

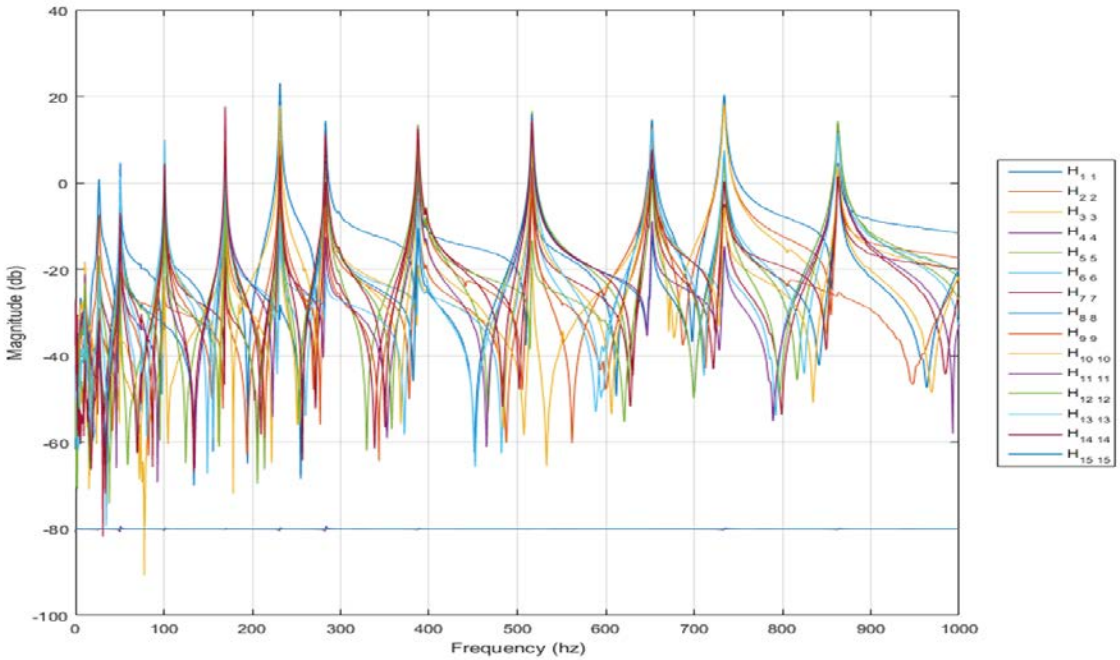

Figure 151. Synthesized Measured Data, 178.579 kg/mm (10,000 lb/in) on Nodes 4 and 15

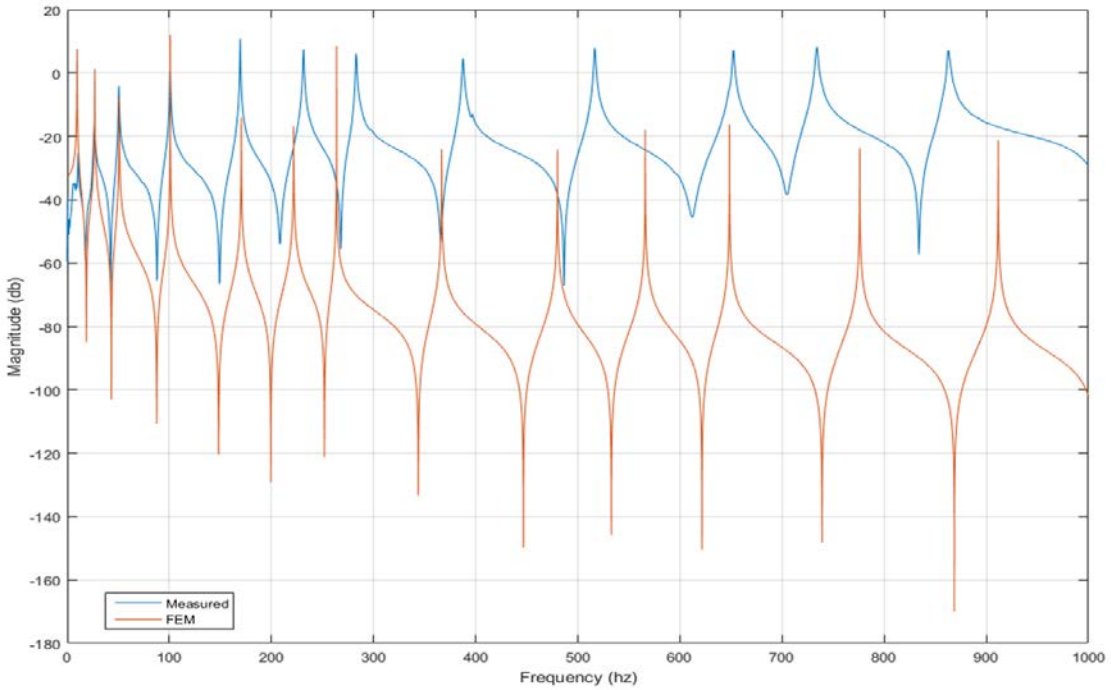

Figure 152. Synthesized Measured Data, Average Driving Points, 1178.579 kg/mm (10,000 lb/in) on Nodes 4 and 15

Again, using the MATLAB findpeaks function [17] on Figure 152, as averaged from Figure 151, we can determine the resonance frequencies of the synthesized measured data and the synthesized FEM. As determined in the development of equation (5.4) the differences in the six highest modes are used in damage detection.

In using the sensitivity matrix identified in equation (4.12) and finding the differences in resonance frequencies of the required modes as identified by equation (5.7), Figure 150, and Figure 152, we can solve for the errors in the FEM flexural rigidity vector:

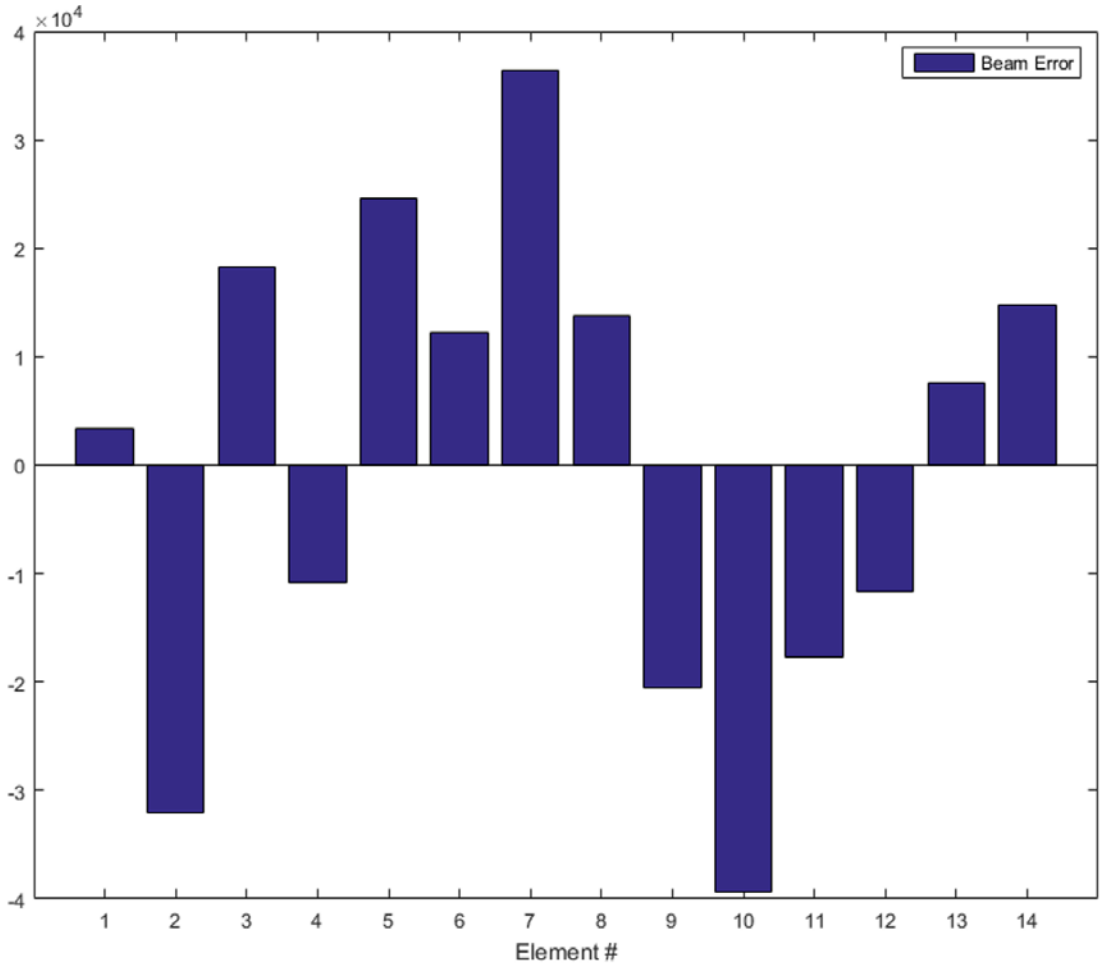

Figure 153. Identified Error in FEM Flexural Rigidity Using Two Spring Synthesis

$$\{\Delta EI\} = \begin{Bmatrix} 3413.727 \\ -32059.664 \\ 18218.355 \\ -10847.512 \\ 24591.878 \\ 12268.331 \\ 36449.882 \\ 13812.577 \\ -20482.147 \\ -39399.042 \\ -17706.379 \\ -11632.960 \\ 7529.408 \\ 14729.118 \end{Bmatrix} \tag{5.8}$$

$$\{\Delta EI\}_{AVERAGE} = -79.602 \tag{5.9}$$

The results of equation (5.7), displayed in Figure 153, equation (5.8), and equation (5.9), provide the necessary corrections to the FEM elements to better reflect the prototype's dynamic response. Using these corrections, the FRF for the FEM was recalculated using the element specific correction identified in equation (5.8), displayed in Figure 154 with Table 19. Separately, the FEM was recalculated using the average element correction identified in equation (5.9) and displayed in Figure 155 with Table 20.

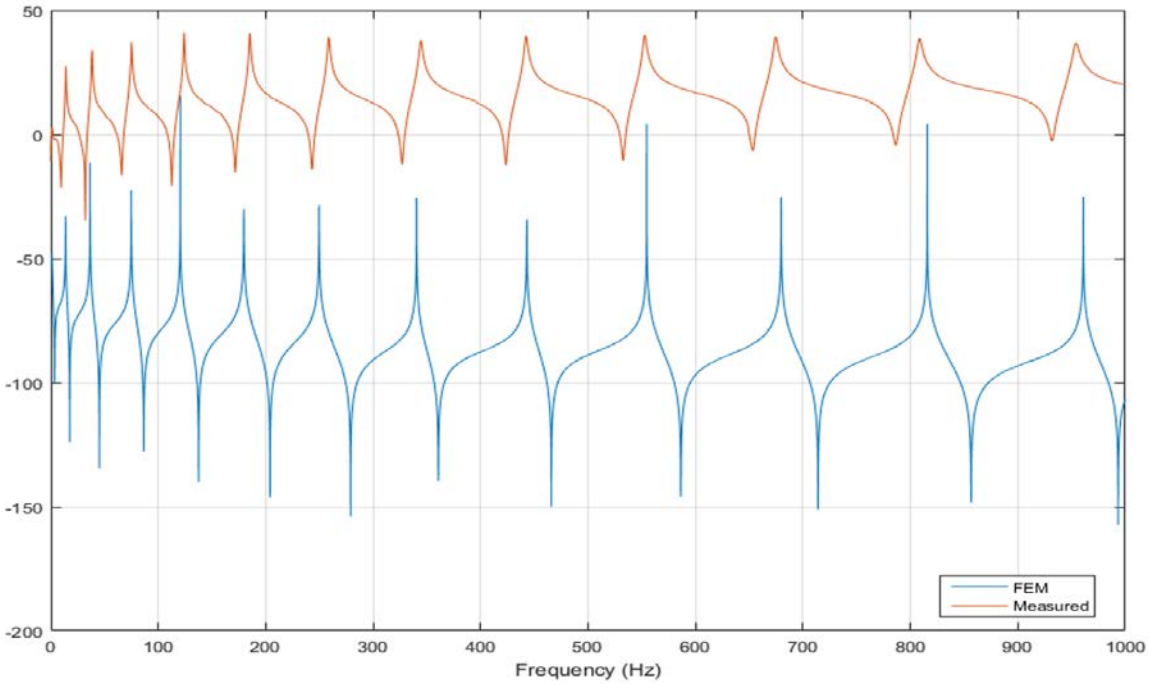

Figure 154. Updated FEM FRF compared to Prototype FRF Using Two Spring Synthesis Element Specific Correction, $H_{1,1}$

Table 19. Updated FEM Resonance Frequencies Using Two Spring Synthesis Element Specific Correction

Previous FEM Frequency(Hz)	Previous % Rel Error	Updated FEM Freq (Hz)	Measured Freq (Hz)	Absolute Error	% Relative Error	% Error Corrected
14.13452	2.3291	13.7422	13.81281	-0.07057	-0.5109	1.81816
38.95759	1.7872	36.4948	38.27358	-1.77878	-4.6475	-2.86038
76.37207	1.7888	74.8184	75.02992	-0.21157	-0.2820	1.50684
126.27156	1.8210	120.4998	124.01327	-3.51352	-2.8332	-1.01217
188.72298	1.8938	179.6513	185.21543	-5.56412	-3.0041	-1.11037
263.83435	2.0310	249.6324	258.58254	-8.95011	-3.4612	-1.43022
351.78075	2.1856	340.3857	344.25651	-3.87084	-1.1244	1.06124
452.81294	2.3864	443.0534	442.25887	0.794519	0.1797	2.20675
567.24773	2.6374	554.6007	552.67146	1.929261	0.3491	2.28834
695.40391	3.0958	679.7198	674.52174	5.198101	0.7706	2.32521
837.35461	3.5819	815.7007	808.39895	7.301723	0.9032	2.67862
991.88069	3.9774	960.9866	953.93877	7.047855	0.7388	3.23858

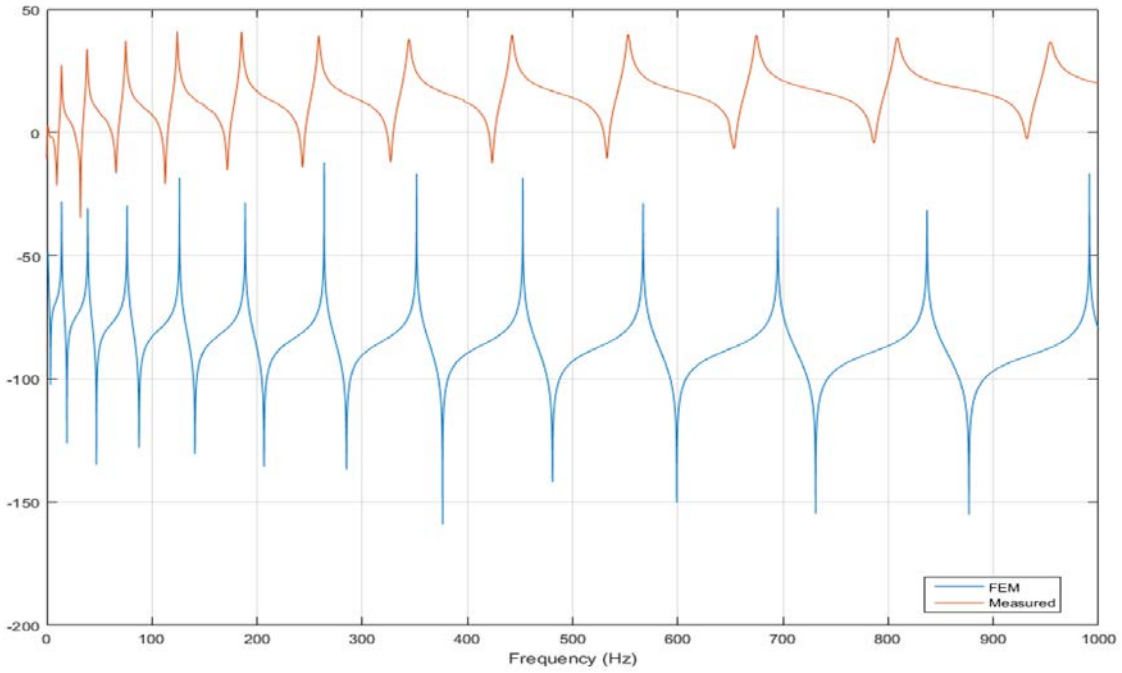

Figure 155. Updated FEM FRF compared to Prototype FRF Using Two Spring Synthesis Average Element Correction, $H_{1,1}$

Table 20. Updated FEM Resonance Frequencies Using Two Spring Synthesis Average Element Correction

Previous FEM Frequency(Hz)	Previous % Rel Error	Updated FEM Freq (Hz)	Measured Freq (Hz)	Absolute Error	% Relative Error	% Error Corrected
14.13452	2.3291	14.1276	13.81281	0.314755	2.2787	0.05035
38.95759	1.7872	38.9384	38.27358	0.664852	1.7371	0.05005
76.37207	1.7888	76.3345	75.02992	1.304595	1.7388	0.05005
126.27156	1.8210	126.2095	124.01327	2.196196	1.7709	0.05007
188.72298	1.8938	188.6302	185.21543	3.414747	1.8437	0.05011
263.83435	2.0310	263.7046	258.58254	5.122073	1.9808	0.05017
351.78075	2.1856	351.6078	344.25651	7.35126	2.1354	0.05025
452.81294	2.3864	452.5903	442.25887	10.3314	2.3361	0.05035
567.24773	2.6374	566.9688	552.67146	14.29734	2.5870	0.05047
695.40391	3.0958	695.0620	674.52174	20.54022	3.0452	0.05070
837.35461	3.5819	836.9429	808.39895	28.54391	3.5309	0.05093
991.88069	3.9774	991.3930	953.93877	37.45419	3.9263	0.05113

F. MODEL UPDATING USING LOWER MODES

The results from model updating with the single spring, single mass, and two spring solutions all utilized the highest six modes from each index in Table 10, Table 12, and Table 14 respectively. Interestingly enough, the highest six modes in the base FEM after updating have the best error correction. Because of this, a short test was conducted using the two spring setup and conditions identified in Table 14, but including some lower modes. As such, the new composite sensitivity matrix was made as follows:

$$\left[S_{comp}\right]_{14x14} = \begin{bmatrix} \left[S^{(N4,11-10,000)}\right]_{2,3,4,5,11,12,13} \\ \left[S^{(N8,15-10,000)}\right]_{6,7,8,9,10,12,13} \end{bmatrix} \tag{5.10}$$

$$\left[S_{comp}\right] = \begin{bmatrix} 0.000 & 0.008 & 0.037 & 0.056 & 0.044 & 0.027 & 0.010 & 0.001 & 0.007 & 0.032 & 0.035 & 0.013 & 0.003 & 0.000 \\ 0.003 & 0.055 & 0.235 & 0.185 & 0.011 & 0.067 & 0.149 & 0.112 & 0.019 & 0.064 & 0.132 & 0.060 & 0.015 & 0.001 \\ 0.014 & 0.164 & 0.437 & 0.139 & 0.665 & 0.762 & 0.095 & 0.573 & 0.996 & 0.247 & 0.317 & 1.098 & 0.723 & 0.075 \\ 0.017 & 0.163 & 0.296 & 0.114 & 0.676 & 0.393 & 0.140 & 0.667 & 0.210 & 1.144 & 0.752 & 1.831 & 2.159 & 0.278 \\ 25.431 & 18.162 & 24.307 & 11.328 & 7.439 & 12.584 & 11.584 & 6.903 & 11.534 & 6.879 & 2.064 & 8.072 & 4.845 & 6.766 \\ 9.239 & 6.057 & 8.434 & 13.133 & 10.829 & 9.297 & 12.989 & 14.299 & 11.124 & 8.846 & 28.775 & 32.559 & 24.815 & 38.110 \\ 19.713 & 14.569 & 13.363 & 25.734 & 33.431 & 30.279 & 27.885 & 28.695 & 31.873 & 30.058 & 21.234 & 18.141 & 18.294 & 25.347 \\ 0.116 & 0.558 & 0.145 & 0.340 & 0.256 & 0.334 & 1.395 & 1.539 & 4.644 & 0.985 & 5.708 & 1.460 & 4.307 & 2.901 \\ 2.168 & 8.441 & 1.553 & 6.928 & 2.102 & 5.066 & 2.155 & 1.217 & 0.118 & 0.060 & 0.245 & 0.130 & 0.179 & 0.159 \\ 0.218 & 0.419 & 0.236 & 0.262 & 0.390 & 0.248 & 0.369 & 6.339 & 4.251 & 12.848 & 3.801 & 12.856 & 4.470 & 8.920 \\ 9.714 & 14.249 & 12.462 & 6.978 & 16.758 & 5.473 & 10.312 & 1.466 & 1.625 & 1.138 & 0.721 & 1.612 & 0.530 & 1.144 \\ 4.408 & 3.555 & 5.485 & 3.375 & 3.158 & 6.100 & 0.688 & 12.001 & 12.386 & 11.240 & 19.563 & 12.537 & 10.988 & 12.415 \\ 13.403 & 9.041 & 9.765 & 11.857 & 11.652 & 9.933 & 7.836 & 19.783 & 26.144 & 21.081 & 19.607 & 23.600 & 29.046 & 4.069 \\ 39.773 & 30.647 & 30.104 & 30.654 & 31.396 & 32.259 & 23.952 & 14.793 & 17.195 & 17.217 & 17.606 & 17.455 & 19.028 & 6.485 \end{bmatrix} \tag{5.11}$$

This composite sensitivity matrix does not include any baseline modes; however, it includes modes 2, 3, 4, 5, 11, 12,and 13 from index 20 and modes 6,7,8,9,10,12, and 13 from index 31 indicated in Table 14. The condition number for this matrix is 4781.7. This matrix conditioning is not great, but within an acceptable magnitude demonstrated during previous tests.

Figure 156 and Figure 157 demonstrate the resulting synthesized FRFs of the measured data for a 178.579 kg/mm (10,000 lb/in) spring synthesized on Nodes 4 and 11. Similarly, Figure 158 and Figure 159 demonstrate the resulting synthesized FRFs of the measured data for a 178.579 kg/mm (10,000 lb/in) spring synthesized on Nodes 8 and 15.

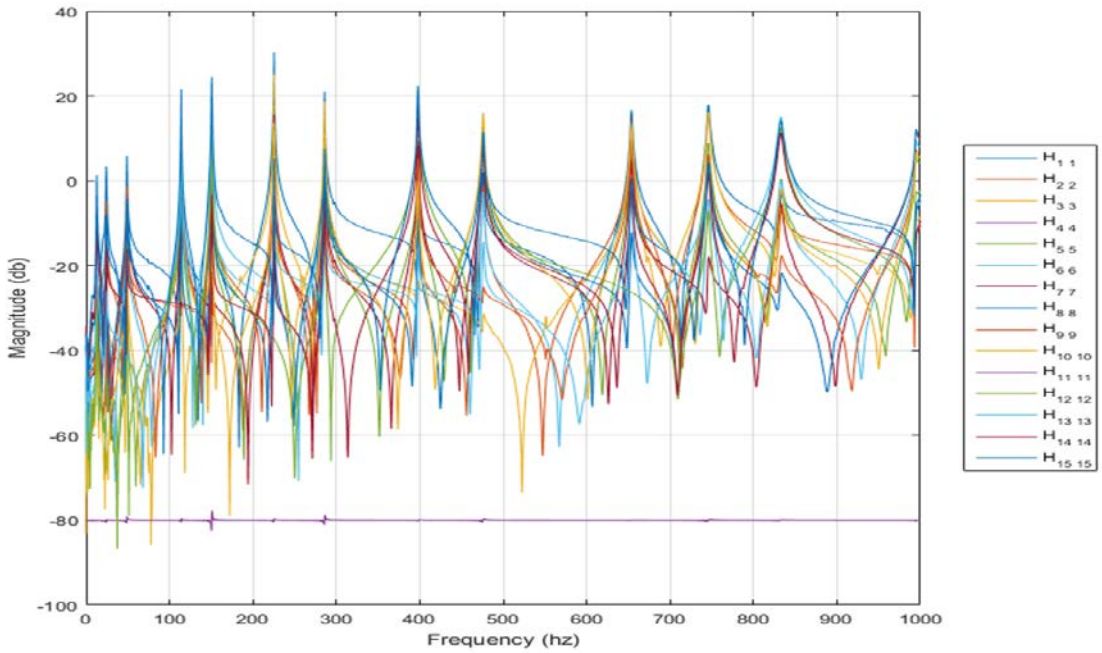

Figure 156. Synthesized Measured Data, 178.579 kg/mm (10,000 lb/in) on Nodes 4 and 11

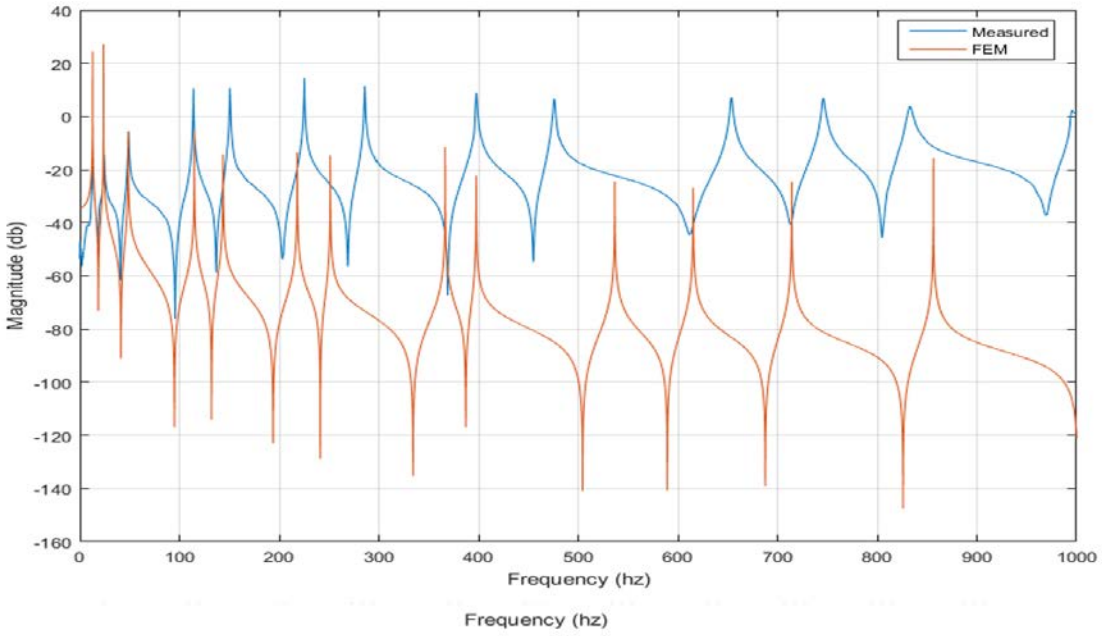

Figure 157. Synthesized Measured Data, Driving Point Average, 178.579 kg/mm (10,000 lb/in) on Nodes 4 and 11

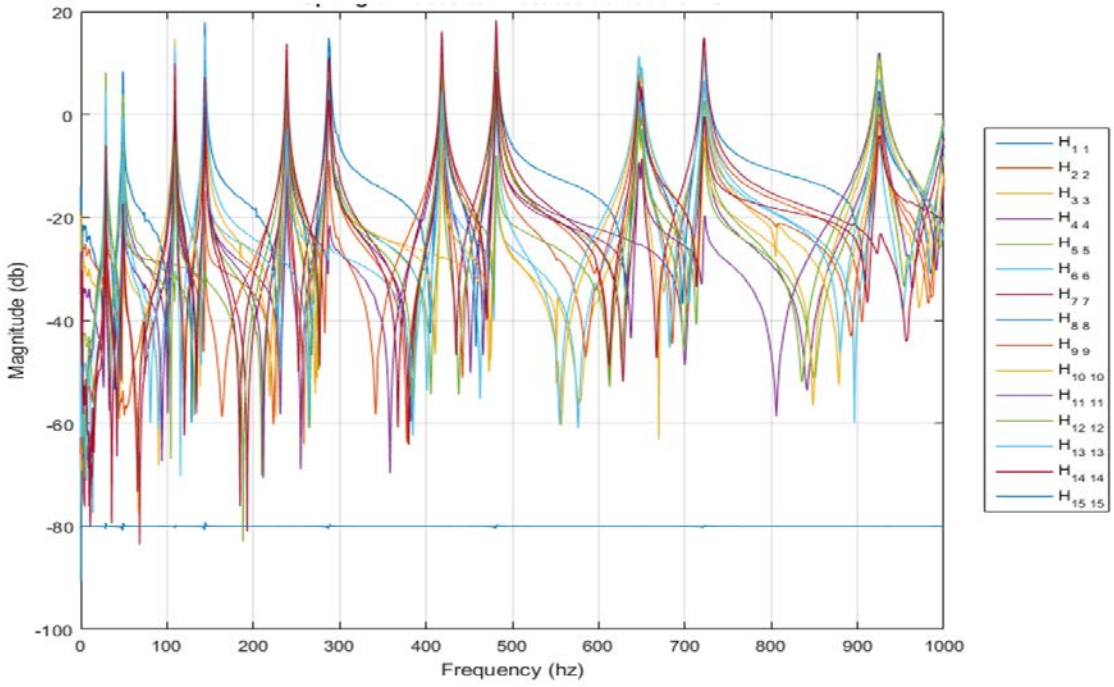

Figure 158. Synthesized Measured Data, 178.579 kg/mm (10,000 lb/in) on Nodes 8 and 15

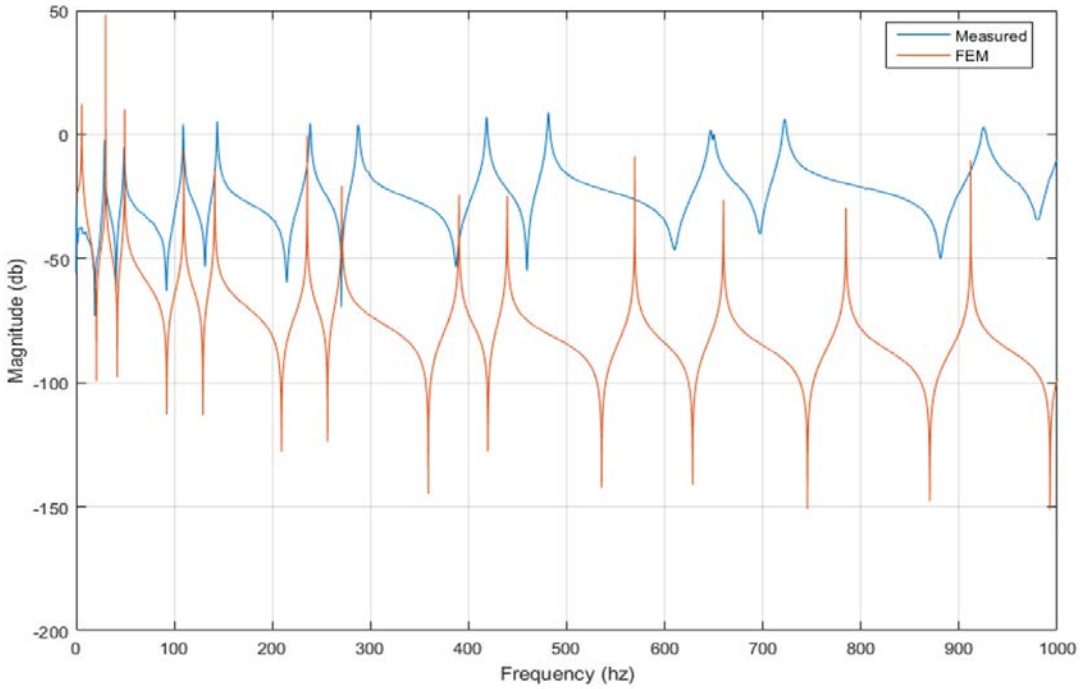

Figure 159. Synthesized Measured Data, Driving Point Average, 178.579 kg/mm (10,000 lb/in) on Nodes 8 and 15

Figure 156 through Figure 159 demonstrate the synthesis of the two spring system for the conditions indicated in equation (5.10). Once synthesized, we extract the frequencies for the specific modes for model updating. By modifying the sensitivity matrix as such, equation (4.23) can be solved with the following modifications:

$$\begin{bmatrix} \left[S^{(N\,4,11-10,000)}\right]_{2,3,4,5,11,12,13} \\ \left[S^{(N\,8,15-10,000)}\right]_{6,7,8,9,10,12,13} \end{bmatrix}^{-1} \begin{Bmatrix} \left\{\Delta\lambda^{(N\,4,11-10,000)}\right\}_{2,3,4,5,11,12,13} \\ \left\{\Delta\lambda^{(N\,8,15-10,000)}\right\}_{6,7,8,9,10,12,13} \end{Bmatrix} = \begin{Bmatrix} \Delta EI_1 \\ \Delta EI_2 \\ \vdots \\ \Delta EI_{14} \end{Bmatrix} \quad (5.12)$$

The identified modifications to the EI vector by solving equation (5.12) are shown in Figure 160.

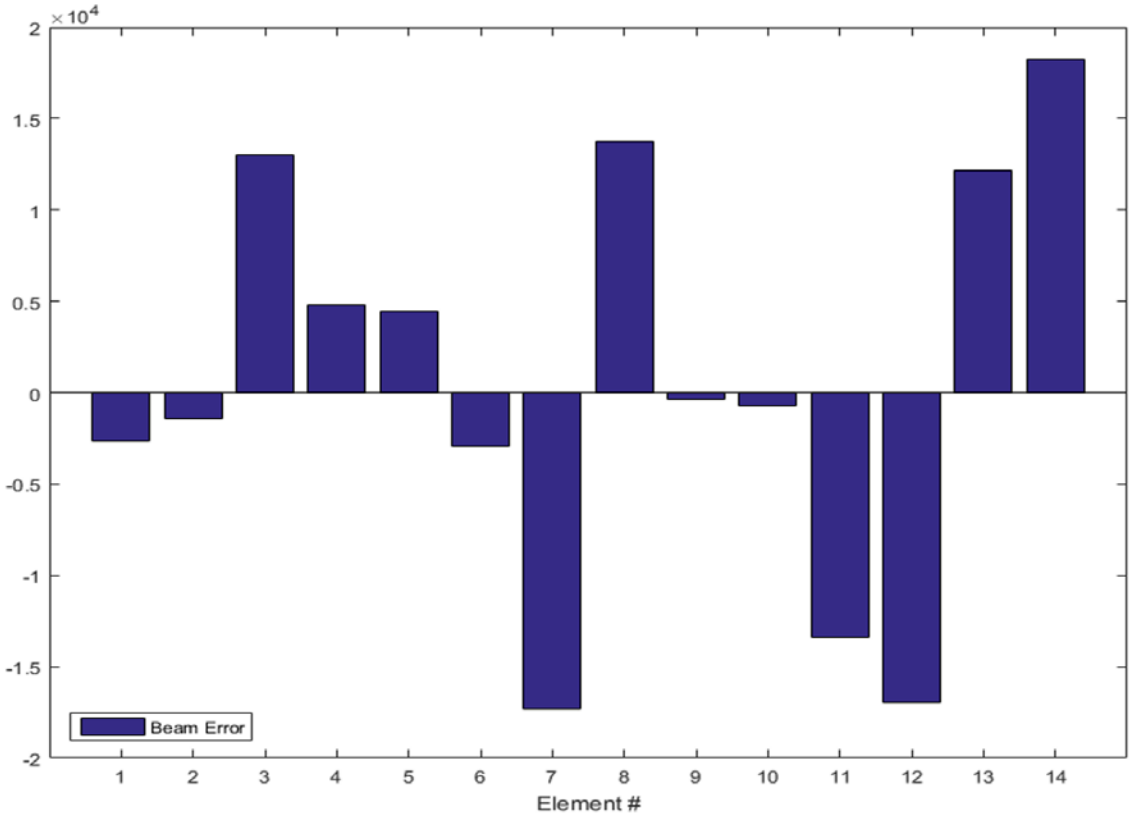

Figure 160. Identified Error in FEM Flexural Rigidity Using Two Spring Synthesis, Low Modes

$$\{\Delta EI\} = \begin{Bmatrix} -2650.899 \\ -1422.751 \\ 13023.016 \\ 4826.005 \\ 4413.373 \\ -2920.809 \\ -17305.534 \\ 13729.188 \\ -323.949 \\ -711.184 \\ -13392.979 \\ -16949.322 \\ 12155.394 \\ 18278.053 \end{Bmatrix} \tag{5.13}$$

$$\{\Delta EI\}_{AVERAGE} = -767.69 \tag{5.14}$$

The modification to the EI vector as displayed in Figure 160 was calculated as equation (5.13) and averaged in equation (5.14). By using the element specific correction, we can modify the dynamic response of the beam as calculated for Figure 161 and Table 21.

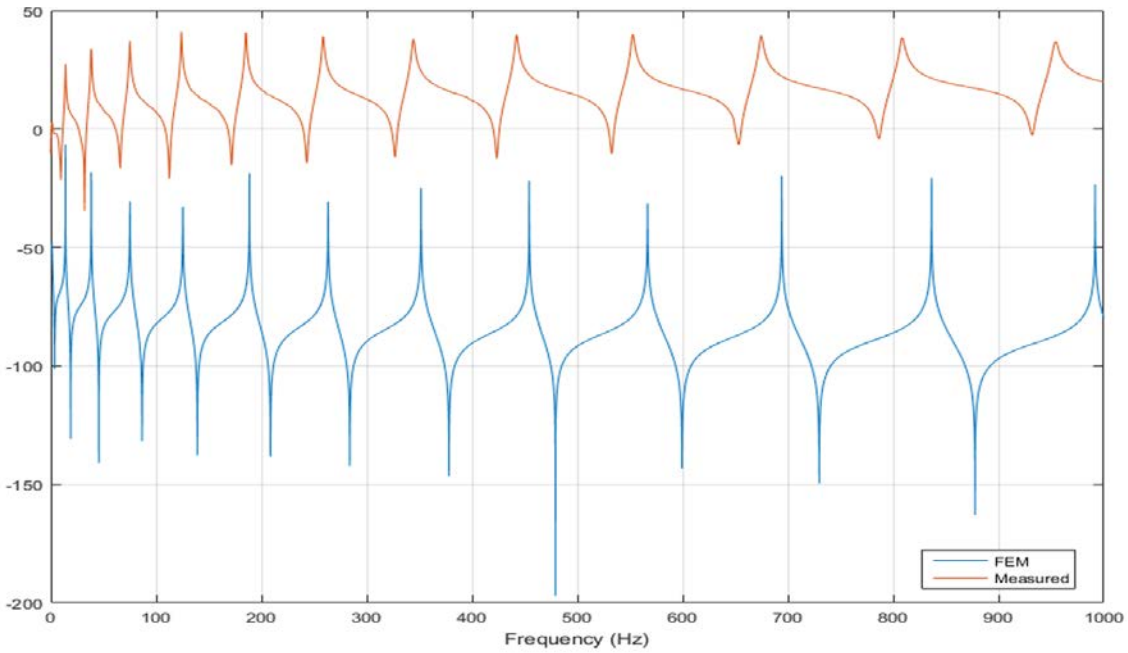

Figure 161. Updated FEM FRF compared to Prototype FRF Using Two Spring Synthesis Element Specific Correction, Low Modes, $H_{1,1}$

Table 21. Updated FEM Resonance Frequencies Using Low Modes Synthesis Element Specific Correction

Previous FEM Frequency(Hz)	Previous % Rel Error	Updated FEM Freq (Hz)	Measured Freq (Hz)	Absolute Error	% Relative Error	% Error Corrected
14.1345	2.3290	13.9022	13.8128	-0.0894	-0.6474	1.6816
38.9576	1.7872	38.3917	38.2736	-0.1181	-0.3086	1.4786
76.3721	1.7888	75.1602	75.0299	-0.1302	-0.1736	1.6152
126.2716	1.8210	125.4511	124.0133	-1.4379	-1.1594	0.6616
188.7230	1.8938	188.6115	185.2154	-3.3960	-1.8336	0.0602
263.8343	2.0310	263.3370	258.5825	-4.7545	-1.8387	0.1923
351.7808	2.1856	351.5785	344.2565	-7.3219	-2.1269	0.0588
452.8129	2.3864	454.3128	442.2589	-12.0539	-2.7255	-0.3391
567.2477	2.6374	566.7458	552.6715	-14.0743	-2.5466	0.0908
695.4039	3.0958	694.1887	674.5217	-19.6669	-2.9157	0.1802
837.3546	3.5819	836.4128	808.3990	-28.0139	-3.4654	0.1165
991.8807	3.9774	991.8157	953.9388	-37.8770	-3.9706	0.0068

G. CONCLUDING REMARKS

As had been developed in Chapter IV, we were able to synthesize a single spring, single mass, and two spring system into the measured data and successfully update the original FEM. Interestingly, the high modes where corrected almost exactly when using the element specific corrections; however, low modes did not see the same amount of correction, or got worse. This may have been due to the use of high modes only when developing the sensitivity for each synthesis type. The correction to the low modes did occur when the low modes where included into the sensitivity matrix, but did not provide a significant correction to the high modes.

Overall, the Single Mass synthesis provided the greatest amount of correction, especially at the higher modes, but had the largest increase in error in the low modes. The Two Spring synthesis provided the greatest benefit with least amount of additional error. Finally, the Two Spring Synthesis with low modes provided the least amount of added error but was minor in the amount of correction.

THIS PAGE INTENTIONALLY LEFT BLANK

VI. CONCLUSIONS AND RECOMMENDATIONS

A. CONCLUSIONS

As identified in Chapter I, the primary purpose of this thesis was to determine the possibility and relevance of using an artificial spring to ground or lumped mass added to a beam in-lieu of a pin connection. In three different types of simulations, we gathered new and relevant information for damage detection and model updating by varying the magnitude of either a single spring, single mass, or two spring system.

As was theorized, by increasing the stiffness of an artificial spring to ground, the beam's dynamic response will change to reflect that of a pin connection; however, there is a lot of useable FRF and sensitivity information in-between the baseline beam with no spring, and a beam with a spring of infinite stiffness. By varying the magnitude of the springs or mass artificially attached, we gathered new frequencies and sensitivity matrices, which we used in creating a new, composite sensitivity matrix.

Following previous thesis work [11], high modes from the new sensitivity matrices where developed into a square, full rank, composite matrix. However, due to the nature of the sensitivity matrix, it was discovered the matrix condition number would dramatically affect the results of any damage detection. As such, multiple sensitivity matrices were developed and evaluated to minimize the matrix condition number. The best-conditioned sensitivity matrix was developed from a combination of two-two spring sensitivity matrices. Similarly, each simulation developed a well-conditioned composite sensitivity matrix.

Each set of conditions was synthesized into FRF data gathered from the prototype beam the finite element model was based on. The resulting element wise correction was compared to a previous thesis where the researcher hand-picked modes from synthesized pin connections based on the QR decomposition of the resulting composite sensitivity matrix. The resulting frequencies are displayed in Table 22 through Table 25 and are compared to previous work developed in [11].

Table 22. Single Mass Solution Comparison to Previous Work

Measured Freq (Hz)	Single Spring Updated FEM Freq (Hz)	Single Spring Absolute Error	Single Spring % Relative Error	Damanakis' Updated Frequencies (Hz) [11]	Pin Synthesis Absolute Error	Pin Synthesis % Relative Error	Pin vs Spring % Relative Error
13.8128	13.996	-0.1832	1.3262	13.8090	-0.0038	0.0275	1.29870
38.2736	36.7333	1.5403	4.0244	38.0604	-0.2132	0.5569	3.4675
75.0299	74.5518	0.4781	0.6372	74.6133	-0.4166	0.5553	0.0819
124.0133	124.5348	-0.5215	0.4205	123.3636	-0.6497	0.5239	-0.1033
185.2154	186.5883	-1.3729	0.7412	184.3768	-0.8386	0.4528	0.2885
258.5825	261.7421	-3.1596	1.2219	257.7584	-0.8241	0.3187	0.9032
344.2565	348.7656	-4.5091	1.3098	343.6795	-0.5770	0.1676	1.1422
442.2589	448.5534	-6.2945	1.4233	442.3850	0.1261	0.0285	1.3948
552.6715	563.0675	-10.3960	1.8811	554.1845	1.5130	0.2738	1.6073
674.5217	687.8183	-13.2966	1.9713	679.3893	4.8676	0.7216	1.2496
808.3990	828.9641	-20.5652	2.5439	818.0711	9.6721	1.1965	1.3475
953.9388	980.0004	-26.0616	2.7320	969.0386	15.0998	1.5829	1.1491

Table 23. Single Mass Solution Comparison to Previous Work

Measured Freq (Hz)	Single Mass Updated FEM Freq (Hz)	Single Mass Absolute Error	Single Mass % Relative Error	Damanakis' Updated Frequencies (Hz) [11]	Pin Synthesis Absolute Error	Pin Synthesis % Relative Error	Pin vs Mass % Relative Error
13.8128	13.6115	0.2013	1.4574	13.8090	-0.0038	0.0275	1.42989
38.2736	35.7128	2.5608	6.6907	38.0604	-0.2132	0.5569	6.1338
75.0299	71.4144	3.6155	4.8188	74.6133	-0.4166	0.5553	4.2635
124.0133	118.0948	5.9185	4.7724	123.3636	-0.6497	0.5239	4.2486
185.2154	184.939	0.2764	0.1492	184.3768	-0.8386	0.4528	-0.3035
258.5825	257.2172	1.3653	0.5280	257.7584	-0.8241	0.3187	0.2093
344.2565	344.0446	0.2119	0.0616	343.6795	-0.5770	0.1676	-0.1061
442.2589	443.6277	-1.3688	0.3095	442.3850	0.1261	0.0285	0.2810
552.6715	553.5058	-0.8343	0.1510	554.1845	1.5130	0.2738	-0.1228
674.5217	679.6416	-5.1199	0.7590	679.3893	4.8676	0.7216	0.0374
808.3990	815.3904	-6.9914	0.8649	818.0711	9.6721	1.1965	-0.3316
953.9388	954.7796	-0.8408	0.0881	969.0386	15.0998	1.5829	-1.4947

Table 24. Two Spring Solution Comparison to Previous Work

Measured Freq (Hz)	Two Spring Updated FEM Freq (Hz)	Two Spring Absolute Error	Two Spring % Relative Error	Damanakis' Updated Frequencies (Hz) [11]	Pin Synthesis Absolute Error	Pin Synthesis % Relative Error	Pin vs Spring % Relative Error
13.8128	13.7422	0.0706	0.5112	13.8090	-0.0038	0.0275	0.48366
38.2736	36.4948	1.7788	4.6475	38.0604	-0.2132	0.5569	4.0906
75.0299	74.8184	0.2115	0.2819	74.6133	-0.4166	0.5553	-0.2734
124.0133	120.4998	3.5135	2.8331	123.3636	-0.6497	0.5239	2.3093
185.2154	179.6513	5.5641	3.0041	184.3768	-0.8386	0.4528	2.5514
258.5825	249.6324	8.9501	3.4612	257.7584	-0.8241	0.3187	3.1425
344.2565	340.3857	3.8708	1.1244	343.6795	-0.5770	0.1676	0.9568
442.2589	443.0534	-0.7945	0.1797	442.3850	0.1261	0.0285	0.1511
552.6715	554.6007	-1.9292	0.3491	554.1845	1.5130	0.2738	0.0753
674.5217	679.7198	-5.1981	0.7706	679.3893	4.8676	0.7216	0.0490
808.3990	815.7007	-7.3017	0.9032	818.0711	9.6721	1.1965	-0.2932
953.9388	960.9866	-7.0478	0.7388	969.0386	15.0998	1.5829	-0.8441

Table 25. Two Spring, Low Modes Comparison to Previous Work

Measured Freq (Hz)	Two Spring Low Updated FEM Freq (Hz)	Two Spring Low Absolute Error	Two Spring Low % Relative Error	Damanakis' Updated Frequencies (Hz) [11]	Pin Synthesis Absolute Error	Pin Synthesis % Relative Error	Pin vs Spring % Relative Error
13.8128	13.9022	-0.0894	0.6472	13.8090	-0.0038	0.0275	0.61962
38.2736	38.3917	-0.1181	0.3086	38.0604	-0.2132	0.5569	-0.2483
75.0299	75.1602	-0.1303	0.1736	74.6133	-0.4166	0.5553	-0.3817
124.0133	125.4511	-1.4378	1.1594	123.3636	-0.6497	0.5239	0.6356
185.2154	188.6115	-3.3961	1.8336	184.3768	-0.8386	0.4528	1.3808
258.5825	263.337	-4.7545	1.8387	257.7584	-0.8241	0.3187	1.5200
344.2565	351.5785	-7.3220	2.1269	343.6795	-0.5770	0.1676	1.9593
442.2589	454.3128	-12.0539	2.7255	442.3850	0.1261	0.0285	2.6970
552.6715	566.7458	-14.0743	2.5466	554.1845	1.5130	0.2738	2.2728
674.5217	694.1887	-19.6670	2.9157	679.3893	4.8676	0.7216	2.1941
808.3990	836.4128	-28.0138	3.4653	818.0711	9.6721	1.1965	2.2689
953.9388	991.8157	-37.8769	3.9706	969.0386	15.0998	1.5829	2.3877

As can be seen from Table 22 through Table 25, the synthesis of an artificial pin connection and time intensive mode evaluation still provides the best model updating; however, there is still a lot of information that can be gathered from continuing research into the synthesis of an artificial spring or mass.

B. RECOMMENDATIONS

Throughout this research, any spring simulation had a self-imposed limit of 178.579 kg/mm (10,000 lb/in) in order to develop an understanding of the reactions of the beam. As indicated in Figure 162 and Figure 163, there may be additional information for the sensitivity matrix with spring values as high as 2678.695 kg/mm (150,000 lb/in) for a single spring system, and 4464.491 kg/mm (250,000 lb/in) for a two spring system.

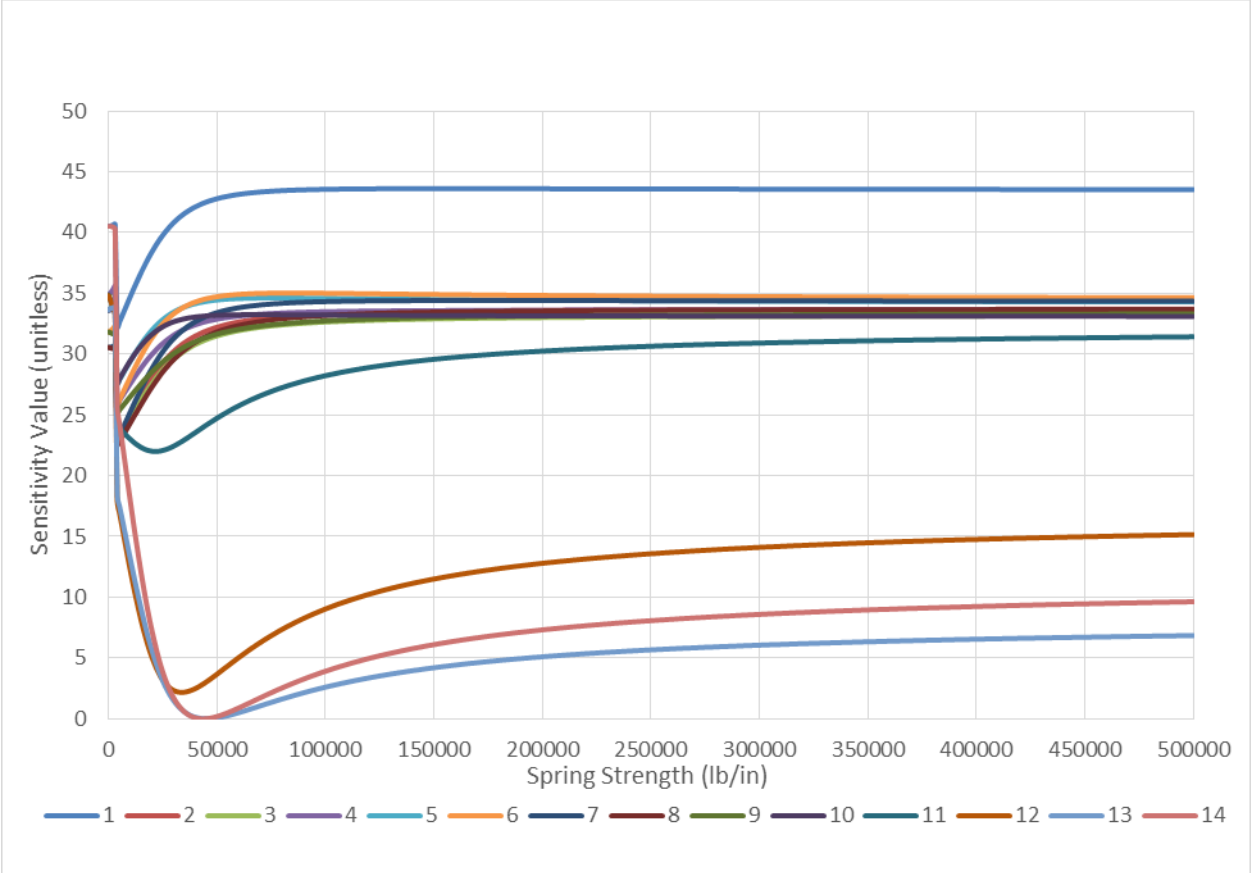

Figure 162. Effect on Sensitivity Value as Single Spring Strength Increases from 0–8928.984 kg/mm (500,000 lb/in) on Node 13

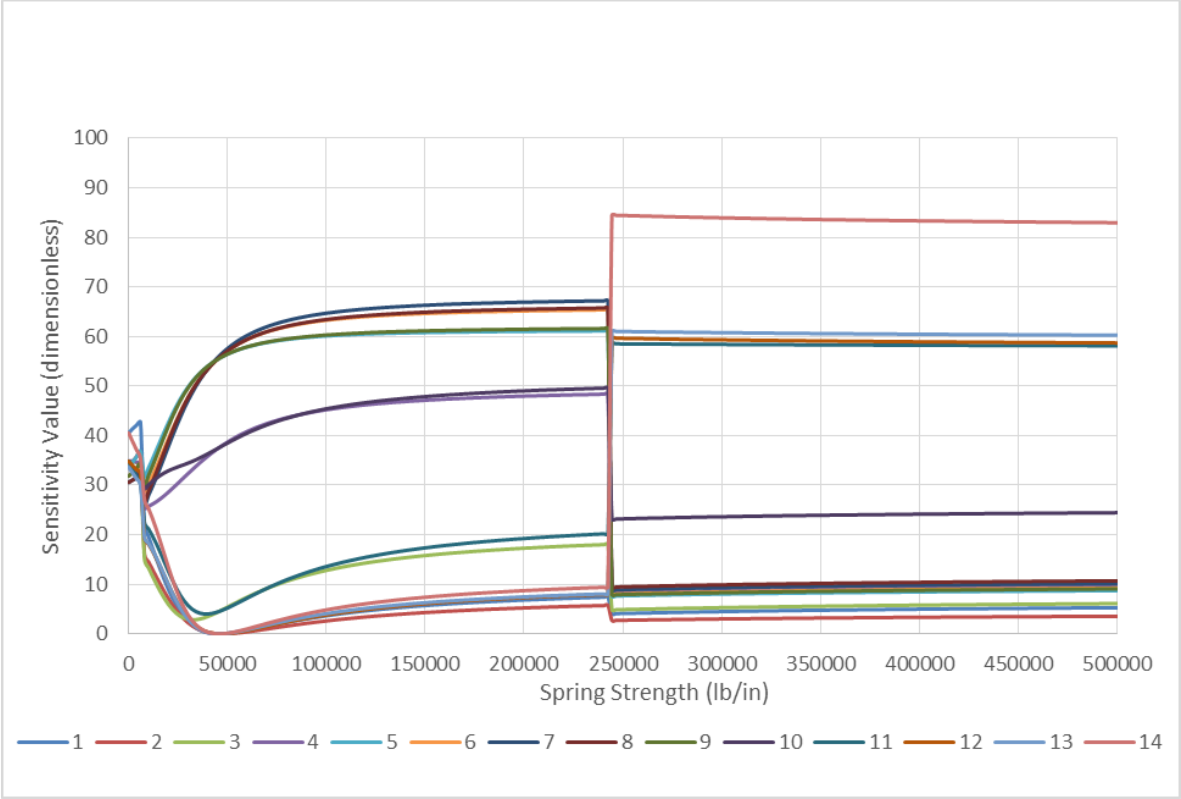

Figure 163. Effect on Sensitivity Value as Two Spring Strength increases from 0–8928.984 kg/mm (500,000 lb/in) on Nodes 5 and 12 equally

As indicated in Chapter IV, the two-spring synthesis was conducted as a proof of concept, and did not include all possibilities for evaluation. There are 105 different node location combinations, and multiple spring strengths that could produce useable FRF and sensitivity matrices from each set of nodes. As such, there may be over 100,000 different sensitivity combinations using the procedure detailed here, and many more depending on how many modes and locations are used in the development of the composite sensitivity matrix.

Another aspect of exploration with this procedure is using springs of different strengths in the two spring synthesis. As indicated in Chapter IV, all two-spring synthesis was done with both springs of equal spring strength. By varying spring strength separately, the dynamic response of the beam should alter

dramatically and provide new FRF and sensitivity data for damage detection and model updating.

Ultimately, because there is so much information available from this procedure, a program should be developed that can build and evaluate the rank and condition of a composite sensitivity matrix based on either existing sensitivity matrices, or have the capability to build new matrices as required. Such a program would decrease a lot of the time required in developing these matrices and reduce the subjectivity in development.

APPENDIX A. BEAM MODIFICATION BASE CODE

```
%% Konze - Thesis
clear,clc,clf,close all
format shortG

% One modification, multiple values, calculates S for each condition and
% pairs down based on selected modes

%% Beam Parameters

% Beam Properties
Beam.elem=16;
Beam.ro=0.0975/386.4; %lbm/in^3 (6061 Aluminum)
Beam.E=10*10^6*.97;   %psi with 0.9 correction factor
Beam.length=72;       %ft to in
Beam.width=1.93;          %in
Beam.depth=0.373;         %in
Beam.dof=2;         %Degrees of freedom per node
Beam.mass=Beam.length*Beam.depth*Beam.width*Beam.ro;     %lbm

%Beam as described by Manos
Beam.nodes=[0 0.5 5.57 10.64 15.71 20.78 25.85 30.92 35.99 41.06...
          46.13 51.2 56.27 61.34 66.41 71.48 71.98];


% Beam.nodes=linspace(lelem_outer,Beam.length-lelem_outer,Beam.elem+1);
BC=2; % Boundry Condition. 1=Cantilevered, 2=FreeFree

Beam.I=Beam.width*Beam.depth^3/12; % Crossectional Moment of Inertia
Beam.gam=Beam.ro*Beam.depth*Beam.width; % Mass per unit length

% Make an array of values for the EI of each element. Used for peturbance
% and stiffness matrix building
EItmp=ones(1,Beam.elem);
EI=(Beam.E*Beam.I);
Beam.EI=EI*EItmp;


% System Limitations
LFreq=1000; % Limiting Frequency (Hz)


% Artifical Boundry Condition Characteristics
ABC.SpringMag=500000; %(lb/in) Artifical Spring maximum magnitude
ABC.MassMag=0;%.35/386.4;     %(lbm)   Artifical Mass maximum magnitude
ABC.Node=[13];     % Node where Artifical Condition is placed
ABC.dof=2.*ABC.Node-1; %Specifies the translational DOF that the ABC is placed

ABC.Interval=500; %How many steps to go from 1 to the magnitude required

if ABC.SpringMag>0
   ABC.Spring = linspace(1,ABC.SpringMag,ABC.Interval);% (lb/ft)
```

```
else
   ABC.Spring=[];
end

% ABC.Spring=[10000];
% ABC.Interval=length(ABC.Spring);

if ABC.MassMag>0
%     ABC.Mass = linspace(ABC.MassMag,10/386.4,ABC.Interval);% (lb/ft)
%       ABC.Mass = [.0001 .001 .01 .1 10 100 1000 10000]/386.4 ;
ABC.Mass=4/386.4;
else
   ABC.Mass=[];
end

ABC.Bmodes=0;   % Baseline higher freq modes (+1) to keep
ABC.Mmodes=0;   % Modified higher freq modes (+1) to keep

% Damage
Damage.elem=5;       % Damaged Element
Damage.mag=5;        % Damage Magnitude (percent)

%% Instrumentation Properties

% Accelerometer
total_accels=15; %number of accelerometers installed
accel_weight=6.5*0.002204 ;% gram to lbs
h_accel=0.487 ; %height (in)
d_accel=0.62 ; %depth (in)

%Screw
screw_weight=.5*0.002204 ;% gram to lbs

%Accelerometers
Inst.accel_mass=accel_weight/386.4 ; %lbs*s^2/in
Inst.massI=Inst.accel_mass /12 *(3*(d_accel/2)^2 +h_accel^2) ; %lbs * s^2 *in Inertial Mass

%Screw
screw_mass=screw_weight/386.4 ; %lbs*s^2/in

%Assy
Inst.assy_mass=screw_mass+Inst.accel_mass ; %total mass of screw-accel assy

Inst.nodes=[0.5 5.57 10.64 15.71 20.78 25.85 30.92 35.99 41.06...
          46.13 51.2 56.27 61.34 66.41 71.48];
for r=1:length(Inst.nodes)
   Inst.Node(r)=find(Beam.nodes==Inst.nodes(r));
end
if length(Inst.Node)~=length(Inst.nodes)
   display('need to fix instrument/node positions')
   return
end

% Remove instrumentation for comparison with analytical frequency assement
% only
```

```
% Inst.assy_mass=0;
% Inst.massI=0;


%% Frequencies Measured

Measured.freqs=[13.81281,38.27358,75.02992,124.01327,185.21543,258.58254,344.25651,442.
25887,552.67146,674.52174,808.39895,953.93877];


%% Calculate global stiffness and mass matricies

[Beam.KGlobal,Beam.MGlobal]=KandMbeam_Global(Beam,Beam.EI,Inst,BC);
%% Analytical frequencies Assessment
% The calculated resonance frequencies are compared to the analytical
% solution using the roots to the chacteristic equation for a uniform,
% cantilevered beam as described using the formula from the Fudamentls of
% Structural Dynamics, 2ed., example 13.3

% Analytic Frequencies
lamL(1)=1.8751;
lamL(2)=4.6941;
lamL(3)=7.8548;
lamL(4)=10.996;


for r=1:length(lamL)
    om(r)=((lamL(r))^2/Beam.length^2)*(max(Beam.EI)/(Beam.ro*Beam.width*Beam.depth))^(1/2);
end

f_act=om/(2*pi());
if BC==1
    KGlobal_BC=Beam.KGlobal;
    MGlobal_BC=Beam.MGlobal;
else
    KGlobal_BC=Beam.KGlobal(Beam.dof+1:end,Beam.dof+1:end);
    MGlobal_BC=Beam.MGlobal(Beam.dof+1:end,Beam.dof+1:end);
end
[phi_BC,lam_BC,fn_BC]=eig_fcn(KGlobal_BC,MGlobal_BC);
Analytical_err=(f_act'-fn_BC(1:4))/f_act'*100;
display('Based off of cantilevered beam analytical assumption:')
vars={'Analytical_Freq','Calculated_Freq','Percent_Rel_Error'};
Comparison=table(f_act',fn_BC(1:4),Analytical_err(:,end),'Variable',vars);
display(Comparison)


%% Eigen Values
format shortG

[Beam.phiFE,Beam.lamFE,Beam.fnFE]=eig_fcn(Beam.KGlobal,Beam.MGlobal);


if BC==1
    display('For a Cantilevered beam, the calculated resonance frequencies are:')
    Freq_Calculated=Beam.fnFE';
```

```
    display(Beam.fnFE)
elseif BC==2
    %comaprison against measured frequencies is only vaid for a free free
    %beam
    display('For a free-free beam, with ridged body modes removed, the calculated resonance
frequencies are:')
    Freq_Calculated=Beam.fnFE(3:14)';
    display(Beam.fnFE(3:end))
    meas_err=abs((Measured.freqs'-Freq_Calculated')/Measured.freqs')*100;
    vars1={'Measured_Freq','Calculated_Freq','Percent_Rel_Error'};
    table(Measured.freqs',Freq_Calculated',meas_err(:,end),'Variable',vars1)

else
    display('Fix the BCs')
end


format short


%% System Frequency Limitations

[Beam.LimitedPhi,Beam.LimitedLam,Beam.LimitedFn]=sys_limit(Beam.phiFE,Beam.lamFE,Bea
m.fnFE,LFreq);

%% Sensitivity Calculation

[Beam.S]=Sensitivity_fcn(Beam,Inst,BC);




[Check]=Sensitivity_Check(Beam,Inst,BC);
display('Sensitivity Relative Error (in percent)')
Check

display('The largest sensitivity error is (percent)')
max(max(Check))

%Beam.S=Beam.S(3:16,:);
R_C.Base.rank=rank(Beam.S);
R_C.Base.cond=cond(Beam.S);
%% Apply simulated spring and mass for FRF analysis
[Delta_fn]=ABC_FRF(Beam,ABC,BC,LFreq);

%% Apply simulated spring and mass for Damage Detection
Pivot.CondS=ones(1,14);
%
% cnt=1
cnt=0;
for CntElem=2:15
    cnt=cnt+1;
    Damage.elem=CntElem;
    fprintf('For element %g \n\n',Damage.elem)
    if LFreq>=Beam.fnFE(end)
```

```
        [phiTest,lamTest,fnTest]=damage_beam(Beam,Inst,BC,Damage);
        [L_phitest,L_lamtest,L_fntest]=sys_limit(phiTest,lamTest,fnTest,LFreq);
        dlam=L_lamtest-Beam.LimitedLam;

        %%%%%%%%%
        %dlam=dlam(3:16);
        %%%%%%%%%

%       deltaP=inv(Beam.S)*dlam;
        deltaP=Beam.S\dlam;
%       deltaP=Beam.S\dlam(1:14);
        figure

        TrueDeltaP=Beam.El';

TrueDeltaP(Damage.elem)=TrueDeltaP(Damage.elem)+TrueDeltaP(Damage.elem)*Damage.ma
g/100;
        TrueDeltaP=Beam.El'-TrueDeltaP;
        TrueDelta_P=TrueDeltaP(2:end-1);

        % Damage Detection Plots
        barThis = [TrueDelta_P deltaP];
        bar(barThis)
        title('Plot: Model Errors vs True Errors Using All Modes')
        legend('True','Indicated','Location','Best')
        xlabel('Element #')
        % axis([0 18 -10000 10000])
    else
        % Perform Damage Detection with Spring
        tic
        [S_s,dlam_s,Pivot]=ABC_Sensistivity(Beam,ABC,LFreq,Inst,Damage,BC,Pivot);

        %%%%%%%%%%%%%%%
        %For testing a composite spring system and using excel

%       [S_s,dlam_s,Pivot]=ABC_CompositeS(Beam,ABC,LFreq,Inst,Damage,BC,Pivot);

        %%%%%%%%%%%%%%%


        deltaP_s=S_s\dlam_s;
        R_C.spring_rank(cnt)=rank(S_s);
        R_C.spring_cond(cnt)=cond(S_s);
        %%%
        SpringRank=rank(S_s)
        Pivot.CondS(cnt)=Pivot.CondS(cnt)*cond(S_s);
        SpringTime=toc
        %%%

        %Perform Damage Detection with Pin
%       tic
%       [S_p,dlam_p,Pivot.pin,Pivot.pin_I]=ABC_Pinned(Beam,LFreq,Inst,Damage,BC,ABC);
%       deltaP_p=S_p\dlam_p;
%       R_C.pin_rank(cnt)=rank(S_p);
%       R_C.pin_cond(cnt)=cond(S_p);
```

```
%       PinTime=toc

      figure

      TrueDeltaP=Beam.EI';

TrueDeltaP(Damage.elem)=TrueDeltaP(Damage.elem)+TrueDeltaP(Damage.elem)*Damage.ma
g/100;
      TrueDeltaP=Beam.EI'-TrueDeltaP;
      TrueDelta_P=TrueDeltaP(2:end-1);

      % Damage Detection Plots
%       barThis = [TrueDelta_P deltaP_s deltaP_p];
      barThis = [TrueDelta_P deltaP_s];
      bar(barThis)
      title('Plot: Model Errors vs True Errors with Limited Freq of 1000Hz')
      legend('True','Spring','Pin','Location','Best')
      xlabel('Element #')
      % axis([0 18 -10000 10000])
   end

end
```

APPENDIX B. STIFFNESS AND MASS MATRIX BUILDING FUNCTION

```
function [KGlobal,MGlobal]=KandMbeam_Global(Beam,EI,Inst,BC)

%-------------------------------------------------------------------------
% Purpose : To develop a Global stiffness and mass matrix for a beam
% Method (Two parts) : (Part 1) Using the shape functions for a beam,
% perform symbolic integration and differentiation to develop the stiffness
% and mass matrix for the element(Longer processing time).
% (Part 2) Using known solutions to the integrations, develop the stiffness
% and mass matrix  for the element (faster processing time)
%
% Variable Description:
% INPUT parameters:
%   Beam: Properties of the beam with the following entries:
%         length
%         width
%         depth
%         elem: Number of elements in the beam
%         nodes: Array of nodal locations
%   EI: Modulus of Elasticity multiplied by the crossectional
%             moment of inertia
%   Inst: Properties of the instruments with the following entries:
%         assy_mass: Any additional mass located at the nodes of the beam
%                   (e.g. Acceleromerters)
%         massI: Innertal mass of the additional mass, againlocated at
%                the nodes
%
% OUTPUT parameters:
%         KGlobal: Global Stiffness Matrix, no boundry conditions
%         MGlobal: Global Mass Matrix, no boundry conditions
%-------------------------------------------------------------------------

syms x y z


% %% Part 1 (uncomment to use)
% sf(1)=1-3*(x/lelem)^2+2*(x/lelem)^3;
% sf(2)=x*(1-2*(x/lelem)+(x/lelem)^2);
% sf(3)=3*(x/lelem)^2-2*(x/lelem)^3;
% sf(4)=-lelem*(x/lelem)^2+lelem*(x/lelem)^3;
%
%
% for i=1:length(sf)
%     for j=1:length(sf)
%         melem(i,j)=gam*int(sf(i)*sf(j),x,0,lelem);
%         kelem(i,j)=EI(j)*int(diff(diff(sf(i),x),x)*diff(diff(sf(j),x),x),x,0,lelem);
%     end
% end
%
% r=1;    %element starting counter
```

```
% v=4; %element ending counter
%
% KGlobal=zeros((elem*dof)+dof); %KGlobal preallocation
% MGlobal=zeros((elem*dof)+dof); %MGlobal preallocation
%
% while r<=elem*dof
%
%
%     % Assemble Stiffness and Mass Global matricies
%     KGlobal(r:v,r:v)=KGlobal(r:v,r:v)+kelem;
%     MGlobal(r:v,r:v)=MGlobal(r:v,r:v)+melem;
%
%     % Moving the number of degrees of freedom for per node in rows and
%     % columns after each loop
%     r=r+dof;
%     v=v+dof;
%     n=n+1;
% end


%%% Part 2 (uncomment to use)

%establish counters and preallocate global matricies
n=1;    % Node starting counter
r=1;    %element starting counter
v=4; %element ending counter

KGlobal=zeros((Beam.elem*Beam.dof)+Beam.dof); %KGlobal preallocation
MGlobal=zeros((Beam.elem*Beam.dof)+Beam.dof); %MGlobal preallocation

while v<=length(Beam.nodes)*Beam.dof

        lelem=Beam.nodes(n+1)-Beam.nodes(n);

        kelem=(EI(n)/(lelem^3))*...
                        [ 12       6*lelem    -12       6*lelem;
                        6*lelem  4*lelem^2  -6*lelem  2*lelem^2;
                        -12     -6*lelem     12      -6*lelem;
                        6*lelem  2*lelem^2  -6*lelem  4*lelem^2];

        melem=(Beam.ro*lelem*Beam.width*Beam.depth/420)*...
                        [ 156     22*lelem   54        -13*lelem;
                         22*lelem  4*lelem^2  13*lelem  -3*lelem^2;
                            54     13*lelem   156       -22*lelem;
                        -13*lelem -3*lelem^2  -22*lelem 4*lelem^2];


    % Assemble Stiffness and Mass Global matricies
    KGlobal(r:v,r:v)=KGlobal(r:v,r:v)+kelem;
    MGlobal(r:v,r:v)=MGlobal(r:v,r:v)+melem;
    % Moving the number of degrees of freedom for per node in rows and
    % columns after each loop
    r=r+Beam.dof;
    v=v+Beam.dof;
    n=n+1;
```

```
end

% Add point and inertial loads due to accelerometers (no accelerometer at
% the ends of the beam)
for rr=1:length(Inst.nodes);
    I_node=find(Inst.nodes(rr)==Beam.nodes);
    dof1=I_node*2-1;
    dof2=dof1+1;
    MGlobal(dof1,dof1)=MGlobal(dof1,dof1)+Inst.assy_mass;
    MGlobal(dof2,dof2)=MGlobal(dof2,dof2)+Inst.massI;

end

if BC==1
    KGlobal=KGlobal(3:end,3:end);
    MGlobal=MGlobal(3:end,3:end);
%     nodes=nodes(find(nodes>0));
elseif BC==2
    KGlobal=KGlobal;
    MGlobal=MGlobal;
%     nodes=nodes;
else
    display('Fix the BCs')
end
```

THIS PAGE INTENTIONALLY LEFT BLANK

APPENDIX C. EIGENVALUE FUNCTION

```
function [phi,lam,fn]=eig_fcn(KGlobal,MGlobal)
%%%%%%%%%%%%%%%%%%%%%%%%%%%%%%%%%%%%%%%%%%%%%%%%%%%%%%%
%%%%%%%%%%%%%%%
% Purpose:
% Take the input stiffness and mass matricies and output the eignenvectors,
% eigenvalues, and frequencies of resonance.
% INPUT parameters:
%       KGlobal: Global Stiffness Matrix
%       MGlobal: Global Mass Matrix
% OUTPUT parameters:
%       phi: Eigenvectors of the matricies
%       lam: Eigenvalues of the matricies
%       fn:  Resonance frequencies of the system (in Hz)
%%%%%%%%%%%%%%%%%%%%%%%%%%%%%%%%%%%%%%%%%%%%%%%%%%%%%%%
%%%%%%%%%%%%%%

[phi,lam] = eig(KGlobal,MGlobal);
lam = diag(lam);
wn = real(sqrt(lam));
fn = wn/(2*pi());
```

THIS PAGE INTENTIONALLY LEFT BLANK

APPENDIX D. SYSTEM FREQUENCY LIMITING FUNCTION

```
function [L_phi,L_lam,L_fn]=sys_limit(phi,lam,fn,LFreq)
%%%%%%%%%%%%%%%%%%%%%%%%%%%%%%%%%%%%%%%%%%%%%%%%%%%%%
%%%%%%%%%%%%%%%%%%%%
% Purpose:
% output an updated eigenvalue and eigenvector based on the limiting
% frequency. The limiting frequency may be due to system bandwidth, and
% will affect the readable eigenvalues and eigenvectors. It can be assumed
% that modes and resonance frequencies above this limiting frequency are
% nolonger "viewable," and may be unuseable in future calculations.
%
% This function also removes free body modes, should they exist.
%
% Input parameters:
%         phi: Eigenvectors of the matricies
%         lam: Eigenvalues of the matricies
%         fn:  Resonance frequencied of the system (in Hz)
%         LFreq: Limiting frequency
%
% Output Parameters
%         L_phi: "viewable" Eigenvectors
%         L_lam: "viewable" Eigenvalues of the matricies
%         L_fn:  "viewable" Resonance frequencies of the system (in Hz)
%%%%%%%%%%%%%%%%%%%%%%%%%%%%%%%%%%%%%%%%%%%%%%%%%%%%%
%%%%%%%%%%%%%%%%%%%%%%

%Below loop limits the usabel modes and frequencies based off of LFreq

r=1;
if LFreq>=fn(end)
   L_phi=phi;
   L_lam=lam;
   L_fn=fn;
else
   while fn(r)<=LFreq && r<=length(fn)
      L_phi(:,r)=phi(:,r);
      L_lam(r,1)=lam(r);
      L_fn(r,1)=fn(r);
      r=r+1;
   end
end

% Below loop removes free body modes.
for rr=1:4
   if L_fn(1)<=10^(-2)
      L_phi=L_phi(:,2:end);
      L_lam=L_lam(2:end);
      L_fn=L_fn(2:end);
   end
end
```

THIS PAGE INTENTIONALLY LEFT BLANK

APPENDIX E. SENSITIVITY MATRIX BUILDING FUNCTION

```
function [S]=Sensitivity_fcn(Beam,Inst,BC,ABC,cnt,LFreq,node)

%-------------------------------------------------------------------------
% Purpose : To develop an Eigen Sensitivity Matrix based on changes to the
% EI values. The Sensitivity matrix assists in predicting changes to
% resonance frequencies based on changes to specific parameters in the
% system. This maxrix is developed by temporarily perturbing the system and
% recording how the finite element model reacts.
%
% Variable Description:
% INPUT parameters:
%   Beam: Properties of the beam with the following entries:
%         phiFE or LimitedPhi: Eigenvectors of the Stiffness and Mass matricies
%         KGlobal: Global Stiffness Matrix
%         EI: Modulus of Elasticity multiplied by the crossectional
%            moment of inertia
%         length : length of the beam
%         width : Width of the beam
%         depth : Depth of the beam
%         elem: Number of elements in the beam
%         nodes: Array of nodal locations
%   Inst: Properties of the instruments with te following entries:
%         assy_mass: Any additional mass located at the nodes of the beam
%                  (e.g. Acceleromerters)
%         massI: Innertal mass of the additional mass, againlocated at
%               the nodes
%   Node: (optional) Node that a simulated pin connection occurs on.
% OUTPUT parameters:
%         S: Eigen Sensitivity matrix
%-------------------------------------------------------------------------
p=exist('node');
c=exist('ABC');
PercentPerturb = 1;    % finite difference step size for calculating sensitivity (unrelated to actual
error in FEM).
NumModes=min(size(Beam.LimitedPhi));
% NumModes=14;
NumSprings=Beam.elem;

% S = zeros(NumModes,NumSprings);        % initialize S matrix

for iCntElem = 1 : NumSprings

   %     KGlobal_Tmp = Beam.KGlobal;

   %Develop an array for the peturbed bar using the EI
   EI_pet=Beam.EI;
   EI_tmp=EI_pet(iCntElem)*(PercentPerturb/100);
   EI_pet(iCntElem)=EI_pet(iCntElem)+EI_tmp;


   [KGlobal_Tmp,MGlobal_Tmp]=KandMbeam_Global(Beam,EI_pet,Inst,BC);
```

```
    if c==1

        if ABC.MassMag>0
            mdelta=ABC.Mass(cnt);
            MGlobal_Tmp(ABC.dof,ABC.dof)=MGlobal_Tmp(ABC.dof,ABC.dof)+mdelta;
        end


        if ABC.SpringMag>0
            kdelta=ABC.Spring(cnt);
            KGlobal_Tmp(ABC.dof,ABC.dof)=KGlobal_Tmp(ABC.dof,ABC.dof)+kdelta;
        end
    end


    if p==1

        [KGlobal_Tmp,MGlobal_Tmp]=Pinned_Dof(KGlobal_Tmp,MGlobal_Tmp,node);
        [KGlobal_Pin,MGlobal_Pin]=Pinned_Dof(Beam.KGlobal,Beam.MGlobal,node);

        [phi_mod,lam_mod,fn_mod]=eig_fcn(KGlobal_Pin,MGlobal_Pin);
        [L_phiPin,L_lamPin,L_fnPin]=sys_limit(phi_mod,lam_mod,fn_mod,LFreq);

        dKdk=(KGlobal_Tmp-KGlobal_Pin)/EI_tmp;

        NumModes=length(L_lamPin);
        for iCntModes = 1 : NumModes  % Using all modes of the system (NumModes = nP = #rows
of [S])
            S(iCntModes,iCntElem) = L_phiPin(:,iCntModes)' * dKdk * L_phiPin(:,iCntModes);
        end
    else
        dKdk=(KGlobal_Tmp-Beam.KGlobal)/EI_tmp;
        for iCntModes = 1 : NumModes  % Using all modes of the system (NumModes = nP = #rows
of [S])
            S(iCntModes,iCntElem) = Beam.LimitedPhi(:,iCntModes)' * dKdk *
Beam.LimitedPhi(:,iCntModes);
        end
    end

end
S=S(:,2:end-1);
```

APPENDIX F. SENSITIVITY MATRIX CHECK FUNCTION

```
function [RelErr]=Sensitivity_Check(Beam,Inst,BC)

%-------------------------------------------------------------------------
% Purpose : To check the accuracy of an Eigen Sensitivity Matrix based on
% changes to the EI values. The Sensitivity matrix assists in predicting
% changes to resonance frequencies based on changes to specific parameters
% in the system. The check is accomplished by comparing the difference
% between the the resonance frequency prediction to change using the Eigen
% Sensitivity Matrix to a system with the change installed.
%
% Variable Description:
% INPUT parameters:
%   Beam: Properties of the beam with the following entries:
%         length
%         width
%         depth
%         ro: material density
%         elem: Number of elements in the beam
%         S: Eigen Sensitivity matrix
%         nodes: Array of nodal locations
%         EI: Modulus of Elasticity multiplied by the crossectional
%            moment of inertia
%         lam_base:Eigenvectors of the Stiffness and Mass matricies
%         KGlobal: Global Stiffness Matrix
%         MGlobal: Global Mass Matrix
%   Inst: Proterties of the instrumentation with the following entries:
%         assy_mass: Any additional mass located at the nodes of the beam
%                    (e.g. Acceleromerters)
%         massI: Innertal mass of the additional mass, againlocated at
%                the nodes
%   BC: Boundry Conditions enforced (cantilevared or free free)
% OUTPUT parameters:
%         RelErr: Relative Error of the predicted eigenvalue compared to
%         the eigen value with the temporary modification installed
%-------------------------------------------------------------------------
%

PercentChange = 1;    % finite difference step size for calculating sensitivity (unrelated to actual
error in FEM).
NumModes=length(Beam.LimitedLam);
% NumModes=14;
NumSprings=Beam.elem-2;


RelErr = zeros(NumModes,NumSprings);        % initialize error check matrix
for iCntElem = 1 : NumSprings

   KGlobal_Tmp = Beam.KGlobal;
   EI_pet=Beam.EI;
   EI_tmp=Beam.EI(iCntElem)*(PercentChange/100);
```

```
    EI_pet(iCntElem)=EI_pet(iCntElem)+EI_tmp;

    [KGlobal_Tmp,~]=KandMbeam_Global(Beam,EI_pet,Inst,BC);

%     kcheck=KGlobal_Tmp-KGlobal;


    [~,LamChanged,~]=eig_fcn(KGlobal_Tmp,Beam.MGlobal);

    %Remove Free Body Modes
    if LamChanged(1)<=10^(-2)
        lamChanged=LamChanged(3:end);
    else
        lamChanged=LamChanged;
    end

    for iCntModes = 1 : NumModes
        % Predict the eigenvalue (and the frequency by extension ) of the
        % system using the base system eigenvalues, the sensitivity matrix,
        % and the total change.

%         lamPredict=lam_base(iCntModes)+S(iCntModes,iCntElem)*EI_pet(iCntElem);

        lamPredict=Beam.LimitedLam(iCntModes)+Beam.S(iCntModes,iCntElem)*EI_tmp;

        %Relative Error of the sensitivity matrix in percent
        RelErr(iCntModes,iCntElem)=abs((lamChanged(iCntModes)-
lamPredict)/lamChanged(iCntModes))*100;
    end
end
```

APPENDIX G. FRF SYNTHESIS FUNCTION

```
function [fn_mod_record,Beam]=ABC_FRF(Beam,ABC,BC,LFreq)

%%%%%%%%%%%%%%%%%%%%%%%%%%%%%%%%%%%%%%%%%%%%%%%%%%%%%%%%%%%%%%%%%%%%%%%
% Variable Description:
% INPUT parameters:
%   Beam: Properties of the beam with the following entries:
%         phiFE or LimitedPhi: Eigenvectors of the Stiffness and Mass matricies
%         KGlobal: Global Stiffness Matrix
%         EI: Modulus of Elasticity multiplied by the crossectional
%             moment of inertia
%         length : length of the beam
%         width : Width of the beam
%         depth : Depth of the beam
%         elem: Number of elements in the beam
%         nodes: Array of nodal locations
%   ABC:  Properties of the Artifical Boundary Conditions
%         SpringMag: The magnitude of artifical spring-to-ground stiffness
%         MassMag: The magnitude of artifical dimensionless mass
%         Node: Node to apply the Artifical beam modifications
%         dof:Degree of Freedom associated to the Node for Beam
%             Modifications
%         Interval: How many steps from 1 to the magnitude of
%                 modification
%         Spring: An array of spring values going from 1 to the magnitude
%                 of modification with ABC.Interval steps
%         Mass:   An array of mass values going from 1 to the magnitude
%                 of modification with ABC.Interval steps
%   Inst: Properties of the instruments with te following entries:
%         assy_mass: Any additional mass located at the nodes of the beam
%                   (e.g. Acceleromerters)
%         massI: Innertal mass of the additional mass, againlocated at
%                the nodes
%   Damage: Properties of the damage to the beam
%         elem: Element that damage occurs on
%         Mag: Manitude of damage
%   BC: Boundary Condition applied to the beam
%   LFreq: Limiting frequency of the system. Modes and resonances above
%         this frequency are not included in calculation
%
% OUTPUT parameters:
%   fn_mod_record: A record of the limited frequencies of the modified beam
%                 for every step of ABC interval,including the baseline
%                 beam
%%%%%%%%%%%%%%%%%%%%%%%%%%%%%%%%%%%%%%%%%%%%%%%%%%%%%%%%%%%%%%%%%%%%%%%
%% Structural Synthisis Properties for Artifical Boundry Condition

Freqs = 1 : 0.1:  1000;
fn_mod=zeros(length(Beam.LimitedFn),ABC.Interval);
fn_record=zeros(length(Beam.LimitedFn)+1,ABC.Interval+1);

if length(ABC.Node)>1
```

```
    ABC.Node=ABC.Node(1);
    ABC.dof=ABC.dof(1);
end


if BC==1
    nodes=Beam.nodes(2:end);
    cset=ABC.dof;
    iset=[0:cset-1,cset+1:2*length(nodes)];
    iset=iset(2:end);
    aset=[cset iset];
else
    nodes=Beam.nodes;
    cset=ABC.dof;
    iset=[0:cset-1,cset+1:2*length(nodes)];
    iset=iset(2:end);
    aset=[cset iset];
end
%% Inital FRF Data
cnt=0;
for freq = Freqs
    cnt = cnt + 1; % counter for plot vectors
    omega = 2*pi*freq; % forcing frequency in rad/sec
    Z = Beam.KGlobal-omega^2*Beam.MGlobal; % impedance matrix at frequency omega
    Beam.H(:,:,cnt) = inv(Z); % FRF matrix at frequency omega
    H11inital(cnt) = Beam.H(2,2,cnt);

    Hcs_inital(cnt)=Beam.H(cset,cset,cnt);
    His_inital(cnt)=Beam.H(iset(end-1),iset(end-1),cnt);
end

%% Pin ABC FRF Synthesis data



cnt=0;
for freq = Freqs
    cnt = cnt + 1;
    Hii = Beam.H(iset,iset,cnt);
    Hic = Beam.H(iset,cset,cnt);
    Hci = Beam.H(cset,iset,cnt);
    Hcc = Beam.H(cset,cset,cnt);
%     HiiStar = Hii - Hic * (Hcc\Hci);
    HStar_pin(:,:,cnt) = Hii - Hic * inv(Hcc) *Hci;
    HiiStar_pin(cnt) = HStar_pin(iset(end-1),iset(end-1),cnt);
    HccStar_pin(cnt) = HStar_pin(cset,cset,cnt);
end

%% Pin FRF Check

[KGlobal_Pin,MGlobal_Pin]=Pinned_Dof(Beam.KGlobal,Beam.MGlobal,ABC.Node);

cnt=0;
for freq = Freqs
    cnt = cnt + 1; % counter for plot vectors
```

```
    omega = 2*pi*freq; % forcing frequency in rad/sec
    Z = KGlobal_Pin-omega^2*MGlobal_Pin; % impedance matrix at frequency omega
    H_pin(:,:,cnt) = inv(Z); % FRF matrix at frequency omega
    H11_pin_chk(cnt) = H_pin(1,1,cnt);
    Hcs_pin_chk(cnt)=H_pin(cset,cset,cnt);
    His_pin_chk(cnt)=H_pin(iset(end)-1,iset(end)-1,cnt);
end


%% Plots

figure(2)
subplot(211)
suptitle('Inital vs Pin FRF response')
plot(Freqs,20*log10(abs(squeeze(Beam.H(iset(end)-1,iset(end)-1,:)))))
hold on
plot(Freqs,20*log10(abs(HiiStar_pin)))
axis([0 150 -160 40])
legend('Inital','Pinned','Location','Best')
title(['|H_{',num2str(iset(end)-1),' ',num2str(iset(end)-1),'}(\Omega)|'])
xlabel('Frequency (Hz)')
subplot(212)
plot(Freqs,angle(squeeze(Beam.H(iset(end)-1,iset(end)-1,:)))*180/pi)
hold on
plot(Freqs,angle(HiiStar_pin)*180/pi)
title('Phase \Theta_{11} (\Omega)')

figure(3)
subplot(211)
suptitle('Pin FRF response check')
plot(Freqs,20*log10(abs(HccStar_pin)))
hold on
plot(Freqs,20*log10(abs(Hcs_pin_chk)),'--')
legend('Check','Synthesized','Location','Best')
title(['|H_{',num2str(iset(end)-1),' ',num2str(iset(end)-1),'}(\Omega)|for pinned DOF Check'])
xlabel('Frequency (Hz)')
subplot(212)
plot(Freqs,angle(HccStar_pin)*180/pi)
hold on
plot(Freqs,angle(Hcs_pin_chk)*180/pi,'--')

title('Phase \Theta_{is is} (\Omega)')



%%

fig_num=5;


for iCntIter=1:ABC.Interval
    %% ABC Mass

    % Add point loads due to Artifical Mass
    MGlobal_Mod=Beam.MGlobal;
```

```
if ABC.Mass>0
  mdelta=ABC.Mass(iCntIter);
  MGlobal_Mod(ABC.dof,ABC.dof)=Beam.MGlobal(ABC.dof,ABC.dof)+mdelta;
end

%% ABC Spring
KGlobal_Mod=Beam.KGlobal;
if ABC.Spring>0
   kdelta=ABC.Spring(iCntIter);
   KGlobal_Mod(ABC.dof,ABC.dof)=KGlobal_Mod(ABC.dof,ABC.dof)+kdelta;
end

%% Beam Modification Integration Sythisis Check
[phi,lam,fn]=eig_fcn(KGlobal_Mod,MGlobal_Mod);
[L_phitest,L_lamtest,L_fntest]=sys_limit(phi,lam,fn,LFreq);


fn_mod(1:length(L_fntest),iCntIter)=L_fntest;
fn_mod_record(1:length(Beam.LimitedFn),iCntIter)=fn(1:length(Beam.LimitedFn));

if ABC.Spring~=0
   vars(iCntIter+1)={sprintf('%s%s%s','Spring',num2str(ABC.Spring(iCntIter)),'lb/in')};
else
   vars(iCntIter+1)={sprintf('%s%s%s','Mass',num2str(ABC.Mass(iCntIter)*386.4),'lb')};
end

cnt = 0;
Hmod=zeros(length(nodes)*Beam.dof,length(nodes)*Beam.dof,length(Freqs));
Hcscheck=zeros(1,length(Freqs));
Hischeck=zeros(1,length(Freqs));
for freq = Freqs
   cnt = cnt + 1;       %  counter for plot vectors
   omega = 2*pi*freq;    % forcing frequency in rad/sec
   Z = KGlobal_Mod-(omega^2*MGlobal_Mod);      % Inversion matrix at frequency omega
   Hmod(:,:,cnt) = inv(Z);
   Hcscheck(cnt)=Hmod(cset,cset,cnt);
   Hischeck(cnt)=Hmod(3,3,cnt);
end


%% Beam Modification Integration Synthisis
cnt = 0;

Hstarcs=zeros(1,length(Freqs));
Hstaris=zeros(1,length(Freqs));
for freq = Freqs
   cnt=cnt+1;

   Haa = Beam.H(aset,aset,cnt);
   Hac = Beam.H(aset,cset,cnt);
   Hca = Beam.H(cset,aset,cnt);
   Hcc = Beam.H(cset,cset,cnt);

   if ABC.Spring~=0
      delZ=ABC.Spring(iCntIter);
```

```
        else
            omega = 2*pi*freq;
            delZ=-omega^2*ABC.Mass(iCntIter);
        end


        Hstar(aset,aset,cnt)=Haa-Hac*inv(Hcc+(inv(delZ)))*Hca;

        Hstar_cssynth(cnt)=Hstar(cset,cset,cnt);
        Hstar_issynth(cnt)=Hstar(3,3,cnt);



    end

    %% Plots
    figure(4)
%     subplot(211)
    plot(Freqs,20*log10(abs(Hstar_cssynth)))
    hold on

%
%     %%%%%%%%%%%%%%%%%%%%
%     % Testing only
            axis([0 150 -160 40])
            grid on
%     %%%%%%%%%%%%%%%%%%%%
%     title(['|H_{',num2str(iset(1)),' ',num2str(iset(1)),'}(\Omega)|'])
%     xlabel('Frequency (Hz)')
%     subplot(212)
%     plot(Freqs,angle(Hstar_cssynth)*180/pi)
%     hold on
% %     title('Phase \Theta_{is is} (\Omega)')

    figure
    subplot(211)
    suptitle('Modified CSET FRF response check')
    plot(Freqs,20*log10(abs(Hcscheck)),'-')
    hold on
    plot(Freqs,20*log10(abs(Hstar_cssynth)),'-.')
    legend('Check','Synthesized','Location','Best')
    if ABC.Spring~=0
        title(['|H_{',num2str(cset),' ',num2str(cset),...
            '}(\Omega)|for k=',num2str(ABC.Spring(iCntIter)),'in/lb spring'])
    else
         title(['|H_{',num2str(cset),' ',num2str(cset),...
             '}(\Omega)|for m=',num2str(ABC.Mass(iCntIter)),'lbm mass'])
    end
    xlabel('Frequency (Hz)')
    subplot(212)
    plot(Freqs,angle(Hcscheck)*180/pi)
    hold on
    plot(Freqs,angle(Hstar_cssynth)*180/pi)
```

```
    title('Phase \Theta_{is is} (\Omega)')

    figure
    subplot(211)
    suptitle('Modified ISET FRF response check')
    plot(Freqs,20*log10(abs(Hischeck)),'-')
    hold on
    plot(Freqs,20*log10(abs(Hstar_issynth)),'-.')
    legend('Check','Synthesized','Location','Best')
    if ABC.Spring~=0
        title(['|H_{',num2str(iset(end-1)),' ',num2str(iset(end-1)),...
            '}(\Omega)|for k=',num2str(ABC.Spring(iCntIter)),'in/lb spring'])
    else
         title(['|H_{',num2str(iset(end-1)),' ',num2str(iset(end-1)),...
             '}(\Omega)|for m=',num2str(ABC.Mass(iCntIter)),'lbm mass'])
    end
    xlabel('Frequency (Hz)')
    subplot(212)
    plot(Freqs,angle(Hischeck)*180/pi)
    hold on
    plot(Freqs,angle(Hstar_issynth)*180/pi)

    title('Phase \Theta_{is is} (\Omega)')

fig_num=fig_num+1;
end
vars(iCntIter+2)={'Pin'};
vars(iCntIter+3)={'Inital'};

figure(4)
% subplot(211)
suptitle('FRF response change')
% plot(Freqs,20*log10(abs(HccStar_pin)))
% hold on
plot(Freqs,20*log10(abs(squeeze(Beam.H(cset,cset,:)))))
hold on

%%%%%%%%%%%%%%%%%%%%
% Testing only
       axis([0 150 -160 40])
       grid on
%%%%%%%%%%%%%%%%%%%%
title(['|H_{',num2str(cset),' ',num2str(cset),'}(\Omega)|'])
xlabel('Frequency (Hz)')
legend(vars(2:end),'Location','EastOutside')
```

APPENDIX H. SENSITIVITY CALCULATION FOR SYNTHESIZED BEAM

```
function [S,dLam,Pivot]=ABC_Sensistivity(Beam,ABC,LFreq,Inst,Damage,BC,Pivot)
%%%%%%%%%%%%%%%%%%%%%%%%%%%%%%%%%%%%%%%%%%%%%%%%%%%%%%%%
%
% Variable Description:
% INPUT parameters:
%   Beam: Properties of the beam with the following entries:
%         phiFE or LimitedPhi: Eigenvectors of the Stiffness and Mass matricies
%         KGlobal: Global Stiffness Matrix
%         EI: Modulus of Elasticity multiplied by the crossectional
%            moment of inertia
%         length : length of the beam
%         width : Width of the beam
%         depth : Depth of the beam
%         elem: Number of elements in the beam
%         nodes: Array of nodal locations
%   ABC:  Properties of the Artifical Boundary Conditions
%         SpringMag: The magnitude of artifical spring-to-ground stiffness
%         MassMag: The magnitude of artifical dimensionless mass
%         Node: Node to apply the Artifical beam modifications
%         dof:Degree of Freedom associated to the Node for Beam
%            Modifications
%         Interval: How many steps from 1 to the magnitude of
%                modification
%         Spring: An array of spring values going from 1 to the magnitude
%                of modification with ABC.Interval steps
%         Mass:   An array of mass values going from 1 to the magnitude
%                of modification with ABC.Interval steps
%   Inst: Properties of the instruments with te following entries:
%         assy_mass: Any additional mass located at the nodes of the beam
%                  (e.g. Acceleromerters)
%         massI: Innertal mass of the additional mass, againlocated at
%                the nodes
%   Damage: Properties of the damage to the beam
%         elem: Element that damage occurs on
%         Mag: Manitude of damage
%   BC: Boundary Condition applied to the beam
%
% OUTPUT parameters:
%         S: Eigen Sensitivity matrixof the beam before damage. This is
%            a composite of every interval of the Spring or Mass array
%         dLam: Change in resonance frequencies of the beam before and
%             after damage. This is a composite of every interval of the
%             Spring or Mass array
%         Pivot: QR pivot properties of the modified beam
%%%%%%%%%%%%%%%%%%%%%%%%%%%%%%%%%%%%%%%%%%%%%%%%%%%%%%%%


MGlobal=Beam.MGlobal;
KGlobal=Beam.KGlobal;
```

```
S=Beam.S;

Bmodes=ABC.Bmodes;   % Baseline higher freq modes (+1) to keep
Mmodes=ABC.Mmodes;   % Modified higher freq modes (+1) to keep

fn_diff=zeros(length(Beam.LimitedFn),ABC.Interval);
fn_rcrd=zeros((length(Beam.LimitedFn)+1),ABC.Interval);

[phiTest,lamTest,fnTest]=damage_beam(Beam,Inst,BC,Damage);
[L_phitest,L_lamtest,L_fntest]=sys_limit(phiTest,lamTest,fnTest,LFreq);
dLam=L_lamtest-Beam.LimitedLam;

Limitedphi=Beam.LimitedPhi;
Limitedlam=Beam.LimitedLam;
Limitedfn=Beam.LimitedFn;

%%%%%%%%%%%%%
   %Modify the Baseline S matrix to account only for some modes.
%   %Lower Modes

%     S=S(2:Bmodes,:);
%     dLam=dLam(2:Bmodes);
%%%%%%%%%%%%%%%
% %   Higher Modes
%
   S=S(end-Bmodes:end,:);
   dLam=dLam(end-Bmodes:end);
%%%%%%%%%%%%%


for cnt=1:ABC.Interval
   %% Damage Beam

   D_mag=(Damage.mag)/100;
   EI_D=Beam.EI;
   EI_D(Damage.elem)=EI_D(Damage.elem)-(EI_D(Damage.elem)*D_mag);
   [Ktest,Mtest]=KandMbeam_Global(Beam,EI_D,Inst,BC);

   if ABC.MassMag>0
      mdelta=ABC.Mass(cnt);
      Mtest(ABC.dof,ABC.dof)=Mtest(ABC.dof,ABC.dof)+mdelta;
   end

   Beam.KGlobal=KGlobal;
   if ABC.SpringMag>0
       kdelta=ABC.Spring(cnt);
       Ktest(ABC.dof,ABC.dof)=Ktest(ABC.dof,ABC.dof)+kdelta;
   end

   % Determine eigenvalues for modified beam, damaged
   [phiTest_mod,lamTest_mod,fnTest_mod] = eig_fcn(Ktest,Mtest);

[Lphitest_mod,Llamtest_mod,Lfntest_mod]=sys_limit(phiTest_mod,lamTest_mod,fnTest_mod,LFr
eq);
```

```
    %% ABC Conditions
    Beam.MGlobal=MGlobal;
    if ABC.MassMag>0
       mdelta=ABC.Mass(cnt);
       Beam.MGlobal(ABC.dof,ABC.dof)=Beam.MGlobal(ABC.dof,ABC.dof)+mdelta;
    end

    Beam.KGlobal=KGlobal;
    if ABC.SpringMag>0
        kdelta=ABC.Spring(cnt)
        Beam.KGlobal(ABC.dof,ABC.dof)=Beam.KGlobal(ABC.dof,ABC.dof)+kdelta;
    end

    Beam.LimitedPhi=Limitedphi;
    Beam.LimitedLam=Limitedlam;
    Beam.LimitedFn=Limitedfn;

    % Determine eigenvalues for modified beam, undamaged
    [phi_mod,lam_mod,fn_mod]=eig_fcn(Beam.KGlobal,Beam.MGlobal);

[Limitedphi_mod,Limitedlam_mod,Limitedfn_mod]=sys_limit(phi_mod,lam_mod,fn_mod,LFreq);

    Beam.LimitedPhi=Limitedphi_mod;
    Beam.LimitedLam=Limitedlam_mod;
    Beam.LimitedFn=Limitedfn_mod;

    dlam_Mod=Llamtest_mod(1:size(Limitedlam_mod))-Limitedlam_mod;
    dfn(1:length(Limitedfn_mod),cnt)=real(sqrt(dlam_Mod))/2*pi;


    %% Sensitivity Modification
%%%%%%%%%%%%%%%%%%%
    fn_rcrd(:,cnt)=fn_mod(2:(length(Limitedfn)+2));
    fn_diff(1:length(Limitedfn_mod),cnt)=Limitedfn_mod-Lfntest_mod(1:length(Limitedfn_mod));
%%%%%%%%%%%%%%%%%%%

    [S_Mod]=Sensitivity_fcn(Beam,Inst,BC,ABC,cnt);

%%%%%%%%%%%%%
    %Modify the S matrix to account only for some modes.
%   %Lower Modes

%     S_Mod=S_Mod(2:Mmodes,:)
%     dlam_Mod=dlam_Mod(2:Mmodes);
%%%%%%%%%%%%%%%
% %   Higher Modes
%
    S_Mod=S_Mod(end-Mmodes:end,:);
    dlam_Mod=dlam_Mod(end-Mmodes:end);
%%%%%%%%%%%%%%%

    [~,~,Pivot.spring_I(cnt,:)]=qr(S_Mod,0);
```

```
    dLam=cat(1,dLam,dlam_Mod);
    S=cat(1,S,S_Mod);

    Srank=rank(S);
    [~,~,Pivot.spring(cnt,:)]=qr(S,0);


end
display('Changes in frequency before and after damage with each spring progression are:')
ABC.Spring
fn_diff

fn_rcrd

end
```

LIST OF REFERENCES

[1] Timoshenko, S., 1953, *History of Strength of Materials*, McGraw-Hill, New York.

[2] Timoshenko, S., 1937, *Vibration problems in Engineering*, D. Van Nostrand Company Inc., New York

[3] Cdang, 2008, “Euler–Bernoulli Beam Theory,” Wikipedia, https://en.wikipedia.org/wiki/Euler%E2%80%93Bernoulli_beam_theory.

[4] Craig Jr., R. R., 1981, *Structural Dynamics: An Introduction to Computer Methods*, John Wiley & Sons, Inc, New York, pp. 385–387.

[5] Gordis, J.H., 1999, “Artificial Boundary Conditions for Model Updating and Damage Detection,” *Mechanical Systems and Signal Processing,* **13**(3):437-48

[6] Wren, J.,2009, “A Simple Frequency Response Function,” Prosig, http://blog.prosig.com/2009/10/19/a-simple-frequency-response-function/.

[7] Pulse Reflex. Version 21.0.0.,2017. Denmark: Bruel & Kjaer. https://www.bksv.com/en/products/PULSE-analysis-software/structural-dynamics-software/operating-deflection-shapes-analysis/reflex-operating-deflection-shapes

[8] Gordis, J. H. and Papagiannakis, K., 2011,”Optimal Selection of Artificial Boundary Conditions for Model Update and Damage Detection,” *Mechanical Systems and Signal Processing*, **25**, pp. 1451–1468.

[9] Imregun, M. and Visser, W. J.,1991, “A Technique to Update Finite Element Models Using Frequency Response Data,” *Proceedings of the 9th International Modal Analysis Conference*, pp. 462–468

[10] Gordis, J.H., “Eigenvector Sensitivity Analysis: An Informal Survey of Selected Contributions to the Literature,” SDRC Engineering Services, Cincinnati, OH.

[11] Damanakis, E., 2017, “Artificial Beam Modifications for Finite Element Model Update and Damage Detection,” M.S. Thesis, Naval Postgraduate School, Monterey, CA.

[12] Benaroya, H., Wei, T., and Han, S.M., 1999, “Dynamics of Transversely Vibrating Beams Using Four Engineering Theories,” *Journal of Sound and Vibration*, **225**(5), pp. 935–988.

[13] Levin, R.I. and Lieven, N.A.J., 1998,"Dynamic Finite Element Model Updating Using Simulated Annealing And Genetic Algorithms," *Mechanical Systems and Signal Processing*, **12**(1), pp. 91–120.

[14] Gordis, J. H.,1996 "Omitted Coordinate Systems and Artificial Constraints in Spatially Incomplete Identification," *Modal Analysis*, **11**, pp. 83–95.

[15] Shumin, L., Stuart, S. and Brown, D., 1955,"Perturbed Boundary Condition Testing," *Proceedings of the 13th International Modal Analysis Conference*, **1**, pp. 902–907.

[16] Jones, K. and Turcotte, J.,2002, "Finite Element Model Updating Using Anti-Resonant Frequencies," *Journal of Sound and Vibration*, **252**(4),pp.17-27.

[17] MATLAB. Version R2016a, 2016. Cambridge, MA: The Mathworks, inc.

[18] Forti, N. C. S., Forti, T. L. D., Jacintho, A. E. P. G. A., and Pimentel, L. L., 2015, "Finite Element Analysis of Composite Concrete-Timber Beams," SciELO, http://www.scielo.br/scielo.php?script=sci_arttext&pid=S1983-41952015000400507.

[19] Parlett, B. N., 1980, *The Symmetric Eigenvalue Problem*, Prentice Hall, New York

[20] O'Callahan, J., 1989, "A Procedure for an Improved Reduction System (IRS) Model," *7th International Modal Analysis Conference*, Las Vegas, NV.

[21] "Frequency domain structural synthesis," class notes for ME 4522, Naval Postgraduate School, Monterey, CA.

[22] Wittrick, W. H., 1962 "Rates of Change of Eigenvalues with Reference to Buckling and Vibration Problems," *Journal of the Royal Aeronautical Society*, **24**, pp. 590–591.

[23] Fritzen, C., and Kiefer, T., 1992, "Localization and Correction of Errors in Finite Element Models Based on Experimental Data," *Proceedings of the 17th International Seminar on Modal Analysis*, pp. 1581–1596.

[24] Lagunes, A. R., 2007, "Finite Element Based Structural Damage Detection Using Artificial Boundary Conditions," M.S. Thesis, Naval Postgraduate School, Monterey, CA.

[25] Erdelyi, N. H. and Hashemi, S. M., 2016 “On the Finite Element Free Vibration Analysis of Delaminated Layered Beams: A New Assembly Technique,” Research Gate, Available: https://www.researchgate.net/publication/289984581_On_the_Finite_Element_Free_Vibration_Analysis_of_Delaminated_Layered_Beams_A_New_Assembly_Technique.

[26] Chang, T. C. and Craig, R. R., 1969, “Normal Modes of Uniform Beams,” Engineering Mechanics Division, *Proceedings of the ASCE*, **95** (EM4), pp. 1027–1031.

[27] Tu, Z. and Lu, Y., 2007, “FE Model Updating Using Artificial Boundary Conditions with Genetic Algorithms,” Computers and Structures, **86**, pp. 714–727.

[28] Tu, Z. and Lu, Y., 2004, “Dynamic Model Updating Using Combined Genetic-Eigensensitivity Algorithm and Application in Seismic Response Prediction,” Earthquake Engineering and Structural Dynamics, **34**(9), pp. 1149–70.

[29] Imregun, M., Viser, W.J. and Ewins, D.J., 1995 “Finite Element Model Updating Using Frequency Response Function Data,” Mechanical Systems and Signal Processing, **9**(2) pp. 187–202.

[30] Nelson, R.B., 1976 “Simplified Calculations of Eigenvector Derivatives,” AIAA, **14**(9), pp. 1201.

[31] Blelloch, P., “Calculation of Eigenvector Derivatives for Structural Systems,” SDRC Engineering Services, Cincinnati, OH.

[32] Fox, R. L. and Kapoor, M. P., 1968, “Rates of Change of Eigenvalues and Eigenvectors,” AIAA, **6**(12), pp.2426-2230.

[33] Gordis, J.H., 1994 “An Analysis of the Improved Reduction System Model Reduction Procedure,” Modal Analysis, **9**(4).

[34] Adams, R. D. and Cawley, P., 1979, “The Location of Defects in Structures From Measurements of Natural Frequencies,” Journal of Strain Analysis, **14**(2),pp.49-57.

THIS PAGE INTENTIONALLY LEFT BLANK

INITIAL DISTRIBUTION LIST

1. Defense Technical Information Center
   Ft. Belvoir, Virginia

2. Dudley Knox Library
   Naval Postgraduate School
   Monterey, California